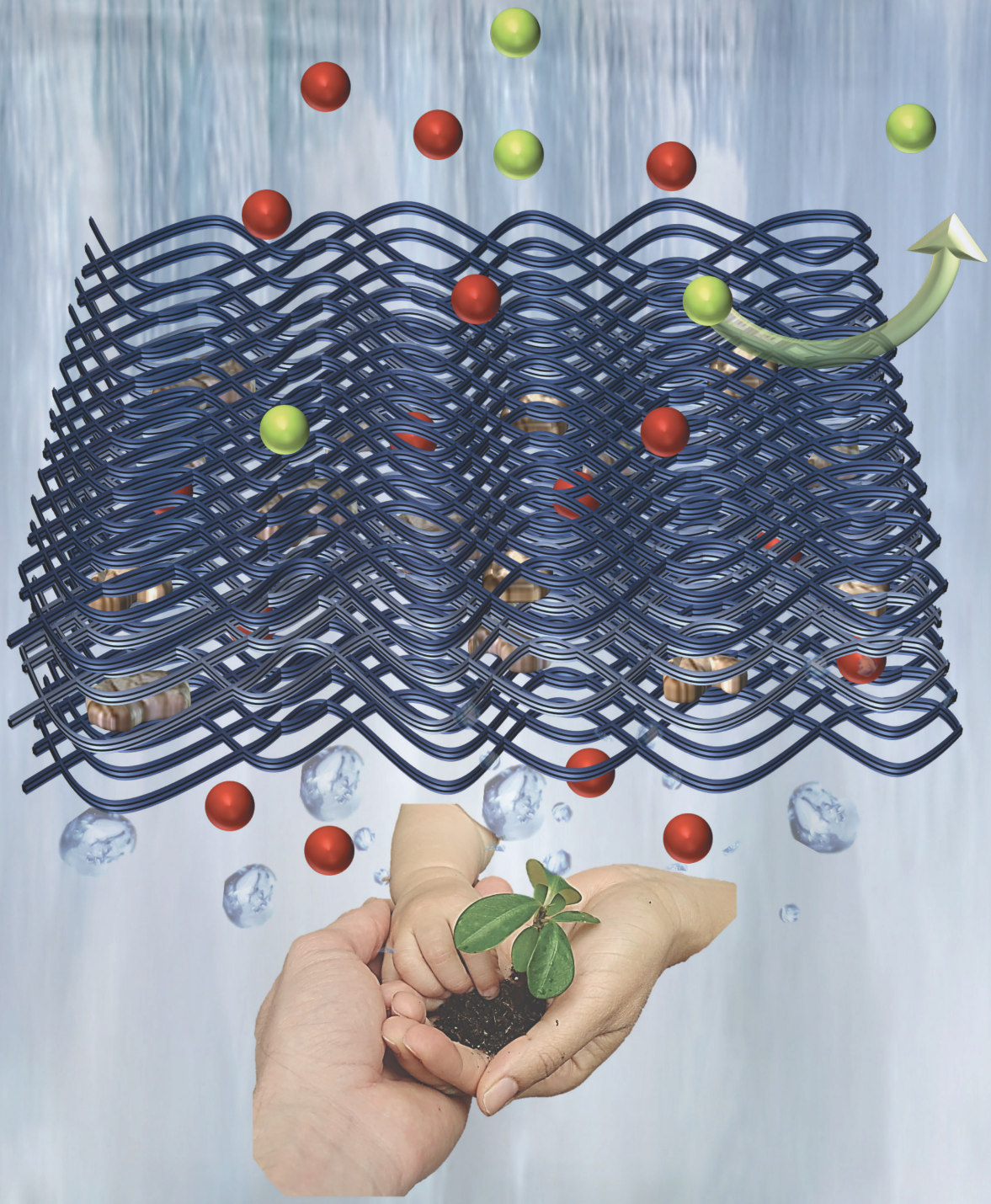

Selective ion removal in electrochemical processes

Tania M. Mubita Zambrano

Propositions

1. In carbon electrodes with pores larger than the hydrated size of the adsorbed ions selectivity is influenced by the ion-carbon surface interactions (this thesis).
2. Selectivity in ion-exchange membranes can be improved by increasing their chemical affinity or their thickness, or by decreasing their charge density (this thesis).
3. By incorporating neuroscience subjects on how the brain works and learns into the curricula of schools, students will acquire the tools to learn more effectively.
4. More breakthrough innovations can be achieved when connections among scientific disciplines are developed.
5. Science should aim for diversifying knowledge rather than meeting a rigid quota based on religion, race, gender, social background, class, or other identifying factors.
6. People with diverse skills and abilities have a better-equipped toolbox to thrive in this ever-changing world as opposed to highly specialized individuals.
7. Society should demand from its leaders to take responsibility for their actions also when things go wrong, and not let them get away by putting the blame on unforeseeable circumstances.

Propositions belonging to the thesis, entitled

Selective Ion Removal in Electrochemical Processes

Tania M. Mubita Zambrano

Wageningen, 19 February 2021.

Selective ion removal in electrochemical processes

Tania M. Mubita Zambrano

Thesis committee

Promotor

Prof. Dr A. van der Wal

Special Professor Electrochemical Water Treatment

Wageningen University & Research

Co-promotors

Dr S. Porada

Principal Scientist

Wetsus, European Centre of Excellence for Sustainable Water Technology,

Leeuwarden

Dr J.E. Dykstra

Assistant Professor, Environmental Technology

Wageningen University & Research

Other members

Prof. Dr R.M. Boom, Wageningen University & Research

Prof. Dr W.M. de Vos, University of Twente, Enschede

Dr M. Stadermann, Lawrence Livermore National Laboratory, United States of America

Dr L.C.P.M. de Smet, Wageningen University & Research

This research was conducted under the auspices of the Graduate School for Socio-Economic and Natural Sciences of the Environment (SENSE)

Selective ion removal in electrochemical processes

Tania M. Mubita Zambrano

Thesis

submitted in fulfilment of the requirements for the degree of doctor
at Wageningen University
by the authority of the Rector Magnificus,
Prof. Dr A.P.J. Mol,
in the presence of the
Thesis Committee appointed by the Academic Board
to be defended in public
on Friday 19 February 2021
at 1:30 p.m. in the Aula.

Tania M. Mubita Zambrano

Selective ion removal in electrochemical processes
218 pages.

PhD thesis, Wageningen University, Wageningen, The Netherlands (2021)
With references, with summary in English

ISBN: 978-94-6395-667-3
DOI: https://doi.org/10.18174/538026

Table of contents

Chapter 1

Introduction

1.1 Water desalination and selective ion removal

Reducing the salinity of water streams, e.g., brackish and seawater, is the most common application of desalination technologies, such as distillation, reverse osmosis (RO), electrodialysis (ED), and capacitive deionization (CDI) [1-3]. Typically, the reduction in salinity is achieved either by removing water molecules from saline waters, e.g., under an applied hydraulic pressure such as in RO, or by removing salts instead of water molecules, e.g., under an applied electrical field such as in ED and CDI [4, 5]. During desalination, the feed water is divided into a diluate and a concentrate stream. Reverse osmosis provides high-quality diluate streams with (close to) complete removal of ions and other dissolved solutes [6, 7]. On the other hand, in technologies such as CDI and ED, the quality of the diluate stream can be controlled by adjusting i) process parameters, e.g., the flow rate of the feed stream and applied electrical potential, and ii) material parameters, e.g., membrane surface area [8, 9].

Desalination is often viewed as a means to obtain freshwater by complete removal of ions, mostly sodium (Na^+) and chloride (Cl^-), the main constituents of natural waters. However, there is a variety of water streams that do not require the removal of all ions, but only the removal/recovery of specific ions mainly because they pose risks to aquatic ecosystems and human health or they have an economic value. Such water streams can be groundwater with a high concentration of nitrate (NO_3^-) or fluoride (F^-), and greenhouse irrigation waters, which often contain high loads of Na^+[10-13] .

The presence of competing ions at high concentrations and with similar physicochemical properties to the target ions (e.g., size and valence) is the main challenge for selective ion removal from water streams. In technologies such as ED and CDI, operational and ion-exchange membrane parameters can potentially be tuned to promote selective ion removal [14]. However, these technologies are not capable yet of achieving this removal in an economically feasible fashion. Major technological developments are expected in the coming years to further expand their application into selective ion separations.

An approach that could advance these technologies in selective ion separation is to develop or modify some of the key components of the electrochemical system, i.e., porous electrodes in CDI and ion-exchange membranes (IEMs) in ED [15-19]. Advancements in membrane technology have prompted the development of different selective IEMs [19, 20]. However, only a few of them have shown significant ion selectivity to reach the commercial market: these membranes mostly show selectivity towards protons or monovalent ions over divalent ions [21]. The pursuit of highly selective membranes is ongoing not only to improve selectivity towards ions with different valence but also ions with the same charge, e.g., potassium (K^+) and ammonium (NH_4^+); NO_3^- and Cl^-.

The need for water desalination and selective ion removal

Water is a precious commodity that forges our society and helps it to meet food, domestic, industrial, and energy needs. Although water is everywhere (water makes up nearly 71% of the earth's surface [22]), many people face barriers in accessing clean water supplies—three out of ten people, including refugees and internally displaced people, do not have access to clean water [23]. Concerns about future water supplies and the strain on the water system are constantly making the headlines due to projections of population growth and economic development in the next decades. A feasible way to meet our increasing water demand is to harness seawater by using desalination processes.

Currently, middle east countries such as Saudi Arabia, United Arab Emirates, and Israel rely on desalination of seawater as a major source of freshwater [24, 25]. The rest of the countries still rely on other natural waters—surface waters, i.e., rivers and lakes, and groundwater. Groundwater supplies nearly 50% of the water consumed worldwide [26]. Most of this water is used for irrigation (**Figure 1.1**)—at the global scale, water used for agriculture represents 69% of the annual water consumption [23]. The availability of groundwater is threatened by the depletion of aquifers and the occurrence of contaminants as a result of human activities [11, 27].

Agriculture is one of the contributors to the pollution of groundwater. High concentrations of nitrate are often found in groundwater due to the excessive use of fertilizers. Nitrates are potentially harmful to humans. It is reduced in the gastrointestinal tract to nitrite, which then reacts with hemoglobin impairing oxygen transport [28]. Due to its negative impact on human health, the World Health Organization has set a limit for nitrate in drinking water of 50 mg/L [29]. Besides nitrate, groundwater can also contain other chemical contaminants, such as fluoride, arsenic, selenium, and heavy metals [11].

There exist different methods to remove chemical contaminants from water. The removal of nitrate, for instance, can be achieved by biological denitrification—mostly used for the treatment of municipal and industrial wastewater—, chemical denitrification, ion-exchange resins, or desalination technologies [30, 31].

State-of-the-art desalination technologies, such as reverse osmosis, lack of selectivity to remove specific ions from multicomponent waters. Therefore, very often after desalination some of the removed ionic species are reintroduced to adjust ion composition to meet water quality standards. For instance, during nitrate removal from groundwater, chloride and some minerals, such as calcium and magnesium ions, are also removed. To improve taste and make the water suitable for human consumption, remineralization is necessary after the completion of the desalination process. Another example is the removal of sodium ions from greenhouse irrigation waters due to its detrimental effect on plant growth (Na^+ in high concentration leads to low yield of crops). Sodium is removed together with other essential nutrients for plant growth, e.g., potassium, magnesium, calcium, and sulfate ions, which are involved in metabolic functions such as enzymatic activation [32]. After desalination, fertilizers are used to add back the required nutrients.

The production of water from saline streams for human consumption is not the only application that requires selective ion removal. Industrial water effluents, such as those from the electroplating and mining industry, often require the selective removal of heavy metals. Conventional methods for removing these ions involve several steps: metal precipitation accompanied by flocculation or coagulation, or

subsequent removal of the precipitate by solid-liquid separation processes [33]. These methods often require the addition of chemicals and generate large amounts of harmful solids [33, 34].

Certainly, it is important to implement relatively simple yet environmentally and economically sustainable technologies to selectively remove ions that represent a potential threat to humans and ecosystems. However, the often low salinity of the polluted water and lack of ion specificity are the biggest hurdles to the adoption of selective desalination technologies in a cost-effective way.

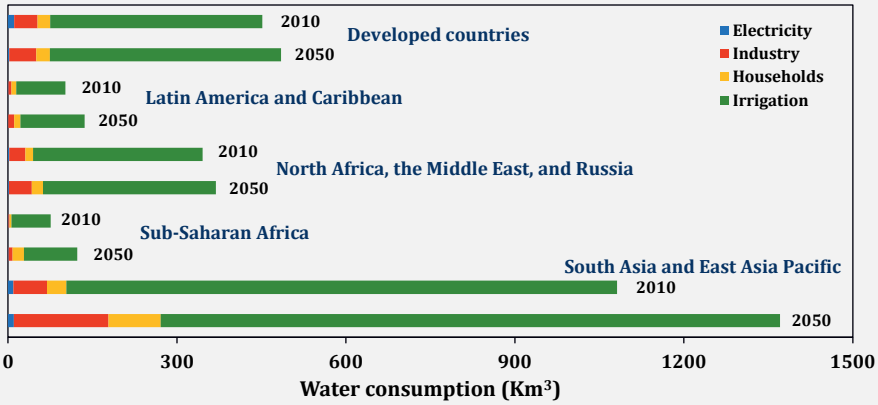

Figure 1.1. Water consumption per sector area in the year 2010 and forecast for the year 2050. Source: Adapted from [35]. Licensed under Creative Commons Attribution 3.0 Unported (CC BY 3.0).

1.2 Desalination technologies

Seawater constitutes about 97% of the water on Earth. Therefore, it is not surprising that desalination is an important means to produce freshwater. Desalination is the separation process in which dissolved compounds—such as salts, and organic matter—are removed from water. Technologies that can achieve this type of separation are commonly divided into two broad categories based on the separation method: 1) thermal evaporation and 2) membrane separation [36-38]. The most commonly used thermal desalination technologies are multi-effect distillation (MED), multi-stage flash (MSF), and vapor compression (VC). The main difference among these technologies is

the temperature to which the feed water is heated to generate the desalinated water vapor. Membrane separation technologies can be further categorized by the driving force that enables the salt-water separation: pressure gradient (osmotic pressure), electrical potential difference, or differential temperature.

The most widely applied desalination method is the pressure-driven membrane technology reverse osmosis with 63% of the capacity share, and MSF and MED, which combined represent 31% of the share [39]. Other desalination technologies, such as CDI, ED, and forward osmosis have not reached a significant share globally because they are in the process of commercialization, or still require further development.

1.3 Electrically-driven desalination technologies

In this PhD project, we focus on electrically-driven technologies, specifically CDI, membrane capacitive deionization (MCDI), and ED. This section gives an overview of the key aspects of these technologies, with emphasis on their application in the selective removal of ions.

1.3.1 Capacitive deionization

Capacitive deionization (CDI) is based on the electrosorption of ions upon the application of an electrical potential difference between two porous electrodes (**Figure 1.2a**). Ions removed from the feed stream are temporarily adsorbed in the electrical double layers (EDLs) of the oppositely polarized electrode (adsorption step) [40, 41]. When the adsorption capacity of the electrode is reached, the electrodes are short-circuited or the voltage is reversed, which releases the ions back into solution generating a concentrated stream (ion desorption step) [42-44]. CDI was initially applied for the desalination of brackish water. However, in recent years the range of CDI applications has expanded to water treatment of domestic and industrial effluents, among others [9, 45, 46].

The main components of the CDI system are a pair of electrodes, mainly composed of highly porous carbon-based materials. Much of the effort to improve CDI performance has been directed to developing materials with high internal surface area to increase

salt adsorption capacity, which is a metric that relates the amount of ions adsorbed in the pores of the electrodes to the total electrode mass. Porous carbon materials, e.g., carbon aerogels, carbon nanotubes, graphene, and especially activated carbon, have been extensively used in the fabrication of electrodes [47, 48]. Recently, a new class of electrodes based on redox-active intercalation materials has been proposed. The removal mechanism of these electrodes is based on ion insertion in the crystalline structure of the material (reversible process) or on redox reactions [49, 50]. In ***section 1.3.1.2***, we give further details about intercalation materials for selective ion separations.

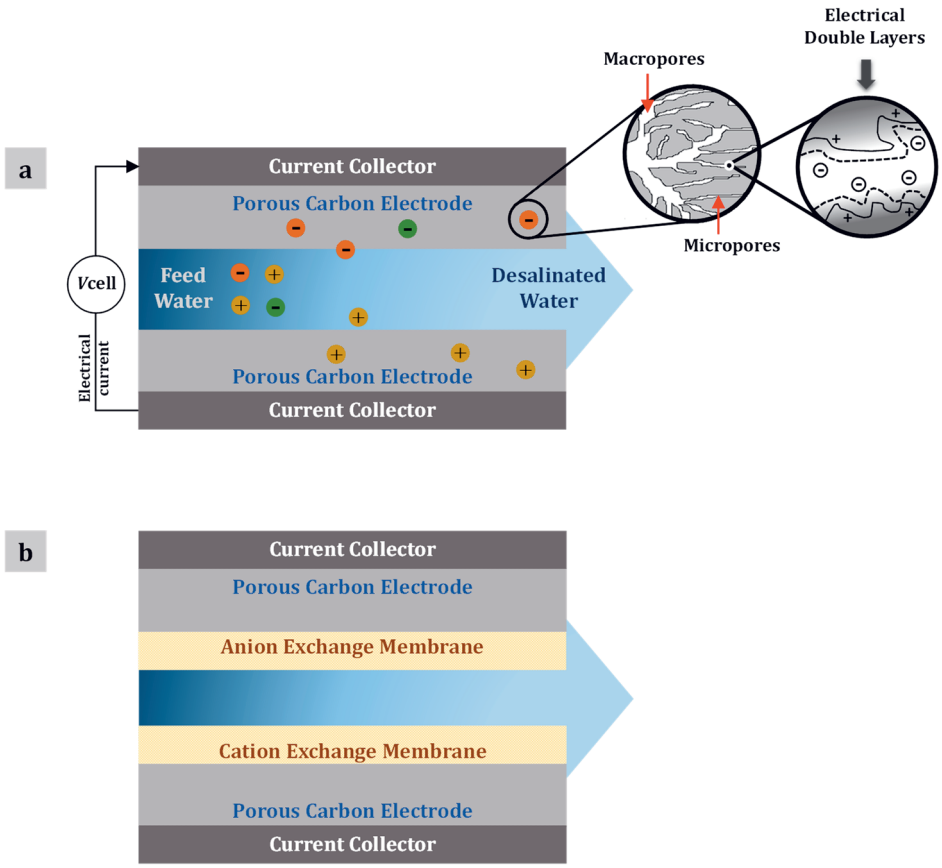

Figure 1.2. Schematic of CDI architectures a) feed water flows in between the electrodes, upon applying an electrical potential, ions are adsorbed in the micropores of the electrodes, where the electrical double layers are formed; b) membranes are placed in front of both electrodes. This architecture is referred to as MCDI.

An important characteristic of porous carbon materials is the preferential adsorption of specific ions. However, ion selectivity in CDI is not only related to the properties of the electrodes, but also to the properties of the ions to be removed, and system conditions. **Figure 1.3** summarizes the main factors that affect ion selectivity in CDI systems. These factors are revised in the following section.

1.3.1.1 Factors affecting ion selectivity in CDI with porous carbon electrodes

- ***The effect of ion properties and ion content on ion selectivity***

Research has shown that ion selectivity in porous carbon materials is largely influenced by the valence and size of the hydrated ions. It has been reported that ions with high valence are preferentially electrosorbed. Gabelich et al. [51] studied the effect of valence, mass, and ion size on electrosorption capacity. They found that ion valence was the main parameter determining ion selectivity. In solutions containing ions with different valences, selectivity was observed towards the ion with the highest valence. Similar results were obtained in the work of Zhao et al. [52] and Hou and Huang [53], who reported preferential electrosorption of Ca^{2+} over Na^{+}, and Li et al. [54], who reported preferential electrosorption of sulfate (SO_4^{2-}) over NO_3^{-}. The selectivity towards multivalent ions seems to prevail even when the concentration of the multivalent ion is much lower than that of the monovalent ion. The selectivity towards Ca^{2+} reported by Zhao et al. [52] was achieved with electrolytes with an initial concentration of Na^{+} five times higher than that of Ca^{2+}.

When ions have the same valence, preferential electrosorption has been observed for ions with smaller hydrated size [53, 55-57]. This selectivity trend, however, has been shown to depend on the pore-size in the electrodes [58]. In electrodes with pore-size similar to the ion-size, salt adsorption capacity, and hence preferential ion electrosorption, decreases with increasing the hydrated size of the ions [59]. On the other hand, when electrodes had a pore-size larger than the ion-size no significant differences in electrosorption capacity of different ions were observed [51, 60].

It is worth mentioning that ion selectivity based on size-affinity is often observed when the concentration of competing ions is the same [54, 61]. This implies that when competing ions have different concentration, selectivity is determined by other factors, which will be discussed later.

For ions with the same valence and similar hydrated size, e.g., NO_3^- and Cl^-, ion selectivity cannot be related to the differences in ion-size. Researchers have tried to relate the observed selectivity to other physicochemical properties of the ions. Li et al. [54] introduced the hydrated ratio, which is the ratio of the hydrated over the bare ion radius, to evaluate the preferential electrosorption of monovalent ions. In this work, Li et al. [54] reported selectivity towards anions with a higher hydrated ratio. A high hydration ratio represents higher screening of the ionic charge, and therefore, less electrostatic attraction of the ion for the carbon electrode. Sun et al. [62] tried to correlate selectivity with electronegativity. They found that ions with higher electronegativity are preferentially electrosorbed.

When looking into the effect of ionic composition, research has shown that preferential ion electrosorption depends on the concentration of the ions in the feed solution and not much on the ion valence or hydrated size. Different studies have reported that ions with higher concentrations in the feed stream are found in higher concentrations adsorbed in the carbon electrodes [63-65].

- ***The effect of system operation on ion selectivity***

Operational parameters can also improve selectivity. Zhao et al. [52] obtained in a CDI stack an effluent with a Ca^{2+}/Na^+ concentration ratio of 300 by performing a stage desalination process, where the desalination stream is repeatedly desalinated in the next desalination cycle. Hou and Huang [53] showed that in a mixture of monovalent cations selectivity towards small size cations increased as the applied voltage increased. At 0 V, there was no preferential adsorption between K^+ and Na^+. However, at higher applied voltages selectivity towards K^+ increased. Yeo and Choi [66] showed that in a mixture containing Cl^-, $NO_3{}^-$, and $SO_4{}^{2-}$ (concentration ratio 5:2:2), $SO_4{}^{2-}$ was preferentially electrosorbed over Cl^- at low current densities. With increasing the current density, adsorption of Cl^- increased.

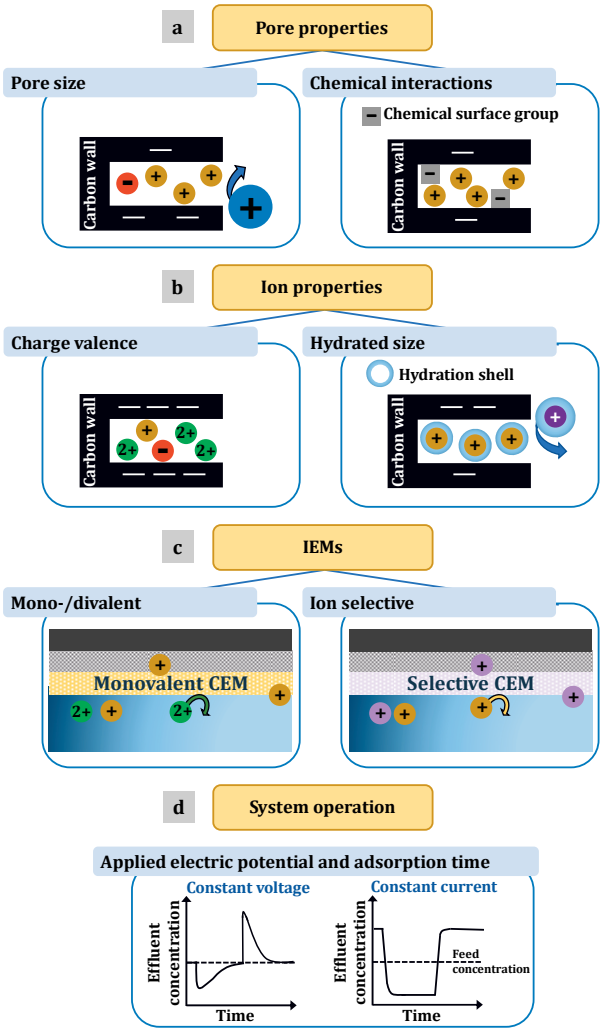

Figure 1.3. Overview of the main factors that affect ion selectivity in CDI with porous carbon electrodes. When multiple ionic species are present in the feed stream the adsorption capacity of individual ions is influenced by a) pore properties, b) ion properties, c) the presence of ion-exchange membranes (IEMs), and d) system operation.

- ***The effect of the electrosorption time on ion selectivity***

The selective behavior of the electrodes in CDI has been shown to vary depending on the electrosorption time [52, 54, 61, 67]. Zhao et al. [52] reported that Na^+ was preferentially removed from the solution at the beginning of the electrosorption

process, but when the electrodes were saturated, Ca^{2+} replaced the adsorbed Na^{+} ions. In addition, when electrosorption was carried out for one hour, the Ca^{2+}/Na^{+} ratio was ~ 7. This ratio increased to ~ 25 when the adsorption time was extended to five hours. Similar to the previous study, in a CDI system, Hassanvand et al. [67] observed that at the start of the electrosorption process monovalent cations (Na^{+} and K^{+}) were preferentially adsorbed over Ca^{2+}. However, after a certain time, Na^{+} and K^{+} were displaced by Ca^{2+}, which increased the concentration of both monovalent ions in the bulk solution compared to that of Ca^{2+}. In the case of mixture of anions, Hassanvand et al. [67] reported that SO_4^{2-} and Cl^{-} are preferentially removed at the early stage of electrosorption, but at later stages these ions are replaced by NO_3^{-}.

- ***The effect of carbon modifications on ion selectivity***

Selective ion adsorption can be achieved by modifying the pore characteristics of carbon materials, e.g., pore size [68, 69]. Avraham et al. [68] used chemical vapor deposition (CVD) to reduce the pore-size of carbon fiber electrodes. After the CVD treatment, their results, obtained with single salt electrolytes, showed that the adsorption capacity for divalent ions decreased, whereas the capacity for monovalent ions did not change. They concluded that only ions that are smaller than the pore opening could enter the pores. Noked et al. [69] modified an AC cloth by CVD to promote the electrosorption of NO_3^{-} over Cl^{-}. The preference for NO_3^{-} was attributed to the formation of narrow pore openings that allowed the passage of NO_3^{-}, with planar shape, and hindered the passage of Cl^{-}, with sphere-like shape.

Oyarzun et al. [70] used carbon electrodes functionalized with quaternary amines (cathode) and benzene sulphonate (anode) to increase selectivity towards NO_3^{-} over Cl^{-}. Guyes et al. [71] reported enhanced selectivity towards K^{+} over Li^{+} when using chemically oxidized cathodes. Lado et al. [72] modified the surface of carbon electrodes with coatings of metal oxides (SiO_2 on the cathode and $\gamma - Al_2O_3$ on the anode) to increase the removal of NO_3^{-}. They showed symmetric removal of cations and anions in $NaNO_3$ electrolyte, but asymmetric ion removal in $Ca(NO_3)_2$ electrolyte, which was characterized by higher electrosorption of Ca^{2+} than NO_3^{-}. In addition, with

multicomponent electrolytes, Lado et al. [72] reported time-dependent ion removal for Na^+ and Ca^{2+} similar to that previously described by Zhao et al. [52].

1.3.1.2 Ion selectivity in CDI with other porous materials

One or both carbon electrodes can be replaced by electrodes composed of intercalation or redox-active materials. CDI systems with two distinct electrodes are considered hybrid. The electrodes in these systems present asymmetric ion removal, which is the result of different removal mechanisms [73]. With intercalation materials, such as Prussian Blue and its analogs (PBAs), ion removal is accompanied by a Faradaic charge transfer. This mechanism of storing charge is often reversible, i.e., ions stored in the interstitial sites can de-intercalate once the electrical potential difference is removed [16]. On the other hand, with redox-active materials, the removed ions are transformed into other chemical species by reaction with the electrode surface [49, 73].

The increasing interest in intercalation/redox-active materials is associated with their high capacitance (capacity for ion storage) and the potential to achieve higher salt removal than porous carbon electrodes at lower voltage [45, 50, 74]. Additionally, intercalation/redox-active materials have shown high ion selectivity. For instance, PBAs, such as nickel hexacyanoferrate (NiHCF), have been intensively studied for their ability to selectively separate alkali metal ions [50, 75]. In aqueous electrolytes, selectivity trends in PBAs-based electrodes are associated with ion size-exclusion: the ion with the lowest hydrated size is preferentially removed [16, 50, 76]. These materials can also achieve high selectivity by charge exclusion. Singh et al. [16] reported selective removal of Na^+ over Ca^{2+} and Mg^{2+} in NiHCF-based electrodes. Sodium selectivity remained high (separation factor Na^+/divalent ions ≈ 20) even in electrolytes with concentrations of the divalent ions three times higher than Na^+.

Transition metal oxides, such as sodium manganese oxide (NMO) and manganese oxide (MnO_2), are other types of intercalation materials. Kim et al. [77] showed that NMO-based electrodes selectively removed Na^+ over K^+, Mg^+, and Ca^+. On the other hand, electrodes containing MnO_2 have shown to be suitable for recovering Li^+ from seawater and brines [78]. Other materials such as lithium–manganese–titanium oxide (LMTO)

and polyanionic phosphates, e.g., lithium iron phosphate ($LiFePO_4$), have also been proposed for the selective removal of Li^+ [79, 80].

Studies conducted by Srimuk et al. [81] demonstrated that intercalation materials can also be used to selectively remove divalent ions. They reported that selectivity can be tuned in intercalation electrodes by adjusting the applied voltage. The changes in selectivity are related to the different potentials of intercalation for different ions. Srimuk et al. [81] achieved selective removal of Mg^{2+} over Cs^+ in electrodes of titanium disulfide and carbon nanotubes (TiS2-CNT). Other studies have also shown that selectivity can be manipulated by changing the operational voltage [82].

In general, much of the research conducted with intercalation/redox-active materials is focused on selective separation of cations, rather than anions. A few relevant studies include mostly redox-active materials. For instance, Hu et al. [83] used layered metal oxide electrodes to remove nitrates. The removal of nitrate is performed in two steps: in the first step, NO_3^- is electrosorbed onto the anode electrode. In the second step, which involves the regeneration of the electrode, NO_3^- is reduced to nitrogen gas. Chloride has been selectively removed using bismuth (Bi) electrodes as an anode [84]. In these, electrodes, Cl^- is stored as a bismuth oxychloride (BiOCl) compound. Removal of Cl^- is approx. 1.5-fold higher than that of SO_4^{2-}. However, this preferential removal of Cl^- decreases with increasing SO_4^{2-} concentrations.

1.3.2 Membrane capacitive deionization

Membrane capacitive deionization (MCDI) is a modification of CDI in which ion-exchange membranes (IEMs) are placed in front of the porous electrode (**Figure 1.2b**) [85]. IEMs increase the desalination efficiency and salt adsorption capacity of the system by blocking the co-ions that are expelled from the micropores. Due to electroneutrality requirements, the accumulation of co-ions at the electrode/membrane interface leads to an increase in counterion concentration, and hence an increase in salt removal capacity [86, 87].

IEMs influence ion kinetics by allowing the preferential transport of specific ions [67, 88]. Ion transport, and therefore ion selectivity, varies depending on the membrane

characteristics, e.g., chemical composition. Studies have shown that the removal of divalent ions is increased in MCDI systems with conventional IEMs [89, 90]. On the other hand, selective monovalent IEMs allow for the selective removal of monovalent ions from electrolytes containing a mixture of multivalent ions [91, 92].

Typically, IEMs are included as free-standing films. However, IEMs can also be coated onto the surface of the electrodes. Kim and Choi [17] coated the anode surface of carbon electrodes with polymeric solutions containing selective ion exchange resins (IERs) to separate NO_3^- from Cl^-. Their system achieved a higher electrosorption of NO_3^- over Cl^- than the MCDI system with conventional IEMs. Gan et al. [93] used a similar approach and coated carboxyl functionalized carbon nanotubes to preferentially electrosorb NO_3^- over SO_4^{2-}, Cl^-, and F^-. Similarly, Zuo et al. [94] reported high selectivity towards SO_4^{2-} even at high Cl^- concentrations in the feed solution.

Although MCDI was initially developed with IEMs, new approaches include other types of membranes such as nanofiltration membranes, which have been used to separate monovalent and divalent ions [95]. Further modifications of MCDI systems include hybrid systems with metal oxides electrodes, such as lithium manganese oxide, which showed high selectivity towards Li^+ over Mg^{2+}, Ca^{2+}, K^+, and Na^+ [96].

1.3.3 Electrodialysis

Electrodialysis is another desalination technology in which ions are transported through IEMs when an electrical potential is applied between two electrodes, i.e., cathode and anode. An ED unit consists of cation-exchange membranes (CEM) and anion-exchange membranes (AEM), placed in alternating order between the electrodes. This membrane arrangement creates two separate compartments, i.e., diluate and concentrate, through which water flows (**Figure 1.4**).

In general, IEMs allow the selective transport of ions with one charge sign, i.e., AEM transports negatively charged ions (anions) and CEM transports positively charged ions (cations). This selectivity is possible due to the presence of ion-exchange sites consisting of functional groups with opposite charge to the ions transported across the IEMs (counterions). These ion-exchange sites can be chemically bound to the

membrane matrix (homogenous membranes) or physically dispersed throughout the membrane matrix (heterogeneous membranes) [21]. Besides the apparent difference in structure between homogenous and heterogeneous membranes, these two types of membranes are also different in terms of their electrochemical properties, e.g., electrical resistance [97-100]. In principle, homogenous membranes have the same properties throughout their thickness due to the uniform distribution of ion exchange sites over the polymeric matrix. In addition, homogenous membranes are considered to have relatively low electrical resistance compared to heterogeneous membranes with the same thickness [100].

The selectivity of the IEMs towards the transport of ions of opposite charge is a property of the IEMs known as permselectivity [101, 102]. This selectivity is often sufficient for most ED applications, e.g., sea and brackish water desalination. However, specific applications, such as water softening, require membranes with an additional selectivity that allows the separation of specific counterions. The ability of IEMs to discriminate different counterions depends on different physical and chemical interactions, e.g., electrostatic attraction and steric hindrance, between the ion-exchange sites in the membrane and the counterions in the feed stream. As a result of these interactions, the IEMs exhibit affinity, or preference to permeate, for one counterion over another.

In ED processes, selective ion separation depends not only on the affinity of the IEMs for specific ions, but also on parameters such as the driving force, e.g., applied electrical potential, and the desalination time. For instance, typically, IEMs (both CEM and AEM) show a higher affinity for multivalent ions, due to stronger electrostatic interactions between the ions and the ion-exchange sites [103, 104]. At low applied electrical potential, this affinity plays an important role in the preferential transport of divalent ions over monovalent ions [105]. However, at high applied electrical potentials, monovalent ions are preferentially transported. In this case, it is argued that kinetics play an important role in determining selectivity: divalent ions are more strongly retained in the IEMs, which in turn results in slow transport compared to the monovalent ions [103, 106].

The affinity of IEMs towards specific ions can be tuned by modifying the way ions interact with the membrane structure i.e., ion-exchange sites and membrane matrix [19, 107, 108]. To that end, modification of the IEM surface is the most common and effective method to date, which has been shown to improve ion selectivity between monovalent and divalent ions [15]. Surface modification can be achieved by i) immobilization of a thin layer of a charged functionalized polymer with the same charge sign as the counterions in solution [109]. In this way, the transport of multivalent counterions is more hindered by strong electrostatic repulsion with the charged layers than that of monovalent ions. ii) Deposition of multiple layers of polyelectrolytes, often referred to as layer-by-layer deposition. The method consists of coating the surface with alternating layers of polyanions and polycations. It has been shown that the modification improves the permeability of the membranes towards small monovalent ions [110-113]. And, iii) increasing the cross-linking degree of the membrane surface. The modification increases the separation of ions with different hydrated size by ion-sieving [114]. Other modification approaches include incorporating in the membrane matrix fine particles of organic and inorganic ion-exchange materials, such as IER and zirconium phosphate [115, 116].

In general, there is often a trade-off between membrane affinity and other membrane properties, such as electrical resistance (ER) and permselectivity [117]. The ER in IEMs with surface modifications or with high cross-linking is often increased as a result of a reduction in ion mobility [110]. On the other hand, the addition of particles to the membrane matrix causes dimensional instability (high degree of swelling or shrinking), which leads to a decrease in the mechanical stability of the membranes [118].

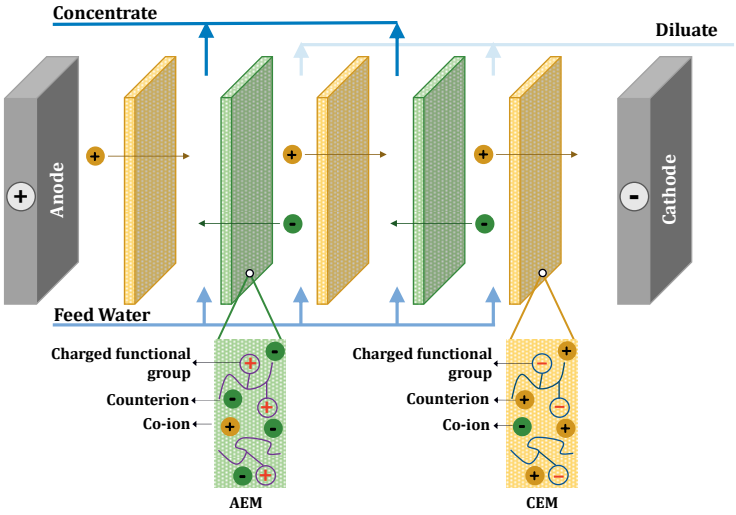

Figure 1.4. Schematic representation of an ED unit. The ED stack consists of alternating cation- and anion-exchange membranes placed between two electrodes, i.e., the anode and the cathode. When an electrical potential is applied, anions migrate through the AEM and cations through the CEM, which creates a concentrate and a diluate stream.

1.4 Numerical frameworks to describe ion transport

1.4.1 Porous electrode theory

Over the years, different theories have been developed to describe electrosorption in porous carbon electrodes in capacitive processes. Key elements of these theories are the description of ion transport inside the electrodes and ion adsorption in the EDLs. A common theoretical approach is to consider the transport of ions from the bulk solution through the interparticle space (macropores), and the transfer of ions from the macropores into the pores inside the carbon particles (micropores), where the EDLs are formed [52, 119]. To describe ion adsorption and charge storage in the micropores, different EDL models have been implemented. Early porous electrode theories used the Gouy-Chapman-Stern (GCS) model for the EDL structure [120, 121]. In the GCS-model, the EDL consists of two layers: i) an inner layer (Stern layer), close to the electrode surface, which is charge-free, i.e., ions are absent. And ii) an outer layer (diffuse layer) at the outside boundary of the Stern layer (**Figure 1.5a**). The diffuse layer contains the ions and extends outwards into the bulk solution—usually several nm in diluate

solutions such as 5~20 mM NaCl. The length of the diffuse layer is often larger than the average micropore diameter (~2nm), which results in double-layer overlap. The GCS model does not take into account the overlap of the EDL, and this is the reason why recent porous electrode theories replaced the GCS model for a more suitable model: the Donnan model (**Figure 1.5b**) and its modified versions. **Chapter 6** describes theory for ion transport that includes a modified version of the Donnan model, which considers the presence of chemical surface charge in the micropores, e.g., protonated groups and acidic groups such as carboxyl.

Existing porous electrode theories capture the dynamics of the electrosorption process, e.g., changes in ion concentration in micropores and the bulk solution. Extended theories capture additional features such as pH changes between feed and outlet stream, Faradaic (redox) reactions, and electrosorption of mixtures of salts [122, 123]. As previously discussed, porous carbon electrodes preferentially electrosorb certain counterions in salt mixtures. Multicomponent theories often predict preferential ion electrosorption based on differences in valence, ion mobility, and size among counterions. However, these theories do not accurately describe preferential ion adsorption between ions with the same charge valence and size. In **Chapter 2**, a theoretical framework is developed to describe preferential ion adsorption based on the affinity of the porous carbon electrodes towards a specific ion.

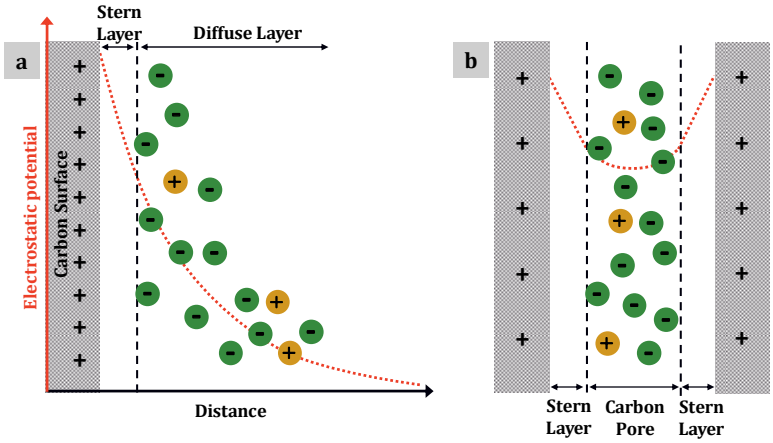

Figure 1.5. Electrical double layer (EDL) representations according to a) Gouy-Chapman-Stern model and b) Donnan model. The EDL forms when the carbon phase is brought in contact with an electrolyte phase. The red dotted line represents the potential drop over the solution side of the carbon/electrolyte interface, when transitioning from the carbon into the bulk liquid.

1.4.2 Theory of ion transport in electrodialysis

Numerical models for ED often use the Nernst-Plank (NP) equation to describe the flux of ions in the system, e.g., across IEMs and bulk solution. In the NP equation, the total flux of ions is the result of diffusional fluxes, i.e., due to a gradient in concentration, and migrational fluxes, i.e., due to a gradient in electrical potential. To fully describe ion transport in ED, the NP equation is often coupled with equations for mass conservation, and the hydrodynamics of the system, among others [124]. These equations are then applied to different regions: i) the diluate and concentrate flow compartments, ii) the thin layers adjacent at each side of the membrane, which are known as boundary layers (BL), and iii) the IEMs. Rigorous models often consider the formulation of ion transport equations for the regions discretized in space and time [125]. Simplified models, on the other hand, assume certain ideal situations to decrease numerical complexity, for instance: i) completely mixed flow channels to neglect the BL, and ii) steady state, i.e., ion transport does not change in time, to avoid temporal discretization.

In general, numerical models consider selectivity in IEMs based on ion charge sign. The common approach is to assume ideally permselective membranes, i.e., only counterions

permeate. However, some models relax this assumption by considering leaky membranes, i.e., counterions and a limited number of co-ions permeate the membrane. Numerical models for ED that also include membrane selectivity between different counterions are insufficient. Ion selectivity between counterions is captured by introducing parameters that are related to differences in ion mobilities between the membrane matrix and the bulk solution or BL. This approach has been used to capture ion selectivity between ions with marked differences in mobilities, e.g. monovalent and divalent ions [105]. In **Chapter 4,** a dynamic transport model is developed to describe selectivity between two different monovalent ions. An important characteristic of the approach used in this model is that it includes a parameter related to the affinity of the membrane for a specific ion.

1.5 Scope and outline of the thesis

Studies mentioned in previous sections have shown that selective ion separation is possible with CDI and ED. However, the degree of the separation that is achieved with these technologies is still modest and limited to certain ionic species, mostly multivalent/monovalent separation. This thesis aims to provide insights to promote the selective removal of ions in CDI and ED. More specifically, this thesis intends to i) study the selective separation of monovalent ions, ii) analyze the factors that affect selective ion removal in CDI, i.e., applied electrical potential and ion concentration, iii) synthesize selective ion-exchange membranes and evaluate their performance in electrodialysis systems, and iv) propose numerical frameworks to describe and predict ion selectivity in CDI and ED.

Chapter 2 focuses on the study of adsorption and electrosorption of NO_3^- and Cl^- in an activated carbon material. The chapter includes a systematic study on ion selectivity over a range of ion concentrations and applied electrical potentials. Moreover, it presents a comparison between preferential ion adsorption onto the carbon material at equilibrium (no electrical potential is applied) and electrosorption onto the carbon electrode. The chapter also describes a theoretical model based on a modification of the Donnan model and includes a parameter that relates to the affinity of the carbon particles towards a specific counterion.

Chapter 3 explores the fabrication of heterogeneous IEMs selective towards NO_3^-. The chapter provides i) a comprehensive characterization of the electrochemical properties of the membranes and ii) an analysis of the effects of hydrophobic groups in the membranes and competing anions, such as Cl^-, IO_3^-, and SO_4^{2-} on NO_3^- selectivity.

Chapter 4 deals with the evaluation of NO_3^- selectivity in commercial and home-made membranes in an ED system. The performance of the different membranes is compared and a numerical model for ion transport that captures ion selectivity is proposed.

Chapter 5 shows a "proof of concept" to fabricate IEM with biopolymers, i.e., alginate and extracellular polymeric substances (EPS) extracted from anaerobic activated

granular sludge. The membranes are intended to selectively separate monovalent cations, specifically K^+ and Na^+.

Chapter 6 is focused on the electrosorption of ions in an MCDI system consisting of wire-shaped carbon electrodes coated with ion-exchange polymeric solutions. Two procedures to fabricate the layer of porous carbon in the electrodes were examined. The salt adsorption capacity of the resulting electrodes was described using a model that considers the presence of acidic and basic groups on the carbon surface (amphoteric Donnan model).

Finally, **Chapter 7** gives an overview of the main findings of this thesis and provides additional perspectives on ion selectivity in electrically driven processes.

Chapter 2

Selective adsorption of nitrate over chloride in microporous carbon.

This chapter has been published as:
T.M. Mubita, J.E. Dykstra, P.M. Biesheuvel, A. van der Wal, S. Porada, Selective adsorption of nitrate over chloride in microporous carbons, Water Research, 164 (2019) 114885.

Abstract

Activated carbon is the most common electrode material used in electrosorption processes such as water desalination with capacitive deionization (CDI). CDI is a cyclic process to remove ions from aqueous solutions by transferring charge from one electrode to another. When multiple salts are present in solution, the removal of each ionic species can be different, resulting in selective ion separation. This ion selectivity is the result of combined effects, such as differences in the hydrated size and valence of the ions. In the present work, we study ion selectivity from salt mixtures with two different monovalent ions, chloride and nitrate. We run adsorption experiments in microporous carbons (i.e., without applying a voltage), as well as electrosorption experiments (i.e., based on applying a voltage between two carbon electrodes). Our results show that i) during adsorption and electrosorption, activated carbon removes much more nitrate than chloride; ii) at equilibrium, ion selectivity does not depend strongly on the composition of the water, but does depend on charging voltage in CDI; and iii) during electrosorption, ion selectivity is time-dependent. We modify the amphoteric Donnan model by including an additional affinity of nitrate to carbon. We find good agreement between our experimental results and the theory. Both show very high selectivity towards nitrate over chloride, $\beta_{NO_3^-/Cl^-} \sim 10$, when no voltage is applied, or when the voltage is low. The selectivity gradually decreases with increasing charging voltage to $\beta_{NO_3^-/Cl^-} \sim 6$ at V_{ch}=1.2 V. Despite this decrease, the affinity-effect for nitrate continues to play an important role also at a high voltage. In general, we can conclude that our work provides new insights into the importance of carbon-ion interactions for electrochemical water desalination.

2.1 Introduction

Capacitive deionization (CDI) is a cyclic process to remove ions from aqueous solutions by electrostatic interactions with charged electrodes often made of porous carbon [126, 127]. This cyclic process is performed by alternatingly charging and discharging the electrodes. During charging, ions are electrosorbed from the feed water, and a desalinated stream is produced. The ions are temporarily stored in electrical double layers (EDLs), which are formed at the electrode-solution interface [59, 128, 129]. During discharge, ions are released from the electrodes and a concentrated stream is produced.

When multiple salts are present in the feed water, the adsorption of each ionic species can be different, resulting in selective removal of ions [56, 63, 130]. As we mentioned in **Chapter 1**, several factors influence the ion adsorption capacity of individual ions from salt mixtures, including i) the material of the electrode, for instance, an intercalation material [131], or porous carbons, as we will focus on in this work; ii) for carbons, the pore characteristics, such as size [132] and chemical surface charge [59]; iii) ion properties, such as ion valence [53], hydrated size [51], electronegativity [62], and the affinity of the ion to the carbon; and iv) operational conditions, such as charging and discharge voltage and initial ion concentration.

When ions have different valencies, it has been shown that a large selectivity can be obtained [52]. However, for mixtures with two anions or two cations with the same valence (namely both monovalent), the results are more ambivalent. In some cases, the selectivity is quite small [55, 56] and in some cases much more significant [70]. It would seem that an affinity difference between the two ions, i.e., their non-electrostatic interaction with the carbon (micropores), can play a significant role when the carbon is uncharged (in an adsorption experiment) [133], but most likely is overruled when two carbons are charged in a CDI-cell (electrosorption). In the second case, the electrostatic forces are strong (the voltage applied is many times the thermal voltage), and this is expected to overwhelm the affinity effect, which is voltage-independent. Our findings, as we will report below, are that indeed with increasing voltage the selectivity between two ions of the same valence decreases when the charging voltage increases. However,

as we also show, both experimentally and theoretically, the separation factor (β) for the ion pair NO_3^-/Cl^- remains very high, also at a voltage of V_{ch}=1.2 V, where a value of $\beta_{NO_3^-/Cl^-} \sim 6$ is found, dropping from a value ~10 in an adsorption experiment.

In the present chapter, we focus on studying selective removal of NO_3^- and Cl^- by porous carbons. We perform two different types of experiments: i) adsorption to study selective removal without electrically charging the carbon material, and ii) electrosorption with charging the carbon, i.e., CDI. The CDI experiments are performed as a function of the NO_3^- over Cl^- concentration ratio in the water and charging voltage. For both types of experiments, we find significant preferential removal of NO_3^- over Cl^-. We show that, in both cases, experimental data can be well described with the amphoteric Donnan model for ion adsorption in the EDLs. In the model, we include a term to account for the affinity of the carbon surface for NO_3^-. We show that this affinity term leads to a high selectivity between the two ions in case of absence of a charging voltage (or a low voltage). Furthermore, we show that the affinity-effect remains important at a high voltage (V_{ch}=1.2 V) where electrostatic effects also come to play a role.

2.2 Theory

To describe ion adsorption in the EDLs formed in microporous carbon materials, we use the amphoteric Donnan (amph-D) model. This model takes into account EDL overlap in sufficiently small micropores (smaller than the Debye length), which is typically the case for CDI with microporous carbons, and the model includes the presence of chemical charge on the surface of the carbon, i.e., lining the micropore regions [134-137]. The amph-D model considers that there are two types of surface charge located in two different regions in the micropores: one region with acidic groups (region-A), and one region with basic groups (region-B). The two regions are expected to be near one another, quite well “mixed” throughout the electrode, but nevertheless, each has its distinct ionic composition, resulting from the difference in nearby surface charge.

Chemical interactions between ions and chemical groups present at the carbon surface can be included in the amph-D model, e.g., positively charged chemical groups at the surface, for which we use the general symbol B^+, can chemically bind ions, for example, NO_3^-, according to the reaction $B^+ + NO_3^- \leftrightarrows B - NO_3$. This adsorption process can be modeled in equilibrium using a pK-constant, which describes the state of the equilibrium as a function of the concentration of ionic species, and the number of free and occupied adsorption sites [138, 139]. These chemical interactions between ions and chemical groups affect the adsorption of specific ions, as well as the chemical surface charge. Related is the pH-dependency of the acidic and basic groups as considered by Hemmatifar [140] in a model with acidic and basic groups, co-existing in the same micropore region (no separation in A- and B-regions).

Instead of considering the binding constants of ions with the different chemical groups, in the present work we use a simplified approach to describe chemical interactions by making use of a term (μ) that describes the affinity of the micropore for certain ions. This term is incorporated in the description of the ion concentration in the micropores ($c_{\mathrm{mi,i,j}}$) according to the Boltzmann equilibrium. The resulting expression is

$$c_{\mathrm{mi,i,j}} = c_{\mathrm{mA,i}} \cdot \exp\left(-z_{\mathrm{i}} \cdot \Delta\phi_{\mathrm{D,j}} + \mu_{\mathrm{i}}\right) \qquad \text{Eq. 2.1}$$

where subscript 'i' refers to the ionic species, and subscript 'j' to the micropore region, which can be either A or B. The concentration in the macropores is $c_{\mathrm{mA,i}}$, z_{i} is the valence of the ion, and $\Delta\phi_{\mathrm{D,j}}$ is the dimensionless Donnan potential. For all species, except for NO_3^-, we set μ to zero. Thus, only for NO_3^-, we assume that the binding to chemical groups can be appreciable. For the other ions (Cl^- and K^+), we assume they do not have a significant chemical binding to the surface, and that they behave as inert species for which the normal Boltzmann distribution applies, i.e., Eq. 2.1 with $\mu = 0$. We use the same value of μ in both the A- and B- regions, i.e., the present model assumes the affinity effect for NO_3^- does not depend on the nature of the chemical charge.

In each region in the micropores, the amph-D model describes three types of charge: electronic charge in the carbon matrix (σ_{elec}), ionic charge in solution (σ_{ionic}), and

chemical charge at the carbon surface (σ_{chem}). Overall, each region in the micropores is charge-neutral, and thus

$$\sigma_{elec,j} + \sigma_{chem,j} + \sigma_{ionic,j} = 0. \quad \text{Eq. 2.2}$$

The acidic region has a negative value of σ_{chem}, whereas the basic region has a positive value of σ_{chem}. To calculate $\sigma_{ionic,j}$ in each region we use

$$\sigma_{ionic,j} = \sum_{i} z_i \cdot c_{mi,i,j}. \quad \text{Eq. 2.3}$$

In the micropores, the ionic charge and electronic charge cannot come infinitely close; therefore, a dielectric layer is considered in between, which is called the Stern layer. The potential over this layer ($\Delta\phi_{S,j}$) is related to the Stern layer capacitance (C_S) and $\sigma_{elec,j}$ according to

$$\sigma_{elec,j} \cdot F = V_T \cdot \Delta\phi_{S,j} \cdot C_S \quad \text{Eq. 2.4}$$

where F is Faraday's constant, and V_T the thermal voltage, given by $V_T = RT/F$, with R the gas constant and T the temperature.

In each electrode (anode or cathode), the potential drop over the EDLs ($\Delta\phi_{EDL}$) is the sum of $\Delta\phi_D$ and $\Delta\phi_S$, and is equal for region A and B [141]

$$\Delta\phi_{EDL} = \Delta\phi_{D,A} + \Delta\phi_{S,A} = \Delta\phi_{D,B} + \Delta\phi_{S,B}. \quad \text{Eq. 2.5}$$

In addition, for each electrode, we calculate the average value for σ_{elec} and σ_{ionic} using

$$\sigma_{elec} = \sum_{j=A,B} \alpha_j \cdot \sigma_{elec,j}, \text{ and } \sigma_{ionic} = \sum_{j=A,B} \alpha_j \cdot \sigma_{ionic,j} \quad \text{Eq. 2.6}$$

where α_j is the fraction of each region relative to the total micropore volume, $\upsilon_{mi,AC}$ (mL/g electrode).

At equilibrium (no transport of ions), the cell voltage is related to $\Delta\phi_{EDL}$ in the anode (an) and in the cathode (ca) by

$$\frac{V_{cell}}{V_T} = \Delta\phi_{EDL_{an}} - \Delta\phi_{EDL_{ca}}. \quad \text{Eq. 2.7}$$

The ion adsorption capacity of the electrodes (IAC) is calculated from the difference between the ion concentration in the micropore (c_i) at the end of the adsorption step (superscript "ads, end"), and the concentration at the end of the desorption step (superscript "des, end"), and when both electrodes have the same mass is given by [142]

$$\mathrm{IAC_i} = \frac{1}{2} \cdot \upsilon_{\mathrm{mi,AC}} \cdot \left(\left(c_\mathrm{i}^{\mathrm{ads,end}} - c_\mathrm{i}^{\mathrm{des,end}} \right)_{\mathrm{ca}} + \left(c_\mathrm{i}^{\mathrm{ads,end}} - c_\mathrm{i}^{\mathrm{des,end}} \right)_{\mathrm{an}} \right) \qquad \text{Eq. 2.8}$$

where

$$c_\mathrm{i} = \sum_{\mathrm{j=A,B}} \alpha_\mathrm{j} \cdot c_{\mathrm{mi,i,j}}. \qquad \text{Eq. 2.9}$$

The electrode charge (in C/g: defined per gram of two electrodes combined) is given by

$$\Sigma_\mathrm{F} = ½ \cdot \mathrm{F} \cdot \upsilon_{\mathrm{mi,AC}} \cdot \left| \sigma_{\mathrm{elec}}^{\mathrm{ads,end}} - \sigma_{\mathrm{elec}}^{\mathrm{des,end}} \right|. \qquad \text{Eq. 2.10}$$

Next, we define the charge efficiency for a mixture of monovalent ions as the ratio of the total number of ions adsorbed, divided by a factor 2, over the charge transferred,

$$\Lambda = \frac{\mathrm{F}}{2} \cdot \frac{\sum_\mathrm{i} \mathrm{IAC_i}}{\Sigma_\mathrm{F}}. \qquad \text{Eq. 2.11}$$

Where 'i' runs over all adsorbed ions.

Finally, to describe ion selectivity in the EDLs, we use the separation factor (β), which is explained in detail by Suss [56] and is expressed as

$$\beta_{1/2} = \frac{\mathrm{IAC_1}}{\mathrm{IAC_2}} \cdot \frac{c_{\mathrm{mA,2}}}{c_{\mathrm{mA,1}}} \qquad \text{Eq. 2.12}$$

where the subscripts 1 and 2 refer to the two different ionic species, e.g., NO_3^- and Cl^-.

The set of Eq. 2.1-Eq. 2.12 describes ion adsorption in the micropores for a process that at the end of each step (charging step, discharge step) reaches equilibrium, i.e., there is no longer transport of ions into the micropores, and is valid irrespective of the valences of the participating ions (except Eq. 2.11).

2.3 Materials and methods

2.3.1 Adsorption experiments

Batch experiments were conducted to study the adsorption of ions in activated carbon (AC) powder, which is equilibrated with a salt solution. A mass of 2 g of dry AC (YP50-F, Kuraray Chemical, Japan) was immersed in 20 mL of multi-ionic solutions containing either: i) one dissolved salt, either 20 mM KNO_3 or 20 mM KCl; or ii) salt mixtures with different NO_3^- to Cl^- concentration ratios, such as 1:2 and 2:1 (21 mM total ionic strength), and 1:3, 1:1, and 3:1 (20 mM total ionic strength). The solution was continuously stirred for 24 h, which is sufficiently long to reach equilibrium in the ion transport between bulk solution and micropores. After this time, the solution was filtered and the concentration of each ion in the filtrate was analyzed by ion chromatography (IC). The ion concentration in the micropores ($c_{\mathrm{mi,i}}$) was calculated from the ion mass balance

$$V_{\mathrm{sol}} \cdot c_{\mathrm{initial,i}} = \upsilon_{\mathrm{mi,AC}} \cdot \mathrm{m_{AC}} \cdot c_{\mathrm{mi,i}} + \left(V_{\mathrm{sol}} - \upsilon_{\mathrm{mi,AC}} \cdot \mathrm{m_{AC}}\right) \cdot c_{\mathrm{final,i}} \qquad \text{Eq. 2.13}$$

where V_{sol} is the volume of solution, $\mathrm{m_{AC}}$ the mass of AC, and $\upsilon_{\mathrm{mi,AC}}$ is the AC micropore volume. $c_{\mathrm{initial,i}}$ is the initial concentration of ion i, and $c_{\mathrm{final,i}}$ is the concentration of ion i at the end of the adsorption experiment.

2.3.2 Electrosorption experiments

CDI experiments were conducted in a stack with four cells. Each cell consisted of two graphite current collectors, a pair of carbon electrodes (Materials & Methods, PACMM™ 203, Irvine, CA, electrode area = 33.8 cm^2) and a spacer channel (Glass fiber filter, cat No. AP2029325, Millipore, $\delta_{sp} \sim 250$ μm) placed in between the electrodes, through which an aqueous solution flows. The electrodes used in the present study have been electrochemically characterized by other researchers [70, 143]. The stack was ensembled as described by Porada et al. [144] in which an aqueous solution flows in between the electrodes through the spacer channel. The aqueous solution with a total volume of 160 mL was pumped through the stack with a flow rate of 30 mL/min. The system was operated in batch-mode: the solution was pumped from the feed container

into the stack, and the effluent of the stack was recirculated to the feed container. The charging voltage (V_{ch}) and discharge voltage (V_{dch}) were controlled and the current was measured using a potentiostat (Ivium Technologies, the Netherlands). For each experiment, we ran three cycles (charging /discharge) to achieve dynamic equilibrium, i.e., when the dynamic data of effluent concentration and current of a particular cycle is the same as of the previous cycle. Thereafter, the fourth cycle was performed, and we took samples from the feed container at different times during charging and discharge. The ion concentration in solution was measured by IC. With this concentration and the volume of solution, we obtain the mole of ion in solution. The difference between the mole of ions at the beginning of the electrosorption experiment and at equilibrium is the total ion adsorption. This total ion adsorption was divided by the total mass of electrodes to obtain IAC in mol/g. The half-cycle time (HCT), which is the duration of each step (charging or discharge), was always 90 min unless otherwise noted. We present an overview of the experimental conditions in **Table 2.1**.

Table 2.1. Overview of electrosorption experimental conditions.

Experiment type	Initial salt concentration	Operational mode
Effect of the initial ion concentration (**Figure 2.2**)	$[NO_3^-]$:$[Cl^-]$ 1:2; 2:1 (total = 21 mM) 1:3; 1:1; 3:1 (total = 20 mM)	CV V_{ch} = 1.2 V V_{dch} = 0 V
Effect of the charging voltage (**Figure 2.3**)	$[NO_3^-]$= 10 mM $[Cl^-]$= 10 mM	CV V_{ch} = 0.6; 0.8; 1.0; 1.2 V V_{dch} = 0 V
Preferential ion electrosorption (**Figure 2.4a**)	$[NO_3^-]$= 10 mM $[Cl^-]$= 10 mM	CV V_{ch} = 1.2 V V_{dch} = 0 V
Ion displacement (**Figure 2.4b**)	Step I: $[Cl^-]$= 20 mM* Step II: $[NO_3^-]$= 20 mM#	CV V_{ch} = 1.2 V, t_{ch} = 30 min CV V_{ch} = 1.2 V, t_{ch} = 90 min

CV=constant voltage; * first step: CV charging for 30 min, 20 mM KCl solution; # second step: addition of 20 mM KNO_3 while keeping V_{ch} = 1.2 V for t_{ch} = 90 min

2.4 Results and discussion

2.4.1 Adsorption experiments: activated carbon is selective towards NO_3^-

Figure 2.1 shows the NO_3^- and Cl^- concentration in the micropores of the carbon particles as a function of the NO_3^- to Cl^- equilibrium concentration ratio in solution. Preferential NO_3^- adsorption is observed, even when the concentration of Cl^- is three times higher than that of NO_3^-. Experiments performed with single salt solutions (either NO_3^- or Cl^- in solution) showed that the concentration of Cl^- ions in the micropores is 34 % lower than that of NO_3^-: c_{mi,Cl^-}=86 mM and c_{mi,NO_3^-}=130 mM. These results show that commercial activated carbon materials, which are often used to fabricate electrodes for CDI [145-147], have an affinity that favors the adsorption of NO_3^- in carbon micropores.

Pore size and surface chemistry are affected by the fabrication and activation method of AC and play an important role in the adsorption capacity of AC [148-150]. In the present work, we report data obtained with microporous AC: 80% of the total pore volume is due to pores with a size between 0.6 and 2 nm [129]. These pores are larger than the hydrated size of the ions used in this study, and thus, are accessible for ions. Therefore, we consider that the surface chemistry, rather than the pore size, has an effect on the preferential adsorption of ions.

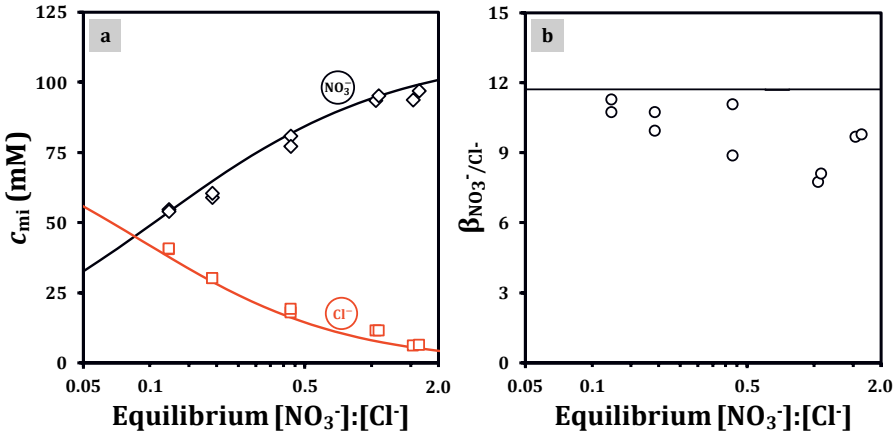

Figure 2.1. Adsorption in uncharged carbon powder. a) Experimental data (symbols) and theoretical curves of the ion concentration in the micropores (c_{mi}) of activated carbon, and b) the separation factor ($\beta_{NO_3^-/Cl^-}$) both as a function of equilibrium concentration ratio in solution, $[NO_3^-]$: $[Cl^-]$. In all calculations, we assumed that the volume of solution is 160 mL and that the total initial ionic strength was 20 mM, although in experiments with an initial concentration ratio of 2:1 and 1:2, the total initial ionic strength was 21 mM.

The surface chemistry of the AC is related to the presence of functional groups, which are: i) acidic groups, primarily oxygen-containing groups, such as phenolic, carboxylic, and lactonic, and ii) basic groups, such as nitrogen-containing functional groups, or π-electrons on the graphene layer [151, 152]. Depending on the conditions, such as the pH and solvent characteristics, these functional groups can be dissociated or protonated, thereby inducing attractive or repulse interactions with the ions in solution [153]. As the strength of the interactions between ions and functional groups is not the same for all ions, we observe an effect on the preferential adsorption of ions [154].

In **Figure 2.1,** we also show theory curves for NO_3^- and Cl^-. We used the affinity term (μ), which describes the interaction between each ion in solution with the uncharged carbon material, as a fitting parameter. Theory describes our data very closely when the value of $\mu_{NO_3^-}$ is 2.46.

Table 2.2. Parameters used in the theory to describe ion selectivity in the EDLs.

amph-D model			
$\sigma_{chem,A}$	Chemical surface charge - acidic region	- 0.26	M
$\sigma_{chem,B}$	Chemical surface charge - basic region	+0.26	M
$\upsilon_{mi,AC}$	Micropore volume carbon powder (adsorption)	0.82	mL/g
	Micropore volume electrode (electrosorption)	0.49	mL/g
C_S	Stern capacitance (adsorption)	145	F/mL
	Stern capacitance (electrosorption)	175	F/mL
$\mu_{NO_3^-}$	Affinity term for NO_3^- adsorption in micropores	2.46	
α_j	Fraction of region A and B relative to $\upsilon_{mi,AC}$	½	
R	Gas constant	8.314	J/mol/K
F	Faraday constant	96485	C/mol
T	Temperature	298	K

2.4.2 Effect of the initial ion concentration and charging voltage on ion selectivity in CDI

Figure 2.2a and **Figure 2.2b** show equilibrium electrosorption data of $\beta_{NO_3^-/Cl^-}$ and the ion adsorption capacity (IAC) as a function of the NO_3^- to Cl^-concentration ratio in the feed solution. We observe that $\beta_{NO_3^-/Cl^-}$ increases with the NO_3^- to Cl^-concentration ratio in feed solution (**Figure 2.2a**). In **Figure 2.2b**, we see that with increasing initial NO_3^- to Cl^-concentration ratio, the difference between the concentration of NO_3^- and Cl^- in the micropores increases. Before equilibrium is reached, however, preferential ion electrosorption is determined by the initial concentration ratio: the ion with the highest concentration in solution was predominantly electrosorbed (data not shown).

Figure 2.3a shows that $\beta_{NO_3^-/Cl^-}$ decreases with charging voltage, but the affinity-effect does not diminish much and continues to play an important role also at a high voltage. Charge and IAC increase with charging voltage (**Figure 2.3b** and **Figure 2.3c)**. **Figure**

2.3d shows that the charge efficiency is much lower than unity, which can be explained by the desorption of co-ions (ions with the same charge as the electrode) from the carbon surface at the beginning of the charging step [67, 146, 155].

To describe the experimental data in **Figure 2.2** and **Figure 2.3,** we use the theory outlined in **Section 2.2.** For the calculations, values for parameters σ_{chem}, $\upsilon_{mi,AC}$, C_S, and μ_i are required. The parameter value for σ_{chem} was obtained from Ref. [156], while the other parameters were fitted (see **Table 2.2**). We find that both the adsorption and electrosorption data are theoretically described using the same value for μ_i. For the adsorption experiments, for which activated carbon powder was used, we found a micropore volume significantly higher than the micropore volume of the electrosorption experiments, for which electrodes were used. This finding is supported by previous work that showed that the micropore volume of activated carbon (Kuraray YP-50F) (0.67 mL/g AC) was significantly higher than the micropore volume of the electrode material per gram of dry activated carbon used for synthesis (0.56 mL/g AC) [146].

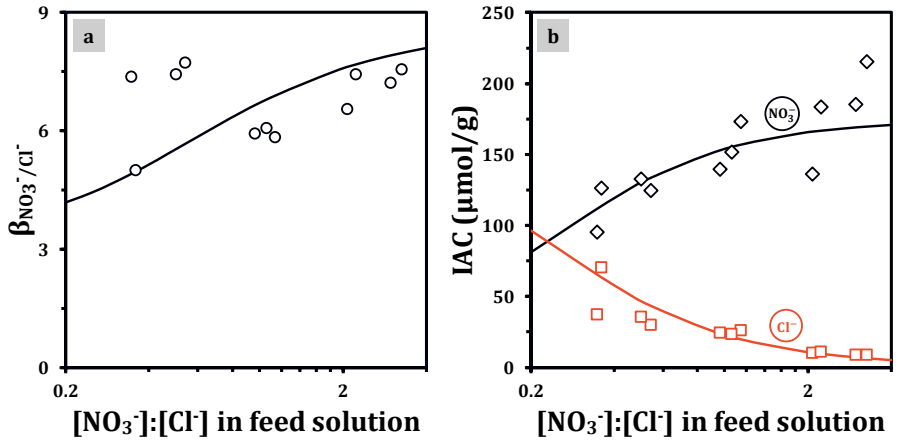

Figure 2.2. Ion electrosorption in CDI ($V_{ch} = 1.2$ V). Data measured at equilibrium at different initial NO_3^- to Cl^- concentration ratio in solution. a) Separation factor; b) ion adsorption capacity per gram of both electrodes. Solid lines are the predictions of the numerical model.

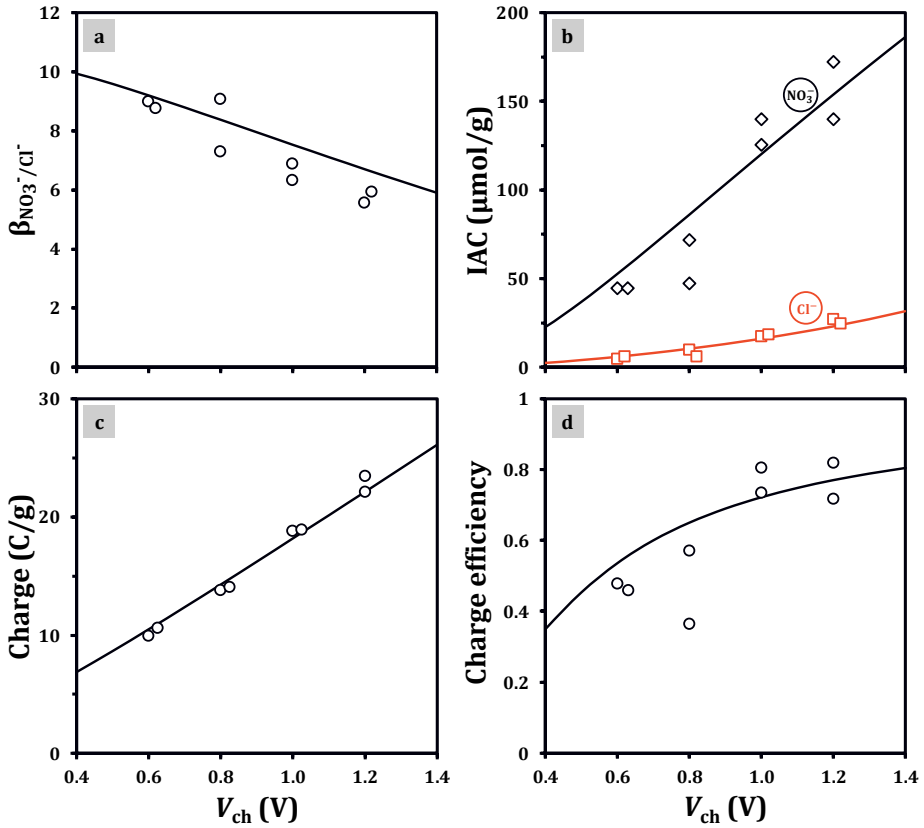

Figure 2.3. Ion electrosorption in CDI. a) Separation factor; b) ion adsorption capacity per gram of both electrodes; c) charge; and d) charge efficiency, as a function of the charging voltage (V_{ch}) Each plot shows two experimental data sets, both obtained at $c_{initial,NO_3^-}$~10 mM and $c_{initial,Cl^-}$~10 mM. Solid lines are the predictions of the numerical model.

2.4.3 Electrosorption of nitrate and chloride: ion selectivity is controlled by kinetics and equilibria

Next, we analyze the dynamics of preferential electrosorption (**Table 2.1**). **Figure 2.4a** shows that the NO_3^- concentration continuously decreases for about 30 min until it reaches a constant value, whereas the Cl^- concentration decreases only for about 15 min. Thereafter, we observe an increase of the Cl^- concentration in solution, which means that NO_3^- ions gradually displace Cl^- ions. This phenomenon was previously reported by Chen et al. [61] for the same mixture of ions.

According to Hassanvand et al. [67], ion selectivity can be explained as a two-step phenomenon: the first step is controlled by ion kinetics and the second by adsorption equilibria. We will analyze both phenomena. To quantify ion selectivity, we use $\beta_{NO_3^-/Cl^-}$, which we show in **Figure 2.4a** as function of time. Values of $\beta_{NO_3^-/Cl^-}$ higher than 1 indicate that NO_3^- ions are preferentially electrosorbed over Cl^- ions. As **Figure 2.4a** shows**,** the separation factor increases over time, which indicates that preferential ion electrosorption is a time-dependent process. At the beginning of the charging step more Cl^- than NO_3^- is electrosorbed in the EDLs: $\beta_{NO_3^-/Cl^-} = 0.7$. At this stage, it is likely that ion selectivity is governed by ion transport to the micropores: the faster ion, in this case Cl^-, is preferentially electrosorbed (see diffusion coefficients of the ions in **Table 2.3**). As electrosorption progresses, $\beta_{NO_3^-/Cl^-}$ increases as a consequence of the displacement of Cl^- by NO_3^-. At equilibrium, $\beta_{NO_3^-/Cl^-}$ reaches a maximum value of ~6.0 at $V_{ch} = 1.2$ V.

Ions in aqueous solution are surrounded by layers of water molecules that form the hydration shell [157]. The ion hydration energy indicates how strong the ions hold these water molecules [158]. The structure of the hydration shell can suffer rearrangements (partial dehydration or complete loss of the water molecules) depending on the interaction of ions with the surface through which they flow [159, 160]. Ions with lower hydration energy can more easily rearrange their hydration shell compared to ions with higher hydration energy. It has been shown that ions need to strip off or deform their hydration shell to enter pores with smaller size than the ion hydrated size [161]. The mean size of the pores contained in our electrodes is larger than the ion hydrated size. Thus, the pore size might not induce large perturbations in the hydration shell of NO_3^- and Cl^-, when these ions enter the pores. Therefore, structural changes on the hydration shell are probably not the main cause of preferential electrosorption of NO_3^-. Ion-carbon surface interactions may play a more important role in determining ion selectivity.

To support our findings of preferential adsorption of NO_3^- over Cl^- at equilibrium, we also conducted two-stage electrosorption experiments (**Figure 2.4b**). In the first stage, we charged the cell to 1.2 V with only K^+ and Cl^- ions in solution. After 30 min, a 20 mM

KNO_3 solution was added to the feed container (same volume as the KCl solution in the feed container, thus the resulting ion concentrations in the feed container are $[K^+]$ = 20 mM, $[Cl^-]$ = 10 mM, and $[NO_3^-]$ = 10 mM), and the charging voltage was maintained for another 90 min. As **Figure 2.4b** shows, Cl^- starts to desorb from the EDLs immediately after NO_3^- is added to the solution. We observe an increase in the Cl^- concentration, while the NO_3^- concentration decreases. Approximately 15 min after the addition of NO_3^-, we observe only minor concentration changes.

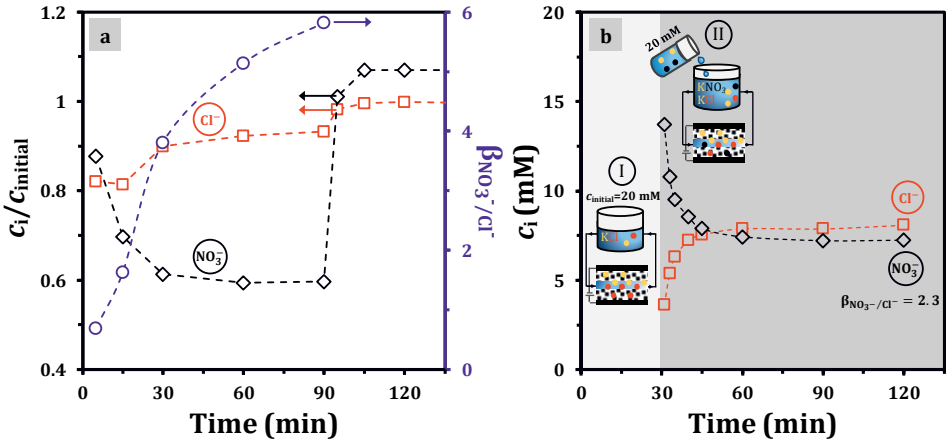

Figure 2.4. a) Anion concentration in solution and separation factor as a function of time; V_{ch} = 1.2 V; $c_{initial,NO_3^-}$~10 mM and $c_{initial,Cl^-}$~10 mM. b) Concentration of NO_3^- and Cl^- ions as a function of time (ion displacement experiment). At step I, only Cl^- ions are electrosorbed for 30 min (NO_3^- ions were not present in the feed solution). Thereafter, a 20 mM KNO_3 solution is added to the feed container (step II). Dashed lines serve to guide the eye.

Table 2.3. Physicochemical properties of the anions studied in the present work.

Ion	Ionic radius (Å) *	Hydrated radius (Å) *	Hydration energy (kJ/mol) **	Diffusion coefficient (10^{-9} $m^2 \cdot s^{-1}$)***
Cl^-	1.81	3.32	-381	2.03
NO_3^-	2.64	3.35	-314	1.90
K^+	1.33	3.31	-322	1.96

*Nightingale [162]; **Smith [163]; ***Haynes [164]

2.5 Conclusions

In this work, we present adsorption and electrosorption data for nitrate and chloride ions. At equilibrium, we observe preferential adsorption of nitrate over chloride in the micropores. Several factors can contribute to the preferential electrosorption of ions, such as the hydrated size of the ions and the interactions between the ions and the carbon surface. As the hydrated size of nitrate and chloride are equal, we conclude that the preferential adsorption of nitrate over chloride is due to chemical interactions between the ions and the carbon surface.

We also presented theory based on the amphoteric Donnan (amph-D) model to predict selectivity between nitrate and chloride in the micropores. The theory can be extended to describe preferential adsorption of other monovalent ions as well. Until now, the amph-D model has not been used to describe ion selectivity. We included an affinity term to describe the preferential adsorption of nitrate into the micropores. Although this affinity term is not associated with any particular property of the ion or micropore, it certainly describes the interaction between ions and the uncharged carbon particles. We acknowledge that this interaction is influenced by the surface chemistry and ion properties. Both theory and data underpin that a specific adsorption effect is not overruled by electrostatic phenomena.

2.6 Supplementary information (S.I)

2.6.1 Electrosorption of nitrate and iodide

A different mixture of monovalent ions, namely NO_3^- and I^-, was used to study preferential ion electrosorption in porous carbon. Nitrate and I^- have equal hydrated size, but different hydration energy: the hydration energy of I^- is lower than that of NO_3^- (see **Table S.I. 2.1)**.

Results in **Figure S.I. 2.1** show that the carbon electrodes are more selective towards I^-, rather than NO_3^-. We observe that I^- displaces NO_3^- in the EDLs. Consequently, there is a continuous increase in I^-adsorption capacity, whereas NO_3^- adsorption capacity increases only at the early stages of the electrosorption step (**Figure S.I. 2.1b**).

These results show that ion displacement occurs when two ions with different affinity compete for space in the micropores. In this case, the ion with higher hydration energy is displaced from the EDLs.

Table S.I. 2.1. Ionic and hydrated radius, and Gibbs free energies of hydration of the anions studied in the present work.

Ion	Ionic radius (Å) [162]	Hydrated radius (Å) [162]	Hydration energy (kJ/mol) [163]
Cl^-	1.81	3.32	-381
NO_3^-	2.64	3.35	-314
I^-	2.16	3.31	-305

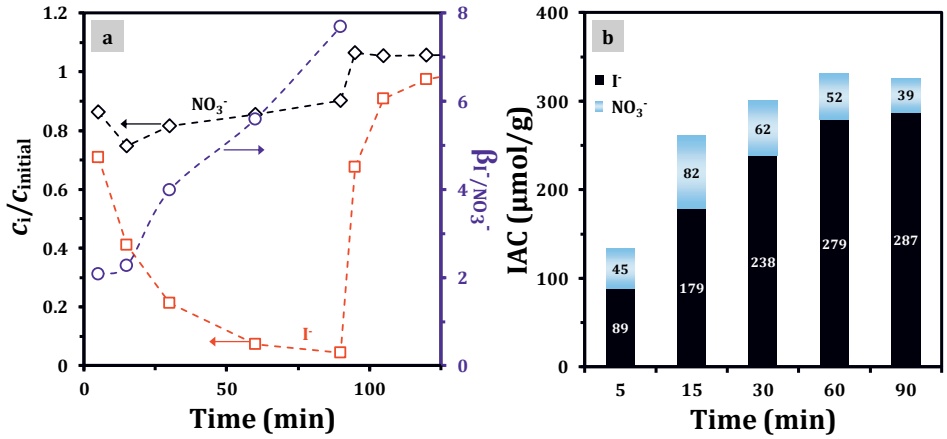

Figure S.I. 2.1. Nitrate and iodide concentration in solution and separation factor (β_{I^-/NO_3^-}); b) ion adsorption capacity (IAC) as a function of time. $c_{initial,NO_3^-}$ =$c_{initial,I^-}$ =10 mM. Dashed lines serve to guide the eye. We applied 1.2 V during the charging step and 0.0 V during discharge. The HCT was 90 min.

Chapter 3

Heterogeneous anion exchange membranes with nitrate selectivity and low electrical resistance.

This chapter has been published as:
T. Mubita, S. Porada, P. Aerts, A. van der Wal, Heterogeneous anion exchange membranes with nitrate selectivity and low electrical resistance,
J. Mem. Sci., 607 (2020) 118000.

Abstract

Selective transport of specific ions across ion-exchange membranes can be enhanced by controlling membrane properties such as hydrophobicity. Previous studies have shown that hydrophobic membranes enhance the transport of ions with low hydration energy, although such membranes often have increased electrical resistance. In the present work, we study the separation of monovalent ions, specifically nitrate and chloride, using newly-designed heterogeneous anion-exchange membranes. These membranes show high selectivity for nitrate over chloride and at the same time have low electrical resistance. We use a functionalized polymeric binder (ionomer) and three ion-exchange resins with different hydrophobic groups, i.e., resins with quaternary ammonium groups and methyl, ethyl, and propyl substituents, respectively. We find that in electrolyte solutions with nitrate and chloride, nitrate over chloride selectivity in our membranes increases with the increasing length of the alkyl groups. The membrane with propyl groups, i.e., which has the highest selectivity for nitrate, was further tested in electrolyte solutions containing nitrate, chloride, sulfate, and nitrate, chloride, iodate. The transport of sulfate and iodate ions across the membranes with propyl groups was 6% and 2% of the total counterions transport, respectively. For monovalent ions with similar hydrated size, it is possible to report selectivity trends based on hydration energy. We find that the chemical structure of the membrane can either promote or hinder the transport of ionic species.

3.1 Introduction

Ion-exchange membranes (IEM) act as selective barriers that enable the separation of anions from cations [15, 20, 67, 165-167]. Certain membranes also enable the separation between mono- and divalent ions [19, 168], but they have limitations when it comes to the separation of ions with the same charge and valence, e.g., nitrate (NO_3^-) and chloride (Cl^-) or sodium (Na^+) and potassium (K^+). The selective separation of ions is particularly challenging because most of the water sources contain other competing ions with similar physicochemical properties that may even be present at much higher concentrations.

Technologies that use IEM for water desalination, such as electrodialysis (ED) and membrane capacitive deionization (MCDI), can benefit from the use of ion-selective membranes, e.g., because of the possibility of removing ions that are toxic to humans and/or ecosystems, or by recovering ions with high economic value from various water streams without using harsh chemicals [169-173]. A potential application of these technologies is the removal of NO_3^- ions from groundwater. Nitrate is ubiquitous in most natural waters. However, its concentration in several water sources, especially in groundwater, has increased due to the use of fertilizers [174, 175]. The potentially harmful effects of NO_3^- on human health have prompted research to selectively remove this ion species [17, 29, 176-181].

The increasing number of potential applications for selective IEMs has led to research focused on modifying the electrostatic interactions between counterions (ions with opposite charge to the charged functional groups in the membrane) and ion-exchange sites in the membrane as well as the membrane matrix [15, 108, 182-184]. The ion-exchange sites in IEMs determine most of the membrane properties such as water uptake, electrical resistance, and selectivity [185]. There are two main classes of IEMs: homogeneous and heterogeneous [21, 117]. In homogeneous membranes, the ion-exchange sites are chemically bound to the membrane matrix [20], whereas in heterogeneous membranes particles that contain ion-exchange sites are dispersed in a polymer matrix [186]. These particles can be organic such as ion-exchange resins (IERs) [187, 188], inorganic with ion-exchange sites such as silicates and zirconium

phosphates [189, 190], or a combination of the two [191]. The binder in heterogeneous membranes is often an uncharged binder such as polyethylene [116], polystyrene [192], polyvinyl chloride [118], polycarbonate [193]. The main drawback of heterogeneous membranes is that the ion-exchange sites are not uniformly distributed. Hence, for the same membrane thickness heterogeneous membranes have higher electrical resistance than homogeneous membranes [194-196]. A large variety of heterogeneous IEMs can be modified by using blends of polymeric binders [186], varying the concentration of IER [197], applying an electrical field to arrange the distribution of the IER particles [198], using binders with charged functional groups [199].

To increase the selectivity of IEMs towards monovalent ions, one possible route is to apply a charged layer on top of the membrane surface, which repels counterions with higher valence [111, 200, 201]. Another approach is to decrease the mobility of large ions inside the membrane by increasing the degree of crosslinking [202] or by changing the hydrophobicity. Previous work has shown that hydrophobic membranes are more selective to the transport of ions with low hydration energy [176, 203, 204]. Membrane hydrophobicity has been used to achieve the separation of NO_3^- from Cl^-. For example, by varying the length of the alkylated quaternary ammonium groups [203, 205] or by incorporating hydrophobic additives, i.e., activated carbon particles (AC) [206]. Results show that the increase in alkyl length leads to more selectivity for NO_3^-, but also to an increase in electrical resistance [203]. On the other hand, it has been shown that the addition of AC particles increases membrane hydrophobicity, but this did not result in an increase in NO_3^- selectivity [206].

The present study focuses on the separation of different monovalent ions, and therefore we designed new heterogeneous anion-exchange membranes (hAEMs). In our study, we use resin particles with different hydrophobicity and a polymeric binder with charged functional groups to decrease the electrical resistance of the membrane. In this work, we characterize and quantify the effect of hydrophobicity of ion-exchange groups on selective ion transport. Our results show that selective transport of NO_3^- over Cl^- can be achieved with our membranes while also achieving low electrical resistance. In

addition, we also show that the hydrophobic membrane effectively rejects bulky ions such as iodate and sulfate.

3.2 Materials and methods

3.2.1 Membrane fabrication

Three heterogeneous anion exchange membranes, which we refer to as CB-hAEMs (conductive binder heterogeneous anion-exchange membranes), were prepared using different commercial IERs with quaternary ammonium groups: Amberlite PWA15, PWA5, and Ionac SR7. These IERs are specially designed for the removal of NO_3^- from water streams. To bind the IER particles together an ionomer solution (fumion FAS solution, FumaTech GmbH, Germany) was used as a polymeric binder. Relevant physicochemical properties and specifications for the IER and polymeric binder as reported by suppliers are given in **Table 3.1**.

For comparison, two commercial AEM were used, a homogeneous membrane (Neosepta AMX, ASTOM Corporation, Tokyo, Japan), and a heterogeneous membrane (Ralex AMH-PES, Mega a.s., Czech Republic).

Table 3.1. Physicochemical properties of the IERs and polymeric binder used to fabricate CB-hAEMs.

	PWA15	PWA5	Ionac SR7	Fumion FAS
Matrix	Crosslinked copolymer	Crosslinked copolymer	Crosslinked polystyrene	Polyaromatic polymer
Structure	Gel	Macroporous	Macroporous	--
Amine	$(C1)_3N$	$(C2)_3N$	$(C3)_3N$	Quaternary ammonium
IEC	≥ 1.3 eq/L	≥ 1.0 eq/L	0.8 eq/L	1.7-1.9 meq/g
Counterion	Chloride	Chloride	Chloride	Bromide

C1, C2, and C3 refer to methyl, ethyl, and propyl substituents, respectively

First, ion-exchange resins were dried in a vacuum oven at 40 °C for 24 h and then ground in a ball mill. The resulting powder was sieved using a mesh size of 40 μm. Then, a suspension was prepared by mixing the IER powder with the ionomer solution containing N-methyl-2-pyrrolidone as solvent. The weight ratio of polymeric binder to

IER was 60:40. To obtain a homogenous distribution of the IER particles in the membranes, the suspension was stirred for 1 h and then sonicated for 6 min. The resulting mixture was cast using a doctor blade knife onto a glass plate heated at 50 °C. The cast solution was exposed to the environment until complete evaporation of the solvent. In the final synthesis step, all membranes were immersed in deionized water for 12 h and stored in a 0.5 M NaCl solution. Four different AEMs were fabricated: three membranes containing IER (CB-hAEMs) and one membrane consisting only of the polymeric binder (PB-membrane).

3.2.2 Membrane characterization

- ***Morphological analysis of membranes***

Morphology of the membranes was visualized by scanning electron microscopy (SEM) using a JEOL, JSM-6480LV scanning electron microscope at an accelerating voltage of 10 kV. Before analysis, membranes were coated with gold using a sputter coater (JFC-1200 Fine Coater, JEOL, Tokyo, Japan).

- ***Water uptake***

Water uptake was determined as the weight difference between the wet and dry membrane. First, membrane pieces of 12 cm^2 were immersed in deionized water for 24 h, and the wet weight was measured after removing excess water from the membrane surface. Thereafter, the membranes were dried at 55 ºC for 24 h and the dry weight was measured. Water uptake was calculated as follows:

$$\text{Water uptake } \% = \left(\frac{W_{wet} - W_{dry}}{W_{dry}}\right) \cdot 100 \qquad \text{Eq. 3.1}$$

where W_{wet} and W_{dry} are the wet and dry mass of the membrane, respectively.

- ***Ion-exchange capacity***

Ion-exchange capacity (IEC) was calculated by measuring the number of equivalents of Cl^- exchanged with NO_3^-. First, the membranes were immersed in 0.5 M NaCl solution for 48 h and then excessive Cl^- was removed from the membrane surface by washing in deionized water. Subsequently, the membranes were immersed in 0.5 M $NaNO_3$

solution for 24 h, and the concentration of Cl^- in solution was measured by ion chromatography (IC) using a Metrohm Compact IC 761 with conductivity detector and chemical suppression. IEC was related to the equivalent of exchanged ions (a) according to:

$$IEC = \frac{a}{W_{dry}}. \quad \text{Eq. 3.2}$$

- ***Electrical resistance***

Electrical resistance (ER) in the membranes was measured using a six-compartment electrochemical cell (**Figure 3.1**) following the procedure described by Galama et al. [207]. The six-compartment electrochemical cell consisted of four-electrodes: i) two Haber-Luggin capillaries, on either side of the tested membrane; and ii) the cathode and anode. The capillaries were filled with 3 M potassium chloride solution and connected to a reservoir with Ag/AgCl electrodes. The effective membrane area was 7.0 cm^2. Four compartments of the cell were filled with 0.5 M NaCl solution (compartments A, B, and C in **Figure 3.1**). Electrode compartments (compartments D in **Figure 3.1**) were filled with 0.5 M Na_2SO_4 solution. All solutions were circulated through the compartments at 170 mL/min. The potential across reference electrodes was measured at different current densities (mA/cm^2) in the cell with and without the tested membrane. Electrical resistance is obtained from the slope of voltage (mV) versus current density. The membrane area resistance ($\Omega \cdot cm^2$) was calculated by subtracting the resistance obtained without the membrane from the value obtained with the membrane. In this work, we report the specific membrane resistance, ρ in Ω·cm [208], which is the area resistance normalized by the thickness of the membrane in a hydrated form (δ_{wet}) [209]. Therefore, ρ is given by

$$\rho = \frac{\text{Area resistance}}{\delta_{wet}}. \quad \text{Eq. 3.3}$$

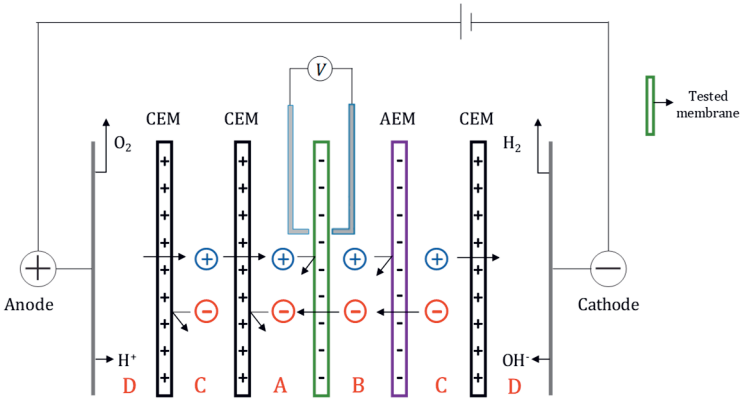

Figure 3.1. Schematic of the six-compartment electrochemical cell used to measure electrical resistance and ion selectivity**.**

3.2.3 Ion selectivity in ion-exchange membranes

Ion selectivity was investigated under equilibrium conditions, i.e., adsorption experiments to measure the number of adsorbed counterions inside the membranes, and dynamic conditions to measure ion transport through the membranes under electrical potential driving force.

- ***Equilibrium conditions***

Membranes of 12 cm^2 were placed in a 0.05 M NaCl and 0.05 M $NaNO_3$ solution and stirred for 24 h. Thereafter, the membranes were transferred to 200 mL of a 0.05 M K_2SO_4 solution for 48 h to exchange NO_3^- and Cl^- for SO_4^{2-}. Aliquots of the solutions were taken and analyzed with IC to determine NO_3^- and Cl^- concentration. To ensure the complete exchange of NO_3^- and Cl^-, the membranes were immersed once more in a smaller volume of SO_4^{2-} solution for 24 h. The NO_3^- and Cl^- concentration in the second SO_4^{2-} exchange solution was below the detection limit. We calculate the NO_3^- to Cl^- selectivity inside the membranes (SE) by

$$SE_{NO_3^-/Cl^-} = \left(\frac{c_{NO_3^-}}{c_{Cl^-}}\right)_{\text{exchanged in } SO_4^{2-} \text{ solution}} . \qquad \text{Eq. 3.4}$$

- ***Dynamic conditions***

To study the preferential transport of ions across the AEMs, selectivity tests were conducted in the six-compartment cell (**Figure 3.1**). Before each experiment, all membranes were equilibrated in the test solution for 24 h. At the beginning of each experiment, compartments A, B, and C were filled with the same solution, whereas compartment D was filled with a 0.1 M K_2SO_4 solution. In compartments C and D, solutions were recirculated at a flow rate of 170 mL·min^{-1} using a peristaltic pump. A fixed volume of 130 mL of a multicomponent solution (0.1 M ionic strength) was continuously stirred in compartments A and B, and after applying certain current density samples were taken from these compartments at different time intervals to measure ion concentration by IC.

Two sets of experiments were conducted to study the effect of competing ions on NO_3^- selectivity. In the first set, ion selectivity of all AEMs, i.e., CB-hAEMs and commercial membranes, was tested in a solution containing anions with similar size and valence, i.e. Cl^- and NO_3^- (Solution I, **Table 3.2**). Ion selectivity was measured at two current densities, i.e., 20 A·m^{-2} for 5 h and 50 A·m^{-2} for 2 h. In the second set of experiments, the effect of competing ions with different size and valence on ion selectivity was further studied. To that end, the CB-hAMs with the highest selectivity towards NO_3^- was tested in two multicomponent solutions containing: i) Cl^-, NO_3^-, and SO_4^{2-} (Solution II, **Table 3.2**), and ii) Cl^-, NO_3^-, and IO_3^- (Solution III, **Table 3.2**). The applied current density for these experiments was 20 A·m^{-2} for 5 h.

Ion selectivity under dynamic conditions (SD) is defined as

$$SD_{i/j} = \left(\frac{\Delta c_i}{\Delta c_j}\right)_A \cdot \left(\frac{c_j}{c_i}\right)_B \quad \text{Eq. 3.5}$$

$$\Delta c = c_t - c_{initial} \quad \text{Eq. 3.6}$$

where subscript 'i' indicates NO_3^- ions and 'j' another anionic species present in the solution. $c_{initial}$ and c_t are the initial concentration and the concentration at time t; subscripts A and B refer to compartment A (receiving solution) and compartment B, respectively. In compartment B, the concentration of both anions 'i' and 'j' was the same

at the beginning of each experiment and remain constant throughout the experiment. This implies that $\left(\frac{c_j}{c_i}\right)_B$ =1 in Eq. 3.5.

The current efficiency (λ) was calculated by

$$\lambda = \frac{(J_i + J_j) \cdot F}{I} \cdot 100\% \qquad \text{Eq. 3.7}$$

where J_i and J_j are the flux of nitrate and other ions respectively across the membrane in mol/m^2/s; F is Faraday's constant; and I is the applied current density in A/m^2.

Table 3.2. Composition of electrolyte solutions and current densities applied in the electrochemical cell to measure ion selectivity.

Solution	Composition compartments A, B, and C	Current density (A·m^{-2})	Tested membrane
I	50 mM KCl + 50 mM KNO_3	20; 50	CB-hAEMs and commercial
II	20 mM KCl + 20 mM KNO_3 + 20 mM K_2SO_4	20	CB-hAEM with propyl groups and commercial
III	33 mM KCl + 33 mM KNO_3 + 33 mM KIO_3	20	CB-hAEM with propyl groups

3.3 Results and discussion

3.3.1 Membrane characterization

- ***Membrane morphology***

SEM images of heterogeneous AEMs with the conductive binder (CB-hAEMs) with propyl groups show the polymeric matrix as well as the dispersed resins. Irregularities on the membrane surface (**Figure 3.2a**) are the result of agglomerates of IER particles. We also observed that IERs particles are covered by the polymeric binder and are uniformly distributed throughout the membrane matrix. The cross-section micrograph (**Figure 3.2b)** shows a dense structure and the absence of empty spaces.

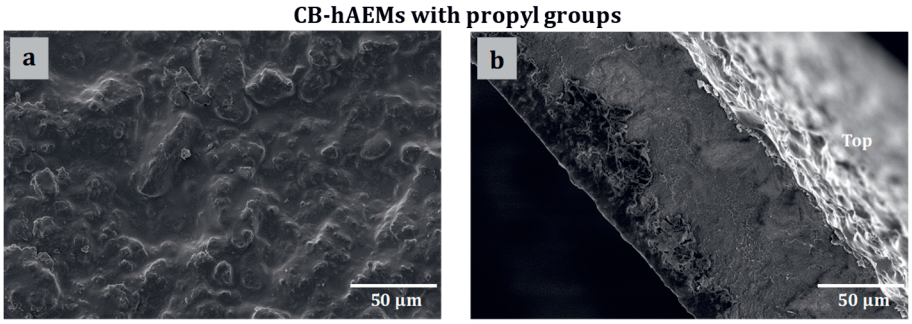

Figure 3.2. SEM micrographs of (a) the surface and (b) the cross-section of CB-hAEM with propyl groups.

- ***Ion-exchange capacity, water uptake, and electrical resistance***

Figure 3.3 shows the effect of IEC on water uptake and ER (shown as specific membrane resistance, ρ) in CB-hAEMs and commercial membranes, which are used as a reference. Overall, we observe an increase in water uptake (**Figure 3.3a**) and a decrease in ρ (**Figure 3.3b**) as IEC in the membranes increases, which is in line with the trends observed in other IEMs [186, 209]. For CB-hAEMs, **Figure 3.3** shows that water uptake and ER are influenced by the chemical structure of the membranes, i.e., the structure of functional groups with methyl (C1), ethyl (C2), and propyl (C3) substituents. The effect of the length of alkyl chain on water uptake (**Figure 3.3a**) can be explained by the increase in hydrophobicity of the ion-exchange sites with the addition of methylene groups ($-CH_2-$) to the alkyl chain [210].

Importantly, the ER in CB-hAEMs is lower in comparison with commercial membranes. The use of conductive binder creates an extra pathway for ion transport, in addition to the ones via IER and the liquid film between resin particles and the polymeric binder [211].

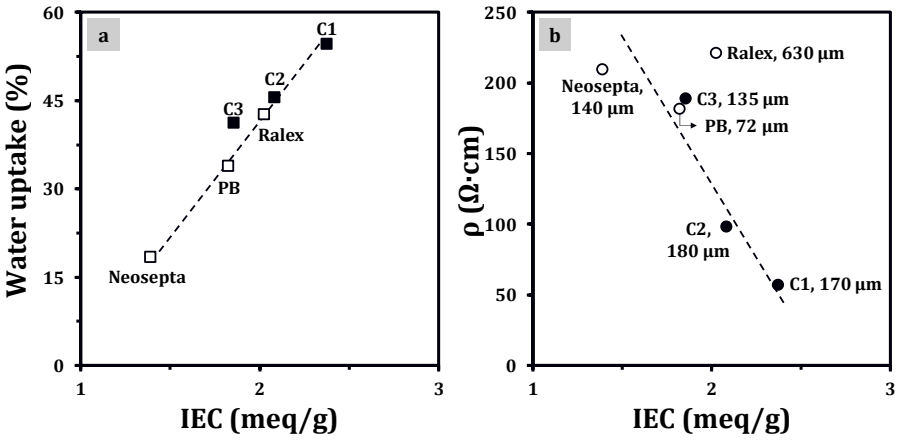

Figure 3.3. a) Water uptake and b) specific membrane resistance (ρ) of CB-hAEMs and commercial homogeneous (Neosepta) and heterogeneous (Ralex) membranes as a function of the ion-exchange capacity. C1, C2, and C3 refer to methyl, ethyl, and propyl groups in the IERs, respectively. PB refers to the polymeric binder membrane without IER. Dashed lines are to guide the eye. The numbers in panel (b) indicate the thickness of wet membranes (δ_{wet}) to help the reader with the conversion to the membrane area resistance (in $\Omega \cdot cm^2$).

3.3.2 Selectivity between nitrate and chloride

- ***Equilibrium conditions***

Figure 3.4 shows the preferential adsorption of NO_3^- over Cl^-—i.e., $SE_{NO3^-/Cl^-} > 1$ (Eq. 3.4), in CB-hAEMs and commercial membranes. In CB-hAEMs, NO_3^- selectivity increases with increasing the length of the alkyl group, and the highest value of $S_{NO3^-/Cl^-} = 5.3$ is obtained for the membrane with propyl groups. Ion selectivity at equilibrium is influenced by specific electrostatic interactions between the ion-exchange sites in the membranes and the counterions. The strength of these interactions depends on ion hydrated size and hydration energy [203, 204]. Our results suggest that NO_3^-, with lower hydration energy (**Table 3.3**), can establish stronger electrostatic interactions with the ion-exchange sites in AEMs, owing to the presence of fewer water molecules around this ion. We believe that the strength of these interactions is what leads to the preferential adsorption of NO_3^- over Cl^- ions. In addition, in CB-hAEMs, the increase in hydrophobicity and size of the ion-exchange sites with increasing alkyl chain can induce partial loss of water molecules in the hydration shells of the counterions [212-214]. It

has been pointed out that the required energy to rearrange hydration shells is compensated by stronger interactions between ions and ion exchange sites in the membranes [204].

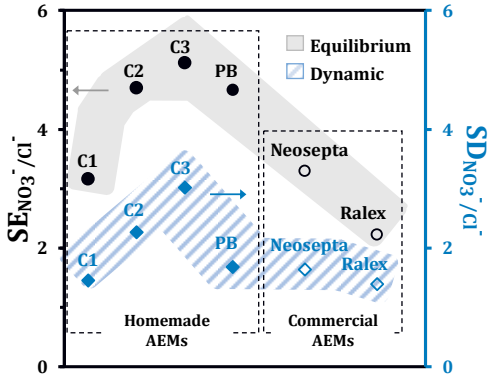

Figure 3.4. Nitrate selectivity of CB-hAEMs, polymeric binder (PB) and commercial anion exchange membranes at equilibrium (SE) and under dynamic conditions (SD). Selectivity in dynamic conditions was measured in solution I (50 mM KCl + 50 mM KNO_3) at 20 A·m^{-2}.

Table 3.3. Ionic and hydrated radii, and hydration energies of the anions studied in the present work

Ion	Ionic radii (Å) [162]	Hydrated radii (Å) [162]	Hydration energy (kJ/mol) [163]
Cl^-	1.81	3.32	-381
NO_3^-	2.64	3.35	-314
IO_3^-	3.30	3.74	-326
SO_4^{-2}	2.90	3.79	-1059

- ***Dynamic conditions***

Under dynamic conditions, when ions are transported through the membranes due to the electrical field, NO_3^- selectivity (SD) significantly decreases compared to selectivity at equilibrium conditions (**Figure 3.4**)**.** Despite this decrease**,** we observe the same selectivity trend in CB-hAEMs: propyl-membrane > ethyl-membrane > methyl-membrane, which is related to a higher transport of NO_3^- across the membranes compared to that of Cl^- (**Figure 3.5).** Both PB- and methyl-membranes show the same flux of NO_3^- and Cl^- (**Figure 3.5a)**, and therefore the same selectivity towards nitrate (**Figure 3.4,** SD). The difference between selectivity values obtained at equilibrium and

under dynamic conditions may be seen as the result of different mechanisms occurring during ion adsorption in and transport across the membrane. As we mentioned before, at equilibrium conditions ion selectivity is associated with differences in affinity, related to chemical/physical interactions, between the charged functional groups in the membranes and the counterions. Under dynamic conditions, however, ion selectivity is determined by coupled effects that include kinetic effects, i.e., relative transport of ions, as well as affinity effects. At current densities of 20 and 50 A·m^{-2}, the current efficiency (λ) was on average 90% and 95%, respectively. The lower λ at 20 A·m^{-2} is the result of undesirable transport of co-ions (potassium ions) and water molecules across the membrane due to the longer experimental time (5 h compared to 2h at 50 A·m^{-2}).

Figure 3.6 shows the change in ion concentration with time at 20 A·m^{-2} in compartment A. The slope 'm' of the fitted lines in **Figure 3.6** and **Figure 3.7** represents the rate of ion concentration change. In **Figure 3.6**, the ion concentration change rate of NO_3^- is higher for CB-hAEMs with propyl groups (m=2.7) in comparison to the PB (m=2.3) and commercial Neosepta (m=2.2) and Ralex (2.1) membranes. In compartment B the ion concentration change is negligible (data not shown). Additionally, in **Figure 3.7**, we further show the effect of the IER particles on NO_3^- selectivity at 50 A·m^{-2}.

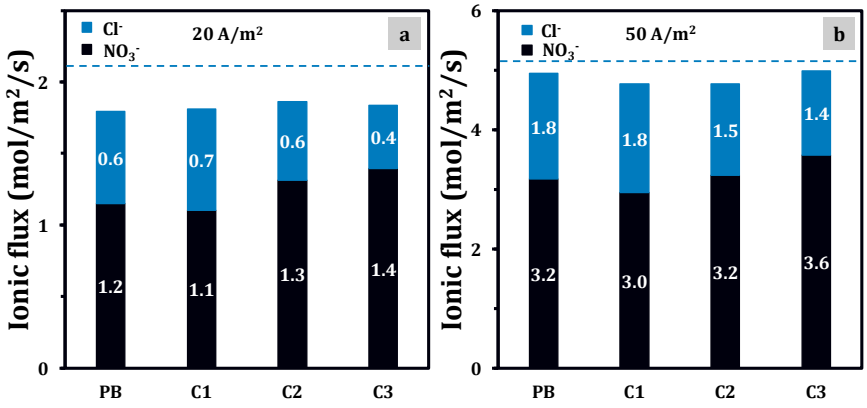

Figure 3.5. Nitrate and chloride flux through fabricated membranes at a) 20 A·m^{-2}, and b) 50 A·m^{-2}. Membranes were tested in solution I (**Table 3.2**), whereby the ionic flux is the average over 5 hours. Dashed lines indicate the expected total ionic flux through the membranes.

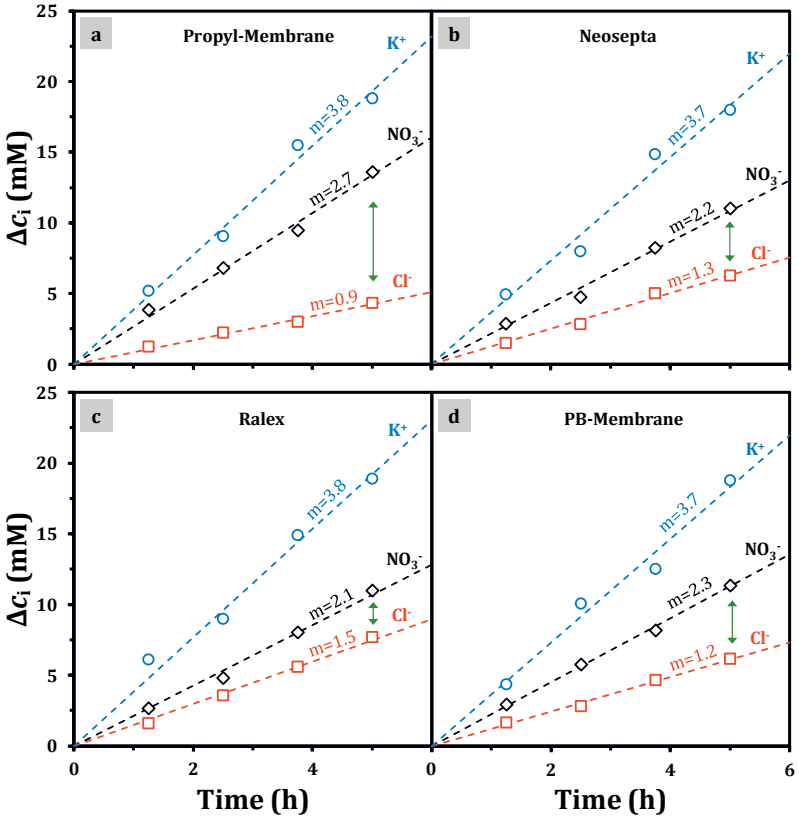

Figure 3.6. Experimental data (symbols) for the changes in bulk ion concentration at 20 A·m^{-2} with a) propyl-membrane; b) Neosepta membrane; c) Ralex membrane; and d) PB membrane. Dashed lines are the linear regression of experimental data. The value of m indicates the slope of dashed lines. Membranes were tested in solution I (**Table 3.2**).

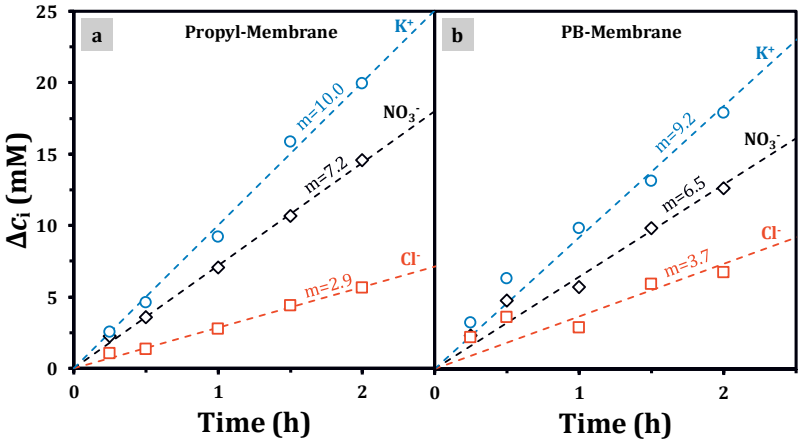

Figure 3.7. Experimental data (symbols) for the changes in bulk ion concentration at 50 A/m² with a) propyl-membrane; and b) PB membrane. Dashed lines are the linear regression of experimental data. The value of m indicates the slope of dashed lines. Membranes were tested in solution I (**Table 3.2**).

3.3.3 Selectivity between anions with different valence and size

In previous sections, we showed that for monovalent ions with similar hydrated size it is possible to report selectivity trends based on hydration energy. In this section, we show that when ions have different valence or size, hydration energy is not sufficient to predict ion selectivity. **Figure 3.8a** shows that overall AEMs are more selective to monovalent (NO_3^- and Cl^-) than to divalent ions (SO_4^{2-}). The low transport of SO_4^{2-} can be explained by i) hydrophobic effects, the membranes allow the preferential transport of ions with low hydration energy, i.e., NO_3^- and Cl^-, and limit the transport of ions with high hydration energy, i.e., SO_4^{2-}, (**Table 3.3**), ii) steric hindrance, related to the large size of SO_4^{2-} (**Table 3.3**), and iii) stronger electrostatic interactions between SO_4^{2-} and ion-exchange sites [103]. In CB-hAEMs with propyl groups and PB-membrane, the flux of monovalent ions is similar, with significantly lower transport of SO_4^{2-} compared to Neosepta and Ralex membranes. The difference in SO_4^{2-} transport between commercial membranes and CB-hAEMs with propyl groups and PB-membranes may be related to variations in the distance between ion-exchange sites, i.e., the transport of SO_4^{2-} requires the presence of two closely-spaced ion-exchange sites [215, 216]. Results in **Figure 3.8b** show that in mixtures of monovalent ions with different hydrated size, the decrease in hydration energy, i.e., $NO_3^- < IO_3^- < Cl^-$ (**Table 3.3**), cannot account for the

observed preferential ion transport, which follows the sequence NO_3^->Cl^->IO_3^-. In this case, the difference in size between IO_3^- and the other anions seems to play a more important role. In addition to the large size of IO_3^-, some studies have reported that this ion behaves as a cation in aqueous solutions [217, 218], which can lead to electrostatic repulsion with the ion-exchange sites. The low selectivity of the AEMs towards IO_3^- was also measured at equilibrium in which on average for CB-hAEMs with propyl groups and PB membranes IO_3^- concentration represents ~ 3% compared to 15% for Cl^- and 82% for NO_3^-, whereas for Neosepta membrane the IO_3^-, Cl^-, NO_3^- concentration are 4%, 20%, and 76%, respectively. Our results show low adsorption and transport of IO_3^-, but they do not allow to make conclusions about whether the observations are related to the large size of these ions or their cation-like behavior.

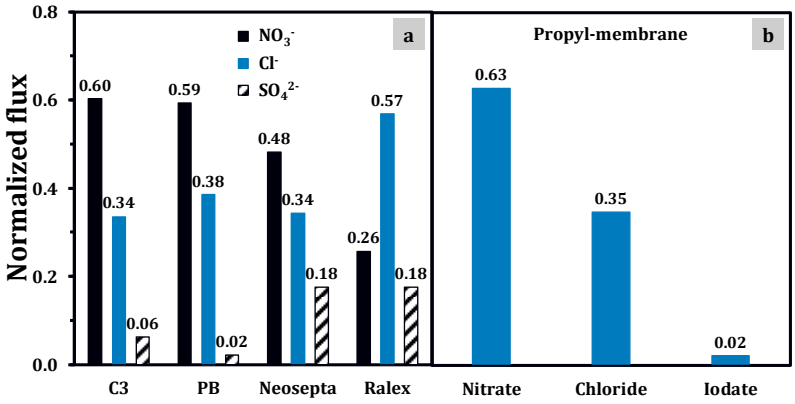

Figure 3.8. a) Normalized flux of ions, i.e., the ratio of the flux of one anion to the total flux of anions, through propyl-and PB-membrane as well as commercial membranes in solution II, b) normalized flux through propyl-membrane in solution III. Experiments conducted at 20 A·m^{-2}

3.4 Conclusions

Heterogeneous anion-exchange membranes (CB-hAEMs) were fabricated with ion-exchange resins with different alkyl groups and a polymeric binder with charged functional groups. We showed that nitrate selectivity in CB-hAEMs correlates with the hydrophobicity of the alkyl groups in the membrane. CB-hAEM with the longest alkyl group (propyl-membrane) showed high nitrate selectivity under dynamic conditions, about two times higher than commercial AEM.

Selectivity is the consequence of the interplay between different factors among whereby the hydration energy is a dominant factor. We observed that for monovalent ions with the same size such as nitrate and chloride, the selectivity is linked to the difference in hydration energy. In solutions containing ions with different size and valence it is not possible to relate ion selectivity to one single parameter. Ion selectivity is the combination of electrostatic interactions between ions and ion-exchange sites, and steric hindrance due to the size of the ions and structure of the ion-exchange sites.

The use of a charged polymeric binder enables the fabrication of selective membranes with low electrical resistance, comparable to commercially available non-selective membranes. These membranes can potentially be used in electrochemical desalination technologies such as electrodialysis and membrane capacitive deionization to obtain selective removal of ions.

Chapter 4

Experimental and theoretical results point towards strategies to increase ion selectivity in electrodialysis.

This chapter will be submitted as:
T.M. Mubita, S. Porada, P.M. Biesheuvel, A. van der Wal, J.E. Dykstra, Experimental and theoretical results point towards strategies to increase ion selectivity in electrodialysis.

Abstract

We developed a dynamic theory based on the Nernst-Planck equation to describe the transport of ions across ion-exchange membranes (IEMs) in multi-ionic electrolytes. In the theory, we introduced a membrane parameter, the chemical affinity, to account for the preference of membrane materials towards specific ionic species. The value of the chemical affinity was determined from adsorption experiments with anion-exchange membranes (AEMs) immersed in an electrolyte with mixtures of ions, specifically nitrate and chloride ions. We found that in equilibrium nitrate ions are preferentially adsorbed by the AEMs. We validate the dynamic theory with data of batch-mode electrodialysis experiments, and we find that the transport of nitrate and chloride is well described for different IEMs. Results indicate that strategies to increase nitrate selectivity in AEMs are to i) increase the chemical affinity, ii) increase the membrane thickness, or iii) decrease the membrane charge density.

4.1 Introduction

Ion-exchange membranes (IEMs) are the key component of technologies such as electrodialysis (ED) and membrane capacitive deionization (MCDI), which allow the separation of ions from saline streams [15, 219-221]. In the present study, we focus on ion separation using ED. Main applications of ED technology require the removal of a large part of the total salt from the water stream. However, there are specific applications that require separation between ions with the same charge sign but different valence, e.g., separation of sodium (Na^+) and calcium (Ca^{2+}) in water softening; or with the same valence, e.g., nitrate (NO_3^-) removal from groundwater, which also contains chloride (Cl^-). In this chapter, we focus on this last example, the separation of ions with the same sign and the same valence.

In ED, the selective separation of ions with the same charge sign is mostly determined by the structure of the IEMs, e.g., the density of ion-exchange sites and the pore structure of the membrane matrix, and physicochemical properties of the counterions, e.g., hydrated size and hydration energy [97, 104, 107, 222-224]. Additionally, operational conditions, such as applied current and volumetric flow rate, and properties of the water stream, such as ion concentration and composition, also affect the separation of counterions [106, 166, 182].

Experimental and theoretical studies have been carried out to measure ion selectivity in IEMs and to understand the mechanisms underlying ion transport through the membranes [124, 204, 225, 226]. Theoretical models often use the Nernst–Planck equation to describe the transport of ions subject to diffusional and migrational forces. These transport models also include a set of parameters related to membrane characteristics (porosity, charge density), and to other factors, such as ion partitioning at the membrane-solution interface, and ion diffusion coefficients [227-229].

Several studies have focused on describing the transport of counterions in multicomponent solutions. The competitive transport between mono- and divalent ions is often described by considering ion transport in the diffusion layers adjacent to the IEMs and the influence of the applied current density [230, 231]. Kim et al. [231]

reported that at high current densities the polarization of the boundary layer favors the transport of monovalent ions, whereas at low current densities the divalent ions are preferentially transported. Galama et al. [105] studied the influence of divalent ions present in seawater on the electrochemical properties of anion- and cation-exchange membranes under low current conditions. This study presented a transport theory in which ion selectivity is introduced as the result of the differences in diffusion coefficients between mono- and divalent ions inside the membrane.

Interestingly, only a limited number of studies focus on numerical models to describe preferential transport of ions with equal valence [232, 233]. These transport models use the modified form of the Boltzmann equation, which describes the equilibrium distribution of ions in the membranes by adding different hydration terms for the ions as a function of their size. Using this approach, for instance, Yang and Pintauro [233] described the preferential adsorption and transport of alkali-metal cations in multicomponent solutions in a dialysis system.

In the present work, we introduce a theoretical model to describe the transport of monovalent ions through IEMs. In this theory, the ion concentration at the membrane-solution interface is described using a modified Boltzmann equation. We introduce in this equation a term that accounts for the affinity of the membrane towards an ion. We use this approach to describe the transport of Cl^- and NO_3^- across different IEMs, i.e., commercial membranes (homogenous and heterogeneous) and a home-made heterogeneous anion-exchange membrane (CB-hAEMs). In **Chapter 3**, we reported the fabrication and characterization of the CB-hAEMs, which showed an increased selectivity towards NO_3^- over Cl^-. The present study builds upon our previous work and focuses on understanding the selective NO_3^- transport in an ED system. We provide experimental and theoretical data that give insight into the selective separation of monovalent ions in batch ED experiments. In addition, we analyze the results of the theoretical calculations to develop strategies for enhancing the selectivity for NO_3^-. The strategies consist of modifying membrane properties such as the magnitude of the affinity term, membrane thickness, and membrane charge density.

4.2 Theory. Selective ion transport in ion-exchange membranes

Theory presented in this section considers the dynamic transport of ions in an ED system. The ED system is operated in batch-mode and consists of i) the ED stack with multiple cell pairs. Each cell pair includes one anion-exchange membrane (AEM), one cation-exchange membrane (CEM), and the spacer channels: diluate and concentrate, and ii) two containers with the diluate and concentrate solutions. These solutions are kept separate from one another and are continuously recirculated between the containers and the ED stack (**Figure 4.1**).

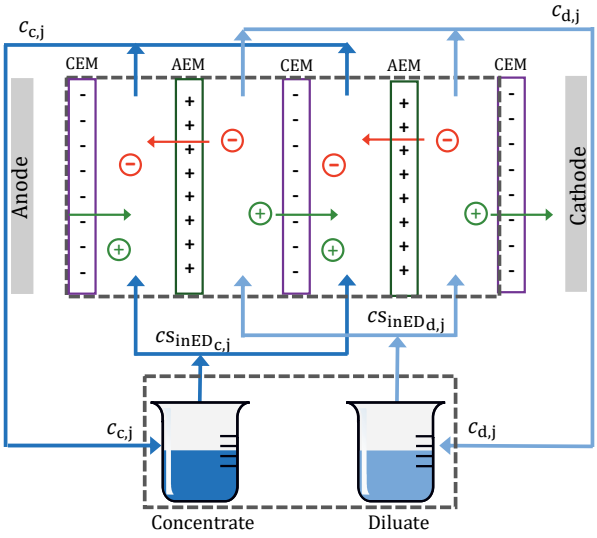

Figure 4.1. Schematic representation of an electrodialysis system operated in batch-mode. Dashed grey lines illustrate the computational domain used to set up the mass balances.

First, we describe the ionic flux (J in mol/m^2/s) through non-ideal IEMs, i.e., membranes that besides the transport of counterions allow the transport of co-ions. We assume that diffusion and electromigration only occur in the direction perpendicular to the membrane surface (x-direction), and we neglect water transport through the IEMs. Thus, we use a version of the Nernst-Planck equation that does not describe advective transport, which is given by [234]

$$J_{\mathrm{j}} = -\mathrm{D}_{\mathrm{m,j}}\left(\frac{\partial \mathrm{c}_{\mathrm{m,j}}}{\partial x} + \mathrm{z}_{\mathrm{j}}\mathrm{c}_{\mathrm{m,j}}\frac{\partial \phi}{\partial x}\right) \qquad \text{Eq. 4.1}$$

where subscript 'j' refers to the ionic species, c_{m} is the concentration per volume of solution in the membrane (mol/m^3), x the position inside the membrane, z the ion valence, ϕ the dimensionless electrical potential, and $\mathrm{D_m}$ the diffusion coefficient in the membrane (m^2/s), which is assumed to be lower than the ion diffusion coefficient in free solution, i.e., $\mathrm{D_{m,j}} = \mathrm{D_{\infty,j}}/\mathrm{f_{red,j}}$, where $\mathrm{f_{red,j}}$ is empirically obtained from fitting the model to data. We consider that the values of $\mathrm{D_m}$ are different between the different counterions, and will also be different for the co-ion.

At each position in the membrane, mass conservation of the ions at any time, t, is given by

$$\frac{\partial c_{\mathrm{m,j}}}{\partial t} = -\frac{\partial J_{\mathrm{j}}}{\partial x}. \qquad \text{Eq. 4.2}$$

Equation 4.2 is evaluated for each ionic species present, except for one, which can be arbitrarily chosen. To evaluate the concentration of the remaining species, we use the electroneutrality condition, which holds at each position in the membrane

$$\rho_{\mathrm{m}} = \sum_{\mathrm{j}} z_{\mathrm{j}} c_{\mathrm{m,j}} + \omega X = 0 \qquad \text{Eq. 4.3}$$

where ρ_{m} is the local ionic charge density, ω is the sign of the membrane charge, i.e., ω =+1 for the AEM and ω =-1 for the CEM, and X is the charge density of the membrane defined per unit volume of solution in the membrane.

The local charge density is invariant in time and space

$$\frac{\partial \rho_{\mathrm{m}}}{\partial t} = -\frac{\partial}{\partial x}\sum_{\mathrm{j}} \mathrm{z}_{\mathrm{j}} J_{\mathrm{j}} = 0. \qquad \text{Eq. 4.4}$$

The current density (I, in A/m^2) is independent of x, i.e., it has the same value at each position in the membranes and the spacer channels, and is defined by

$$I = \mathrm{F} \cdot \sum_{\mathrm{j}} z_{\mathrm{j}} J_{\mathrm{j}} \qquad \text{Eq. 4.5}$$

where F is Faraday's constant (96485 C/mol).

The ion concentration inside the membrane at the solution/membrane interface ($c_{\mathrm{sc/m}}$) is often described by the Boltzmann equation [227, 235, 236]. In the present work, we modify this equation and include a term (μ) to account for the ability of the IEMs to preferentially adsorb one counterion over another, from multi-ionic solutions. Thus, the ion concentration inside the membrane at the solution/membrane interface is given by

$$c_{\mathrm{sc/m,j}} = c_{\mathrm{sc,j}} \cdot \exp\left(-z_{\mathrm{j}} \cdot \Delta\phi_{\mathrm{D,sc/m}} + \mu_{\mathrm{j}}\right) \qquad \text{Eq. 4.6}$$

where subscript 'sc' refers to either the concentrate or diluate spacer channel, subscript 'm' refers to AEM or CEM, and $\Delta\phi_{\mathrm{D,sc/m}}$ is the Donnan potential at the specific interface.

Next, we set up expressions for the ion concentration in the spacer channels, $c_{\mathrm{sc,j}}$. In the spacer channels, we assume ideally-stirred volumes, and hence ion concentration invariant in the x-direction (from membrane to membrane). We calculate ion concentration at the entrance ($c_{s_{\mathrm{inED_j}}}$) and the exit ($c_{\mathrm{d,j}}$) of each spacer channel, i.e., along the membranes in the y-direction. The overall mass balance relates the ion concentration to the flux of ions at the solution/membrane interface. In the diluate and concentrate channels, the concentration is evaluated for each ionic species, except for one. Therefore, we set up the balance for the anions, which is given by

$$\frac{\partial c_{\mathrm{d,j}}}{\partial \mathrm{t}} = \frac{\Phi_{\mathrm{d}}}{\mathrm{V_{sc,d}}}\left(c_{s_{\mathrm{inED}_{\mathrm{d,j}}}} - c_{\mathrm{d,j}}\right) + \frac{1}{\delta_{\mathrm{d}}}\left(J_{\mathrm{j,d/AEM}} - J_{\mathrm{j,d/CEM}}\right) \qquad \text{Eq. 4.7}$$

$$\frac{\partial c_{\mathrm{c,j}}}{\partial \mathrm{t}} = \frac{\Phi_{\mathrm{c}}}{\mathrm{V_{sc,c}}}\left(c_{s_{\mathrm{inED}_{\mathrm{c,j}}}} - c_{\mathrm{c,j}}\right) + \frac{1}{\delta_{\mathrm{c}}}\left(J_{\mathrm{j,c/CEM}} - J_{\mathrm{j,c/AEM}}\right) \qquad \text{Eq. 4.8}$$

where subscripts 'd' and 'c' refer to diluate and concentrate, respectively; Φ_{d} and Φ_{c} are the flow rate through each spacer channel ($\mathrm{m^3/s}$), $\mathrm{V_{sc}}$ is the volume of the spacer channel ($\mathrm{m^3}$), $J_{\mathrm{j,d/AEM}}$, $J_{\mathrm{j,d/CEM}}$, $J_{\mathrm{j,c/AEM}}$, and $J_{\mathrm{j,c/CEM}}$ are the ionic fluxes inside the membrane at the solution/membrane interface, δ is the thickness of the spacer channel (m), and $c_{s_{\mathrm{inED}}}$ is the ion concentration in the solution that enters the spacer channel

(mol/m^3). Here, we assume the porosity of each spacer channel to be unity, i.e., we neglect the presence of a spacer mesh.

The electroneutrality condition is also maintained in each compartment

$$\sum_{\mathrm{j}} \mathrm{z_j} c_{\mathrm{sc,j}} = 0. \qquad \text{Eq. 4.9}$$

Besides a mass balance for each separate (set of) spacer channels (i.e., either c or d), we also have two solution containers. What exits the cells goes to the containers, is mixed there, and this mixture is fed back to the cells. The mass balance for the diluate and concentrate containers is given by

$$\mathrm{V_c} \frac{\partial c_{s_{\mathrm{inED_{sc,j}}}}}{\partial t} = \Phi \left(c_{\mathrm{sc,j}} - c_{s_{\mathrm{inED_{sc,j}}}} \right) \qquad \text{Eq. 4.10}$$

where $\mathrm{V_c}$ is the container's volume (m^3) and Φ is the flow rate (m^3/s) at the inlet and outlet of the ED stack.

Finally, the preferential transport of ions is quantified by a time-dependent separation factor (β) given by

$$\beta_{\mathrm{i/j}} = \frac{J_{\mathrm{i,c/AEM}}}{J_{\mathrm{j,c/AEM}}} \cdot \frac{c_{\mathrm{d,j}}}{c_{\mathrm{d,i}}}. \qquad \text{Eq. 4.11}$$

The above equations (Eq. 4.1-Eq. 4.11) result in a model that can be solved for an ED system containing a mixture of monovalent ions. We use these equations to describe the selective transport of ions through three different IEMs, i.e., two commercial IEMs (one homogenous and one heterogeneous), and newly-designed heterogeneous anion-exchange membranes (CB-hAEMs), see **Chapter 3**. **Tables 4.1** and **4.2** summarize the parameters used in the model for a system with KCl and KNO_3 and also provides key properties of the ion-exchange membranes.

Table 4.1. Parameters used in the ED model to describe ion selectivity in IEMs.

Operational			
I	Current density	20	A/m^2
Φ_{sc}	Flow rate per spacer channel	5	mL/min
N_{Cell}	Number of cell pairs	4	
V_C	Volume of the solution container		
	Diluate	75	mL
	Concentrate	72	mL
Spacer channels (diluate and concentrate)			
δ	Spacer channel thickness	450	µm
V_{sc}	Volume of one spacer channel	0.27	mL
Anion Exchange Membranes			
$f_{red,j}$	Reduction factor for ion diffusion coefficient in AEM		
	Potassium	140	
	Chloride	140	
	Nitrate	115	
Cation Exchange Membranes			
$f_{red,j}$	Reduction factor for ion diffusion coefficient in CEM	10	
Diffusion coefficient of ions in free solution ($D_{\infty,j}$)			
D_{∞,K^+}	Potassium	$1.96 \cdot 10^{-9}$	m^2/s
D_{∞,Cl^-}	Chloride	$2.03 \cdot 10^{-9}$	m^2/s
D_{∞,NO_3^-}	Nitrate	$1.90 \cdot 10^{-9}$	m^2/s

Table 4.2. Properties of the membranes used in the present study.

	Charge density *X* (M)*	Thickness δ_m (μm)	Derived affinity term, $\mu_{NO_3^-}$
AEM			
CB-hAEM	4.52	135	1.83
Commercial homogeneous (C.HM, Neosepta, AMX)	7.56	150	1.35
Commercial heterogeneous (C.HT, Ralex, AMH-PES)	4.75	590	0.77
CEM			
Commercial homogeneous (Neosepta, CMX)	8.70	150	-
Commercial heterogeneous (Ralex, CMH-PES)	5.75	590	-

* Charge density measured experimentally.

4.3 Experimental

Adsorption experiments (***section 4.3.1***), as well as electrodialysis experiments (***section 4.3.2***), were carried out with three different anion exchange membranes (AEMs): i) the commercial homogeneous membrane Neosepta AMX (ASTOM Corporation, Tokyo, Japan), ii) the commercial heterogeneous membrane Ralex AMH-PES (Mega a.s., Czech Republic), and iii) a home-made heterogeneous membrane, which we refer to as CB-hAEM. The fabrication and characterization of CB-hAEM are described in **Chapter 3**.

4.3.1 Adsorption equilibrium experiments

To determine the chemical affinity of the IEMs for NO_3^- ($\mu_{NO_3^-}$), we measured the concentration of anions in IEMs in an adsorption experiment. First, membrane pieces of 12 cm^2 were immersed for 24 h in 100 mL of aqueous solution (solution A) containing salt mixtures with different concentration ratio of Cl^- to NO_3^- (total ionic strength 100 mM). Then, the membranes were immersed for a short time, around 2 seconds, in deionized water to remove the salt solution from the membrane surface. Subsequently,

the membranes were transferred into an exchange solution (100 mL, 0.25 M Na_2SO_4) for 24 h. After this period, the ion concentrations in the exchange solution were measured by ion chromatography (IC). To ensure a complete release of Cl^- and NO_3^-, the membranes were once more placed in a smaller volume of fresh exchange solution for 24 h. The Cl^- and NO_3^- concentrations in the second exchange solution were below the detection limit, implying that most of $Cl^-$and NO_3^- was released into the first exchange solution. The NO_3^- to Cl^- adsorption selectivity (S) of the IEMs was calculated by

$$S_{NO_3^-/Cl^-} = \left(\frac{c_{NO_3^-}}{c_{Cl^-}}\right)_{\text{exchange solution}} \cdot \left(\frac{c_{Cl^-}}{c_{NO_3^-}}\right)_{\text{solution A,after 24 h}} . \quad \text{Eq. 4.12}$$

4.3.2 Electrodialysis experiments

The ED experiments were conducted using a micro-ED stack (ED 08002, PCCell GmbH, Germany) consisting of two electrode compartments, one with a Pt/Ir coated titanium anode and the other with a stainless-steel cathode, and four cell pairs. Each cell pair consists of a CEM, a diluate channel, an AEM, and a concentrate channel. The IEMs (6 cm^2 of area available for ion transport) were separated by a silicone/polypropylene spacer (thickness 450 μm). The stack is comprised of nine IEMs in total: 4 AEMs and 5 CEMs. Two of the CEM (PC SC for ED 08002) were used to separate the electrode compartments from the cell pairs. The ED system was operated in batch-mode. The initial salt concentration in the diluate and concentrate containers was 50 mM KCl + 50 mM KNO_3, and in the electrode rinse solution container was 0.1 M Na_2SO_4.. Samples were taken from the diluate and concentrate containers every 30 minutes to measure the ionic concentration by IC.

The separation factor (β) is defined as

$$\beta_{i/j} = \frac{\Delta c_{i,c}}{\Delta c_{j,c}} \cdot \frac{c_{d,j}}{c_{d,i}} \quad \text{Eq. 4.13}$$

$$\Delta c_i = c_{i,t} - c_{i,t-1}$$

where subscript *t* indicates the sampling time.

Additionally, the current efficiency (λ) is quantified by

$$\lambda = \frac{(J_i + J_j) \cdot F}{I} \cdot 100\% \qquad \text{Eq. 4.14}$$

4.4 Results and discussion

4.4.1 Adsorption equilibrium experiments

The concentrations of NO_3^- and Cl^- in the AEMs were determined through adsorption experiments (***section 4.3.1***). Within the membranes, the total counterion concentration (Cl^- + NO_3^-) is approximately equal to the concentration of the ion-exchange sites in the membranes, i.e., the charge density (X) (**Figure 4.2a**). The concentrations of co-ions in the membranes was below the detection limit of the IC equipment. These results show that highly charged IEMs—such as the membranes used in the present study—adsorb high concentrations of counterions that balance the functional groups in the membranes [237]. Interestingly, the three studied AEMs show higher adsorption of NO_3^- over Cl^- regardless of the initial NO_3^-:Cl^- concentration ratio, which translates into adsorption selectivity $S_{NO_3^-/Cl^-} > 1$ (**Figure 4.2b**). However, the adsorption selectivity is markedly different among the membranes: the CB-hAEM is more selective for NO_3^- than the C.HM and C.HT membranes.

We measured the adsorption of NO_3^- and Cl^-in AEMs to determine the value of the chemical affinity (μ), which is introduced in the theory section as a parameter to quantify the preferential adsorption of ions in the IEMs. The affinity term is only calculated for NO_3^- ($\mu_{NO_3^-}$), and hence for the other ions, we set μ to zero. We used the modified Boltzmann equation (see Eq. 4.6) to calculate the ion concentration in the membranes. This equation describes the ion distribution at the membrane/solution interface by taking into account the contributions of ion charge, concentration, and chemical affinity. The value of $\mu_{NO_3^-}$ is derived by fitting theory to experimental data (the best-fit values are reported in **Table 4.2**). Experimental and theoretical data of ion transport across the AEMs are presented in the next sections.

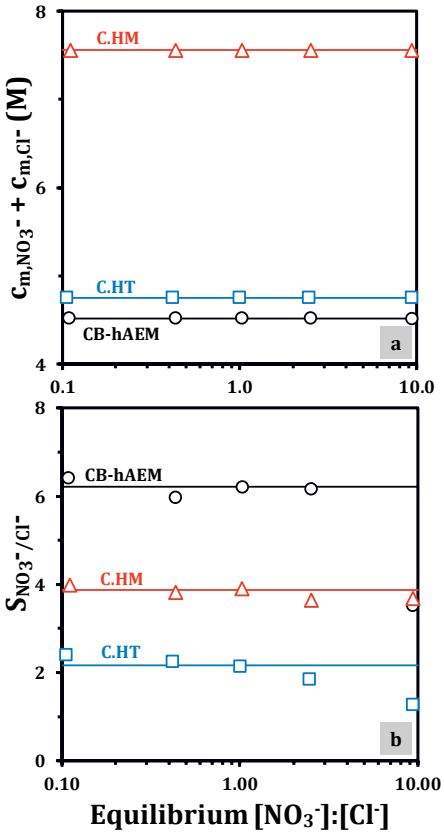

Figure 4.2. Experimental results (symbols) of adsorption experiments. The membranes were immersed in electrolyte solutions with different NO_3^- and Cl^- concentrations (total ionic strength 100 mM). The x-axis gives the equilibrium NO_3^- : Cl^- concentration ratio in solution. a) Total anion concentration in the AEMs ($c_{m,NO_3^-} + c_{m,Cl^-}$). Lines represent the charge density (X) in the membranes (**Table 4.2**) ; b) Nitrate selectivity ($S_{NO_3^-/Cl^-}$, Eq. 4.12) in the AEMs as a function of the ion concentration ratio in the bulk solution. Lines are based on theory.

4.4.2 Experiments and theory of ion transport in batch-mode ED

In this section, we report experimental data and output of theoretical calculations of the competitive transport of Cl^- and NO_3^- through three different AEMs in ED. In batch-mode ED experiments, the concentrations of Cl^- and NO_3^- continuously decrease in the diluate container and increase in the concentrate container (**Figure 4.3a** and **Figure S.I. 4.2**). As shown in **Figure 4.3b-d,** $\beta_{NO_3^-/Cl^-}$ is higher in the CB-hAEM than in C.HM and C.HT. Furthermore, **Figure 4.3** shows that the theory, which includes the values of $\mu_{NO_3^-}$

obtained by fitting the equilibrium adsorption data (**Figure 4.2** and **Figure S.I. 4.1**) closely describes measured ion concentrations and $\beta_{NO_3^-/Cl^-}$. **Figure 4.3** also shows that, in batch-mode ED, $\beta_{NO_3^-/Cl^-}$, and hence the NO_3^- selectivity decreases over time as a result of the continuously changing ion concentrations in the solution containers. Therefore, it is difficult to report the selectivity of the membrane material based on a single value of $\beta_{NO_3^-/Cl^-}$ that is independent of the solution composition.

In general, the flux of NO_3^- is markedly higher than that of Cl^- for all membranes(**Figure 4.4a**). Nevertheless, the magnitude of the flux in each membrane is different. Nitrate flux is higher in CB-hAEM compare to C.HT membranes, even though these two membranes have similarities in their structure, which are related to their heterogeneous nature [186, 224]. On the other hand, the NO_3^- flux through CB-hAEM is equal to that of the C.HM membrane. However, CB-hAEM shows higher selectivity toward NO_3^- because of the lower Cl^- flux in comparison with C.HM membranes. **Figure 4.4a** also shows the current efficiency (λ) in the ED system with different AEMs.

Overall, results show that AEMs are selective to NO_3^-, but this selectivity varies depending on desalination time and the type of membrane. In further studies with CB-hAEM, we found that NO_3^- selectivity also depends on membrane thickness. Interestingly, results show that an increase in membrane thickness increases $\beta_{NO_3^-/Cl^-}$ (**Figure 4.4b**). In the next section, we analyze how the transport of anions is affected by the membrane thickness and other membrane parameters.

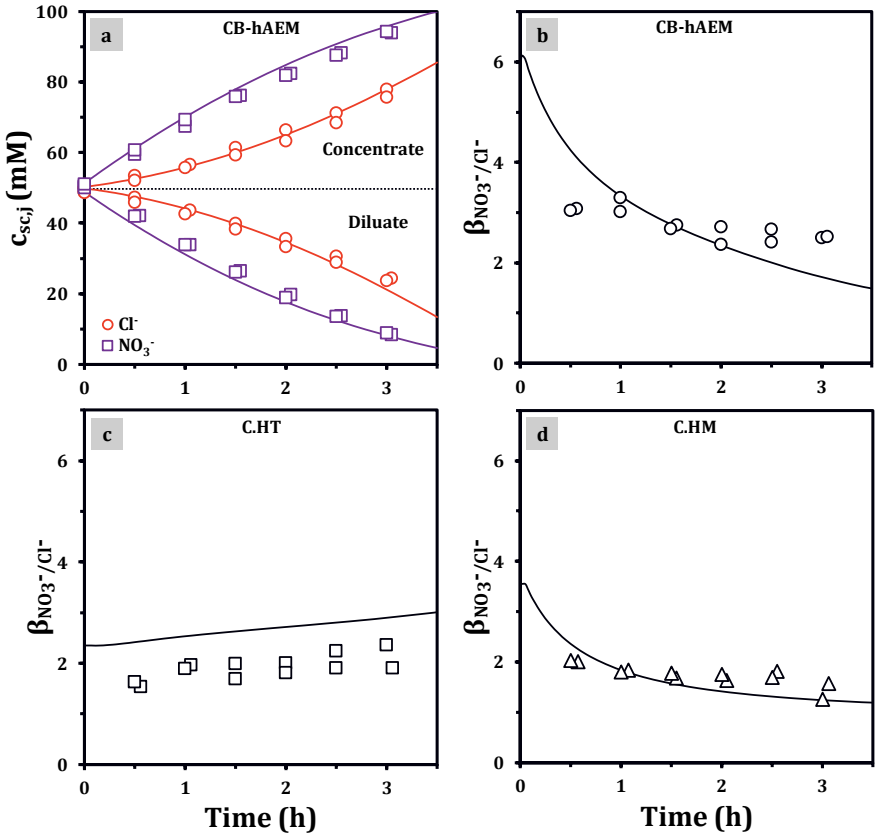

Figure 4.3. Experimental data (symbols) and theory (lines) as a function of time for: a) Ion concentration in the solution containers, i.e., diluate and concentrate, for the ED system with CB-hAEM; b-d) separation factor ($\beta_{NO_3^-/Cl^-}$) obtained with different AEMs. Duplicate symbols represent two independent sets of experiments.

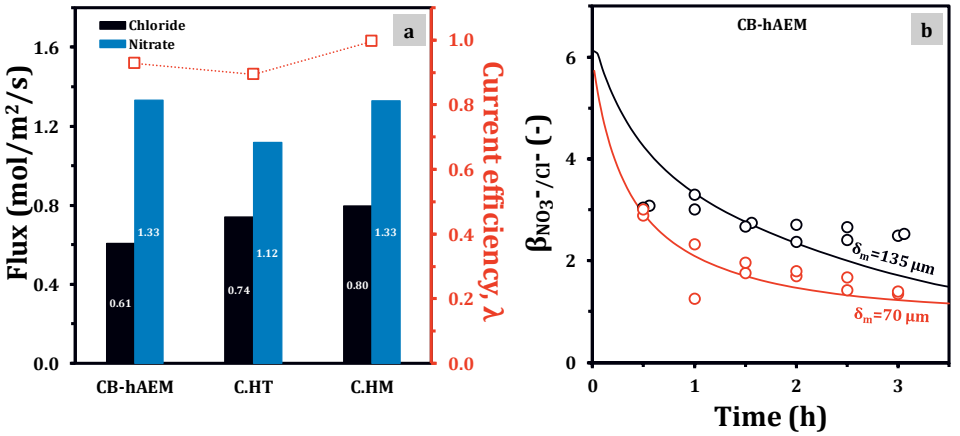

Figure 4.4. a) Average ionic flux and current efficiency (λ) through AEMs; b) separation factor ($\beta_{NO_3^-/Cl^-}$) for CB-hAEMs with different membrane thickness (δ_m) as a function of time.

4.4.3 Theoretical predictions of ion transport in continuous ED

In this section, we present theoretical results of the transport of ions through the home-made membrane, CB-hAEM, in continuous ED, instead of batch ED. In continuous ED, the system is in steady-state: the ion concentrations are not changing over time, which allows us to better understand and predict how the selective transport of NO_3^- through IEMs is affected by membrane properties. Our study of preferential ion transport in continuous ED is also relevant because this operational mode is often used in large-scale ED desalination plants. In a continuous process, the aim is to achieve the desired concentration of the diluate stream within a single pass, depending on, among others, operational parameters such as the applied current and flow rate, and the dimensions of the system

To analyze ion transport in continuous ED, we include certain modifications in the theory presented in ***section 4.2***. Consequently, the theory does not include a mass balance for the solution containers (Eq. 4.10), and hence $cs_{\mathrm{inED}_{sc,j}}$ in Eq. 4.7 does not change in time and is equal to the ion concentration in the feed solution. We consider an ED system with 10 cell pairs in which the membranes have an active area of 100 cm^2. The flow rate per spacer channels is set to 1.5 mL/min. We systematically analyze the effect of parameters such as $\mu_{NO_3^-}$ and D_m on the ion concentration profile in the

membrane. In addition, we also study the effect of thickness and charge density on $\beta_{NO_3^-/Cl^-}$.

- ***Effect of the chemical affinity and the diffusion coefficients on the concentration profiles across the membrane***

This section shows the analysis of the effect of $\mu_{NO_3^-}$ and of D_m on the concentration profiles of ions in the membranes based on three different scenarios. In the first scenario, we set $\mu_{NO_3^-}$=0 and assume that the value of D_m is for both anions the same. In this scenario, there is no preferential transport between NO_3^- and Cl^- across the membrane, and hence $\beta_{NO_3^-/Cl^-} = 1$ and the concentration profile of the anions are identical (**Figures 4.5a-b**). In the second scenario, we set $\mu_{NO_3^-}$=0 and assume that NO_3^- and Cl^- have different D_m. In this case, we observe low membrane selectivity ($\beta \cong 1.1$) towards the ion with higher D_m (data not shown). In addition, results show that the concentration profiles of anions are in opposite directions (**Figure 4.5a-b**). For the ion with the lowest D_m, the concentration profile inside the membrane is in the opposite direction as one would intuitively predict based on the concentrations in the spacer channels. The phenomenon in which one ion diffuses across the membrane in the direction of increasing concentration or against the external concentration gradient is in some work referred to as uphill diffusion [238-240]. Uphill diffusion is the result of the requirement of electroneutrality in the membrane to avoid charge imbalance. Our theory predicts uphill diffusion of Cl^-, i.e., the Cl^- concentration at the interface with the concentrate compartment is lower than that at the interface with the diluate compartment, when $D_{m,NO_3^-} > D_{m,Cl^-}$ (**Figure 4.5a**). The concentration profile of NO_3^- is opposite to that of Cl^- (**Figure 4.5b**). Other studies have reported uphill diffusion in different multicomponent systems with ion-exchange materials, e.g., membranes, resins, and have also used the Nernst-Plank equation to numerically describe this phenomenon [239-241].

In the last scenario, we set $\mu_{NO_3^-}$>0 and assume that the anions have different D_m. The theory predicts the affinity of the AEM for NO_3^- and the membrane concentration profiles of NO_3^- and Cl^- are opposite regardless of their values of D_m. With an increase

in $\mu_{NO_3^-}$, the NO_3^- concentration in the membrane increases while the Cl^- concentration decreases (**Figure 4.5c-d**). In summary, NO_3^- and Cl^- have membrane concentration profiles opposite when their D_m is different or when the membrane shows a higher affinity towards either ion.

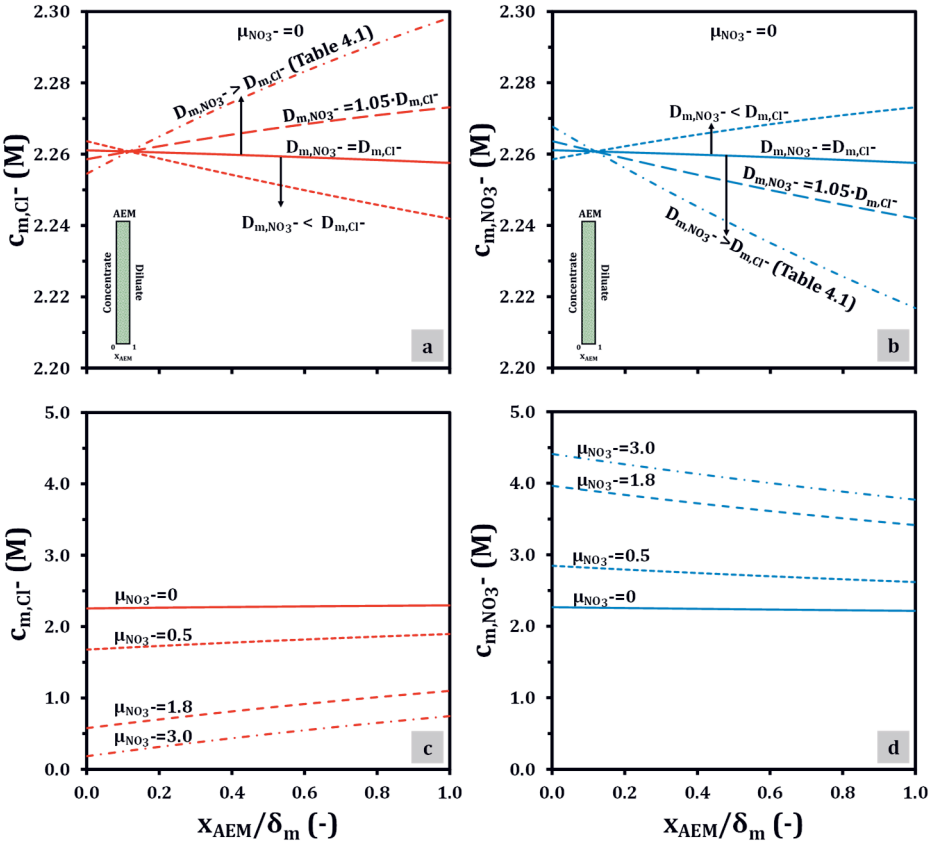

Figure 4.5. Theoretical results for concentration profile of Cl^- and NO_3^- across the CB-hAEM: a-b) concentration obtained with different values of ion diffusion coefficients (D_m) when $\mu_{NO_3^-} = 0$; c-d) concentration obtained with different values of $\mu_{NO_3^-}$. x_{AEM} is the x-direction and δ_m is the thickness of the membrane.

- ***Effect of membrane parameters on ion selectivity***

We also evaluated the effect of membrane thickness (δ_m), charge density (X), and magnitude of $\mu_{NO_3^-}$ on NO_3^- selectivity in CB-hAEM (**Figure 4.6**). Firstly, results in **Figure 4.6b** show that increasing δ_m leads to an increase in the NO_3^- concentration and a decrease in the Cl^- concentration in the concentrate compartment. The opposite trend is observed in the diluate compartment.

On the other hand, we observe that an increase or decrease in δ_m have a pronounced effect on the anion concentration in the membrane at the membrane interface with the diluate compartment (**Figure 4.7**). At the interface with the concentrate compartment, the NO_3^- and Cl^- concentration are not significantly affected by δ_m (**Figure 4.7**). To understand the relationship between δ_m and the ion concentration at the membrane interfaces, we evaluate the transport of anions across the CB-hAEM in terms of total flux and the contribution of diffusion, i.e., flux of ions due to concentration gradients, and migration, i.e., flux of ions due to the influence of electrical potential, (**Figure S.I. 4.3**). For NO_3^- , the diffusion and migration fluxes at either interface do not markedly change with increasing δ_m (**Figure S.I. 4.3a-b**). However, δ_m has a more dominant effect on the Cl^- fluxes, especially at the membrane-diluate interface. Results in **Figure S.I. 4.3c** show that increasing δ_m causes a decrease in Cl^- diffusion, while its migration flux increases across the membrane-diluate interface.

Secondly, **Figure 4.6c-d** show the effect of X on $\beta_{NO_3^-/Cl^-}$ and of the anion concentration in the spacer channels, when δ_m is kept constant (135 μm). Overall**,** increasing X in the membrane decreases selectivity towards NO_3^- (**Figure 4.6c**). The change in X has a more pronounced effect on the Cl^- concentration than on the NO_3^- concentration in the spacer channels (**Figure 4.6d**). When we analyze the contribution of diffusion and migration to the total flux of Cl^- (**Figure S.I. 4.4c-d**), we observe that diffusion increases with increasing X, whereas migration decreases. Interestingly, for highly charged membranes (above 4.5 M) diffusion becomes the dominant contributor to Cl^- transport. Thirdly, increased selectivity towards NO_3^- is observed as $\mu_{NO_3^-}$ increases (**Figure 4.6e**)**.**

Overall, our results show that NO_3^- selectivity can be enhanced when thick or low charge density AEMs are used. These results contrast with the commonly accepted view of using membranes with reduced membrane thickness [242] and increased charge density to optimize ED performance. This view is mainly based on the effect that the aforementioned membrane properties have on electrical resistance and permselectivity, which in turn affect the energy consumption of the ED system. However, selectivity between counterions is often not considered when analyzing membrane properties and their impact on ED operation. The effect of these membrane properties in systems with multiple salts was not investigated before, probably due to limitations on how to account for the affinity of the IEMs towards certain counterions, a topic we resolved in the present work.

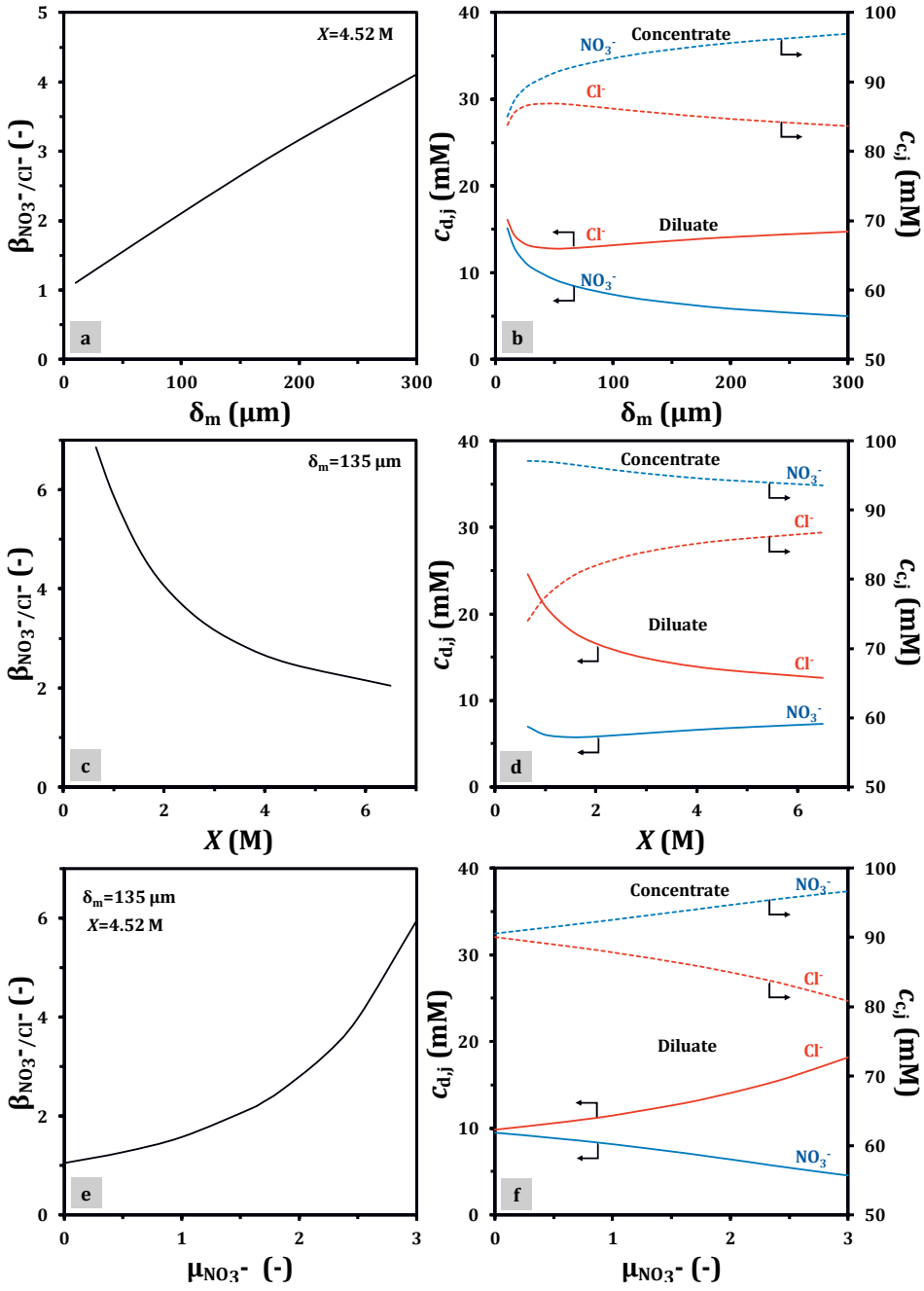

Figure 4.6. Theoretical results for: a, c, e) Separation factor ($\beta_{NO_3^-/Cl^-}$), and b, d, f) concentration of anions in the spacer channels as a function of the membrane thickness (δ_m), charge density (X), and the affinity term ($\mu_{NO_3^-}$).

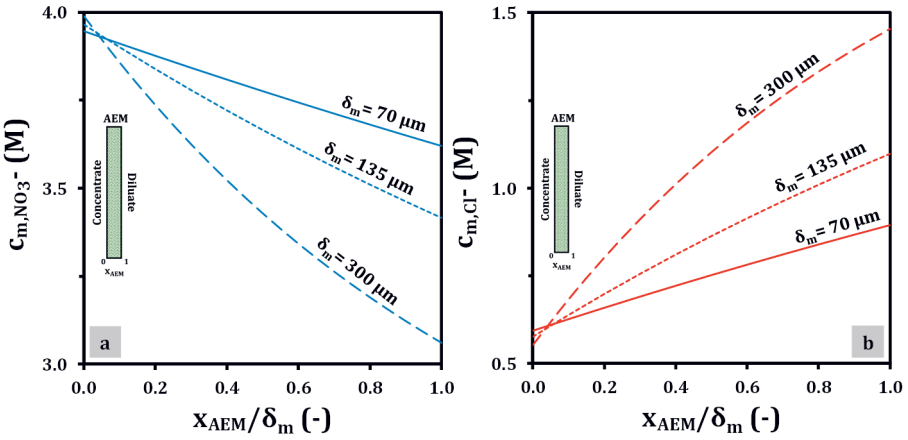

Figure 4.7. Theoretical results for concentration profiles of a) nitrate and b) chloride across CB-hAEM obtained with different membrane thickness (δ_m). x_{AEM} is x-direction and δ_m is the thickness of the membrane.

4.5 Conclusions

We used a theoretical model to describe the transport of monovalent anions, i.e., chloride and nitrate, through AEMs, and we described the nitrate selectivity observed in batch-mode ED experiments. In our theory, we introduced an affinity term to describe the preferential adsorption of specific ions by the membrane material. In this work, the affinity term is not related to a particular interaction (chemical or physical) between counterions and the AEMs, but treated as a general correction to account for higher adsorption.

Overall, we developed an understanding of the relationship between membrane properties, i.e., thickness, charge density, and their effect on nitrate selectivity. An important aspect of the theory is that it allows the characterization of the transport properties of IEMs when experimental data is difficult to obtain, e.g., ion concentration profiles in the membranes. In addition, it also allows the analysis of the contribution of the different mechanisms, diffusion and migration, to ion transport.

4.6 Supplementary information (S.I)

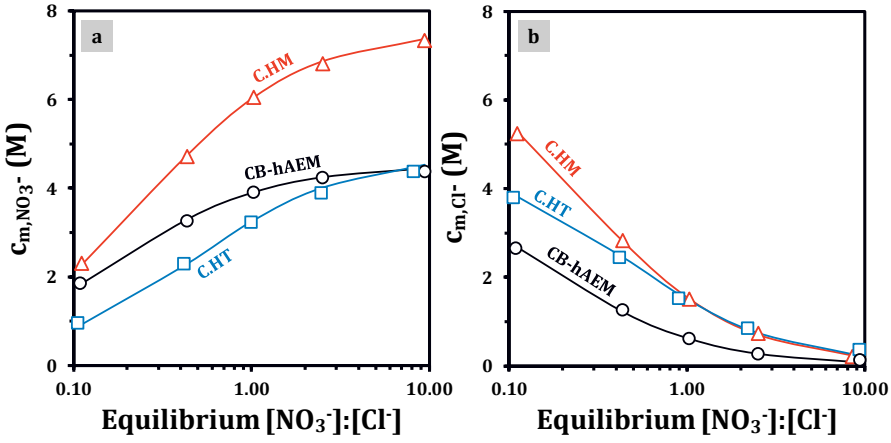

Figure S.I. 4.1. Experimental results (symbols) of adsorption experiments. The membranes were soaked in electrolyte solutions with different NO_3^- and Cl^- concentrations (total ionic strength 100 mM). The x-axis gives the $NO_3^-:Cl^-$ equilibrium concentration ratio in solution. a) Nitrate and b) chloride concentration in the membranes. Lines are based on theory.

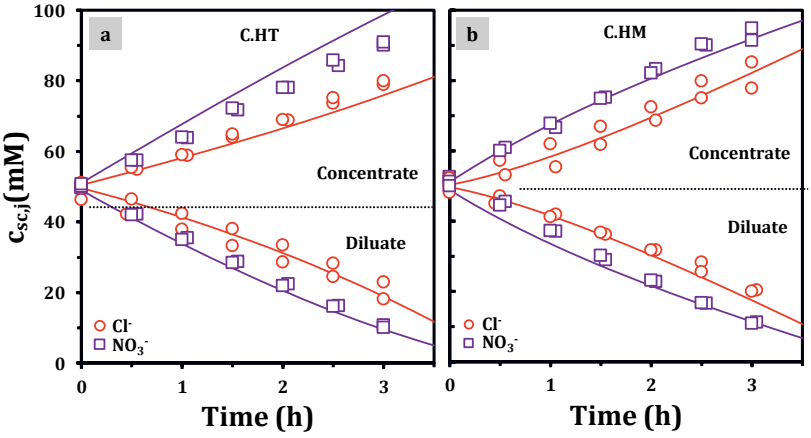

Figure S.I. 4.2. Experimental data (symbols) and theory (lines) of the ion concentration in diluate and concentrate containers as a function of time for: a) the heterogeneous commercial AEM (C.HT), namely Ralex; and b) the homogeneous commercial AEM (C.HM), namely Neosepta.

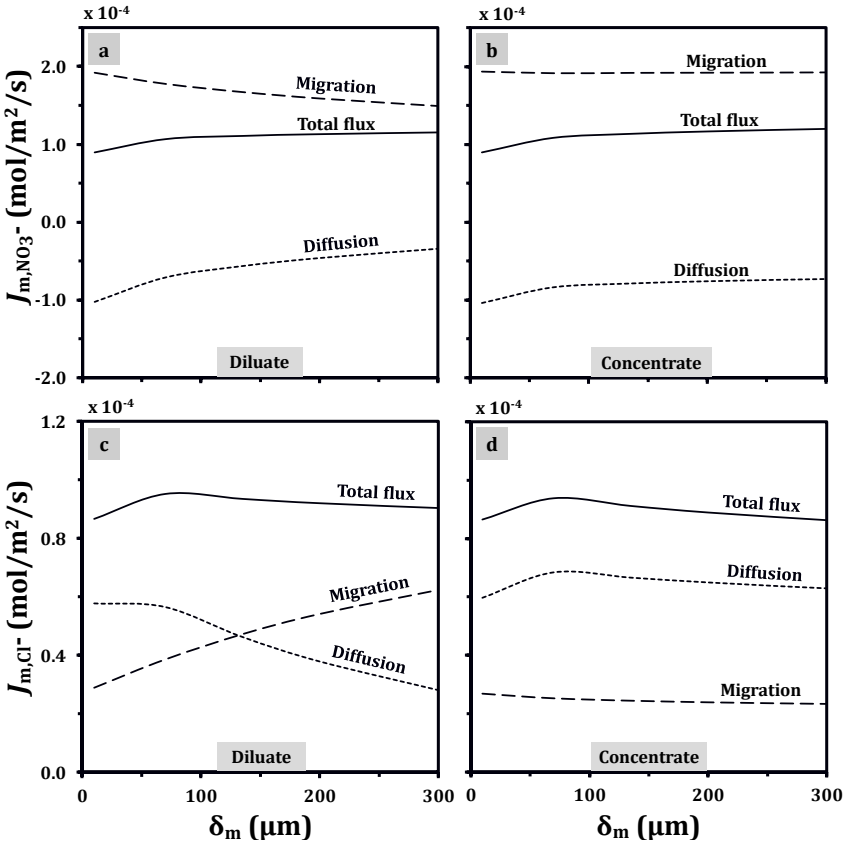

Figure S.I. 4.3. Theoretical curves for continuous ED with CB-hAEM. Influence of membrane thickness (δ_m) on ionic flux at the membrane/solution interface. Nitrate flux at the interface with a) diluate and b) concentrate solution. Chloride flux at the interface with c) diluate and d) concentrate solution. Theory lines for an ED system operated in continuous mode with CB-hAEM.

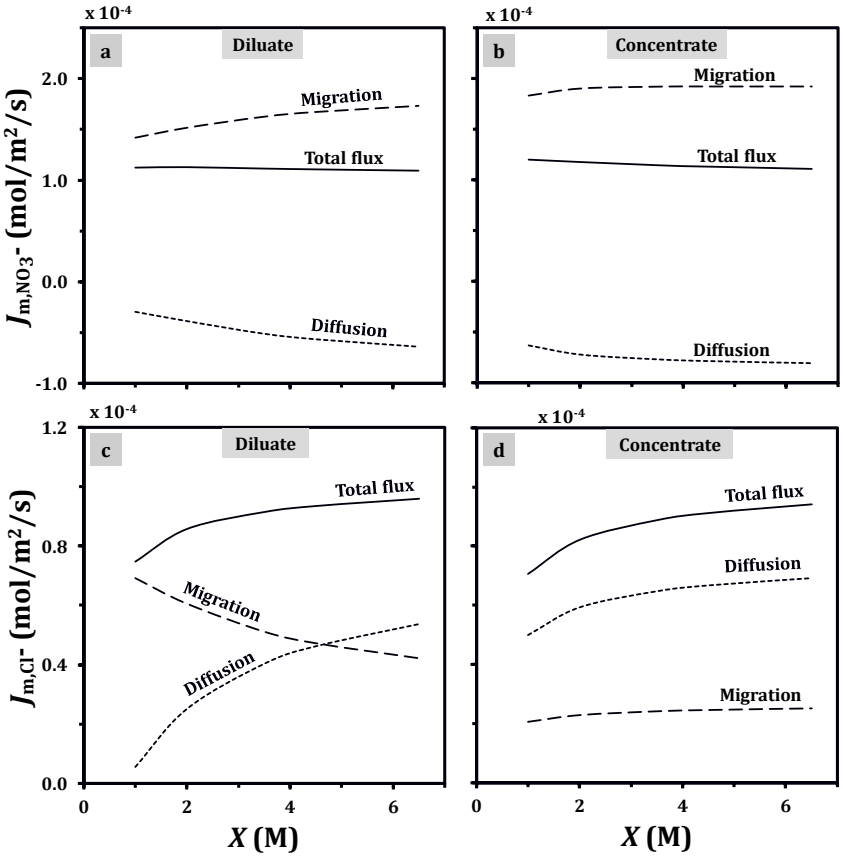

Figure S.I. 4.4. Theoretical curves for continuous ED with CB-hAEM. Influence of membrane charge density (*X*) on ionic flux at the membrane/solution interface. Nitrate flux at the interface with a) diluate and b) concentrate solution. Chloride flux at the interface with c) diluate and d) concentrate solution. Theory lines for an ED system operated in continuous mode with CB-hAEM.

Chapter 5

Cation exchange membrane behavior of extracellular polymeric substances (EPS) in salt adapted granular sludge.

This chapter has been published as:
D. Sudmalis, T.M. Mubita, M.C. Gagliano, E. Dinis, G. Zeeman, H.H.M. Rijnaarts, H. Temmink, Cation exchange membrane behaviour of extracellular polymeric substances (EPS) in salt adapted granular sludge, Water Research, 178 (2020) 115855.

Abstract

In compact bioreactors such as upflow anaerobic sludge blanket (UASB) reactors, microorganisms grow as mixed consortia entangled and "glued" together by extracellular polymeric substances (EPS). EPS act as a protective barrier against harsh environments, e.g., increased salt concentrations. The present work aims to elucidate the role of EPS in regulating ion concentrations in anaerobic granular sludges adapted to high salinity. To that end, we exposed salt adapted anaerobic granules to different monovalent electrolytes to i) study their effect on the methanogenic activity of the granules, and ii) measure ion concentration inside the granules and in the bulk solution. Results from batch-adsorption experiments show that the concentration of cations in the granules is significantly higher than that of the anions. Furthermore, the cation concentration in the granules was found to be higher compared to that in the bulk solution. For the anions, the opposite trend was observed: higher concentrations in the bulk solution than in the granules. The increased affinity of the granules for cations suggests a cation-exchange process in which EPS is directly involved. To study the ion-exchange properties of EPS, we devised a novel approach. We fabricated membranes with EPS embedded in an inert binder (PVDF-HFP). The membrane was characterized in an electrodialysis cell using a mixed electrolyte solution with KCl and NaCl. Results show that the membrane with EPS preferentially transports cations. Furthermore, the EPS-membrane shows selectivity for potassium ions over sodium. The performance of the EPS-membrane was compared with a membrane containing alginate, a well-studied EPS model compound, and a commercial cation-exchange membrane. Results reveal the potential use of EPS-like compounds for ion separation applications.

5.1 Introduction

In anaerobic wastewater treatment systems, high monovalent salt concentrations are considered to negatively affect microbial activity, especially the methanogenic activity, and formation of anaerobic granular sludge [243-246]. It was only recently shown that anaerobic granules adapted to approximately 0.35 M NaCl can increase in size [247] and can even be formed from dispersed biomass [248] at NaCl concentrations as high as 0.87 M. In such high concentrations, it was also shown that microorganisms can maintain high methanogenic activity for successful high rate anaerobic reactor operation [247, 248]. The high methanogenic activity could in part be explained by the production of osmolytes that balance the osmotic pressure between the microbial cells and the bulk liquid [249]. The osmo-toxic effect of highly saline environments on anaerobic microbial consortia has mainly been attributed to cations rather than anions [245, 250-255]. The toxicity of cations has been attributed to a mechanism that involves their ability to i) replace metallic enzyme cofactors thereby disrupting the biological function of these cofactors, ii) induce redox reactions with cellular thiols, provoking Fenton-type reactions that produce reactive oxygen species, and iii) interfere with membrane transport processes [256, 257].

In anaerobic granular sludge, microorganisms are entangled in a matrix of extracellular polymeric substances (EPS) forming a dense spherical biofilm structure [258, 259]. Extracellular polymeric substances generally have a net negative charge [260, 261], which enables them to adsorb cations. Studies have shown the tendency of bacterial EPS to adsorb multivalent ions, specifically heavy metals [262-267]. The adsorption of monovalent ions has also been reported. However, results differ depending on the type of culture used in the study. The EPS of *Halomonas sp.* were shown to poorly adsorb monovalent cations [268], whereas the EPS of *Pseudoalteromonas* showed high affinity towards K^+[269].

Extracellular polymeric substances can alleviate toxicity of low concentrations (mg/L range) of heavy metals towards microorganisms [257, 270-272] by binding and coordination reactions between the metals and the negatively charged functional groups of EPS. These binding reactions prevent the cations to diffuse into the deeper

parts of the biofilm [271, 273, 274]. A recent study has shown that mannose-rich EPS surrounding methanogenic cells from high salinity adapted granular sludge adsorb high concentrations of sodium ions (Na^+), while the concentration within active cells remains low [275]. These results suggested that even at high salinity EPS may have a protective role against monovalent cations such as Na^+ by hindering their diffusion into microbial cells [275].

Few studies have shown the toxic effects of anions on bacterial communities. Only at relatively high salt concentrations (0.2 M), the flux of chloride (Cl^-) into microbial cells was shown to alter the intracellular pH of aerobic acidophilic microorganisms [276]. Typically, anions are reported to be less toxic for anaerobic microorganisms than cations. This relatively low toxicity of anions so far has not been extensively addressed. Anions and cations both contribute to osmotic pressure in water [277], and therefore microorganisms should have a strategy to cope with high concentrations of either of them. In principle, the negative charge of EPS could prevent or hinder the transport of anions to microbial cells, thereby lowering their toxicity towards the microorganisms present in porous biofilm structures.

Studies that evaluate the transport of ions, rather than adsorption, across EPS layers are scarce. Furthermore, often these studies do not provide enough insights into ion transport dynamics. Siegrist and Gujer [278] experimentally determined the diffusion coefficients of Br^- and Na^+ through a heterogeneous biofilm. They reported that the diffusion coefficient of Br^- was slightly higher compared to Na^+. In another study, Horn and Morgenroth [273] studied the diffusion of NaCl and $NaNO_3$ in biofilms. However, in the latter study, the transport of individual ionic species could not be distinguished because conductivity rather than individual ion concentrations was measured.

In the current study, the distribution of monovalent ions (K^+, Na^+, and Cl^-) was investigated in microbial granules adapted to 0.87 M and 0.22 M of NaCl. Preliminary results indicated that Cl^- is repelled from the granular sludge by EPS surrounding the microorganisms. These results suggest that EPS may act as a barrier for anions with cation-exchange properties. We investigated the ion-exchange nature of EPS by implementing a novel approach. EPS extracted from granular sludge were used to

fabricate EPS layers (EPS-membranes). These membranes were tested in an electrodialysis cell to evaluate the transport of K^+, Na^+, and Cl^-. To further evaluate the role of EPS on regulating ion concentration inside granules (osmo-protection), studies were conducted with the salt adapted granular sludge to evaluate the impact of different monovalent salts on the methanogenic activity.

5.2 Materials and methods

5.2.1 Source of anaerobic granular sludge

Anaerobic granular sludge was obtained from laboratory scale Upflow Anaerobic Sludge Bed (UASB) reactors. The reactors were operated at sodium concentrations of 0.22 (R5) and 0.87 (R20) M as described in [248].

5.2.2 Ion distribution and concentration within salt adapted granular sludge

- ***Scanning electron microscopy with energy dispersive X-ray spectroscopy (SEM-EDX)***

Samples of granules for SEM-EDX analysis were prepared with a modified procedure described in Ref. [279]. The modifications included dehydration with graded series (10, 30, 50, 70 and two times 100%) of ethanol instead of acetone and sputter coating with tungsten instead of platinum. The granules were imaged at an acceleration voltage of 10 kV and a beam current of 0.4 nA, at room temperature in a field emission scanning electron microscope (Magellan 400, FEI Company, Oregon, USA) equipped with an energy dispersive X-ray detector. The images were processed using AZtec software (OXFORD Instruments).

- ***Ion concentration in hydrated granular sludge***

Approximately 20 g of sludge samples were taken directly from R5 and R20 for the determination of ion concentration in hydrated granular sludge. For ionic composition measurements of hydrated granular sludge, the sludge was first separated from the liquid phase by centrifugation at 10000 xg and 4^{o}C for 15 min. Further, the sludge

samples were carefully homogenized with a spatula and two samples (approximately 0.5 g each) of homogenized solids were taken for microwave digestion (ETHOS 1 - Advanced Microwave Digestion Labstation, Milestone S.r.l., Italy) with 10 mL of 65% HNO_3 (For Analysis Emsure® ISO). Digested samples were brought up to 50 mL with mili-Q water and further diluted for analysis. As a blank for ionic composition of solids mili-Q was treated in the same way as the samples. The supernatant after centrifugation was filtered through 0.2 μm cellulose acetate membrane filter (VWR® Syringe Filters) and diluted with mili-Q for further analysis. Measurements of bulk liquid were made in one replicate to confirm the expected bulk liquid concentrations of ions. Differences between measurements and expected values were below 2% in all cases.

Additionally, to elucidate the cation exchange properties of EPS in sludge granules, the distribution of Cl^-, Na^+, and K^+ in granules of R20 upon granular sludge exposure to equimolar K^+ (0.87 M) concentration was investigated. To do this, 1 g of R20 granular sludge was immersed in 1L of a modified ($NaHCO_3$ and NaCl replaced with $KHCO_3$ and KCl, respectively) nutrient medium of R20 [248] for 24 h before analysis of ionic composition with sample preparation as described above. A period of 24 h for ion exchange was chosen to ensure that an equilibrium between the sludge granules and the modified nutrient medium is reached. As a control R20 granular sludge was also exposed to its original medium containing 0.87 M of Na^+ [248].

The analysis of Na^+ and K^+ was carried out by inductively coupled plasma optical emission spectroscopy (ICP-OES, Varian, Australia) as described in Ref. [275]. Chloride content was measured on Dionex ICS-2100 Ion Chromatography System (Breda, The Netherlands) equipped with a Dionex IonPac AS19 column (4 x 250 mm) and data were processed with Chromeleon 6.80 SR13 software. The results are presented on weight bases ($mmol_{ion}/g_{medium}$ and $mmol_{ion}/g_{wet\ sludge}$) to prevent introduction of errors due to differences in the density of the medium and the granular sludge.

5.2.3 Ion exchange properties of EPS

- ***Extraction and purification of EPS***

Extracellular polymeric substances (EPS) were extracted from granular sludge adapted to 0.87 M of Na^+ (R20) by using an alkaline extraction method as reported in Ref. [280]. In short, 3 g of granular sludge (wet weight) were put into a 0.5% (w/v) Na_2CO_3 solution, heated to 80°C and stirred at 400 rpm for 35 min. After extraction, the cell debris and insoluble fraction of the extract were separated by centrifugation at 4000 xg and 4°C for 20 min. Finally, the EPS solution was dialyzed (SnakeSkin™, 3.5K MWCO) against milli-Q for 24 hours. To obtain purified EPS in a dry state, the EPS solution was further lyophilized at -84°C and 0.001 mbar.

- ***Fabrication of alginate gel membranes (ALG – membranes)***

Alginate is a well-known EPS model compound [270, 281]. Therefore, alginate membranes were prepared as a control for comparison with membranes fabricated with EPS extracted from granular sludge. The alginate gel layers (ALG-membranes) were cast with an external gelation method adapted from Ref. [282] in the following steps: i) dissolving the polymer in 10 mL milli-Q; ii) degassing the solution for 24 hours at 4°C; iii) casting the solution on a petri dish (ID = 5.7 cm) and drying at 40°C in a leveled oven; iv) crosslinking the casted layers in a 2% (w/v) calcium chloride solution with 30% (v/v) of ethanol. For casting a mixture of 0.4 g of sodium alginate (SA) and 0.004 g of guar gum (GG) as a plasticizer were used, resulting in 0.016 g SA/cm^2. The resulting membrane was washed with demi-water and equilibrated in a solution with 10 mM NaCl and 10 mM KCl for 8 h before ion selectivity tests.

- ***Fabrication of membranes with EPS (EPS-membranes)***

First, a polymeric solution was prepared by dissolving poly(vivylidene fluoride-co-hexafluoropropene) (PVDF-HFP) in dimethylacetamide (DMAc) in a ratio 1:9.5 w/v for 3h at 80 °C. Then, a weighed amount of EPS was dispersed in the polymeric solution and the materials were blended in a ball mill for 4 h. The resulting mixture contained 70:30 weight ratio of PVDF-HFP to EPS. The mixture was cast onto a glass plate at 50 °C

until complete evaporation of the solvent. The resulting membrane/layer was washed with demi-water and equilibrated in a solution with 10 mM NaCl and 10 mM KCl for 8 h before ion selectivity tests. The content of EPS in the membranes was approximately 0.0027 g EPS/cm^2 of dry membrane. This was calculated from the total area of the membrane by assuming a uniform EPS distribution.

- ***Confocal laser scanning microscopy (CLSM) for visualization of EPS distribution in the polymeric binder PVDF-HFP***

To visualize the EPS distribution in the EPS-membranes, the membranes were first equilibrated in a buffer solution (10 mM KCl and 10 mM NaCl) overnight. For the staining of the protein fraction of EPS, the EPS-membranes were placed in PBS 1X and SYPRO Ruby for 1 hour in the dark. Finally, the membranes were washed with the buffer solution and immediately observed under CLSM. To guarantee that SYPRO Ruby does not stain PVDF-HFP, a pure PVDF-HFP membrane was processed in the same way as EPS-membranes. Before the CLSM analysis, autofluorescence of PVDF-HFP was tested, as described in **S.I. 5.6.1**. Microscopy analysis was performed with an inverted AxioObserver Zeiss LSM 880 CLSM (Carl Zeiss, Germany) with a 40 x/1.3 Oil DIC M27 Plan-Apochromat objective lens. Autofluorescence of PVDF-HFP in the membranes was visualized with 488 nm excitation wavelength, at a maximum emission of 510 nm. SYPRO Ruby signal was visualized with 458 nm excitation wavelength at a maximum emission of 656 nm. The argon laser was set to 1% power for both excitation wavelengths. A series of Z-axis images (212.5 µm x 212.5 µm x 70 µm) were generated by optical sectioning with a slice thickness of 1 µm. Maximum projection intensity and orthogonal 3D reconstruction were generated with Zen Blue software (Zen imaging Software, ZEISS, Germany). The choice of emission wavelengths and the dye for EPS protein staining is explained in detail in **S.I. 5.6.1**.

5.2.4 Electrochemical characterization and ion selectivity

The performance of the membranes was evaluated in a six-compartment electrodialysis cell as shown in **Figure 5.1**. Different membranes separated the compartments inside the cell: i) the membrane under investigation, placed in between compartments A and

B. This membrane was either the EPS-membrane, the ALG-membrane, or a commercial ion-exchange membrane (Neosepta CMX, ASTOM Corporation, Tokyo, Japan). ii) Commercial ion exchange membranes, i.e., Neosepta AMX and CMX, which separated the other compartments.

Compartments A, B, and C were filled with a solution containing 10 mM NaCl and 10 mM KCl, whereas compartments D were filled with 0.1 M Na_2SO_4 solution. Solutions in compartments A and B (130 mL) were continuously stirred. For compartments C and D, one-liter solutions were circulated at a flow rate of 170 mL/min. A current density of 10 A/m^2 was applied to the cell for 1h. Samples from compartments A and B were taken over time and ion concentration was measured by ion chromatography. An increase in chloride concentration was calculated from compartment A, whereas increases in sodium and potassium concentration were calculated from compartment B. Ion selectivity (S) in the membranes is based on the concentration changes between potassium and sodium and is given by

$$S_{K^+/Na^+} = \frac{\Delta c_{K^+}}{\Delta c_{Na^+}}, \qquad \text{Eq. 5.1}$$

and

$$\Delta c = c_t - c_{initial} \qquad \text{Eq. 5.2}$$

where t, $c_{initial}$ and c_t are the sampling time, the initial concentration and the concentration at time t measured in compartment B, respectively.

We measure the current efficiency (λ) in the membranes as

$$\lambda = \sum_{i}^{i=2} \frac{(c_{t,i} - c_{initial,i}) \cdot V_{cell} \cdot F}{I \cdot t} \qquad \text{Eq. 5.3}$$

where subscript 'i' refers to cation species in solution, i.e., K^+ and Na^+, V_{cell} is the volume of liquid in compartment B, F is Faraday's constant, and I is the applied current.

The value of λ gives an indication of how selectively ions are transported across the membrane [166], i.e., it indicates if the ionic current is mainly transported by potassium and sodium (cation-exchange membrane), or the membranes also allow the transport of chloride.

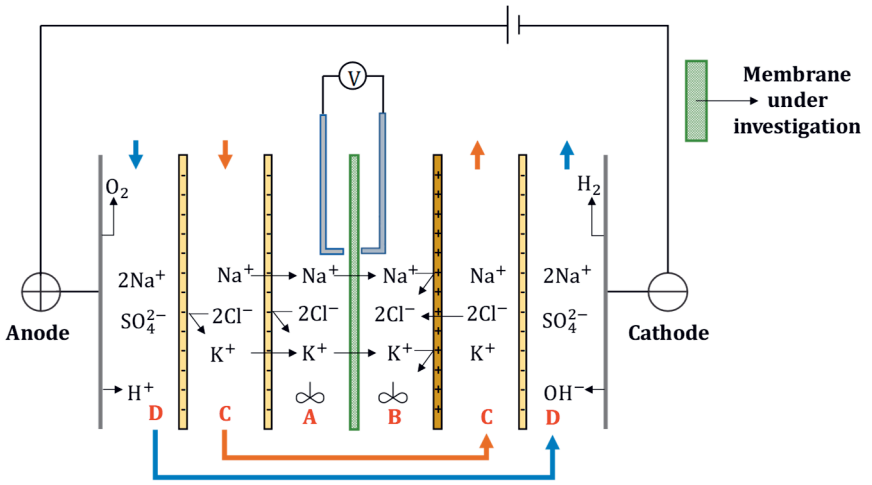

Figure 5.1. Schematic representation of the electrochemical cell used to evaluate the performance of the membranes. The membrane under investigation separates compartments A and B. After applying a potential difference, cations move from compartment A to B. For an ideal cation-exchange membrane, the transport of chloride from compartment B to A is zero. Water splitting was not significant in these experiments.

5.2.5 Effect of anions and cations on specific methanogenic activity

To study the effect of monovalent anions and cations on specific methanogenic activity (SMA) of salt adapted granular sludge, batch experiments in 118 mL serum bottles at a working volume of 50 mL, 120 RPM mixing speed and 35°C were performed. The VSS concentration was set to 1 g/L and the COD:VSS ratio was 4:1 (w/w). Sodium acetate was used as the electron donor and carbon source. The SMA was calculated through measurements of pressure build-up curves with a pressure meter equipped with an absolute pressure probe (GMH3151, Greisinger Electronic, Germany). The biogas composition at the end of experiments was measured as described in Ref. [283]. Unless stated otherwise, the experiments were performed in triplicate. All results were corrected for the atmospheric pressure and pressure build-up in blank experiments without added acetate.

The first set of experiments was performed to study the SMA of granular sludge adapted to 0.22 (R5) and 0.87 (R20) M of Na as NaCl, when exposed to an equimolar concentration of cations by addition of NaBr, KCl, and KBr. The second set of experiments was performed to study the SMA of R5 granular sludge upon exposure to

hyper-salinity shocks (i.e., an abrupt increase of salinity by spiking a nutrient medium with increased ion concentration) of NaCl, NaBr, KCl, and KBr. The final cation concentration in these experiments was 0.43 M. Bromide salts were tested (NaBr and KBr), to investigate if different anions at very high salinity would also have a substantial effect on SMA, as is frequently reported for cations [245, 252, 253]. All experiments contained 0.08 M of Na^+ originating from inocula and sodium acetate as a carbon source. This was taken into account when calculating the desired concentration of cations in the experiments. The nutrient medium was the same as reported in Ref. [249].

5.3 Results

5.3.1 Equilibrium of sodium, chloride, and potassium in granules at different salinities

The measured ion concentrations (**Figure 5.2**) and distributions (**Figure 5.4**) in the anaerobic, salt adapted, granular sludges suggest a cation exchange nature of EPS in the granules. **Figure 5.2** shows the sodium and chloride concentrations in bulk liquid and in granular sludges of R5 and R20. Sodium concentration in the granular sludge was 0.24 ± 0.004 (~0.24 M) and 0.71 ± 0.01 (~0.71 M) $mmol/g_{wet\ sludge}$ in R5 and R20, respectively. The sodium concentration in R5 granular sludge was 9% higher compared to the bulk liquid, whereas in R20 it was 17% lower compared to the bulk liquid, probably due to metal cations other than sodium also being present in the granular structure and interacting with the negatively charged EPS groups. The chloride concentration was 0.11 ± 0.002 (~0.11 M) and 0.52 ± 0.001 (~0.52 M) $mmol/g_{wet\ sludge}$ in R5 and R20, respectively (**Figure 5.2**). These concentrations correspond to a 31.2 and 35.8% lower chloride concentration compared to the bulk liquid in R5 and R20, respectively. Thus, apparently, EPS of granular sludge acclimated to 0.22 and 0.87 M of Na^+ preferentially repel anions, such as Cl^-, probably due to the anionic nature of EPS, as will be discussed in more detail in ***section 5.4.1***.

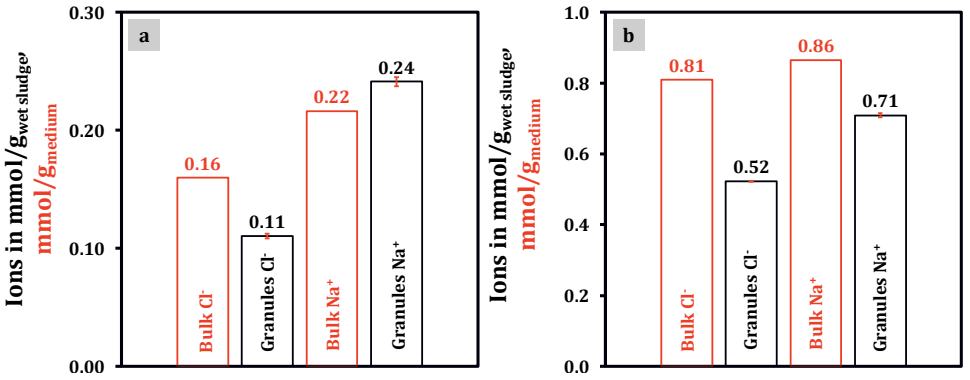

Figure 5.2. Na^+ and Cl^- concentration in salt adapted granular sludge. a) granular sludge and bulk liquid composition of R5 adapted to 0.22 M Na^+; b) granular sludge and bulk liquid composition of R20 adapted to 0.87 M Na^+. The error bars show absolute deviation from measurements of two separately prepared and digested 0.5 g sludge samples.

Potassium concentration in the R20 granular sludge before changing the medium was 0.05 mmol/$g_{wet\ sludge}$ (~ 0.02 g/$g_{sludge\ VS}$) (**Figure 5.3**). This corresponds to a 28-fold increase compared to the growth medium. Such a high concentration of K^+ can be found within methanogenic cells upon exposure to high osmotic stress, even after the accumulation of osmolytes within the microbial cells [284]. When placing the R20 granules, previously exposed to 0.87 M NaCl, in a nutrient medium with KCl (0.87 M) the Cl^- concentration in the granular sludge did not change (**Figure 5.3**). However, Na^+ had almost completely been displaced with K^+ within 24 hours (**Figure 5.3**). After the medium change, the K^+ concentration within the granular sludge reached a concentration of 0.81 ± 0.04 mmol/$g_{wet\ sludge}$ (~0.32 g/$g_{sludge\ VS}$), which is higher compared to the Na^+ concentration of 0.73 ± 0.002 mmol/$g_{wet\ sludge}$ in the control sample. This indicates a higher affinity of K^+ towards EPS in granular sludge compared to Na^+.

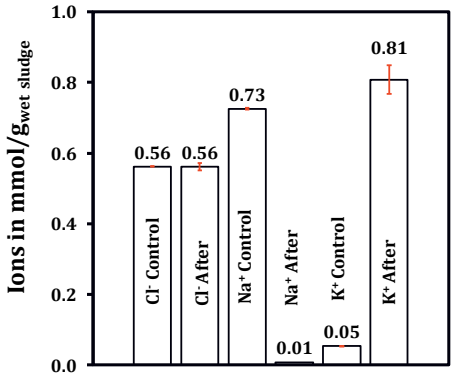

Figure 5.3. Ionic composition of R20 granular sludge after 24 hours in 0.87 M Na^+ medium (control) and 0.87 M K^+ medium (after). The error bars show absolute deviation from duplicate measurements.

Scanning electron microscopy with energy-dispersive X-ray spectroscopy (SEM-EDX) of sliced microbial granules adapted to 0.87 M of NaCl showed a uniform distribution of sodium ions throughout the granules (**Figure 5.4a**), confirming the ionic composition results in **Figure 5.2**. In contrast to the ion chromatography results (**Figure 5.2**), chloride could not be detected in the granules with SEM-EDX imaging (**Figure 5.4b**). This could be a result of chloride ions removal together with water from the pores of the granular sludge during the dehydration steps of the SEM samples preparation (see Materials and Methods). This removal of chloride, coupled with sodium retention in the granules, suggests that sodium was bound to the EPS, whereas chloride was mainly present in the water phase of the granule pores as will be further discussed in ***section 5.4.2***.

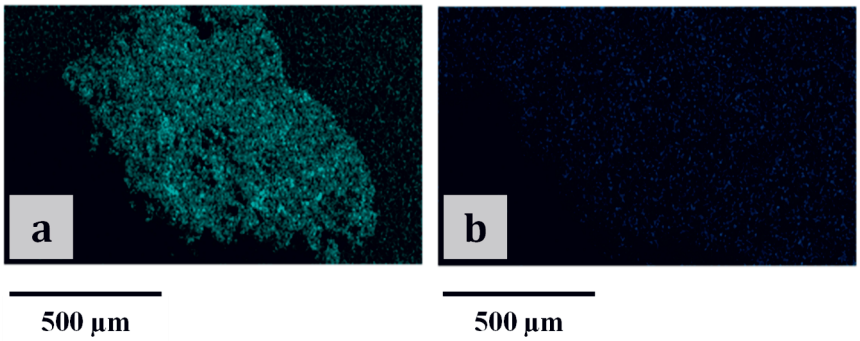

Figure 5.4. SEM – EDX micrographs of a sliced microbial granule adapted to 0.87 M NaCl. a) distribution of sodium throughout the granular structure; b) distribution of chloride throughout the granular structure. The black corner in the bottom left of the micrographs is a region from which the detector could not receive any signal due to the structure of the granule. No clear shape of a granule in panel (b) indicates that the background signal was as strong as the signal from the granule.

5.3.2 The ion exchange properties of EPS-membrane and ALG-membrane

The CLSM analysis showed that binding of EPS with PVDF-HFP was successful. Micrographs in **Figure 5.5a** and **Figure 5.5c** show a uniform distribution of EPS (in red, stained with SYPRO RUBY) as a thin layer on the surface of the PVDF-HFP (in green). Such a distribution is likely due to the hydrophobic nature of the inert binder (PVDF-HFP), which could interact with the hydrophobic moieties of EPS, and did not allow for mixing of EPS throughout the depth of the membrane. The negative control staining (**Figure 5.5b** and **d**) confirmed that SYPRO Ruby does not bind to the PVDF-HFP membrane and that the signal in **Figure 5.5a** and **c** indeed originated from SYPRO Ruby bound to the proteinaceous fraction of EPS.

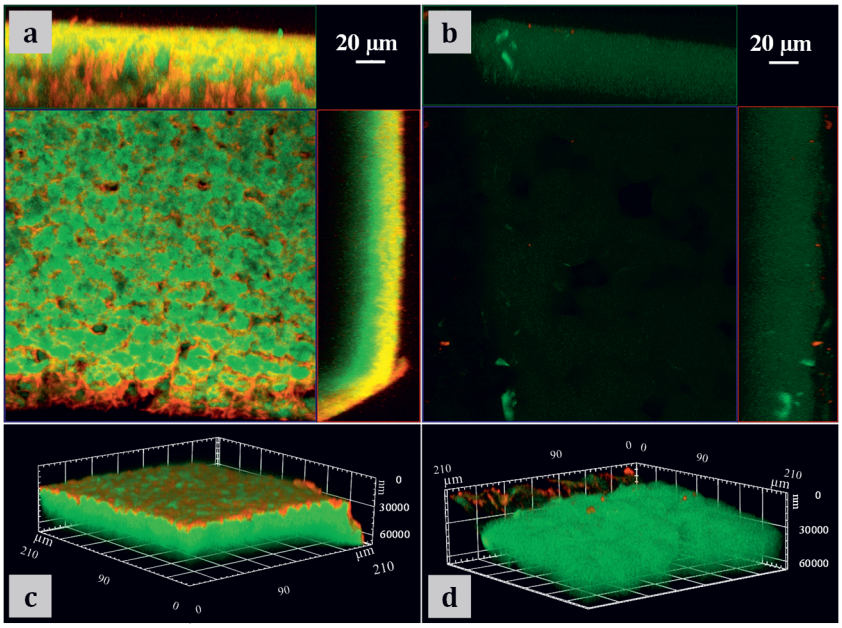

Figure 5.5. a-b) Orthogonal view of CLSM micrographs of membranes using maximum intensity projection and the respective 3D reconstructions in panels (c) and (d). The membrane with the EPS in A, C. The green signal shows auto-fluorescence of the binder. The red signal shows EPS proteins stained with SYPRO Ruby. The bright yellow signal originates from the combination of green and red. The reference membrane composed solely of inert binder (PVDF-HFP) in panels (b) and (d).

After the successful preparation of the membranes, as shown in **Figure 5.5a and Figure 5.5c,** their selectivity towards transport of potassium, sodium, and chloride was tested in an electrodialysis cell. **Figure 5.6a-c** shows changes in cation concentration (potassium and sodium) in compartment B and of chloride concentration in compartment A, for the ALG-membrane, EPS-membrane, and the commercial membrane, respectively. Cations (sodium and potassium) were preferentially transported across the membranes, whereas chloride ions were partially repelled. In addition, a preferential transport of potassium over sodium across the ALG and EPS-membrane was measured (**Figure 5.6a-b**). The rate of change in ion concentration (determined by the slopes of the curves, m value) shows that in the ALG-membrane the potassium transport was 11 % higher and sodium transport was 23 % lower than in the EPS-membrane. The resulting potassium selectivity ($S_{K^+/Na^+} > 1$) is depicted in **Figure 5.6d** and was higher for the ALG-membrane compared to the EPS-membrane.

With the commercial ion exchange membrane, there was no marked difference in the transport between potassium and sodium (**Figure 5.6c**). In **Figure 5.6d,** the current efficiency shows how much of the current was transported by cations. Despite the non-ideal cation selectivity of the "bio-membranes", the current efficiency (λ) was relatively high: 79% for the ALG-membrane and 83% for the EPS-membrane. The commercial membrane gave the highest current efficiency of 92%.

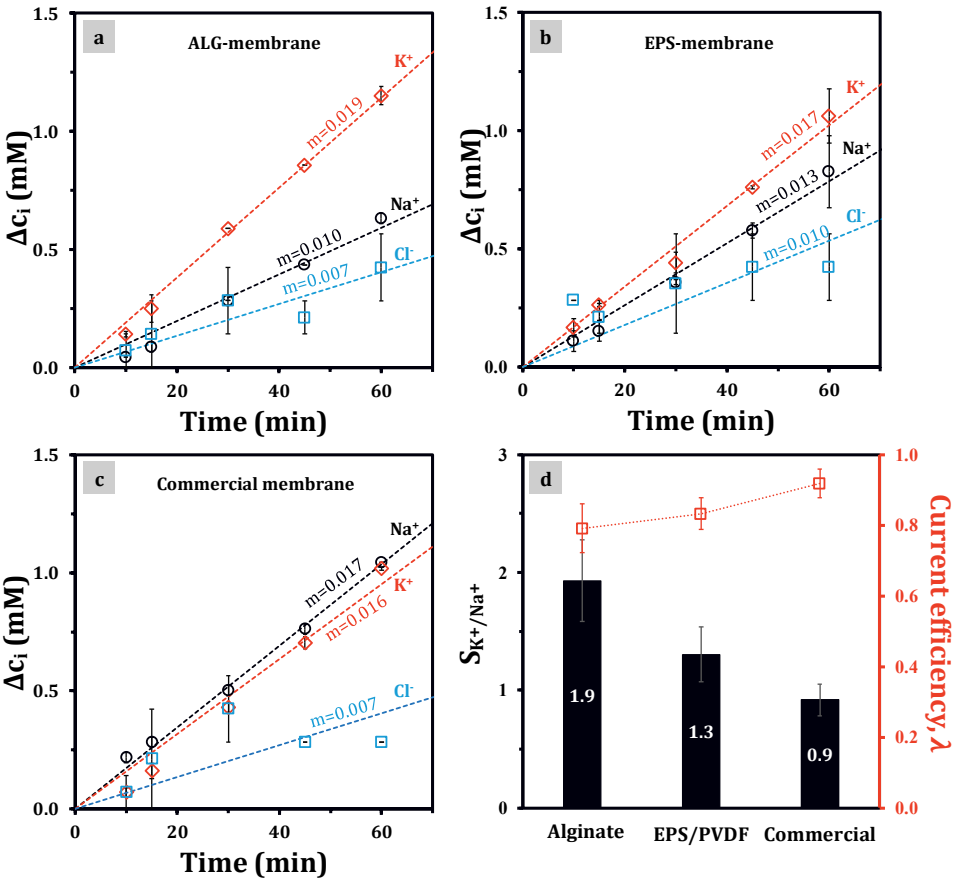

Figure 5.6. a-c) Ion concentration changes (symbols) as a function of time. The concentration changes of cations were measured in compartment B, whereas the concentration changes of anions were measured in compartment A. The m value indicates the slope of the dashed lines. d) Potassium selectivity (S_{K^+/Na^+}) and current efficiency (λ) of the membranes. The error bars show absolute deviation in duplicate measurements.

5.3.3 Effect of anions and cations on specific methanogenic activity

Figure 5.7a shows that exposure of 0.22 M Na^+ adapted granular sludge to equimolar concentration of KCl and KBr salts resulted in a decrease of methanogenic activity by 25.3 and 11.7%, respectively, when compared to the reference at 0.22 M of Na^+. Doubling the ion concentration to 0.43 M of KCl and KBr resulted in SMA decrease by 49.2 and 44.1%, respectively. The negative effect of Na^+ salts on the SMA of granular sludge at increased molarity of 0.43 M was considerably less pronounced compared to K^+ salts (**Figure 5.7b**). The SMA decreased by 19.9 and 11.1% with NaCl and NaBr salts, respectively. It seems that in general Br^- salts had a slightly smaller negative effect on SMA compared to Cl^- salts. However, the results obtained with NaBr at 0.22 M did not follow the overall trend, therefore additional experiments are needed in the future to confirm this. Finally, **Figure 5.8** shows that granular sludge adapted to 0.87 M NaCl retains its methanogenic activity when exposed to NaBr. However, SMA in the granules completely ceased when they were exposed to potassium salt solutions. Overall, results indicate that cations, specifically K^+, have a stronger impact on the methanogenic activity of salt adapted granular than the anions (Cl^- and Br^-).

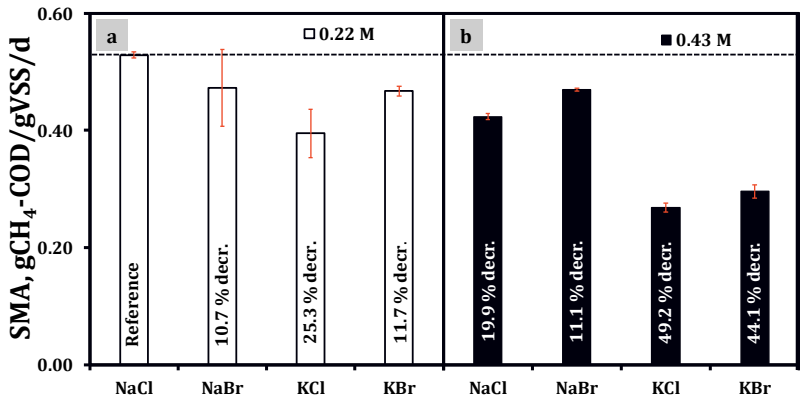

Figure 5.7. SMA of granular sludge exposed to various chloride and bromide salts. Granular sludge was first adapted to 0.2 M NaCl and then exposed to 0.22 M (panel a) and 0.43 M (panel b) electrolyte solutions of NaCl, NaBr, KCl, and KBr. Error bars show standard deviations from triplicate in Cl^- salts. Error bars with Br^- salts show absolute deviations from average in duplicate experiments. % decr. - % SMA decrease with respect to the reference. Horizontal dashed line shows the SMA of the reference.

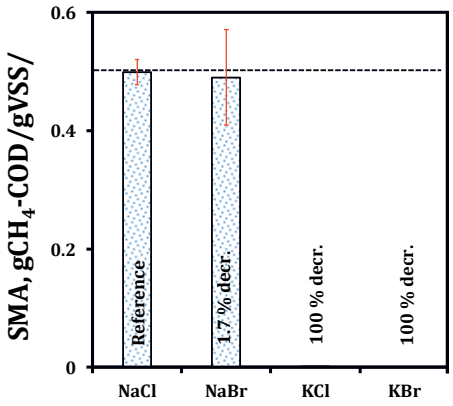

Figure 5.8. SMA of granular sludge exposed to various chloride and bromide salts. Granular sludge was first adapted to 0.87 M NaCl and then exposed to 0.87 M electrolyte solutions of NaCl, NaBr, KCl and KBr. Error bars show standard deviations from triplicate experiments. % SMA decrease with respect to the reference. Horizontal dashed line shows the SMA of the reference.

5.4 Discussion

5.4.1 Cation exchange membrane properties of EPS and potassium selectivity

The ability of EPS to partially repel anions, and act as a cation-exchange membrane, has been clearly shown in the present study (**Figure 5.2, Figure 5.4, Figure 5.6a-b**). Different studies have shown that both EPS and EPS-like substances, such as alginate, exhibit affinity for cations [285-288]. This cation affinity is also visible in EPS- and ALG-membranes in which the transport of cations (potassium and sodium) represented ~ 80% of the total ionic current (**Figure 5.6d**). The cation affinity in EPS-membrane is probably the result of the abundant presence of different negatively charged functional groups such as carboxylic, phenolic, and phosphoric groups in EPS [264]. Alginate compounds also have negatively charged groups, mainly carbonyl, at neutral pH [289, 290].

Evidently, the membranes do not show ideal permselectivity (λ < 100%)—however, such non-ideal behavior is expected. EPS can not completely repel ions since it would prevent the diffusion of important substrates, such as phosphate or acetate, to the

microbial cells. Furthermore, EPS and alginate have hydrogel properties. Hydrogels are known for their hydrophilic structure, and hence high water uptake, which leads to swelling and even dissolution when exposed to water [289, 291]. Swelling can cause structural changes in the membranes that impact the ability of the membrane to preferentially transport counterions (ions with opposite charge to the charged functional groups in the membranes) and exclude co-ions (mobile ions with the same charge to the charged functional groups in the membranes) [292, 293]. Therefore, when ion-exchange membranes are not able to effectively block the transport of co-ions, λ is < 100. Optical coherence tomography (OCT) analysis (**Figure S.I. 5.2**) showed that a hydrated PVDF-HFP membrane was 50 µm thick, while the addition of 10% w/w EPS increased the membrane thickness by 89 µm, clearly showing that swelling of EPS indeed took place.

Surprisingly, the EPS and particularly the ALG-membrane were more selective to K^+ than to Na^+, (**Figure 5.6d**). Such selectivity was higher than that measured in the commercial membrane (**Figure 5.6d**). It is not clear, which EPS and alginate properties resulted in such selectivity and this certainly should be further looked into.

The current efficiency of ALG-membrane was very similar to that of the EPS-membrane (**Figure 5.6d**). Measurements of charge density show a marked difference between alginate and EPS (***S.I. 5.6.2***). In principle, membranes with high charge density are also more permselective [209]. Alginate had a charge density of 7.0 meq/g and EPS a charge density of 2.5 meq/g as measured for free dissolved polymers in solution. These values may be significantly different in the membranes themselves due to charge shielding. In ALG-membranes, the crosslinking with calcium ions may have led to a reduction of charged functional groups available for ion-exchange. In the EPS-membranes, some functional groups may have been completely embedded in the matrix of the supporting polymers (PDVF). Therefore, in future studies, the real charge densities in the membranes themselves should be assessed, for example by acid-base titration [186].

5.4.2 Methanogenic activity inhibition by various ions

The methanogenic activity of 0.87 M NaCl adapted granular sludge was completely inhibited when it was exposed to an equimolar concentration of KCl (**Figure 5.8**). Also,

exposure of 0.22 M NaCl adapted granular sludge to 0.22 M of KCl led to a 25 % decrease in methanogenic activity. The decrease of SMA was smaller (19.9 %) when exposing the same granular sludge to 0.43 M NaCl (**Figure 5.7b**). Kugelman and McCarty [252] showed that potassium had a higher negative effect on methanogenic activity than sodium, using low salinity adapted sludge and equimolar concentrations of sodium and potassium bicarbonates. Our results extend this finding with chloride salts and high salinity adapted sludge and demonstrate that anions at equimolar concentrations have little influence on the SMA (**Figure 5.7** and **Figure 5.8**). The mechanism of a potential Br^- or Cl^- toxicity on methanogens is not known. Possibly anion toxicity is "masked" by the ability of EPS to repel these anions, as was shown in this study (**Figure 5.2, Figure 5.6**). This "masking" would occur if the granular structure could be viewed upon as a membrane (**Figure 5.9**). In this regard, the concentration of ions in the membrane is determined by the concentration of fixed charged functional groups in it. Inside the membranes, electroneutrality is reached according to Ref. [236]:

$$c_{\text{counterion}} - c_{\text{co-ion}} - X = 0$$

where $c_{\text{counterion}}$ is the counterion concentration, $c_{\text{co-ion}}$ is the co-ion concentration, and X is the concentration of charged functional groups (negative for EPS). Due to the fixed negative charges of EPS, the concentration of negatively charged co-ions in the porous granular structure is potentially reduced, while positively charged counterions are allowed to accumulate (**Figure 5.9**). The extent to which the amount of co-ions is reduced in the granular structure compared to the bulk liquid depends on X. Due to the fixation and electrostatic interaction between the cations and the charged functional groups in EPS, the osmotic pressure experienced by the microbial cells can be reduced.

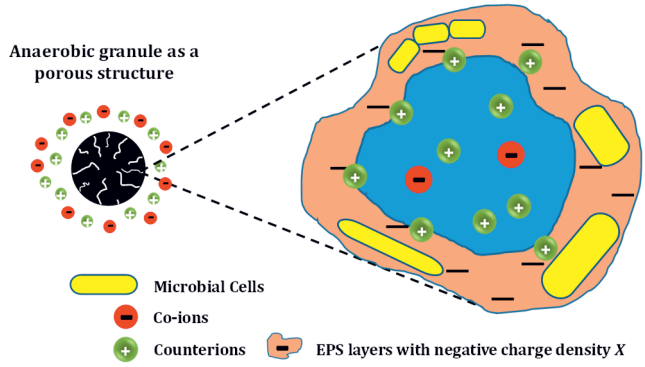

Figure 5.9. Granular sludge as a porous structure with fixed negative charges in EPS.

This hypothesis can potentially be tested with EPS deficient mutants of methanogens in toxicity experiments, and by comparing their sensitivity to different anions with EPS covered methanogens. Such an approach has been used by Wang et al. [272] to study the role of EPS in osmo-protection upon exposure of *Klebsiella pneumoniae* to 100 mM of $CaCl_2$. This showed that in EPS deficient microbial cells the turgor pressure decreased upon exposure to salt, whereas in cells covered with EPS the turgor pressure remained unaffected. This suggests that EPS helps to counteract the osmotic pressure experienced by microbial cells in high salinity environments.

The mechanism by which high K^+ concentrations inhibit methanogenic activity is not exactly known. Toxicity studies with high concentrations of metallic cations and other types of microorganisms demonstrated interference with membrane transport processes, either by competitively inhibiting membrane transporter proteins or by affecting the membrane potential [257]. Acetoclastic methanogens couple sodium transport across the cytoplasmic membrane with the transfer of the methyl group from tetrahydrosarcinapterin (H_4SPT) to coenzyme M (HS-CoM). This precedes the final reduction step for methane production from acetate [294]. Also, acetoclastic methanogens make use of both proton and sodium gradients across the cell membrane for ATP synthesis [294]. Abrupt exposure of the microorganisms to high concentrations of potassium could potentially interfere with these processes. Prolonged periods (more than a month) of exposure can result in the adaptation of methanogens to K^+

concentrations of up to 0.19 M [295]. However, further increases of K^+ concentration in completely stirred continuously operated tank reactor resulted in decreasing methanogenic activity, similar to the results of batch experiments in this study [295]. This suggests that the adaptation of methanogens to high K^+ concentration is more difficult than adaptation to Na^+.

5.4.3 Can the EPS-membranes be applied for the separation of sodium and potassium in practice?

Separation of two monovalent cations is a serious challenge, even for the most advanced technologies, such as electro-membrane processes. This is because these ions possess similar physicochemical properties, e.g., hydrated size. Most state-of-the-art ion exchange membranes lack selectivity for one specific ion [15]. With the mimicked "bio-membranes" (ALG and EPS-membranes) as prepared in this study, relatively high selectivity towards potassium over sodium ($S_{K^+/Na^+} > 1$), was observed, particularly for the ALG-membrane. Such selectivity was absent in a commercial cation-exchange membrane (**Figure 5.6d**). However, the membranes prepared in this study cannot be considered for commercial applications at this stage due to their limited stability. Approximately 48 hours of exposure of membranes to water leads to EPS detachment from the PVDF EPS-membrane and to water leakage in the ALG-membrane (data not shown). In the EPS-membrane, this is likely due to weak adhesion between EPS (hydrophilic with hydrophobic moieties) and PVDF (hydrophobic), whereas in the ALG-membrane this is likely due to Ca^{2+} exchange with Na^+, leading to disintegration of the 3D structure of the gel [289]. Future studies need to focus on the EPS and sodium alginate properties that dictate the selective transport of K^+ over Na^+, which may help to develop analogous synthetic membranes. Such investigations should include fractionation of EPS extracts in their constituents and also preparation of membranes with EPS model constituents other than alginate (e.g., proteins and glycoproteins) to elucidate how these affect the membrane transport properties.

5.5 Conclusions

We have shown that electrochemical methods can be used to measure and characterize the affinity of EPS towards cations. With the fabrication of membranes containing EPS (EPS-membrane), we were able to demonstrate that EPS from anaerobic granular sludge adapted to high salinity have cation-exchange properties. The cation-exchange behavior was also exhibited by membranes fabricated with alginate (ALG-membrane), a well-studied EPS model compound. Both EPS and ALG- membrane showed not only cation selectivity but also selectivity between different cations. Potassium ions were selectively transported over sodium ions. These results may open doors to consider biopolymers for the fabrication of selective ion-exchange membranes.

In addition, selectivity experiments carried out with EPS-membrane and adsorption experiments with granular sludge showed that EPS of the granules function as a protective barrier against anions. Moreover, we showed that the ion concentration and composition of the bulk solution markedly affect the specific methanogenic activity (SMA) of anaerobic granular sludge. A higher decrease of SMA was measured with potassium monovalent salts solutions than with sodium salt solutions.

5.6 Supplementary information (S.I)

5.6.1 Membranes morphology

- ***Confocal laser scanning microscopy (CLSM)***

For the visualization of PVDF-EPS membranes under CLSM, the auto-fluorescence of PVDF-HFP was tested on pure a PVDF-HFP membrane, previously hydrated in a solution containing 10 mM KCl and 10 mM NaCl. The PVDF membrane was analyzed for autofluorescence with an inverted AxioObserver Zeiss LSM 880 confocal laser scanning microscope (CLSM; Carl Zeiss, Germany) using fluorescence excitation/emission filters with a 20×/0.8M27 Plan-Apochromat objective lens. The emission scans were performed with 9 nm bandwidth increments in the range of 410-695 nm excitation wavelength. The argon laser power was set to 1% for 488 and 458 nm excitation wavelengths. Acquired CLSM images were processed with the Zen Blue software (ZEISS, Germany). The obtained images are shown in **Figure S.I. 5.1**.

The PVDF membrane has high emission intensity in the range from 486 nm to 575 nm at excitation wavelength of 458 nm (**Figure S.I. 5.1A**). The emission spectrum at excitation wavelength of 488 nm showed a maximum emission intensity in the range from 477 to 521 nm (**Figure S.I. 5.1B**). This excludes the possibility to apply on the PVDF-EPS membranes fluorescent dyes falling in the same emission range.

SYPRO Ruby was chosen for EPS protein staining because it has its maximum excitation at 458 nm and its maximum emission at 656 nm. This allowed to simultaneously scan the auto-fluorescence of PVDF (excitation 488 nm, max. emission 510 nm) and the protein portion of EPS by the fluorescence of SYPRO Ruby (excitation 458 nm, max. emission 656 nm).

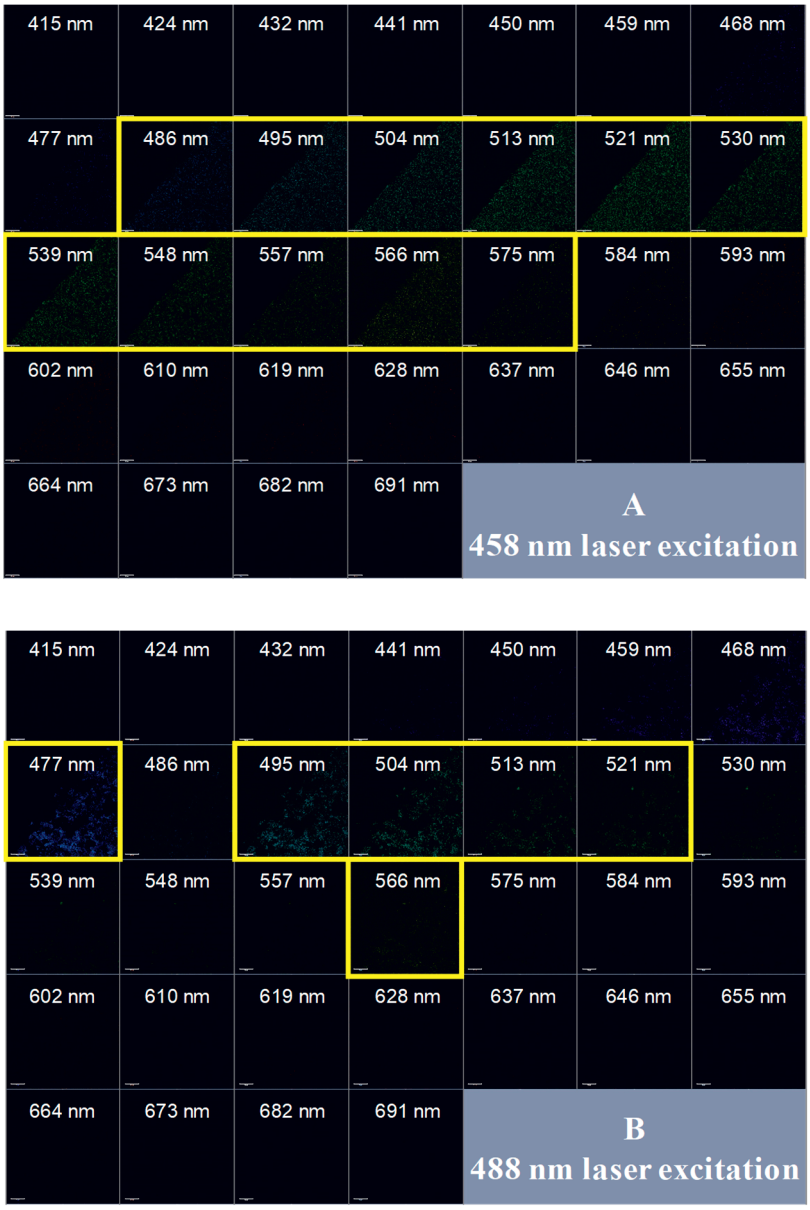

Figure S.I. 5.1. Single pictures show the isolated emission spectra of the PVDF membrane after excitation with 458 nm (panel A) and 488 nm (panel B) lasers in the emission range from 415 nm to 691 nm. In yellow, the emission spectra with highest intensities are identified.

- ***Optical Coherence Tomograph (OCT)***

To study the thickness of the hydrated membranes (in 10 mM NaCl + 10 mM KCl), a spectral domain OCT (Thorlabs Ganymede OCT System, USA) was used. The OCT was equipped with a 5x telecentric scan lens (Thorlabs LSM03BB, USA) with a maximum scan area of 100 mm^2. The OCT engine was configured to provide high-resolution images with a sensitivity of 106 dB at 1.25 kHz scan rate.

The results in **Figure S.I. 5.2** show a large increase of membrane swelling upon mixing PVDF with EPS. Upon addition of 10% (w/w) of EPS to PVDF the thickness of the PVDF membrane increased from 50 μm (**Figure S.I. 5.2A**) to 139 μm (**Figure S.I. 5.2B**).

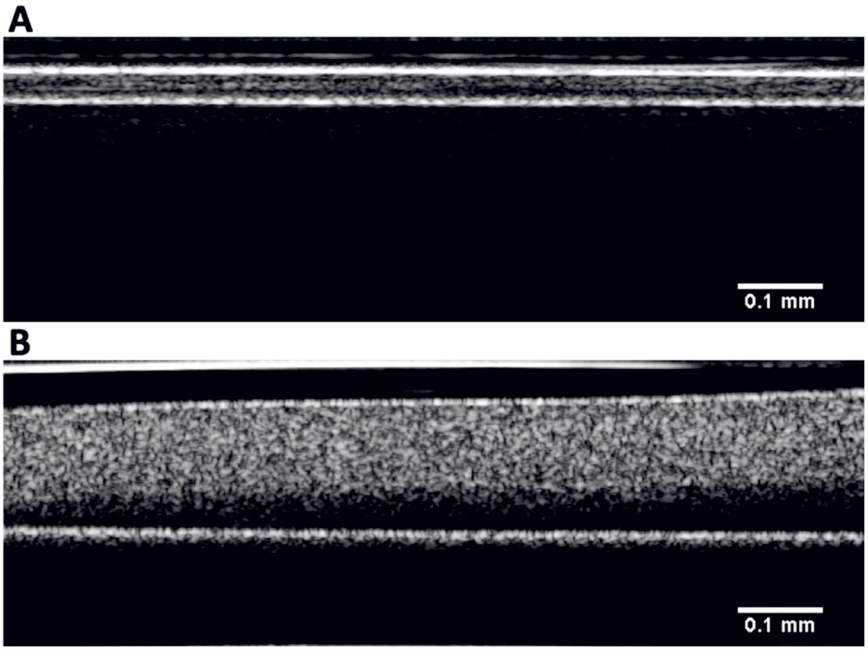

Figure S.I. 5.2. OCT micrographs of membranes fabricated with : A) PVDF; and B) PVDF mixed with 10% (w/w) EPS. The thickness of the membrane was 50 μm in A and 139 μm in B.

5.6.2 Charge density measurement

To compare the charge density of EPS and alginate used for preparation of the EPS-PVDF and SA-gel membranes, a colloid titration method was used, as described in Ref. [260]. In short, 10 mL of samples (1 mg/L) were titrated against 0.01 mM poly-diallyldimethylammonium chloride (pDADMAC) using a Mütek Particle Charge Detector (PCD03) with an automatic titrator (Metrohm titrando 888). The titrant was added in steps of 0.02 mL, while simultaneously recording the streaming potentials (mV). The charge density was then calculated on the basis of titrant volume added to reach the point of 0 charge (streaming potential equals to 0 mV). The charge densities of samples were measured at their original pH (below 6) in mili-Q and at pH adjusted to 7. A solution 0.1 M of NaOH/HCl was used for the pH adjustment.

Figure S.I. 5.3 shows the charge density of EPS extracted from several sludges grown in laboratory scale reactors at 20 g Na^+/L and 5 g Na^+/L and of alginate used to prepare SA-gel membranes. The charge density of EPS used to prepare EPS-PVDF membranes corresponds to the sample *Tryptone 20 g Na*. A variety of EPS was tested to confirm if EPS from anaerobic sludge of various reactors would have similar charge density.

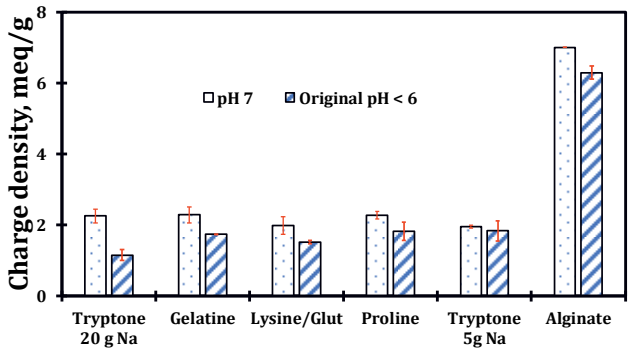

Figure S.I. 5.3. Charge density of various anaerobic sludges grown at 20 g Na^+/L (Tryptone 20 g Na^+, Gelatine, Lysine/Glut, Proline), at 5 g Na^+/L (Tryptone 5 g Na^+) and of alginate used for SA-gel membrane preparation.

Chapter 6

Capacitive deionization with wire-shaped electrodes.

This chapter has been published as:
T.M. Mubita, S. Porada, P.M. Biesheuvel, A. van der Wal, J.E. Dykstra, Capacitive deionization with wire-shaped electrodes, Electrochim. Acta, 270 (2018) 165-173.

Abstract

Capacitive deionization is a desalination technology to remove ions from aqueous solutions in a cyclic manner by applying a voltage between pairs of porous electrodes. We describe the dynamics of this process by including a possible rate limitation in the transport of ions from the interparticle pore space in the electrode into intraparticle pores, where electrical double layers are formed. The theory includes the effect of chemical surface charge located in the intraparticle pores, which is present in the form of acidic and basic groups. We present dynamic data of salt adsorption for electrodes with and without coated ion-exchange membranes. Experiments were conducted in a CDI cell geometry based on wire-shaped electrodes placed together. The electrodes consisted of graphite rods coated with a layer of porous carbon. To fabricate this layer, we examined two procedures that involve the use of different solvents: acetone and N-methyl-2-pyrrolidone (NMP). We found that electrodes prepared with acetone had lower salt adsorption compared to electrodes prepared with NMP. At equilibrium, the theory is in agreement with data, and this agreement underpins the effect of chemical surface groups on electrode performance. Under dynamic conditions, our theory describes reasonably well desalination cycles.

6.1 Introduction

Water desalination using capacitive deionization (CDI) is based on the removal of ions from aqueous solutions by electrosorption [41, 45, 296]. For CDI with porous carbon electrodes, after applying a voltage between the electrodes, cations are adsorbed into the negatively polarized electrode while anions are adsorbed into the positively polarized electrode (adsorption step). When the adsorption capacity of the electrodes is reached, the electrodes can be short-circuited for regeneration, and ions are released (desorption step) [42, 297, 298]. During desalination two processes jointly occur in the carbon electrodes: ion transport and adsorption. Ions are transported through the interparticle space, the macropores. Ion adsorption occurs in the intraparticle space, the micropores, where electrical double layers (EDLs) are formed [126, 143, 299].

Several mathematical models describe adsorption phenomena in EDLs. The Helmholtz and Gouy-Chapman-Stern models are well-known [52, 300, 301], but do not accurately describe ion adsorption for CDI [142]. The Donnan model and its extended versions, however, describe ion adsorption to a very accurate degree [128, 142, 302]. The latest version of the Donnan model, the amphoteric Donnan (amph-D) model, includes the effect of charged surface groups in EDLs [134, 156]. These charged surface groups are present in the form of acidic groups, e.g., carboxyl structures, or basic groups, e.g., amine structures. Different from previous Donnan models [43, 142, 302, 303], the amph-D model does describe the sometimes-observed phenomenon of ion desorption at the start of an adsorption cycle [304-306].

In the present work, we use the amph-D model and couple it to a transport model to dynamically describe the desalination process. In the transport theory, we include a transport limitation for ions between macro- and micropores. This approach is different from the often-used assumption of infinitely fast ion adsorption into micropores [146, 299, 307, 308].

To compare our dynamic theory with experimental data, we use a CDI cell with rod-shaped electrodes (“wire-CDI cell”), **Figure 6.1a.** The wire-CDI cell is a simple cell design (compared to conventional CDI), which consists of graphite rods (wires) coated

with a thin porous carbon layer [309]. To enhance salt adsorption, we coat ion-exchange membranes (IEMs) on the carbon layer. The inclusion of IEMs in the system is referred to as membrane capacitive deionization (MCDI) [44, 143]. The carbon layer on the electrodes is prepared by mixing activated carbon with a polymeric binder dissolved in an organic solvent. Often, N-methyl-2-pyrrolidone (NMP) is used as a solvent [299, 309]. In this work, we tested a new method to fabricate the carbon layer by using acetone as a solvent. Acetone is a less toxic alternative to NMP [310, 311]. In addition, acetone evaporates faster than NMP, which decreases the preparation time of the electrodes.

One of our aims is to present a modified theory to dynamically describe salt adsorption and charge storage in CDI and MCDI. Our theory is not only valid for wire-CDI systems but can also be applied to other CDI cell designs and other electrosorption processes. In this study, we validate the theory with experiments conducted with wire-shaped electrodes with and without coated IEMs. Furthermore, we compare salt adsorption and charge storage of porous carbon electrodes prepared with two different organic solvents, acetone, and NMP.

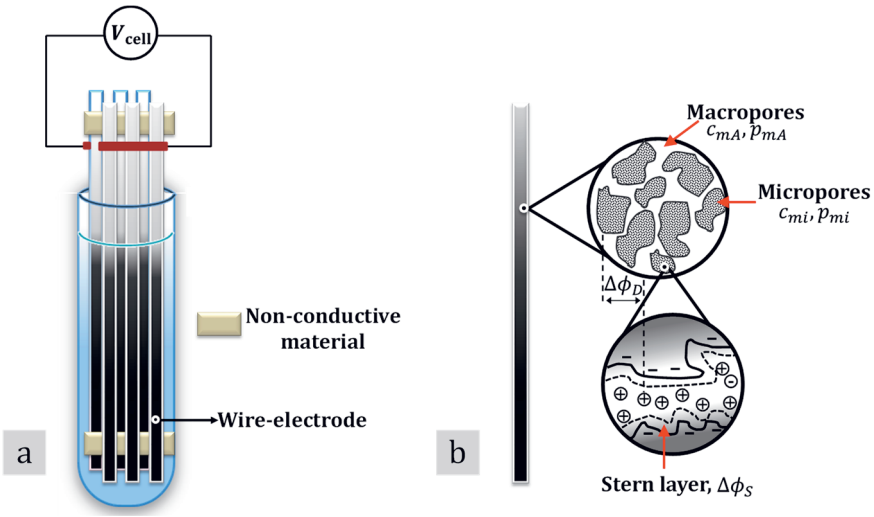

Figure 6.1. a) Capacitive deionization cell used in this study. The cell consists of three pairs of porous carbon electrodes. Ions are adsorbed from solution upon applying a voltage between pairs of electrodes. b) In the electrodes, ions are adsorbed in electrical double layers formed in the micropores.

6.2 Theory

In this Section we present i) the theory used to calculate salt adsorption and charge in equilibrium, when there is no transport of ions either through the macropores or from macro- to micropores, and ii) our dynamic theory to describe electrosorption.

6.2.1 Equilibrium theory

To describe salt adsorption in equilibrium for CDI, we use the amphoteric Donnan (amph-D) model [141, 156]. This model includes the effect of charged surface groups in EDLs. These groups are fixed to the carbon surface and can be formed during the activation process of the carbon material or cell operation [151, 312, 313]. In each electrode, we model two different micropore regions: the A- and B-region. The A-region contains acidic groups, such as carboxyl-, lactone- or phenol- groups [314]. The B-region contains basic groups (i.e., protonated groups). In the A- and B-region, three types of charge are present: i) electronic charge in the carbon matrix, σ_{elec}, ii) ionic charge in the micropores, σ_{ionic}, and iii) chemical surface charge fixed to the carbon surface, σ_{chem}. Each region is overall charge-neutral, thus

$$\sigma_{elec,j} + \sigma_{ionic,j} + \sigma_{chem,j} = 0 \qquad \text{Eq. 6.1}$$

where subscript *j* refers to region A or B. Charge $\sigma_{chem,A}$ has a negative sign, and $\sigma_{chem,B}$ has a positive sign.

Similar to the classical Donnan model [130, 303], the amph-D model also considers overlapping EDLs and assumes that the electrical potential inside the micropores, in each region, does not depend on the distance to the pore wall. Therefore, the concentration of ion 'i' in a micropore region 'j', $c_{mi,i,j}$ can be related to the concentration in the macropores, $c_{mA,i}$, according to the Boltzmann equilibrium

$$c_{mi,i,j} = c_{mA,i} \cdot \exp\left(-z_i \cdot \Delta\phi_{D,j}\right) \qquad \text{Eq. 6.2}$$

where parameter z_i is the charge number of an ion, and $\Delta\phi_{D,j}$ the dimensionless Donnan potential.

From now on, we consider an electrolyte containing only a dissolved 1:1 salt in water, such as NaCl. In the macropores, we assume electroneutrality, which is given by

$$c_{\mathrm{mA,cation}} = c_{\mathrm{mA,anion}} = c_{\mathrm{mA}} \qquad \text{Eq. 6.3}$$

while the ionic charge in each micropore region is

$$\sigma_{\mathrm{ionic,j}} = c_{\mathrm{mi,cation,j}} - c_{\mathrm{mi,anion,j}}. \qquad \text{Eq. 6.4}$$

The Stern layer, which is located between the carbon surface and the aqueous phase in the micropore, is considered in the amph-D model. The Stern layer potential, $\Delta\phi_{\mathrm{S,j}}$, is related to the Stern layer capacitance ($\mathrm{C_S}$) and $\sigma_{\mathrm{elec,j}}$ according to

$$\sigma_{\mathrm{elec,j}} \cdot \mathrm{F} = \mathrm{V_T} \cdot \Delta\phi_{\mathrm{S,j}} \cdot \mathrm{C_S} \qquad \text{Eq. 6.5}$$

where F is Faraday's constant, and V_{T} the thermal voltage ($V_{\mathrm{T}} = \mathrm{RT/F}$).

The potential drop over the EDL, $\Delta\phi_{\mathrm{EDL}}$, is the sum of the Stern and Donnan potentials and (in a given electrode) is equal for the acidic and basic region

$$\Delta\phi_{\mathrm{EDL}} = \Delta\phi_{\mathrm{D,A}} + \Delta\phi_{\mathrm{S,A}} = \Delta\phi_{\mathrm{D,B}} + \Delta\phi_{\mathrm{S,B}}. \qquad \text{Eq. 6.6}$$

For each electrode, the average electronic charge, σ_{elec}, ionic charge, σ_{ionic}, and average ion concentration in the micropores, c_{ions}, are given by

$$\sigma_{\mathrm{elec}} = \sum_{\mathrm{j=A,B}} \alpha_{\mathrm{j}} \cdot \sigma_{\mathrm{elec,j}} \qquad \text{Eq. 6.7}$$

$$\sigma_{\mathrm{ionic}} = \sum_{\mathrm{j=A,B}} \alpha_{\mathrm{j}} \cdot \sigma_{\mathrm{ionic,j}} \qquad \text{Eq. 6.8}$$

$$c_{\mathrm{mi,ions}} = \sum_{\mathrm{j=A,B}} \alpha_{\mathrm{j}} \cdot (c_{\mathrm{mi,cation,j}} + c_{\mathrm{mi,anion,j}}) \qquad \text{Eq. 6.9}$$

where α_{j} is the fraction of each region relative to the total micropore volume ($\upsilon_{\mathrm{mi,AC}}$, mL/g electrode). Note that $\alpha_{\mathrm{A}} + \alpha_{\mathrm{B}} = 1$.

We calculate the charge, Σ_{F}, from the difference between the micropore charge at the end of the adsorption step (superscript "ads, end") and that at the end of the desorption step (superscript "des, end") [299]

$$\Sigma_F = ½ \cdot F \cdot \upsilon_{mi,AC} \cdot \left|\sigma_{elec}^{ads,end} - \sigma_{elec}^{des,end}\right|. \quad \text{Eq. 6.10}$$

The salt adsorption is calculated according to

$$\Gamma_{salt} = ¼ \cdot M_{w,NaCl} \cdot \upsilon_{mi,AC} \cdot \left(\left(c_{mi,ions}^{ads,end} - c_{mi,ions}^{des,end}\right)_{ca} + \left(c_{mi,ions}^{ads,end} - c_{mi,ions}^{des,end}\right)_{an}\right) \quad \text{Eq. 6.11}$$

where $M_{w,NaCl}$ is the molecular weight of NaCl. We relate the cell voltage, V_{cell}, to $\Delta\phi_{EDL}$ according to

$$\frac{V_{cell}}{V_T} = \Delta\phi_{EDL_{an}} - \Delta\phi_{EDL_{ca}} \quad \text{Eq. 6.12}$$

where subscripts 'an' refers to the anode and 'ca' to the cathode.

Equations Eq. 6.1-Eq. 6.12 describe, together with a mass balance of the cell (**see S.I. 6.6.1**), salt adsorption in equilibrium for CDI. For MCDI, however, we need to consider the IEMs. Previous work [309] assumed that the membranes are perfectly selective, which means that co-ions (ions with the same sign as the membrane fixed charge) cannot go through. In our work, we relax this assumption and consider non-ideal permselectivity, which we will describe in ***section 6.2.2***.

6.2.2 Dynamic theory

To model dynamics of ion adsorption from macropores into each micropore region in the electrodes, we use an expression similar to the one used to calculate the transfer rate of electrons in redox reactions at electrode surfaces [315]. However, instead of using this equation for a redox reaction, in this work, we use it to describe the transfer rate of ions between macro- and micropores, given by

$$j_{i,j} = k \cdot \left(c_{mA} \cdot \exp\left(-½ \cdot z_i \cdot \Delta\phi_{D,j}\right) - c_{mi,i,j} \cdot \exp\left(½ \cdot z_i \cdot \Delta\phi_{D,j}\right)\right) \quad \text{Eq. 6.13}$$

where $j_{i,j}$ is the transfer rate of each type of ion per unit macropore volume into micropore region j (mol/m^3/s), and k is the rate constant, which we assume to have the same value for cations and anions.

For monovalent salt solutions, we derive expressions for the transfer rate of ions, j_{ions}, and charge, j_{charge}, between macro- and micropores, expressed in mol/m^3/s

$$j_{\mathrm{ions,j}} = j_{\mathrm{cation,j}} + j_{\mathrm{anion,j}} \quad \text{Eq. 6.14}$$

$$j_{\mathrm{charge,j}} = j_{\mathrm{cation,j}} - j_{\mathrm{anion,j}}. \quad \text{Eq. 6.15}$$

We insert Eq. 6.13 in Eq. 6.14 and Eq. 6.15 to arrive at

$$j_{\mathrm{ions,j}}/k = 2 \cdot c_{\mathrm{mA}} \cdot \cosh\left(\tfrac{1}{2} \cdot \Delta\phi_{\mathrm{D,j}}\right) - \left[c_{\mathrm{mi,ions,j}} \cdot \cosh\left(\tfrac{1}{2} \cdot \Delta\phi_{\mathrm{D,j}}\right) + \sigma_{\mathrm{ionic,j}} \cdot \sinh\left(\tfrac{1}{2} \cdot \Delta\phi_{\mathrm{D,j}}\right)\right] \quad \text{Eq. 6.16}$$

$$j_{\mathrm{charge,j}}/k = -2 \cdot c_{\mathrm{mA}} \cdot \sinh\left(\tfrac{1}{2} \cdot \Delta\phi_{\mathrm{D,j}}\right) - \left[c_{\mathrm{mi,ions,j}} \cdot \sinh\left(\tfrac{1}{2} \cdot \Delta\phi_{\mathrm{D,j}}\right) + \sigma_{\mathrm{ionic,j}} \cdot \cosh\left(\tfrac{1}{2} \cdot \Delta\phi_{\mathrm{D,j}}\right)\right]. \quad \text{Eq. 6.17}$$

For both anode and cathode, we set up an ion balance over the macropore volume, which includes the flux of the ion from the bulk solution into the electrode, J_{i} (mol/m^2/s), and the flux of ions from macro- to micropore, j_i, according to

$$\mathrm{V_{mA}} \frac{\partial c_{\mathrm{mA,i}}}{\partial \mathrm{t}} = \mathrm{A_e} \cdot J_{\mathrm{i}} - \mathrm{V_{mA}} \sum_{\mathrm{j=A,B}} \alpha_{\mathrm{j}} \cdot j_{\mathrm{i,j}} \quad \text{Eq. 6.18}$$

where $\mathrm{V_{mA}}$ is the total volume of macropores in the anode or cathode, and $\mathrm{A_e}$ is the outer area of the electrode. As electroneutrality holds in the macropores, summing Eq. 6.18 over cat- and anions results in

$$2 \cdot \frac{\partial c_{\mathrm{mA}}}{\partial \mathrm{t}} = \frac{J_{\mathrm{ions}}}{\mathrm{p_{mA}} \cdot \lambda_{\mathrm{e}}} - j_{\mathrm{ions}} \quad \text{Eq. 6.19}$$

where λ_{e} is the ratio of electrode volume over electrode surface area, $\lambda_{\mathrm{e}} = \mathrm{V_e}/\mathrm{A_e}$, $\mathrm{p_{mA}}$ is the macroporosity, and where J_{ions} and j_{ions} are given by

$$J_{\mathrm{ions}} = J_{\mathrm{cation}} + J_{\mathrm{anion}} \quad \text{Eq. 6.20}$$

$$j_{\mathrm{ions}} = \sum_{\mathrm{j=A,B}} j_{\mathrm{ions,j}}. \quad \text{Eq. 6.21}$$

In (each region of) the micropores we relate $c_{\mathrm{mi,i,j}}$ to $j_{\mathrm{i,j}}$ by

$$\alpha \cdot p_{mi} \cdot \frac{\partial c_{mi,i,j}}{\partial t} = p_{mA} \cdot j_{i,j} \qquad \text{Eq. 6.22}$$

where p_{mi} is the microporosity.

We substitute Eq. 6.22 into Eq. 6.4 to derive a mass balance for $\sigma_{ionic,j}$

$$\alpha \cdot p_{mi} \cdot \frac{\partial \sigma_{ionic,j}}{\partial t} = p_{mA} \cdot j_{charge,j}. \qquad \text{Eq. 6.23}$$

The average ionic charge in the micropores, σ_{ionic}, can be related to ionic current density, J_{charge} (mol/m^2 s), which is defined per projected area of an electrode, according to

$$p_{mi} \cdot \frac{\partial \sigma_{ionic}}{\partial t} = \frac{J_{charge}}{\lambda_e}. \qquad \text{Eq. 6.24}$$

We relate J_{charge} to the potential drop over the bulk solution, $\Delta\phi_{bulk}$, and a constant describing the conductance of the bulk solution, κ_D, by

$$\Delta\phi_{bulk} = -\frac{J_{charge}}{\kappa_D \cdot c_{bulk}}. \qquad \text{Eq. 6.25}$$

We set up an overall salt balance over the bulk solution in the cell, which is operated in batch mode, given by

$$2 \cdot V_{bulk} \cdot \frac{\partial c_{bulk}}{\partial t} = -A_e \sum_{e=an,ca} J_{ions,e} \qquad \text{Eq. 6.26}$$

where V_{bulk} is the volume of the bulk solution and where e runs over the anode, an, and cathode, ca. To complete the description of the CDI cell we consider that

$$c_{mA} = c_{bulk}. \qquad \text{Eq. 6.27}$$

Equations 6.13-6.27 are the basis of the dynamic theory of salt adsorption in CDI. For MCDI, we include membranes and consider non-ideal permselectivity (i.e., besides counterions, co-ions can also go through the membranes). Therefore, the flux of ions through the membrane is calculated using the Nernst–Planck equation. We assume that: i) at each position in the membrane, the electroneutrality condition holds, $c_{mem,cation} - c_{mem,anion} + \omega X = 0$, where ωX is the membrane fixed charge defined per

unit aqueous phase [236, 316]; ii) the concentration profile and potential profile across the membrane are linear, which is only correct for ωX very large; iii) the cat- and anions have equal diffusion coefficients; iv) the transport of ions through the membranes can be described in steady state condition.

These assumptions lead to an expression for J_{ions} given by [220]

$$J_{\mathrm{ions}} = -\kappa_{\mathrm{mem}} \cdot \left(\Delta c_{\mathrm{T,mem}} - \omega X \cdot \Delta\phi_{\mathrm{mem}}\right) \qquad \text{Eq. 6.28}$$

where κ_{mem} is the membrane transport rate constant, which is directly linked to the membrane porosity and thickness, and the mobility of ions within membrane pores. The term $\Delta c_{\mathrm{T,mem}}$ is the difference between the total ion concentration in the membrane at the membrane-macropore interface, $c_{\mathrm{T,mem-elec}}$, and in the membrane at the membrane-bulk solution interface, $c_{\mathrm{T,mem-bulk}}$, and $\Delta\phi_{\mathrm{mem}}$ is the difference in potential between the aforementioned interfaces.

The concentration at each membrane interface (membrane/bulk, mem − bulk, and membrane/electrode, mem − elec), $c_{\mathrm{T,mem}}$, is given by [236]

$$\begin{aligned} c_{\mathrm{T,mem-bulk}} &= \sqrt{\mathrm{X}^2 + (2 \cdot c_{\mathrm{bulk}})^2} \\ c_{\mathrm{T,mem-elec}} &= \sqrt{\mathrm{X}^2 + (2 \cdot c_{\mathrm{mA}})^2}. \end{aligned} \qquad \text{Eq. 6.29}$$

The potential drop over the membrane, $\Delta\phi_{\mathrm{mem}}$, is related to ionic current density and average membrane concentration, $c_{\mathrm{T,mem}}$, by

$$J_{\mathrm{charge}} = -\kappa_{\mathrm{mem}} \cdot c_{\mathrm{T,mem}} \cdot \Delta\phi_{\mathrm{mem}}. \qquad \text{Eq. 6.30}$$

The ionic current density, J_{charge}, is invariant across membranes and bulk solution. Therefore, the value of J_{charge} in Eqs. Eq. 6.24, Eq. 6.25, and Eq. 6.30 is the same.

At the mem − bulk and mem − elec interfaces, we consider Donnan equilibrium [317]. The Donnan potential, $\Delta\phi_{\mathrm{D}}$, at these interfaces is given by

$$\begin{aligned} \Delta\phi_{\mathrm{D,mem-bulk}} &= \operatorname{asinh}\left(\frac{\omega X}{2 \cdot c_{\mathrm{bulk}}}\right) \\ \Delta\phi_{\mathrm{D,mem-elec}} &= \operatorname{asinh}\left(\frac{\omega X}{2 \cdot c_{\mathrm{mA}}}\right). \end{aligned} \qquad \text{Eq. 6.31}$$

Finally, the cell voltage is calculated according to

$$\frac{V_{\mathrm{cell}}}{V_{\mathrm{T}}} = \left(\Delta\phi_{\mathrm{EDL}} + \Delta\phi_{\mathrm{mem}} + \Delta\phi_{\mathrm{D,mem-bulk}} - \Delta\phi_{\mathrm{D,mem-elec}}\right)_{\mathrm{an}} - \left(\Delta\phi_{\mathrm{EDL}} + \Delta\phi_{\mathrm{mem}} + \Delta\phi_{\mathrm{D,mem-bulk}} - \Delta\phi_{\mathrm{D,mem-elec}}\right)_{\mathrm{ca}} + \Delta\phi_{\mathrm{bulk}}. \quad \text{Eq. 6.32}$$

6.3 Experimental

6.3.1 Preparation of wire electrodes

All experiments in this study were performed using wire-shaped electrodes. Graphite rods (Poco EDM-3, diameter ~ 3.0 mm, Saturn Industries, Inc., USA) were used as inner support and current collector. These graphite rods were coated with a porous carbon layer using a carbon slurry. A polymeric binder, polyvinylidene fluoride (PVDF) (Kynar HSV 900, Arkema Inc., Philadelphia, PA), was dissolved in a solvent: either acetone or N-methyl-2-pyrrolidone (NMP). For the preparation of electrodes using acetone (A-electrodes), PVDF was dissolved in boiling acetone (56 °C) in a weight ratio PVDF : acetone of 1 : 45 and stirred for 1 h. Thereafter, activated carbon (YP50-F, Kuraray Chemical, Japan) and carbon black (Vulcan XC72R, Cabot Corp., Boston, MA) were added to the solution in a weight ratio activated carbon : carbon black : PVDF of 85 : 5 : 10. The resulting slurry was stirred for an additional hour at 50 °C. Graphite rods were repeatedly dipped into the slurry until a carbon layer with a thickness of ~ 370 µm and a length of 12 cm was obtained. The coated electrodes were dried at 100 °C overnight. For the preparation of electrodes using NMP (NMP-electrodes), we followed the procedure described in Ref. [309].

6.3.2 Preparation of wire electrodes coated with ion-exchange membranes

Commercially available Fumion® ionomer (FumaTech GmbH, Germany) was used in this study; FKS for cation exchange membranes (CEM), and FAS for anion exchange membranes (AEM). Membranes were coated onto the acetone-based electrodes (A-electrodes) by dipping the electrodes into the solution with ionomer. Three layers of

ionomer were coated on the electrode. Each layer was dried before coating a new one. The thickness of the resulting membranes was ~100 µm. The membrane-coated electrodes were dried in a tubular oven with a temperature ramp from 60 °C to 120 °C for 3 hr. Before use, the electrodes were soaked in a 20 mM NaCl solution for at least 24 h.

6.3.3 CDI and MCDI experiments

The CDI and MCDI experiments were conducted in a batch-wise operated wire-CDI cell. The cell consisted of three pairs of electrodes separated by a piece of non-electrically conductive material (1.5 mm thick) located at the top and bottom of the electrodes, **Figure 6.1a,** to avoid electrical connection between anodes and cathodes. In CDI and MCDI experiments, aqueous solutions of NaCl with an initial concentration of 20 mM were continuously stirred and purged with nitrogen. The cell voltage was controlled and the current was measured using a potentiostat (Iviumstat, Ivium Technologies, the Netherlands). The conductivity of the solution was also monitored and its value recalculated according to a calibration curve to obtain salt concentration. To perform the experiments, we followed three procedures that are described below.

- ***Method i***

To calculate salt adsorption, charge, and charge efficiency as a function of charging voltage, desalination experiments were conducted with alternating adsorption and desorption steps in the same container, while we continuously monitor the conductivity of the solution. During the adsorption step, we applied different charging voltages, V_{ch}, of 0.6, 0.8, 1.0 and 1.2 V, for 35 min. This time was long enough to assure that equilibrium was reached. During the desorption step, we short-circuited the electrodes for regeneration i.e., we applied a discharging voltage of 0 V for 35 min. For each charging voltage, we conducted four consecutive adsorption and desorption cycles, and we determined salt adsorption, charge, and charge efficiency of the last cycle. These equilibrium experiments were conducted with A- and NMP-electrodes. Results are presented in **Figures 6.2a-c**.

- ***Method ii***

To evaluate salt adsorption, charge, and charge efficiency in a more realistic setting, with actual desalination, experiments were conducted in two different containers, one container for adsorption, and another container for desorption. At the beginning of each experiment, the volume and salt concentration of the two solutions were the same. For adsorption, a charging voltage of 1.2 V was applied for 35 min. For desorption, the electrodes were moved from the adsorption to the desorption container and short-circuited for 35 min. Each experiment consisted of four consecutive desalination cycles. In these experiments, at the end of each adsorption or desorption step, the electrodes are moved to the other container and the conductivity is measured. Results are presented in **Figure 6.2d-f** and **Figure 6.3.**

- ***Method iii***

To evaluate dynamic salt adsorption and charge, desalination cycles were conducted with consecutive adsorption and desorption steps in the same container, as in method i. We applied a charging voltage of 1.2 V for 1.1 h, and thereafter we short-circuited the electrodes for 1.1 h. The experiments were conducted with A-electrodes with and without coated membranes. Results are presented in **Figure 6.4.**

6.4 Results and discussion

In the first part of this Section, we present results of equilibrium CDI experiments, conducted with A- and NMP-electrodes, as a function of charging voltage (method i), and results of experiments conducted during real desalination (method ii). We compare the results of experiments with the amph-D model. In the second part, we show the dynamic evolution of salt adsorption and charge in (M)CDI, and compare the experimental data with our dynamic theory.

6.4.1 Performance A- and NMP-electrodes

Equilibrium experiments were conducted using A- and NMP-electrodes (method i and ii). **Figure 6.2** compares the performance of both sets of electrodes in terms of salt adsorption, charge, and charge efficiency. Panels **a**, **b**, and **c** show an increase of these

variables as a function of charging voltage. Panels **d**, **e**, and **f** show data obtained when consecutive desalination cycles are carried out.

Compared to NMP-electrodes, salt adsorption and charge efficiency of A-electrodes are considerably lower. We considered two explanations for this behavior: i) differences in pore size distribution and ii) presence of an additional chemical surface charge, σ_{chem}, in the micropores of the carbon material for the A-electrode. To test the first explanation, we conducted gas sorption analysis to measure the porosity and surface area of the electrodes. Results show no evidence of a significant difference in the physical structure between the two sets of electrodes, **Table S.I. 6.1.**

The second explanation considers the modification of the chemical surface on carbon particles during the fabrication of the electrodes using acetone. Carbon-oxygen groups are the main surface groups present in activated carbon (AC) [318]. Functional groups such as carboxyl, lactone, and phenol impart the acidic behavior of AC [61, 128]. We assume that electrode preparation with acetone increases the number of acidic groups in the carbon pores. To investigate this hypothesis, we measured the concentration of acidic groups in both sets of electrodes, NMP- and A-electrodes, following the procedure described in Ref. [134]. Results in **Figure S.I. 6.2** show that the total concentration of acidic groups is about -0.43 M for A-electrodes and -0.18 M for NMP-electrodes. These results underline the possibility that acetone modifies the chemical surface of carbon electrodes by increasing the concentration of acidic surface groups. This increase may be responsible for the decrease in salt adsorption exhibited in experiments conducted with A-electrodes.

In our theory, we include the effect of chemical surface charge to predict salt adsorption and charge. For NMP-electrodes, we assumed that the density of acidic and basic surface charge groups is the same in value and opposite in sign. We used values for surface charge determined in Ref. [156], which is for the acidic region $\sigma_{\mathrm{chem,A}} = -0.26$ M and for the basic region $\sigma_{\mathrm{chem,B}} = +0.26$ M. For A-electrodes, we determined the chemical surface charge by adding to each region additional acidic groups with a concentration set to -0.35 M. The additional groups are assumed to be equally present in both A- and B-region in both anode and cathode. As shown in **Figure 6.2**, the theory describes

experimental data very closely for both types of electrodes, thus the amph-D model underpins that chemical surface charge has an impact on the performance of the electrodes [134].

Additional parameters required for the theory are micropore volume, $\upsilon_{mi,AC}$, which was measured using gas sorption and Stern layer capacitance, C_S, which was obtained from Ref. [146]. A list of all parameters is given in **Table 6.1** and **Table 6.2**.

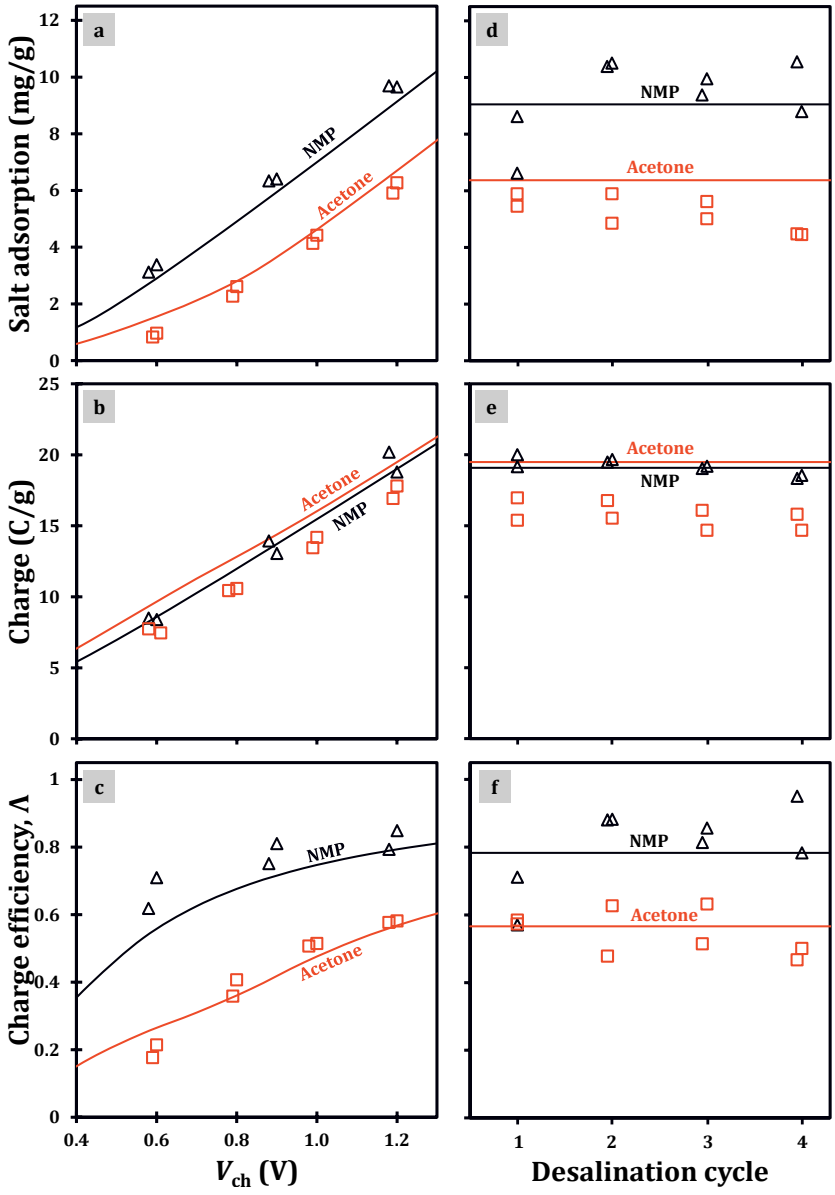

Figure 6.2. Comparison of the amph-D theory (lines) with experimental data (open symbols) for A- (squares) and NMP-electrodes (triangles); $c_{\text{salt initial}} = 20$ mM. Equilibrium salt adsorption, charge, and charge efficiency as a function of: a-c) charging voltage, V_{ch} (discharge 0 V, method i) and d-f) desalination cycle (method ii, *section 6.3.3*). Salt adsorption and charge are given per total mass of electrodes.

Table 6.1. Parameters for A-electrodes.

Experimental			
λ_e	Thickness of porous carbon layer	1.83	mm
A_e	Area of electrode (cathode or anode)	6.90	cm^2
M_e	Total mass of porous carbon layer (anode and cathode)	1.27	g
ρ_{elec}	Electrode mass density	0.52	g/mL
V_{bulk}	Volume bulk solution	40	mL
amph-D theory			
$\sigma_{chem,A}$	Chemical surface charge - acidic region (-0.26-0.35)	-0.61	M
$\sigma_{chem,B}$	Chemical surface charge - basic region (+0.26-0.35)	-0.09	M
υ_{mi}	Micropore volume	0.49	mL/g
C_S	Stern capacitance	160	F/mL
Dynamic theory			
p_{mA}	Macroporosity	0.48	
p_{mi}	Microporosity	0.25	
ωX	Membrane charge density	(-)2.5	M
k	Kinetic rate constant for macropore-micropore transport	1	s^{-1}
κ_D	Fitting parameter for the conductance of the bulk solution	$2.7 \cdot 10^{-6}$	m/s
κ_{mem}	Membrane transport rate constant	$1.0 \cdot 10^{-8}$	m/s

Table 6.2. Parameters for NMP-based electrodes.

Experimental			
M_e	Total mass of porous carbon layer	0.90	g
ρ_{elec}	Electrode mass density	0.40	g/mL
V_{bulk}	Volume bulk solution	40	mL
amph-D theory [299]			
$\sigma_{chem,A}$	Chemical surface charge acid region	-0.26	M
$\sigma_{chem,B}$	Chemical surface charge base region	+0.26	M
υ_{mi}	Micropore volume	0.47	mL/g
C_S	Stern capacitance	160	F/mL

6.4.2 Consecutive desalination cycles

Next, we show the results of salt adsorption for CDI and MCDI experiments conducted with A-electrodes. These experiments were conducted by alternatingly transferring the electrodes from the adsorption to the desorption container, as described in

section 6.3.3 (method ii). Theory lines shown in **Figure 6.3a** are based on equilibrium theory for CDI, and on dynamic theory for MCDI. The dynamic theory was adopted to include the non-ideal behavior of the IEMs. **Figure 6.3a** shows the salt concentration in the container at the end of each adsorption step as a function of the number of desalination cycles. With IEMs, after 4 desalination cycles, we see a decrease in the initial salt concentration of about 87%, while for CDI the decrease was about 52%. **Figure 6.3b** compares experimental data for energy consumption per mole of salt removed in CDI and MCDI. Energy consumption is calculated by integrating the current over time for the adsorption step and then multiplying by the charging voltage. As previously reported [44, 319], IEMs do not only enhance the performance of the system by increasing the salt adsorption, but also decrease the energy required for the adsorption of ions. Our results show that MCDI requires, on average, 57% less energy to remove an ion than CDI. When we compare our data with data reported in Ref. [143] for CDI, we observe that the energy consumption in our system is higher. We attribute the increased energy consumption to the presence of additional acidic groups in the A-electrodes and to higher resistance in bulk solution.

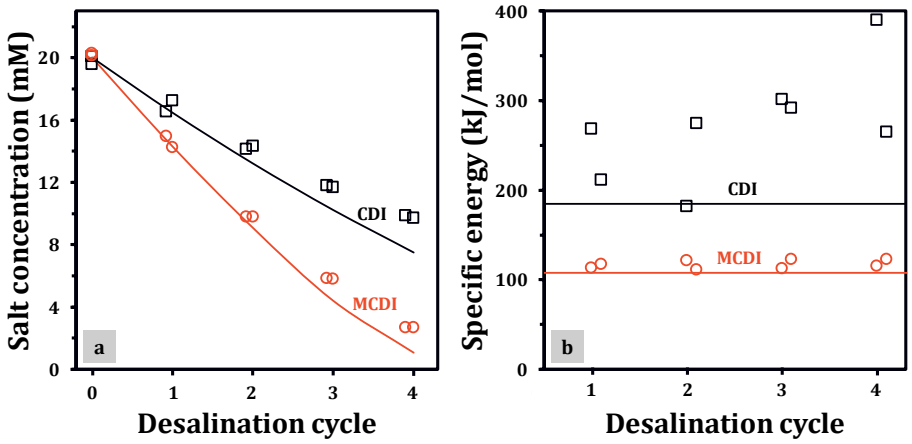

Figure 6.3. a) Concentration in the desalination chamber as a function of the cycle number. Two sets of experiments (symbols) are compared with theory (lines). b) Specific energy, i.e., energy per salt removed. Data is reported for A-electrodes without ion-exchange membranes (CDI) and with membranes (MCDI).

6.4.3 Dynamic salt adsorption

In this Section, we discuss experimental and theoretical results of dynamic ion adsorption in CDI and MCDI. For electrodes prepared with acetone, the theory includes parameters used in the amph-D model and additional parameters such as p_{mi}, p_{mA}, ωX, κ_D, κ_{mem}, and k. Porosities, p_{mi} and p_{mA}, are calculated as described in **S.I. 6.6.2**. The remaining parameters are treated as fitting parameters. When fitting κ_D and k using data from CDI experiments, we found that there is not a unique set of values that describe the experimental data, see **Figure S.I. 6.3a** and **Figure S.I. 6.3b**. Consequently, we decided to set k= 1 s^{-1}, which is in line with the approach taken in previous work [146, 299], because when $k \geq$ 1 s^{-1} there is no longer a rate limitation in the transport of ions from macro- to micropore; instead ion transport from macro- to micropore is at equilibrium.

With the value of k fixed, we then fitted κ_D. The values of ωX and κ_{mem} were fitted with MCDI experimental data. Both CDI and MCDI calculations include the additional surface charge that we assumed is present in A-electrodes.

Despite our theory describes CDI and MCDI data reasonably well, **Figure 6.4**, it is unclear whether the ion transport from macro- to micropore is rate-limiting since more than one set of values for k and κ_D can closely describe our experimental data. Although we did not include in our approach rate-limitation between macro- and micropores, this phenomenon may be important when we model ion adsorption in carbons with very small pores (sub-nm) [161], or thin electrodes with long macro- to micropore transport distances [45].

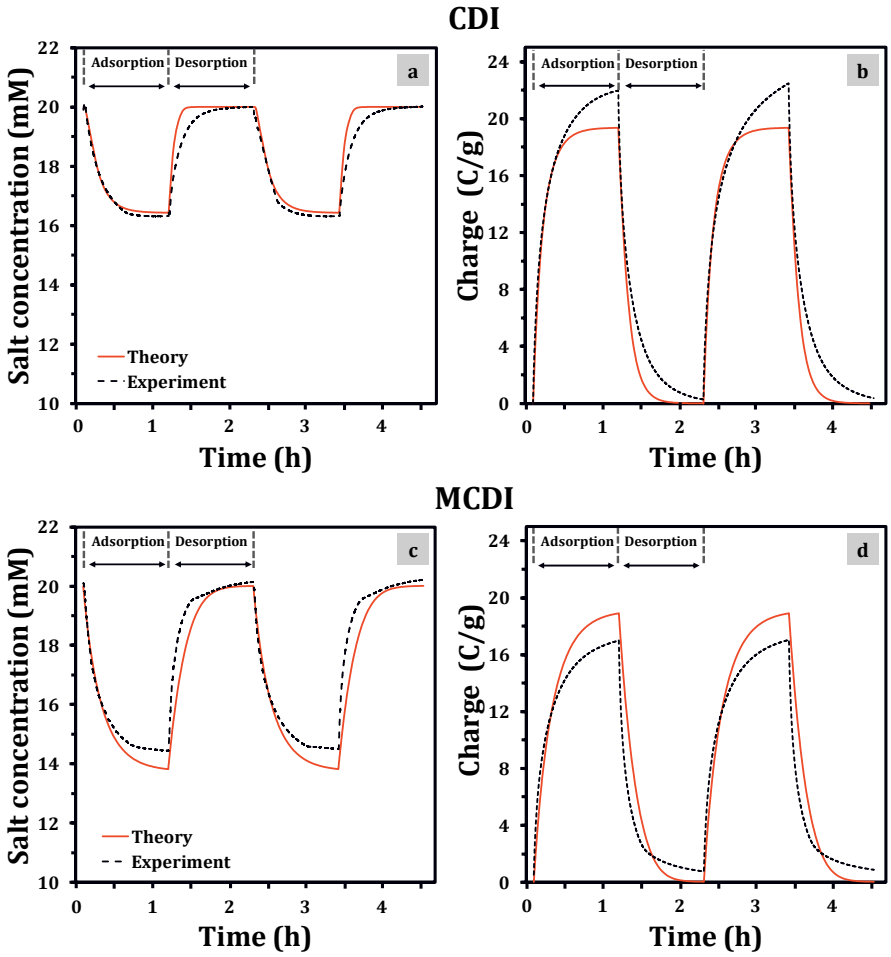

Figure 6.4. Comparison of the dynamic theory with experimental data. For CDI (A-electrodes without IEMs): a) salt concentration in the bulk, and b) charge per total mass of carbon as a function of time. For MCDI, i.e., A-electrodes with ion-exchange membranes: c) salt concentration in the bulk, and d) charge per total mass of the carbon coating as a function of time. From time 0 onwards, V_{ch}=1.2 V is applied, which is reduced to zero for the desorption step.

6.5 Conclusions

We extended dynamic theory for electrosorption of ions in porous carbon electrodes by including i) a chemical charge on the carbon surface to describe the electrical double layers and ii) a finite transport rate of ions from macro- to micropores. We used the theory to describe experimental data obtained in a CDI system. The CDI system has wire-shaped electrodes with and without coated ion-exchanges membranes. As we showed, the extended theory closely describes fundamental aspects of desalination cycles: salt concentration and charge. Additionally, it also captures the influence of chemical surface groups on the performance of the electrode.

Regarding ion transport from macro- to micropores, it was not possible to verify the influence of this phenomenon on the dynamics of the electrosorption process. This is because numerically we found more than one set of values for the kinetic rate constant, k, and the conductance of the bulk solution, κ_D, that describe our experimental data to the same degree.

We also compared salt adsorption of electrodes fabricated using two solvents, namely acetone and N-methyl-2-pyrrolidone (NMP). Results show lower salt adsorption for acetone-based electrodes (A-electrodes). This difference is not explained by differences in pore size distribution or pore volumes. We suggest that the lower salt adsorption for A-electrodes is due to an increase in the density of acidic groups on the surface of the electrodes. Titration experiments indeed confirm that A-electrodes possess a higher concentration of acidic groups compared to NMP-electrodes.

6.6 Supplementary information (S.I)

6.6.1 Mass balance for equilibrium theory

In a batch mode operated cell, the total amount of salt in the system remains the same over the whole process of desalination. Thus, for a system without membranes, the concentration of the bulk solution (c_{bulk}) is equal to the concentration in the macropores and the mass balance can be expressed according to the following mathematical expressions.

- At the beginning of the adsorption step

$$\text{Total Salt} = V_{bulk} \cdot c_{bulk,ads} + 2 \cdot V_{mA} \cdot c_{bulk,des} + \Gamma_{salt,des} \qquad \text{Eq. S.I. 6.1}$$

- At equilibrium (end of adsorption)

$$\text{Total Salt} = (V_{bulk} + 2 \cdot V_{mA}) \cdot c_{bulk,ads} + \Gamma_{salt,ads} \qquad \text{Eq. S.I. 6.2}$$

where subscripts 'ads' and 'des' refers to the adsorption step and desorption step, respectively. V_{bulk} is the volume of solution in the container, V_{mA} is the volume of the macropores, and Γ_{salt} is the salt adsorbed in the micropores and the end of each step.

6.6.2 Macro and micro porosities calculations

Considering an electrode structure where three kinds of pores can be distinguished, we can relate them by the following expression

$$p_{ma} + p_{mi} + p_{skeleton} = 1 \qquad \text{Eq. S.I. 6.3}$$

where each porosity is related to the density of the electrode (ρ_e) and the volume of the respective pore by

$$p_m = \upsilon_{mi,AC} \cdot \rho_e. \qquad \text{Eq. S.I. 6.4}$$

In the introduction section, we defined macro- and micropores. The term $p_{skeleton}$ accounts for the fraction of skeleton material (all solid components). This value is calculated by dividing ρ_e by the average mass density of the skeleton material ($\rho_{skeleton}$)

which considers 90% weight fraction of carbon material and 10% of the binder with mass densities of 1.95 g/mL and 1.78 g/mL respectively.

6.6.3 Gas sorption results. NDLFT analysis

We used the non-local density functional theory (NDLFT) method as a tool for calculating pore size distributions in the electrodes, those prepared with acetone and N-methyl-2-pyrrolidone. The results obtained are shown in **Table S.I. 6.1**. In **Figure S.I. 6.1**, we observe that the surface area and volume of the pores of the electrodes do not differ considerably between the acetone and NMP electrodes: this means, that we can obtain a similar pore distribution in the carbon layer by either using NMP or acetone as solvents.

Table S.I. 6.1. Pore area and volume determined by NLDFT method for electrodes prepared by using two different organic solvents.

	ACETONE	NMP
Total pore area, [m^2/g]	1120.6	1070.5
Micropore area, [m^2/g]	1096.1	1048.5
Mesopore area, [m^2/g]	24.5	22.0
Total pore volume, [mL/g]	0.56	0.53
Micropore volume, [mL/g]	0.49	0.47
Mesopore volume, [mL/g]	0.07	0.06

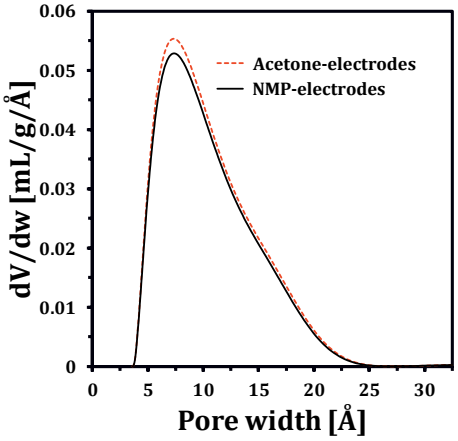

Figure S.I. 6.1. Differential pore size distribution obtained by NLDFT; where V is pore volume and w pore width**.**

6.6.4 Chemical surface charge NMP- and A-electrodes

To determine the total concentration of acidic groups on carbon particles, we performed potentiometric titrations of the electrodes. We used NaOH 0.5 M as reaction base and HCl 0.5 M as titrant. The concentration of acidic groups was obtained from the titration curve, **Figure S.I. 6.2**. At pH 7, when all the acidic groups are completely neutralized, the total concentration of acidic groups is -180 mM for NMP-electrodes and -430 mM for A-electrodes.

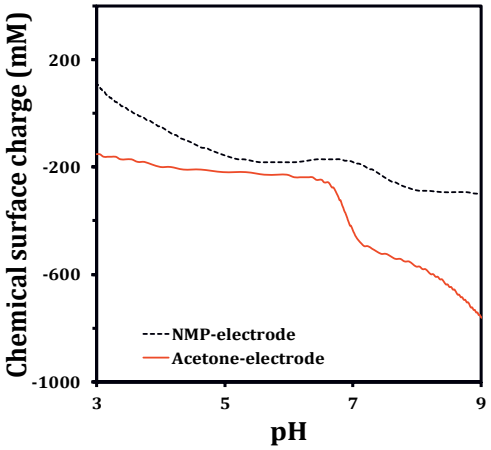

Figure S.I. 6.2. Surface chemical charge of NMP- and acetone-electrodes.

6.6.5 Variation of the fitting parameters k and κ_D

More than one set of values for k and κ_D can fit our experimental data. To obtain a direct view of this behavior we show in **Figure S.I. 6.3a** the salt concentration when k is varied and κ_D is fixed to 2.7e-6 m/s. We can see that when k=1 s^{-1} the theory describes reasonably well the experimental data. On the other hand, when the value of κ_D is varied and k is kept constant to 1e-3 s^{-1}, we obtaine **Figure S.I. 6.3b**. In this case, the theory describes the experiments when κ_D=3.2e-6 m/s.

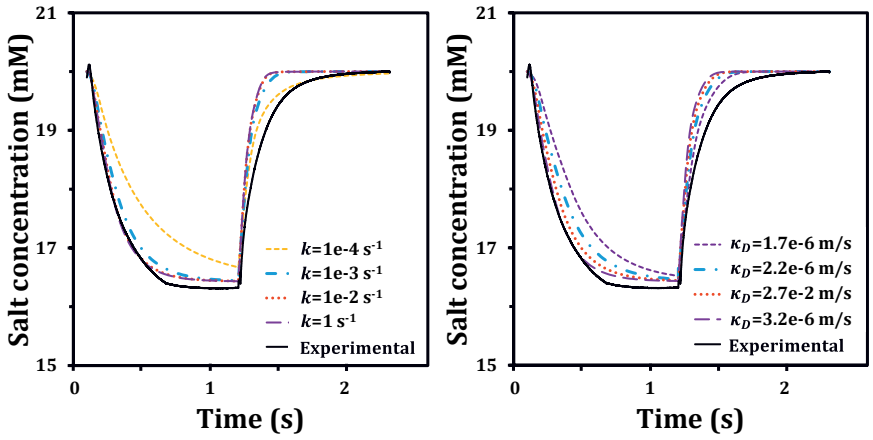

Figure S.I. 6.3. a) Variation of the kinetic rate constant (k) to fit the dynamic ion adsorption theory. In the calculation the value of κ_D was fixed to 2.7e-6 m/s. b) Variation of parameter for the conductance of the bulk solution (κ_D). In the calculation the value of k was fixed to 1.0e-3 s^{-1}.

Chapter 7

General discussion

7.1 Overview of this PhD thesis

This PhD thesis aims to study the selective separation of monovalent ions with similar hydrated size, such as nitrate (NO_3^-) and chloride (Cl^-), potassium (K^+) and sodium (Na^+) ions, using two electrochemical systems, namely capacitive deionization (CDI) and electrodialysis (ED). The research comprises a systematic evaluation of variables that influence ion selectivity (ion concentration, applied electrical potential, presence of competing ions). Additionally, theoretical frameworks were developed to describe ion adsorption in porous carbon electrodes (**Chapters 2** and **6**) and ion transport in IEMs (**Chapter 4**). An overview of the main findings of this thesis is given below.

Chapter 2. Selective adsorption of nitrate over chloride in microporous carbons

In this chapter, the effect of ion concentration and applied cell voltage on the selectivity of activated carbon powders and carbon electrodes is addressed. Results show that:

- activated carbon without any chemical modification, e.g., functionalization or oxidation of the surface, removes much more NO_3^- than Cl^- through adsorption, when no voltage is applied.
- at the beginning of the charging step, ion selectivity is influenced by the initial NO_3^-: Cl^- concentration ratio in the bulk solution. The anion with higher concentration in the bulk solution is predominantly electrosorbed compared to the anion with lower concentration.
- at equilibrium, nitrate is preferentially electrosorbed regardless of its initial concentration in the bulk solution. Overall, at equilibrium, NO_3^- selectivity does not depend on the initial ion concentration in the bulk solution, but it does depend on the applied cell voltage.

Chapter 3. Heterogeneous anion exchange membranes with nitrate selectivity and low electrical resistance

This chapter focuses on the fabrication and characterization of heterogenous anion-exchange membranes (AEMs). The selectivity in the membranes is evaluated in

different electrolyte solutions containing mono- and divalent anions and compared with that of commercial AEMs. This study revealed that:

- fabricating heterogeneous AEMs with a functionalized polymeric binder helps to overcome the high electrical resistance often associated with heterogeneous membranes. The electrical resistance of home-made AEMs was of the same magnitude as that of homogeneous membranes.
- increasing the hydrophobicity of the functional groups in AEMs leads to an increase in selectivity for NO_3^- over Cl^-. The NO_3^- selectivity prevailed even with multivalent ions such as SO_4^{2-} in the feed stream.

Chapter 4. Experimental and theoretical results point towards strategies to increase ion selectivity in electrodialysis

In Chapter 4, the performance of the home-made AEM with the highest selectivity for NO_3^- is further analyzed from an experimental and theoretical point of view in an ED system. We developed a theoretical model to describe selective ion transport across the membranes. Overall, the model describes:

- ion selectivity based on a membrane parameter referred to as the chemical affinity.
- selective transport of NO_3^- not only across the home-made membrane but also across commercial heterogeneous and homogenous AEMs.

Theoretical calculations provide insights into possible strategies to increase ion selectivity, specifically NO_3^- selectivity in AEMs. These strategies include i) increasing the chemical affinity, ii) increasing the membrane thickness, or iii) decreasing the membrane charge density.

Chapter 5. Cation exchange membrane behavior of extracellular polymeric substances (EPS) in salt adapted granular sludge

In this chapter, a novel approach for the fabrication of selective ion-exchange membranes (IEMs) is evaluated, which is based on the use of biopolymers. Two different membranes were fabricated using alginate and extracellular polymeric substances (EPS) extracted from anaerobic granular sludge adapted to high salinity

(NaCl 0.87 M). An important characteristic of the membranes was their preferential transport of cations, and interestingly selective transport of K^+ over Na^+. However, the membranes showed relatively low stability in aqueous electrolytes: visible EPS detachment was observed after 48 h exposure of the membranes to water. Therefore, further research should focus on improving membrane stability.

Chapter 6. Capacitive deionization with wire-shaped electrodes

The removal of ions from aqueous solutions is evaluated in a CDI cell consisting of wire-shaped carbon electrodes, unlike the CDI cell used in **Chapter 2** with flat carbon electrodes. A thin layer of ion-exchange membranes was coated on the surface of each electrode, which leads to an increase in the desalination capacity of the CDI system. Furthermore, **Chapter 6** shows that the type of solvent used in the fabrication of carbon electrodes impacts their salt adsorption capacity. Acetone increases the amount of acidic groups on the surface of carbon electrodes. This increase of acidic groups leads to a reduction in salt adsorption capacity compared to electrodes for which N-methyl-2-pyrrolidone is used as a solvent.

Ion selectivity in CDI and ED

Overall, results obtained throughout this PhD thesis indicate that selectivity results from the interplay between the properties of the ions, the properties of the main constituents of the electrochemical system, i.e., carbon electrodes in CDI and IEMs in ED, and operational parameters. Physicochemical properties of the target and competing ions, especially the hydrated size and hydration energy, were shown to have a significant effect on ion selectivity.

In the following sections, a broader discussion on ion selectivity is given on the basis of one physicochemical property: ion hydration. It is argued that ion hydration is the key property influencing the extent of ion selectivity in porous carbons and IEMs. Further, the implications of the chemical affinity term for describing ion selectivity in IEMs are rationalized. Also, the possible definitions of the separation factor as an indicator of ion selectivity in porous carbon and IEMs are discussed. Finally, an analysis is given on the viability of using IEMs to selectively remove ions with significantly lower

concentrations in the feed stream compared with competing ions. As an example, the selective removal of lithium ions (Li^+) from seawater is analyzed.

7.2 Ion hydration is the key to understand ion affinity in porous carbon

In **Chapter 2**, we show that selectivity between monovalent anions in porous carbon electrodes is a time-dependent process. This time-dependent behavior relates to the constant rearrangement of the electrical double layer (EDL): previously adsorbed anions are exchanged for different anions (ion displacement). Such ion displacement was observed not only in studies conducted with electrolyte solutions containing NO_3^-/Cl^- but also with NO_3^-/I^-, see **Chapter 2*: S.I***.

Our studies with monovalent anions highlight the effect of the EDL dynamics on ion selectivity. At the beginning of the electrosorption step (short adsorption time), kinetics favor the adsorption of the anion with higher mobility, but at equilibrium (longer adsorption time) the adsorption of anions with higher affinity for the micropores is favored. These results give rise to several questions to which we currently have no clear answers, for instance, what factors drive ion affinity in the EDLs? Is ion displacement a phenomenon related to ion properties, e.g., ion size, or to carbon properties, e.g., pore size?

To rationalize the possible factors that influence the distribution and concentration of ions in the EDLs, and overall selective ion adsorption, we first point out that affinity, in the context of this discussion, is viewed as the tendency of an ion to be preferentially adsorbed at the carbon particles. This tendency is the result of a variety of interactions occurring in the micropores, i.e., ion-carbon, ion-water, ion-ion, and it is directly related to the carbon nature and ion properties. Functional surface groups, such as lactones, carboxylic acids, and phenols, influence most of the properties exhibited by carbon materials. These groups can confer a hydrophobic/hydrophilic nature to the surface and also mediate the adsorption of certain ions [152, 153, 320]. On the other hand, water influences most of the physicochemical properties of the ions, e.g., hydration energy and size.

In the constrained environment inside the micropores, ions can undergo a change in size and shape due to dehydration or reorientation/rearrangement of water molecules associated with them. These changes would impact the degree of hydration of the ions and directly affect the distribution and concentration of ions in the EDLs. Numerous studies have reported the important role of hydration in determining specific interactions of ions with charged surfaces and for the structure of EDLs [321-326]. Thus, ion hydration may play an important role in the occurrence of ion displacement in the EDLs, or absence thereof, and more importantly on the ion affinity.

A better understanding of the changes occurring in the EDLs, and the role of ion hydration, requires analyzing the EDL structure not only at the macroscopic level, i.e., EDL formation, but also at the atomistic/nano level to trace the evolution of the ions during electrosorption. Analytical techniques such as x-ray photoelectron spectroscopy (XPS) and x-ray diffraction (SXRD) can provide insights into the structure and composition of the EDLs. These techniques measure the electrostatic potentials, more specifically the energy of electrons, that chemical species experience as they move away from charged surfaces. For instance, analyses of various charged surfaces, e.g., minerals such as mica, have revealed that ions are distributed in the EDLs forming layers, one closer to the charged surface (inner layer) and another farther away (outer layer) [327-329]. In the inner layer, ions are partially dehydrated, whereas in the outer layer ions retain their hydration shell. Numerical simulations that account for the discrete nature of the ions, e.g., molecular dynamics simulations and that consider effective ion size (including hydration) can also help to assess the role of ion hydration on the EDLs formation and ion selectivity. Molecular dynamics (MD) simulations have been used to investigate at the atomic level the mechanisms of ion adsorption on charged surfaces [330-332]. The output of MD simulations provides insights into i) the strength of the interactions among ions, water, and surface, ii) degree of ion hydration, and iii) the effect of ion type on the EDLs structure.

7.3 Ion hydration is the key to understand selectivity in IEMs

In **Chapter 3**, we used the difference in hydration energy between monovalent counterions with similar size as an argument to rationalize selectivity in AEMs. The rationale behind this came from studies that show that ions establish more favorable interactions with the surroundings when they overcome the energy barrier required to undergo dehydration, i.e., the partial or complete loss of water molecules from the hydration shell [213, 333-336]. Calculations of the energy barriers—using Arrhenius-type equations—at membrane-solution interfaces point out a correlation with ion hydration energy [204, 337, 338]. This argument is used to support the validity of membrane selectivity promoted by ion dehydration. However, it does not provide direct evidence that all ions undergo dehydration when permeating the membranes, or to what extent ions dehydrate.

The degree of ion hydration is likely to be affected by the chemical environment in the membranes—polymeric matrix, ion-exchange sites, and the presence of other ions. Consequently, ions would be more or less hydrated depending on the membrane characteristics and even on operational conditions, e.g., applied electrical potential. We argue that ion hydration could explain the selectivity trends observed in different membranes because it relates to the number of water molecules directly associated with the ions [339], and this number influences the interaction with the membrane structure.

Reliable quantification of ion hydration is crucial to understand ion selectivity in different membranes. However, this quantification is challenging mainly due to the limitation of current analytical techniques to separate the signals of water associated with different ions. Additionally, in an ED process, it is difficult to make a clear distinction between water transported by the ions due to friction (electro-osmosis) and water transported in the hydration shells of the ions [340, 341]. Developments in analytical methods are required for a detailed analysis of ion hydration in the membranes. We believe that insight into ion hydration will improve the understanding

of ion selectivity, which in turn will help to predict more consistent selectivity trends for monovalent ions and also mixtures of ions with different charge sign and size.

7.4 The affinity term and the prediction of ion selectivity in IEMs

To numerically describe ion selectivity in IEMs, at least two different approaches, which translate into two different mathematical models, are available. The first approach is to consider that ion selectivity is driven by the affinity of the membranes towards a specific counterion. This approach leads to the transport theory outlined in **Chapter 4.** And, as shown in that chapter**,** selectivity between ions with the same charge sign and hydrated size is well described**.** In this theory, the membrane affinity was not associated with any particular physicochemical property of the ions or the membrane, or any effect resulting from their interaction. Instead, affinity values are derived by fitting theory to experimental data obtained by measuring ion adsorption across a range of solutions with different NO_3^- and Cl^-concentrations.

The second approach assumes that ion selectivity is the result of competitive adsorption involving a specific counterion, e.g., NO_3^-, and the ion-exchange sites (ES). This adsorption can be seen as a reversible reaction given by

$$NO_3^- + ES^+ \rightleftharpoons NO_3^- - ES^+$$

We can use a simple Langmuir isotherm equation to describe the equilibrium state of the adsorption as a function of the counterion concentration and the number of free and occupied adsorption sites.

$$c_{\mathrm{m},NO_3^-,\mathrm{bound}} = \frac{N_{\max} \cdot c_{\mathrm{m},NO_3^-,\mathrm{mobile}}}{k_{NO_3^-} + c_{\mathrm{m},NO_3^-,\mathrm{mobile}}} \qquad \text{Eq. 7.1}$$

where $N_{\max}$ represents the maximum number of adsorption sites, which in the context of IEMs is directly related to the charge density of the membrane (X). The ion-exchange sites can be occupied by nitrate that is bound ($c_{\mathrm{m},NO_3^-,\mathrm{bound}}$) or by nitrate that is mobile and transported across the membranes ($c_{\mathrm{m},NO_3^-,\mathrm{mobile}}$). $k_{NO_3^-}$ is a fitting parameter

related to the number of ion-exchange sites available for ion transport. The higher the value of $k_{NO_3^-}$, the lower the $c_{m,NO_3^-,bound}$.

Therefore, the total concentration of nitrate in the membranes consists of bound and mobile NO_3^-

$$c_{m,NO_3^-,Total} = c_{m,NO_3^-,mobile} + c_{m,NO_3^-,bound}. \quad \text{Eq. 7.2}$$

With this second approach, we derive a theoretical framework to describe ion transport that includes Eq. 7.1 and Eq. 7.2, and the set of equations outlined in **Chapter 4**, except the equation for the ion concentration at the solution/membrane interface, which is now given by

$$c_{sc/m,j} = c_{sc,j} \cdot \exp(-z_j \cdot \Delta\phi_{D,sc/m}). \quad \text{Eq. 7.3}$$

We used this approach to describe selectivity between NO_3^- and Cl^- in the home-made membrane (CB-hAEM). Results in **Figure 7.1a** show that regardless of the value of $k_{NO_3^-}$, we cannot fit the theory to predict the selectivity of NO_3^- over Cl^-observed experimentally. Overall, this approach predicts that there is more NO_3^- than Cl^- in the membrane. However, part of NO_3^- is bound to the exchange sites and does not take part in the transport across the membranes. This implies, that selective ion adsorption does not necessarily lead to selective ion transport through the membranes. This result further supports the approach that ion selectivity is directly linked to the membrane affinity for a specific counterion. However, additional studies are required to find correlations between the membrane affinity and physicochemical properties of the ions. Following the discussion in the previous section, ***section 7.2***, we suggest looking into correlations based on ion hydration. The work of Gur et al. [342] and Guzman et al. [232] can be used as a starting point. They included hydration forces acting on the ions in a solid-water interface as a function of the size and charge of the ions, as well as the dielectric constant of the solvent. Guzman et al. [232] pointed out that not including the hydration effects leads to some inaccuracies in the model, for instance, the flux of co-ions is significantly overestimated.

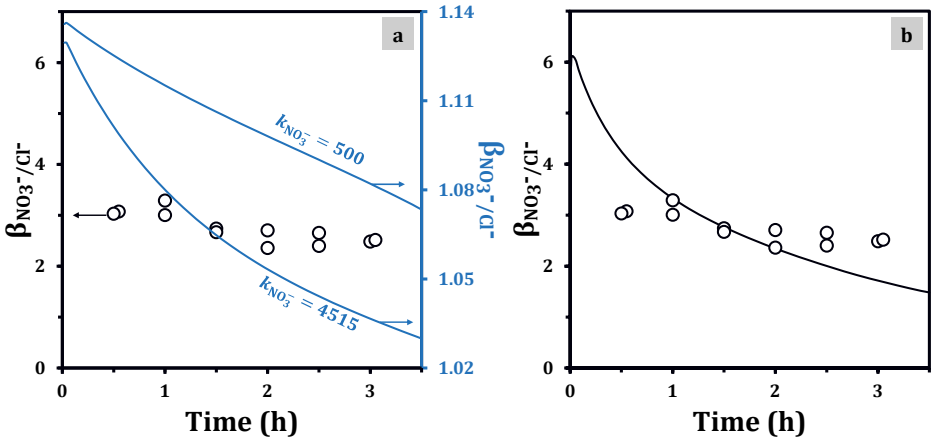

Figure 7.1. Comparison of the separation factor ($\beta_{NO_3^-/Cl^-}$) obtained experimentally for the CB-hAEM (symbols) and using transport theory (lines) that assumes: a) adsorption, and b) chemical affinity. Parameters used in the models are given in **Chapter 4**.

7.5 The separation factor. A metric to compare ion selectivity in CDI with other studies

In the field of CDI, there are standardized metrics to describe the performance of the system and establish comparisons between different CDI systems. These metrics are mostly based on material properties, the throughput of a desalination unit, and energy consumption, e.g., salt adsorption capacity (mg/g of both electrodes: cathode and anode) and energy consumption per mol of salt removed (in kJ/mol kJ/g, or kT /ion) [45, 343]. However, so far, there are no standardized metrics for evaluating electrosorption selectivity in CDI. The problem that arises with this lack of standardization is that often there is not enough data to compare ion selectivity achieved in different studies. Most studies only include data comparing the decrease in ion concentration in the bulk solution.

Several parameters affect ion selectivity in CDI, including the electrosorption time, applied electrical potential, the pore size of carbon particles, and the concentration of target ions, and competing ions. Therefore, the challenge is to establish an insightful

way to quantify ion selectivity. In **Chapter 2**, we quantify ion selectivity by calculating a separation factor given by

$$\beta_{A/B} = \frac{IAC_A}{IAC_B} \cdot \frac{c_{mA,B}}{c_{mA,A}} \qquad \text{Eq. 7.4}$$

where subscripts A and B represent two ionic species, and where IAC is the ion exchange capacity (mg/g of electrode), and c_{mA} is the concentration of ions (A or B) in the macropores, which in CDI with porous carbon electrodes is, in equilibrium, equal to the concentration in the bulk solution.

The separation factor ($\beta_{A/B}$) indicates how effectively ion A is removed from the bulk solution compared to ion B. It is based on a relevant performance metric, the IAC, which can be calculated for electrosorption processes with various time durations. The separation factor measured at any time before equilibrium is reached gives insights into the time-dependent behavior of ion selectivity. On the other hand, the separation factor measured at equilibrium ($eq\beta_{A/B}$) provides information about the maximum ion separation that can be achieved during electrosorption. Importantly, $eq\beta_{A/B}$ is not affected by the initial ion concentration of the feed stream (see **Chapter 2**). It is apparent that measuring $eq\beta_{A/B}$ can be an insightful way to characterize ion selectivity of the electrode material because time effects are excluded. However, if ion selectivity shows strong time-dependency, then $\beta_{A/B}$ values should be reported as a function of time.

In **Chapter 2**, we reported values of $\beta_{NO_3^-/Cl^-}$ measured at equilibrium conditions across a range of applied cell voltages: $\beta_{NO_3^-/Cl^-}$ values ranged from ~ 9 at 0.6 V to ~ 6 at 1.2 V. To put these values into perspective, we calculated $\beta_{A/B}$ for a variety of selectivity studies, which include ion pairs other than the nitrate-chloride pair, carried out over several conditions: constant voltage, constant current, and different ion concentrations. **Figure 7.2** provides a good overview of the maximum $\beta_{A/B}$ values achieved in different CDI configurations: CDI with porous carbon (I), CDI with modified carbon electrodes (II), i.e., electrodes functionalized or oxidized, MCDI with commercial membranes (MCDI, III), MCDI with modified or home-made membranes (IV), and

Hybrid CDI (V). In the case of anion selectivity, most values of $\beta_{A/B}$ are lower than 8. On the other hand, for cations, $\beta_{A/B}$ values of 7 and 24 were obtained with Ca^{2+}/Na^{+} mixtures in CDI [52]. These $\beta_{A/B}$ values are encouraging; however, they were achieved at equilibrium, which often includes long electrosorption times. The long desalination times required to achieve such ion selectivity certainly represent a constraint when considering CDI as an economically viable technology for selective ion separation.

A game-changer in the way ion selectivity can be achieved in CDI systems is by using intercalation or redox materials as electrodes (Hybrid CDI). Hybrid CDI has been increasingly used to selectively separate cations because it achieves significantly higher selectivity compared to other CDI systems (**Figure 7.2b**). Hybrid CDI has not been widely used to selectively separate anions. However, we foresee that more studies will seek to achieve practically valuable ion separations using hybrid CDI.

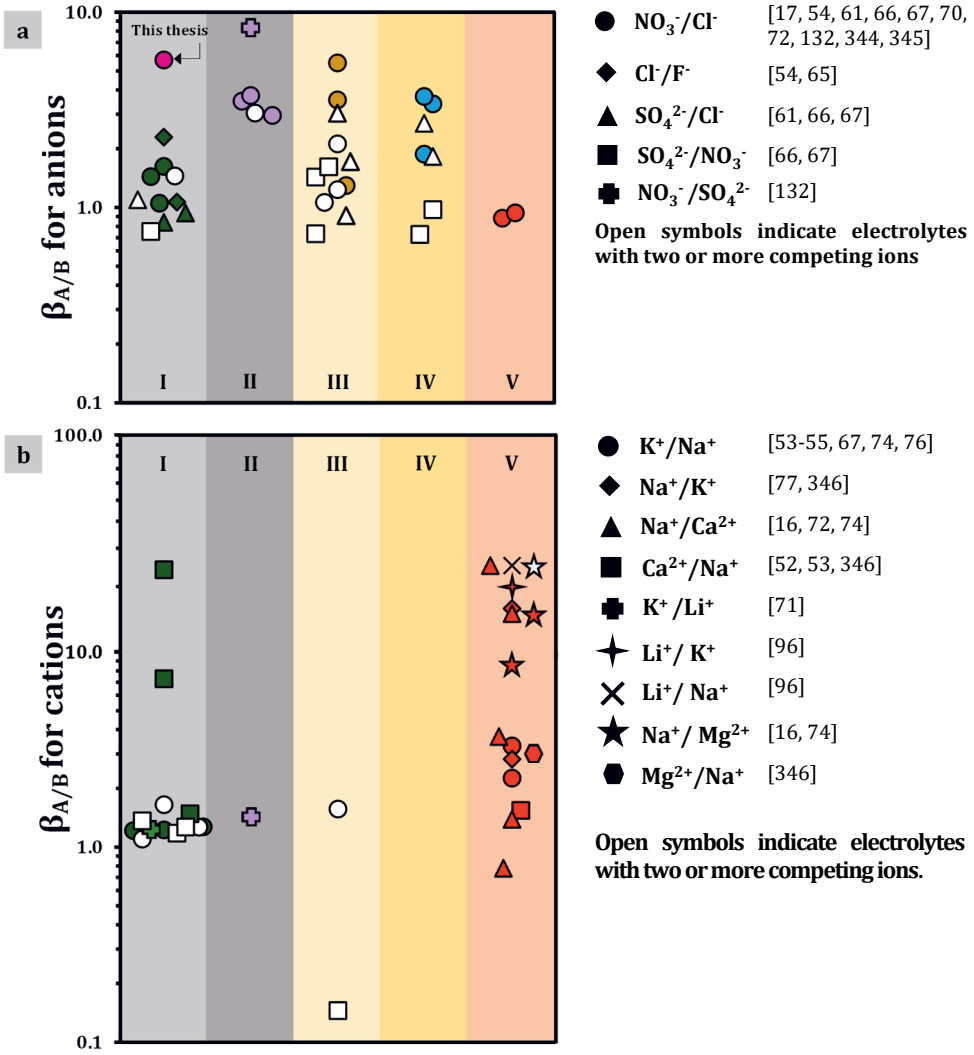

Figure 7.2. Experimental values of the separation factor ($\beta_{A/B}$) calculated for different CDI architectures: I=CDI; II= CDI with carbon modification; III=MCDI; IV=MCDI with membrane modification; and V= Hybrid CDI. Panel (a) shows $\beta_{A/B}$ values for anions, and panel (b) for cations. Data includes studies carried out at constant current (CC) and constant voltage (CV).

7.6 What can the separation factor tell about the performance of IEMs?

The potential application of IEMs for selective ion separations has prompted research focus on developing new membranes with improved selectivity towards specific counterions. Numerous studies have reported IEMs with increased selectivity towards Li^+ [347-349], Na^+ [18, 350] , K^+ [351], NO_3^- [107], among others. However, comparisons between different studies are difficult, given the variety of methods used to measure and quantify ion selectivity. In ED, the selectivity of IEMs for different counterions is often quantified with a separation factor given by [15, 352-355]

$$\beta_{A/B} = \frac{J_A}{J_B} \cdot \frac{c_{d,B}}{c_{d,A}} \qquad \text{Eq. 7.5}$$

where subscripts A and B indicate the ionic species, J is the ionic flux through the membranes, and c_d is the ion concentration in the diluate compartment.

The separation factor ($\beta_{A/B}$) described in Eq. 7.5 is a measure of the transport of ion A relative to that of ion B. It indicates how efficiently the ion separation is performed [354]. In this definition of $\beta_{A/B}$, ion selectivity directly depends on the ion concentration in the feed solution. To assess what impact the ion concentration has on $\beta_{A/B}$, we used the numerical model developed in **Chapter 4**, to calculate $\beta_{NO_3^-/Cl^-}$ for different NO_3^- and Cl^- concentrations in the feed solution and for two current densities: 20 and 10 A/m^2. **Figure 7.3** shows $\beta_{NO_3^-/Cl^-}$ as a function of the NO_3^-:Cl^- concentration ratio in the feed solution for an ED system operated in continuous mode. In **Figure 7.3,** we can distinguish three main regions: the first region, where $\beta_{NO_3^-/Cl^-}$ hardly changes with increasing NO_3^-:Cl^-concentration ratio, includes the lowest value of $\beta_{NO_3^-/Cl^-}$ (~ 1.6 at 20 A/m^2 and ~ 1.4 at 10 A/m^2) obtained when the NO_3^- concentration in the feed solution is almost negligible (NO_3^-:Cl^-concentration ratio ~1e^{-3}). In the second region, we observe a linear relationship between $\beta_{NO_3^-/Cl^-}$ and the NO_3^-:Cl^- concentration ratio. In this region, $\beta_{NO_3^-/Cl^-}$ ranges from 1.8 to 2.9 and from 1.6 to 2.3 at 20 and 10 A/m^2, respectively. The third region shows that increasing the concentration of NO_3^- in the

feed stream does not necessarily lead to a significant increase in $\beta_{NO_3^-/Cl^-}$. The maximum values of $\beta_{NO_3^-/Cl^-}$, obtained at relatively high NO_3^- concentration, are ~ 3.1 at 20 A/m^2 and 2.6 at 10 A/m^2.

Overall, **Figure 7.3** gives a clear indication that for any given membrane, the reported value of $\beta_{A/B}$ only reflects the ion separation attained under specific ion concentrations. In this regard, reporting ion selectivity, $\beta_{A/B}$, as a function of the ion concentration provides more insights into ion separation efficiency, which is more useful from an engineering perspective. Certainly, several other factors affect selectivity in the membranes, such as the applied electrical potential and the presence of competing ions. That is why it is imperative to have consensus about how to measure and quantify ion selectivity to benchmark membrane performance.

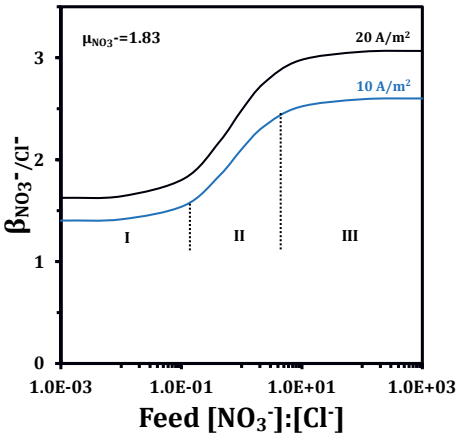

Figure 7.3. Separation factor ($\beta_{NO_3^-/Cl^-}$) as a function of the NO_3^-: Cl^- concentration ratio for two applied current densities: 10 A/m^2 and 20 A/m^2. ED system operated in continuous mode, 10 cell pairs, membrane area= 100 cm^2, and $\phi_{sc} = 1.5$ mL/min.

7.7 Can ED selectively remove ions present at very low concentrations in aqueous solutions?

One potential application of ion-selective technologies is the removal of $Li^+$from seawater. It is estimated that the oceans have around 231 billion tons of Li^+ [356]. This amount is four orders of magnitude higher than the amount reported to exist in brine

deposits and lithium ores combined. The main hurdle for Li^+ removal from seawater is the low concentration, approx. 0.17 ppm [357], compared to the concentrations of 300-700 ppm in salt lake brines (salars) [358]. So, the question is: can technologies such as ED selectively and efficiently remove lithium from seawater?

In this section, we provide a framework to analyze the viability of selective Li^+ removal from seawater based on calculations using the numerical model outlined in **Chapter 4**. To this end, we made the following assumptions: i) ED system operated in continuous mode. ii) The feed solution is comprised of Na^+, Li^+, and Cl^-. iii) The initial concentration of Na^+ and Li^+ are 450 mM and $2.5 \cdot 10^{-2}$ mM, respectively. And iv) the CEMs are selective towards Li^+ with an affinity μ_{Li^+}. All parameters included in the model are listed in **Table 7.1**.

We calculate the separation factor of Na^+/Li^+, β_{Li^+/Na^+}, when the μ_{Li^+} term in the CEMs is varied. The output of the theoretical calculations shows that $\beta_{Li/Na}$, as expected, increases with increasing μ_{Li^+} (**Figure 7.4**). However, increasing μ_{Li^+} is not enough to achieve significantly high Li^+ concentrations in the outlet stream (concentrate spacer channel). The Na^+: Li^+ concentration ratio in seawater (feed stream) is $1.8 \cdot 10^4$. This concentration ratio decreases to $1.67 \cdot 10^4$ (in the concentrate spacer channel) when the affinity of the CEM is $\mu_{Li^+} = 3$, and to $1.38 \cdot 10^4$ when $\mu_{Li^+} = 5$ (**Figure 7.4**).

Overall, the results show that it is possible to remove Li^+ from seawater using selective membranes. However, having CEMs with high selectivity for Li^+ is not a guarantee that the process is economically viable—after the recovery process, the concentration of Li^+ in the concentrate channel remains low: ~0.2 ppm. Note that the concentration of Li^+ reached after solar evaporation of salt lake brines is ≥ 6000 ppm [359]. Thus, the challenge of recovering Li^+ from seawater is not necessarily related to overcoming the low affinity for Li^+ in the membranes, but related to the low concentration in which this ion is found in the feed stream. High volumes of seawater would need to be processed to recover moderate Li^+concentration. Stamp et al. [360] modeled the production of lithium from seawater using ion-exchange technologies. According to the authors, approximately 5000 m^3 of seawater is required to obtain 1 kg of lithium carbonate (Li_2CO_3). To put this number in perspective, a full battery electric vehicle (EV) requires

approx. 1 kg of Li_2CO_3 per kWh of battery's capacity [361]—the Tesla model S EV has a battery of 100 kWh capacity [362].

Certainly, improving the selectivity of CEMs towards Li^+ is of technological relevance. However, efforts should be directed to use selective membranes to remove Li^+ from more concentrated water streams, such as reverse osmosis concentrate or salt lakes brines. But using Li^+-rich streams create other technological challenges mainly associated with the high salinities of the streams—the total dissolved solids (TDS) of salar brines is on average 170-400 g/L [359]. In these high-TDS streams, other ions than Na^+ are in significantly high concentrations, e.g., Mg^{2+}, Ca^{2+}, and K^+, [363]. Therefore, the efficiency of the recovery process will considerably depend on the affinity of the membranes for Li^+ and the high rejection of other counterions. Even when the technical issues associated with high TDS are resolved, achieving significant Li^+ concentration will likely require a multi-stage process in which Li^+ is enriched in the concentrate streams of serially connected ED units. The number of stages will directly depend on the affinity of the membranes towards Li^+: the higher the affinity the fewer stages needed to enrich Li^+ to concentrations that allow economically feasible ED operations.

Sustainability of the widely used lithium mining process

Solar evaporation is the common practice used to concentrate lithium found in salt lake brines [358, 364]. A large amount of water is lost to evaporation during this process, which is then needed in the downstream process to recover and purify lithium compounds (mainly lithium carbonate) [359]. The freshwater used downstream is taken from water reserves surrounding the lithium-brine mines. Most of the world's lithium-brine mining takes place in arid regions—Andean regions of Argentina, Bolivia, and Chile [365, 366]—, all of which often face severe water problems. Thus, this widely used practice of lithium mining puts more stress on fragile water ecosystems, which are vital water supplies for communities living in the proximities of the mining facilities.

Table 7.1. Parameters used in the ED model to predict Li^+ removal from seawater.

Operational			
I	Current density	50	A/m^2
Φ	Flow rate in concentrate and diluate streams	500	L/h
Φ_{sc}	Flow rate in each spacer channel	10	L/h
ED unit			
δ_{sc}	Spacer channel thickness	500	μm
N_{cell}	Number of cell pairs	10	
A_{mem}	Membrane area	0.1	m^2
Ion exchange membranes			
X	Charge density	5	M
δ_m	Membrane thickness	150	μm
Diffusion coefficient of ions in water ($D_{\infty,j}$)			
D_{∞,Li^+}	Lithium	$1.03 \cdot 10^{-9}$	m^2/s
D_{∞,Na^+}	Sodium	$1.33 \cdot 10^{-9}$	m^2/s
D_{∞,Cl^-}	Chloride	$2.03 \cdot 10^{-9}$	m^2/s
Diffusion coefficient of ions in the membrane ($D_{m,j}$)			
D_{m,Li^+}	Lithium	$1.03 \cdot 10^{-11}$	m^2/s
D_{m,Na^+}	Sodium	$1.33 \cdot 10^{-11}$	m^2/s
D_{m,Cl^-}	Chloride	$2.03 \cdot 10^{-11}$	m^2/s

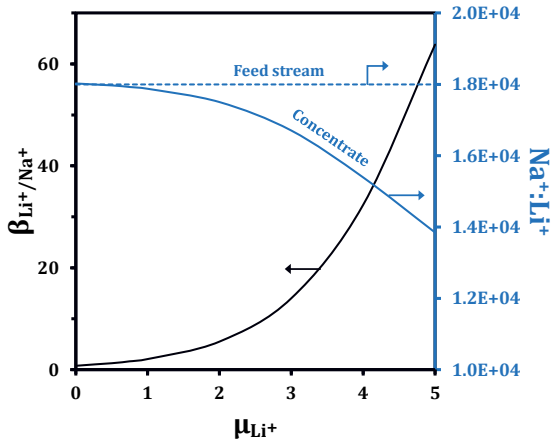

Figure 7.4. Theoretical results for the separation factor, $\beta_{Li/Na}$, and the Na^+: Li^+ concentration ratio in the feed stream (seawater) and the concentrate flow channel of an ED stack.

Summary

Selective ion removal in electrochemical processes

Summary

Ion selectivity is regarded as the ability of a system to remove specific ionic species from multi-ionic mixtures. In this PhD thesis, two electrochemical systems, namely capacitive deionization (CDI) and electrodialysis (ED), were studied for their potential to achieve selective ion separations relevant to a wide variety of applications. One such application is the removal of chemical contaminants from waters intended for human consumption. For instance, in groundwater, chemical substances from natural sources or human activities, such as nitrate, fluoride, arsenic compounds, and heavy metals, can pose a threat to the environment and human health when their concentrations are above a certain threshold. Selective removal of these contaminants is challenging mainly due to the presence of interfering ions with much higher concentrations, e.g., chloride. Another application is the recovery of valuable ions such as lithium from seawater and rare earth elements (REE) from waste streams. Lithium and REE are in high demand because they are used in the fabrication of numerous products and goods. Lithium is the key component of batteries for electronic devices and electric vehicles, whereas REE are used in magnetic, luminescent, and catalytic materials.

This PhD thesis combines the study of the selective separation of monovalent ions in CDI and ED from an experimental and theoretical perspective. The thesis starts with an overview of studies focused on ion selectivity in CDI and ED. **Chapter 1** gives insights into the several factors that affect ion selectivity: ion concentration and composition of the feed stream, applied electrical potential, physicochemical properties of the ions, the carbon electrodes, and the membrane. In **Chapter 2**, selectivity between nitrate (NO_3^-) and chloride (Cl^-) in microporous carbon is studied. The results reveal that during adsorption (i.e., without applying a voltage) and electrosorption (i.e., when a voltage is applied between two carbon electrodes) activated carbon removes much more NO_3^- than Cl^-. During electrosorption, ion selectivity is time-dependent, which indicates that the electrical double layers (EDLs) constantly rearrange their structure. Chloride that has been adsorbed at early stages during electrosorption is displaced by NO_3^-. Consequently, displaced Cl^- ions desorb from the EDLs and return to the bulk solution. When equilibrium is reached, the selectivity of NO_3^- over Cl^- is measured in the EDL.

This selectivity for NO_3^- is observed regardless of the initial NO_3^-: Cl^- concentration ratio in the feed solution. Nevertheless, the NO_3^- selectivity gradually decreases with increasing the charging voltage. When no voltage is applied the separation factor ($\beta_{NO_3^-/Cl^-}$), which is the ratio of ion adsorption capacity normalized by the bulk concentration, is ~ 10. However, when the charging voltage increases to 1.2 V, $\beta_{NO_3^-/Cl^-}$ decreases to ~6.

In this study, it is pointed out that ion selectivity is the result of the affinity between carbon and ions. Moreover, it is assumed that selectivity is not the result of rearrangements of the hydration shell, e.g., partial loss of water molecules, of the ion with lower hydration energy, i.e., NO_3^-. The reasoning behind this assumption is that the mean size of the carbon pores is larger than the hydration shells of the adsorbed ions. Additionally, a numerical model is developed based on a modification of the amphoteric Donnan model, which includes an additional affinity of NO_3^- to carbon. Good agreement between experimental results and the theory is found. Results show that the affinity-effect for NO_3^- plays an important role during adsorption and electrosorption. Overall, the study of ion selectivity in microporous carbon provides new insights into the importance of carbon-ion interactions for electrochemical water desalination.

In **Chapter 3,** ion selectivity is studied in newly-designed heterogeneous anion-exchange membranes (AEMs). The membranes were fabricated using a functionalized (charged functional groups) polymeric binder and three ion-exchange resins with alkyl groups with different hydrophobicity, i.e., methyl, ethyl, and propyl substituents, respectively. The study highlights the influence of hydrophobicity in the membranes on selectivity. Increasing the length of the alkyl group, and therefore hydrophobicity, leads to an increase in the selectivity for NO_3^-. This NO_3^- selectivity is observed in multicomponent solutions containing monovalent ions such as Cl^- and iodate (IO_3^-), and multivalent ions such as sulfate (SO_4^{2-}). In electrolyte solutions containing monovalent ions with similar hydrated size, i.e., NO_3^- and Cl^-, selectivity can be related to the differences in hydration energy of the ions. We argue that the membranes are more selective for the ion with lower hydration energy, i.e., NO_3^-, because it can potentially dehydrate more easily and establish stronger interactions with the ion-

exchange sites. However, for monovalent ions of different size, selectivity trends cannot be reported on the basis of hydration energy. In this case, it is assumed that the chemical structure of the membrane hinders the transport of larger ions.

In **Chapter 4**, we further study the performance of the home-made AEMs that showed the highest selectivity for NO_3^- in an ED cell. The nitrate selectivity of this membrane was higher than that of two commercial AEMs. We explore methods to enhance the NO_3^- selectivity in AEMs using theory. Theoretical results point that suitable strategies to improve ion selectivity are: increasing the chemical affinity or thickness, or decreasing the charge density in the membranes. Overall, this study gives insights into the relationship between membrane properties—affinity, thickness, charge density—and their effect on NO_3^- selectivity.

In **Chapter 5,** we use a novel approach for the fabrication of IEMs, which involves the use of alginate and extracellular polymeric substances (EPS) extracted from anaerobic granular sludge. The membranes fabricated with these two biopolymers showed preferential transport of cations (current efficiency ~80%), which indicates the cation-exchange characteristics of alginate and EPS, and most importantly preferential transport of potassium (K^+) over sodium (Na^+). These results are promising and give an indication of the potential of biopolymers for the selective removal of ions. Nevertheless, further research is needed to improve the stability of the membranes in aqueous electrolytes, as well as to understand the mechanisms involved in the selective transport of ions in these membranes.

In **Chapter 6,** the desalination of water is studied in a wire-CDI system. It is shown that solvents used in the fabrication of the electrodes affect their performance. Electrodes fabricated with acetone showed lower adsorption capacity and charge efficiency compared with electrodes that were fabricated with N-methyl-2-pyrrolidone (NMP). We argue that the lower adsorption capacity is related to a modification of the carbon electrodes chemical surface due to an increase in the concentration of acidic groups. An improvement in the performance of the electrodes was achieved by coating their surface with polymeric solutions (ionomer). This study also includes the development of a theoretical model to describe ion adsorption in CDI systems. The model is based on

the amphoteric Donnan model and includes the effect of the chemical surface charge in the micropores to predict salt adsorption.

Finally, **Chapter 7** presents an overview of the studies conducted in this PhD research. The chapter highlights that it might be possible to give a comprehensive explanation of ion selectivity if we can reliably determine ion hydration in porous carbon electrodes and IEMs. The discussion stresses the importance of ion-water interaction and how this interaction is affected by the presence of other ions and the chemical environment inside the electrodes and IEMs. Additionally, the theoretical and practical implications of our findings are put into perspective.

References

References

1. Ahmed, F.E., R. Hashaikeh, and N. Hilal, *Hybrid technologies: The future of energy efficient desalination – A review.* Desalination, 2020. **495**: p. 114659. DOI: 10.1016/j.desal.2020.114659.
2. Elsaid, K., E.T. Sayed, M.A. Abdelkareem, A. Baroutaji, and A.G. Olabi, *Environmental impact of desalination processes: Mitigation and control strategies.* Sci. Total Environ., 2020. **740**: p. 140125. DOI: 10.1016/j.scitotenv.2020.140125.
3. AlMarzooqi, F.A., A.A. Al Ghaferi, I. Saadat, and N. Hilal, *Application of Capacitive Deionisation in water desalination: A review.* Desalination, 2014. **342**: p. 3-15. DOI: 10.1016/j.desal.2014.02.031.
4. Khawaji, A.D., I.K. Kutubkhanah, and J.-M. Wie, *Advances in seawater desalination technologies.* Desalination, 2008. **221**: p. 47-69. DOI: 10.1016/j.desal.2007.01.067.
5. Bruggen, B.V.d. and C. Vandecasteele, *Distillation vs. membrane filtration: overview of process evolutions in seawater desalination.* Desalination, 2002. **143**: p. 207-218.
6. Greenlee, L.F., D.F. Lawler, B.D. Freeman, B. Marrot, and P. Moulin, *Reverse osmosis desalination: water sources, technology, and today's challenges.* Water Res., 2009. **43**: p. 2317-48. DOI: 10.1016/j.watres.2009.03.010.
7. Fritzmann, C., J. Löwenberg, T. Wintgens, and T. Melin, *State-of-the-art of reverse osmosis desalination.* Desalination, 2007. **216**: p. 1-76. DOI: 10.1016/j.desal.2006.12.009.
8. Strathmann, H., *Electrodialysis, a mature technology with a multitude of new applications.* Desalination, 2010. **264**: p. 268-288. DOI: 10.1016/j.desal.2010.04.069.
9. Xing, W., J. Liang, W. Tang, D. He, M. Yan, X. Wang, Y. Luo, N. Tang, and M. Huang, *Versatile applications of capacitive deionization (CDI)-based technologies.* Desalination, 2020. **482**: p. 114390. DOI: 10.1016/j.desal.2020.114390.
10. Sharma, S. and A. Bhattacharya, *Drinking water contamination and treatment techniques.* Appl. Water Sci., 2016. **7**: p. 1043-1067. DOI: 10.1007/s13201-016-0455-7.
11. Schmoll, O., I.W. Association, W.H.O. Staff, W.H. Organization, G. Howard, J. Chilton, and I. Chorus, *Protecting Groundwater for Health: Managing the Quality of Drinking-water Sources*. 2006: IWA Pub.
12. Jadhav, S.V., E. Bringas, G.D. Yadav, V.K. Rathod, I. Ortiz, and K.V. Marathe, *Arsenic and fluoride contaminated groundwaters: A review of current technologies for contaminants removal.* J. Environ. Manage., 2015. **162**: p. 306-25. DOI: 10.1016/j.jenvman.2015.07.020.

13. Qian, Z., H. Miedema, L.C.P.M. de Smet, and E.J.R. Sudhölter, *Modelling the selective removal of sodium ions from greenhouse irrigation water using membrane technology.* Chem. Eng. Res. Des., 2018. **134**: p. 154-161. DOI: 10.1016/j.cherd.2018.03.040.

14. Dong, T., J. Yao, Y. Wang, T. Luo, and L. Han, *On the permselectivity of di- and mono-valent cations: Influence of applied current density and ionic species concentration.* Desalination, 2020. **488**: p. 114521. DOI: 10.1016/j.desal.2020.114521.

15. Luo, T., S. Abdu, and M. Wessling, *Selectivity of ion exchange membranes: A review.* J. Membr. Sci., 2018. **555**: p. 429-454. DOI: 10.1016/j.memsci.2018.03.051.

16. Singh, K., Z. Qian, P.M. Biesheuvel, H. Zuilhof, S. Porada, and L.C.P.M. de Smet, *Nickel hexacyanoferrate electrodes for high mono/divalent ion-selectivity in capacitive deionization.* Desalination, 2020. **481**: p. 114346. DOI: 10.1016/j.desal.2020.114346.

17. Kim, Y.J. and J.H. Choi, *Selective removal of nitrate ion using a novel composite carbon electrode in capacitive deionization.* Water Res., 2012. **46**: p. 6033-9. DOI: 10.1016/j.watres.2012.08.031.

18. Sahin, S., J.E. Dykstra, H. Zuilhof, R.L. Zornitta, and L. de Smet, *Modification of Cation-Exchange Membranes with Polyelectrolyte Multilayers to Tune Ion Selectivity in Capacitive Deionization.* ACS Appl. Mater. Interfaces, 2020. **12**: p. 34746-34754. DOI: 10.1021/acsami.0c05664.

19. Ge, L., B. Wu, D. Yu, A.N. Mondal, L. Hou, N.U. Afsar, Q. Li, T. Xu, J. Miao, and T. Xu, *Monovalent cation perm-selective membranes (MCPMs): New developments and perspectives.* Chin. J. Chem. Eng., 2017. **25**: p. 1606-1615. DOI: 10.1016/j.cjche.2017.06.002.

20. Ran, J., L. Wu, Y. He, Z. Yang, Y. Wang, C. Jiang, L. Ge, E. Bakangura, and T. Xu, *Ion exchange membranes: New developments and applications.* J. Membr. Sci., 2017. **522**: p. 267-291. DOI: 10.1016/j.memsci.2016.09.033.

21. Xu, T., *Ion exchange membranes: State of their development and perspective.* J. Membr. Sci., 2005. **263**: p. 1-29. DOI: 10.1016/j.memsci.2005.05.002.

22. Boberg, J., *Freshwater Availability*, in *Liquid Assets*. 2005, RAND Corporation. p. 15-28.

23. WWAP, *The United Nations world water development report 2019: leaving no one behind*. 2019: United Nations Education, Scientific & Cultural Organization. 186.

24. Nair, M. and D. Kumar, *Water desalination and challenges: The Middle East perspective: a review.* Desalination Water Treat., 2013. **51**: p. 2030-2040. DOI: 10.1080/19443994.2013.734483.

25. Shevah, Y., *Challenges and Solutions to Water Problems in the Middle East*, in *Chemistry and Water*, S. Ahuja, Editor. 2017. p. 207-258.

26. Cross, K., P. Laban, M. Paden, and M. Smith, *Managing groundwater sustainably*. 2016, IUCN Global Water Programme and IUCN, Water and Nature Initiative (WANI).

27. Boretti, A. and L. Rosa, *Reassessing the projections of the World Water Development Report.* npj Clean Water, 2019. **2**: p. 1-6. DOI: 10.1038/s41545-019-0039-9.

28. Bryan, N.S. and H.v. Grinsven, *The Role of Nitrate in Human Health*, in *Advances in Agronomy*, D.L. Sparks, Editor. 2013. p. 153-182.

29. World Health Organization, *Guidelines for drinking-water quality: fourth edition incorporating the first addendum*. 2017: Geneva.

30. Darbi, A., T. Viraraghavan, R. Butler, and D. Corkal, *Pilot-Scale Evaluation of Select Nitrate Removal Technologies.* J. Environ. Sci. Health A, 2003. **38**: p. 1703-1715. DOI: 10.1081/ese-120022873.

31. Della Rocca, C., V. Belgiorno, and S. Meriç, *Overview of in-situ applicable nitrate removal processes.* Desalination, 2007. **204**: p. 46-62. DOI: 10.1016/j.desal.2006.04.023.

32. Oosterhuis, D.M., D.A. Loka, E.M. Kawakami, and W.T. Pettigrew, *The Physiology of Potassium in Crop Production*, in *Advances in Agronomy*, D.L. Sparks, Editor. 2014. p. 203-233.

33. Dabrowski, A., Z. Hubicki, P. Podkoscielny, and E. Robens, *Selective removal of the heavy metal ions from waters and industrial wastewaters by ion-exchange method.* Chemosphere, 2004. **56**: p. 91-106. DOI: 10.1016/j.chemosphere.2004.03.006.

34. Carolin, C.F., P.S. Kumar, A. Saravanan, G.J. Joshiba, and M. Naushad, *Efficient techniques for the removal of toxic heavy metals from aquatic environment: A review.* J. Environ. Chem. Eng., 2017. **5**: p. 2782-2799. DOI: 10.1016/j.jece.2017.05.029.

35. Ligtvoet, W., A. Bouwman, J. Knoop, S.d. Bruin, K. Nabielek, H. Huitzing, J. Janse, J.v. Minnen, D. Gernaat, P.v. Puijenbroek, J.d. Ruiter, and H. Visser, *The Geography of Future Water Challenges*. 2018, PBL Netherlands Environmental Assessment Agency The Hague.

36. Cherif, H. and J. Belhadj, *Chapter 15 - Environmental Life Cycle Analysis of Water Desalination Processes*, in *Sustainable Desalination Handbook*, V.G. Gude, Editor. 2018, Butterworth-Heinemann. p. 527-559.

37. Jalihal, P. and R. Venkatesan, *Chapter 4 - Advanced desalination technologies*, in *Sustainable Water and Wastewater Processing*, C.M. Galanakis and E. Agrafioti, Editors. 2019, Elsevier. p. 93-131.

38. Mezher, T., H. Fath, Z. Abbas, and A. Khaled, *Techno-economic assessment and environmental impacts of desalination technologies.* Desalination, 2011. **266**: p. 263-273. DOI: 10.1016/j.desal.2010.08.035.

39. Gude, V.G., *Desalination and sustainability - An appraisal and current perspective.* Water Res., 2016. **89**: p. 87-106. DOI: 10.1016/j.watres.2015.11.012.

40. Lee, J.-H., W.-S. Bae, and J.-H. Choi, *Electrode reactions and adsorption/desorption performance related to the applied potential in a capacitive deionization process.* Desalination, 2010. **258**: p. 159-163. DOI: 10.1016/j.desal.2010.03.020.

41. Huyskens, C., J. Helsen, and A.B. de Haan, *Capacitive deionization for water treatment: Screening of key performance parameters and comparison of performance for different ions.* Desalination, 2013. **328**: p. 8-16. DOI: 10.1016/j.desal.2013.07.002.

42. Li, H., Y. Gao, L. Pan, Y. Zhang, Y. Chen, and Z. Sun *Electrosorptive desalination by carbon nanotubes and nanofibres electrodes and ion-exchange membranes*. Water Res., 2008. **42**: p. 4923-4928. DOI: 10.1016/j.watres.2008.09.026.

43. Porada, S., M. Bryjak, A. van der Wal, and P.M. Biesheuvel *Effect of electrode thickness variation on operation of capacitive deionization*. Electrochim. Acta, 2012. **75**: p. 148-156. DOI: 10.1016/j.electacta.2012.04.083.

44. Zhao, Y., Y. Wang, R. Wang, Y. Wu, S. Xu, and J. Wang, *Performance comparison and energy consumption analysis of capacitive deionization and membrane capacitive deionization processes.* Desalination, 2013. **324**: p. 127-133. DOI: 10.1016/j.desal.2013.06.009.

45. Suss, M.E., S. Porada, X. Sun, P.M. Biesheuvel, J. Yoon, and V. Presser *Water desalination via capacitive deionization: what is it and what can we expect from it?* Energy Environ. Sci., 2015. **8**: p. 2296-2319. DOI: 10.1039/c5ee00519a.

46. Choi, J., P. Dorji, H.K. Shon, and S. Hong, *Applications of capacitive deionization: Desalination, softening, selective removal, and energy efficiency.* Desalination, 2019. **449**: p. 118-130. DOI: 10.1016/j.desal.2018.10.013.

47. Zheng-Hong Huang, Z.Y., Feiyu Kang, Michio Inagaki, *Carbon electrodes for capacitive deionization.* J. Mater. Chem. A, 2017. **5**: p. 470-496. DOI: 10.1039/c6ta06733f.

48. Cheng, Y., Z. Hao, C. Hao, Y. Deng, X. Li, K. Li, and Y. Zhao, *A review of modification of carbon electrode material in capacitive deionization.* RSC Advances, 2019. **9**: p. 24401-24419. DOI: 10.1039/c9ra04426d.

49. Elisadiki, J. and C.K. King'ondu, *Performance of ion intercalation materials in capacitive deionization/electrochemical deionization: A review.* J. Electroanal. Chem., 2020. **878**: p. 114588. DOI: 10.1016/j.jelechem.2020.114588.

50. Singh, K., S. Porada, H.D. de Gier, P.M. Biesheuvel, and L.C.P.M. de Smet, *Timeline on the application of intercalation materials in Capacitive Deionization.* Desalination, 2019. **455**: p. 115-134. DOI: 10.1016/j.desal.2018.12.015.

51. Gabelich, C., T. Tran, and I. Suffet, *Electrosorption of Inorganic Salts from Aqueous Solution Using Carbon Aerogels.* Environ. Sci. Technol., 2002. **36**: p. 3010-3019.

52. Zhao, R., M. van Soestbergen, H.H.M. Rijnaarts, A. van der Wal, M.Z. Bazant, and P.M. Biesheuvel, *Time-dependent ion selectivity in capacitive charging of porous electrodes.* J. Colloid Interface Sci., 2012. **384**: p. 38-44. DOI: 10.1016/j.jcis.2012.06.022.

53. Hou, C.-H. and C.-Y. Huang, *A comparative study of electrosorption selectivity of ions by activated carbon electrodes in capacitive deionization.* Desalination, 2013. **314**: p. 124-129. DOI: 10.1016/j.desal.2012.12.029.

54. Li, Y., C. Zhang, Y. Jiang, T.-J. Wang, and H. Wang, *Effects of the hydration ratio on the electrosorption selectivity of ions during capacitive deionization.* Desalination, 2016. **399**: p. 171-177. DOI: 10.1016/j.desal.2016.09.011.

55. Dykstra, J.E., J. Dijkstra, A. van der Wal, H.V.M. Hamelers, and S. Porada, *On-line method to study dynamics of ion adsorption from mixtures of salts in capacitive deionization.* Desalination, 2016. **390**: p. 47-52. DOI: 10.1016/j.desal.2016.04.001.

56. Suss, M.E., *Size-Based Ion Selectivity of Micropore Electric Double Layers in Capacitive Deionization Electrodes.* J. Electrochem. Soc., 2017. **164**: p. E270-E275. DOI: 10.1149/2.1201709jes.

57. Li, Y., T.C. Stewart, and H.L. Tang, *A comparative study on electrosorptive rates of metal ions in capacitive deionization.* J. Water Process Eng., 2018. **26**: p. 257-263. DOI: 10.1016/j.jwpe.2018.10.021.

58. Ying, T.Y., K.L. Yang, S. Yiacoumi, and C. Tsouris, *Electrosorption of ions from aqueous solutions by nanostructured carbon aerogel.* J Colloid Interface Sci, 2002. **250**: p. 18-27. DOI: 10.1006/jcis.2002.8314.

59. Han, L., K.G. Karthikeyan, M.A. Anderson, and K.B. Gregory, *Exploring the impact of pore size distribution on the performance of carbon electrodes for capacitive deionization.* J. Colloid Interface Sci., 2014. **430**: p. 93-99. DOI: 10.1016/j.jcis.2014.05.015.

60. Farmer, J.C., D.V. Fix, G.V. Mack, R.W. Pekala, and J.F. Poco, *Capacitive Deionization of NaCI and $NaNO_3$ Solutions with Carbon Aerogel Electrodes.* J. Electrochem. Soc., 1996. **143**: p. 159-169.

61. Chen, Z., H. Zhang, C. Wu, Y. Wang, and W. Li, *A study of electrosorption selectivity of anions by activated carbon electrodes in capacitive deionization.* Desalination, 2015. **369**: p. 46-50. DOI: 10.1016/j.desal.2015.04.022.

62. Sun, Z., L. Chai, M. Liu, Y. Shu, Q. Li, Y. Wang, and D. Qiu, *Effect of the electronegativity on the electrosorption selectivity of anions during capacitive deionization.* Chemosphere, 2018. **195**: p. 282-290. DOI: 10.1016/j.chemosphere.2017.12.031.

63. Mossad, M. and L. Zou, *A study of the capacitive deionisation performance under various operational conditions.* J. Hazard. Mater., 2012. **213-214**: p. 491-497. DOI: 10.1016/j.jhazmat.2012.02.036.

64. Xu, P., J.E. Drewes, D. Heil, and G. Wang, *Treatment of brackish produced water using carbon aerogel-based capacitive deionization technology.* Water Res., 2008. **42**: p. 2605-2617. DOI: 10.1016/j.watres.2008.01.011.

65. Tang, W., P. Kovalsky, B. Cao, and T.D. Waite, *Investigation of fluoride removal from low-salinity groundwater by single-pass constant-voltage capacitive deionization.* Water Res, 2016. **99**: p. 112-121. DOI: 10.1016/j.watres.2016.04.047.

66. Yeo, J.-H. and J.-H. Choi, *Enhancement of nitrate removal from a solution of mixed nitrate, chloride and sulfate ions using a nitrate-selective carbon electrode.* Desalination, 2013. **320**: p. 10-16. DOI: 10.1016/j.desal.2013.04.013.

67. Hassanvand, A., G.Q. Chen, P.A. Webley, and S.E. Kentish, *A comparison of multicomponent electrosorption in capacitive deionization and membrane capacitive deionization.* Water Res., 2018. **131**: p. 100-109. DOI: 10.1016/j.watres.2017.12.015.

68. Avraham, E., B. Yaniv, A. Soffer, and D. Aurbach, *Developing Ion Electroadsorption Stereoselectivity, by Pore Size Adjustment with Chemical Vapor Deposition onto Active Carbon Fiber Electrodes. Case of Ca2+/Na+ Separation in Water Capacitive Desalination.* J. Phys. Chem. C, 2008. **112**: p. 7385-7389.

69. Noked, M., E. Avraham, Y. Bohadana, A. Soffer, and D. Aurbach, *Development of Anion Stereoselective, Activated Carbon Molecular Sieve Electrodes Prepared by Chemical Vapor Deposition.* J. Phys. Chem C, 2009. **113**: p. 7316-7321.

70. Oyarzun, D.I., A. Hemmatifar, J.W. Palko, M. Stadermann, and J.G. Santiago, *Ion selectivity in capacitive deionization with functionalized electrode: Theory and experimental validation.* Water Research X, 2018. **1**: p. 100008. DOI: 10.1016/j.wroa.2018.100008.

71. Guyes, E.N., T. Malka, and M.E. Suss, *Enhancing the ion size-based selectivity of capacitive deionization electrodes.* Environ. Sci. Technol., 2019. **53**: p. 8447-8454.

72. Lado, J.J., R.E. Pérez-Roa, J.J. Wouters, M.I. Tejedor-Tejedor, C. Federspill, J.M. Ortiz, and M.A. Anderson, *Removal of nitrate by asymmetric capacitive deionization.* Sep. Purif. Technol., 2017. **183**: p. 145-152. DOI: 10.1016/j.seppur.2017.03.071.

73. Su, X., K.-J. Tan, J. Elbert, C. Rüttiger, M. Gallei, T.F. Jamison, and T.A. Hatton, *Asymmetric Faradaic systems for selective electrochemical separations.* Energy & Environmental Science, 2017. **10**: p. 1272-1283. DOI: 10.1039/c7ee00066a.

74. Lee, J., S. Kim, and J. Yoon, *Rocking Chair Desalination Battery Based on Prussian Blue Electrodes.* ACS Omega, 2017. **2**: p. 1653-1659. DOI: 10.1021/acsomega.6b00526.

75. Ikeshoji, T., *Separation of Alkali Metal Ions by Intercalation into a Prussian Blue Electrode.* J. Electrochem. Soc., 1986. **133**: p. 2108-2109.

76. Porada, S., A. Shrivastava, P. Bukowska, P.M. Biesheuvel, and K.C. Smith, *Nickel Hexacyanoferrate Electrodes for Continuous Cation Intercalation Desalination of Brackish Water.* Electrochim. Acta, 2017. **255**: p. 369-378. DOI: 10.1016/j.electacta.2017.09.137.

77. Kim, S., H. Yoon, D. Shin, J. Lee, and J. Yoon, *Electrochemical selective ion separation in capacitive deionization with sodium manganese oxide.* J Colloid Interface Sci, 2017. **506**: p. 644-648. DOI: 10.1016/j.jcis.2017.07.054.

78. Kanoh, H., K. Ooi, Y. Miyai, and S. Katoh, *Electrochemical Recovery of Lithium Ions in the Aqueous Phase.* Sep. Sci. Technol., 1993. **28**: p. 643-651. DOI: 10.1080/01496399308019512.

79. Siekierka, A., E. Kmiecik, B. Tomaszewska, K. Wator, and M. Bryjak, *The evaluation of the effectiveness of lithium separation by hybrid capacitive deionization from geothermal water with the uncertainty measurement application.* Desalination and Water Treatment, 2018. **128**: p. 259-264. DOI: 10.5004/dwt.2018.22870.

80. Pasta, M., A. Battistel, and F. La Mantia, *Batteries for lithium recovery from brines.* Energy & Environmental Science, 2012. **5**: p. 9487. DOI: 10.1039/c2ee22977c.

81. Srimuk, P., J. Lee, S. Fleischmann, M. Aslan, C. Kim, and V. Presser, *Potential-Dependent, Switchable Ion Selectivity in Aqueous Media Using Titanium Disulfide.* ChemSusChem, 2018. **11**: p. 2091-2100. DOI: 10.1002/cssc.201800452.

82. Kim, T., C.A. Gorski, and B.E. Logan, *Ammonium Removal from Domestic Wastewater Using Selective Battery Electrodes.* Environmental Science & Technology Letters, 2018. **5**: p. 578-583. DOI: 10.1021/acs.estlett.8b00334.

83. Hu, C., J. Dong, T. Wang, R. Liu, H. Liu, and J. Qu, *Nitrate electro-sorption/reduction in capacitive deionization using a novel Pd/NiAl-layered metal oxide film electrode.* Chem. Eng. J., 2018. **335**: p. 475-482. DOI: 10.1016/j.cej.2017.10.167.

84. Chang, J., Y. Li, F. Duan, C. Su, Y. Li, and H. Cao, *Selective removal of chloride ions by bismuth electrode in capacitive deionization.* Sep. Purif. Technol., 2020. **240**: p. 116600. DOI: 10.1016/j.seppur.2020.116600.

85. Jung, S.-M., J.-H. Choi, and J.-H. Kim, *Application of capacitive deionization (CDI) technology to insulin purification process.* Sep. Purif. Technol., 2012. **98**: p. 31-35. DOI: 10.1016/j.seppur.2012.06.005.

86. Li, H., C. Nie, L. Pan, and Z. Sun, *A Comparative Study between Membrane Capacitive Deionization and Capacitive Deionization from Isotherms and Kinetics.* Proceedings of Shanghai International Nanotechnology Cooperation Symposium, 2011: p. 110-113. DOI: 10.3786/sincs2011.26.

87. Kim, J.-S. and J.-H. Choi, *Fabrication and characterization of a carbon electrode coated with cation-exchange polymer for the membrane capacitive deionization applications.* J. Membr. Sci., 2010. **355**: p. 85-90. DOI: 10.1016/j.memsci.2010.03.010.

88. Uzun, H.I. and E. Debik, *Economical approach to nitrate removal via membrane capacitive deionization.* Sep. Purif. Technol., 2019. **209**: p. 776-781. DOI: 10.1016/j.seppur.2018.09.037.

89. Wang, L. and S. Lin, *Mechanism of Selective Ion Removal in Membrane Capacitive Deionization for Water Softening.* Environ Sci Technol, 2019. **53**: p. 5797-5804. DOI: 10.1021/acs.est.9b00655.

90. Tang, W., D. He, C. Zhang, and T.D. Waite, *Optimization of sulfate removal from brackish water by membrane capacitive deionization (MCDI).* Water Res., 2017. **121**: p. 302-310. DOI: 10.1016/j.watres.2017.05.046.

91. Pan, J., Y. Zheng, J. Ding, C. Gao, B. Van der Bruggen, and J. Shen, *Fluoride Removal from Water by Membrane Capacitive Deionization with a Monovalent Anion Selective Membrane.* Industrial & Engineering Chemistry Research, 2018. **57**: p. 7048-7053. DOI: 10.1021/acs.iecr.8b00929.

92. Shi, W., X. Liu, C. Ye, X. Cao, C. Gao, and J. Shen, *Efficient lithium extraction by membrane capacitive deionization incorporated with monovalent selective cation exchange membrane.* Sep. Purif. Technol., 2019. **210**: p. 885-890. DOI: 10.1016/j.seppur.2018.09.006.

93. Gan, L., Y. Wu, H. Song, S. Zhang, C. Lu, S. Yang, Z. Wang, B. Jiang, C. Wang, and A. Li, *Selective removal of nitrate ion using a novel activated carbon composite carbon electrode in capacitive deionization.* Sep. Purif. Technol., 2019. **212**: p. 728-736. DOI: 10.1016/j.seppur.2018.11.081.

94. Zuo, K., J. Kim, A. Jain, T. Wang, R. Verduzco, M. Long, and Q. Li, *Novel Composite Electrodes for Selective Removal of Sulfate by the Capacitive Deionization Process.* Environ Sci Technol, 2018. **52**: p. 9486-9494. DOI: 10.1021/acs.est.8b01868.

95. Nativ, P., N. Fridman-Bishop, O. Nir, and O. Lahav, *Dia-nanofiltration-electrodialysis hybrid process for selective removal of monovalent ions from Mg2+ rich brines.* Desalination, 2020. **481**: p. 114357. DOI: 10.1016/j.desal.2020.114357.

96. Lee, D.-H., T. Ryu, J. Shin, J.C. Ryu, K.-S. Chung, and Y.H. Kim, *Selective lithium recovery from aqueous solution using a modified membrane capacitive deionization system.* Hydrometallurgy, 2017. **173**: p. 283-288. DOI: 10.1016/j.hydromet.2017.09.005.

97. Nagarale, R.K., G.S. Gohil, and V.K. Shahi, *Recent developments on ion-exchange membranes and electro-membrane processes.* Adv. Colloid Interface Sci., 2006. **119**: p. 97-130. DOI: 10.1016/j.cis.2005.09.005.

98. Hosseini, S.M., S.S. Madaeni, and A.R. Khodabakhshi, *Preparation and Characterization of Heterogeneous Cation Exchange Membranes Based on S-Poly Vinyl Chloride and Polycarbonate.* Sep. Sci. Technol., 2011. **46**: p. 794-808. DOI: 10.1080/01496395.2010.534122.

99. Vyas, P.V., B.G. Shah, G.S. Trivedi, P. Ray, S.K. Adhikary, and R. Rangarajan, *Characterization of heterogeneous anion-exchange membrane.* J. Membr. Sci., 2001. **187**: p. 39-46.

100. Martí-Calatayud, M.C., D.C. Buzzi, M. García-Gabaldón, A.M. Bernardes, J.A.S. Tenório, and V. Pérez-Herranz, *Ion transport through homogeneous and heterogeneous ion-exchange membranes in single salt and multicomponent electrolyte solutions.* J. Membr. Sci., 2014. **466**: p. 45-57. DOI: 10.1016/j.memsci.2014.04.033.

101. Geise, G.M., M.A. Hickner, and B.E. Logan, *Ionic Resistance and Permselectivity Tradeoffs in Anion Exchange Membranes.* ACS Appl. Mater. Interfaces, 2013. **5**: p. 10294-10301. DOI: 10.1021/am403207w.

102. Strathmann, H., A. Grabowski, and G. Eigenberger, *Ion-Exchange Membranes in the Chemical Process Industry.* Industrial & Engineering Chemistry Research, 2013. **52**: p. 10364-10379. DOI: 10.1021/ie4002102.

103. van der Bruggen, B., A. Koninckx, and C. Vandecasteele, *Separation of monovalent and divalent ions from aqueous solution by electrodialysis and nanofiltration.* Water Res., 2004. **38**: p. 1347-1353. DOI: 10.1016/j.watres.2003.11.008.

104. Chapotot, A., G. Pourcelly, and C. Gavach, *Transport competition between monovalent and divalent cations through cation-exchange membranes. Exchange isotherms and kinetic concepts.* J. Membr. Sci., 1994. **96**: p. 167-181.

105. Galama, A.H., G. Daubaras, O.S. Burheim, H.H.M. Rijnaarts, and J.W. Post, *Seawater electrodialysis with preferential removal of divalent ions.* J. Membr. Sci., 2014. **452**: p. 219-228. DOI: 10.1016/j.memsci.2013.10.050.

106. Kabay, N., Ö. İpek, H. Kahveci, and M. Yüksel, *Effect of salt combination on separation of monovalent and divalent salts by electrodialysis.* Desalination, 2006. **198**: p. 84-91. DOI: 10.1016/j.desal.2006.09.013.

107. Sata, T., *Studies on anion exchange membranes having permselectivity for specific anions in electrodialysis — effect of hydrophilicity of anion exchange membranes on permselectivity of anions.* J. Membr. Sci., 2000. **167**: p. 1-31.

108. Yaroslavtsev, A.B. and V.V. Nikonenko, *Ion-exchange membrane materials: Properties, modification, and practical application.* Nanotechnol. Russ., 2009. **4**: p. 137-159. DOI: 10.1134/s199507800903001x.

109. Pan, J., J. Ding, R. Tan, G. Chen, Y. Zhao, C. Gao, B.V. der Bruggen, and J. Shen, *Preparation of a monovalent selective anion exchange membrane through constructing a covalently crosslinked interface by electro-deposition of polyethyleneimine.* J. Membr. Sci., 2017. **539**: p. 263-272. DOI: 10.1016/j.memsci.2017.06.017.

110. Abdu, S., M.-C. Martí-Calatayud, J.E. Wong, M. García-Gabaldón, and M. Wessling, *Layer-by-Layer Modification of Cation Exchange Membranes Controls Ion Selectivity and Water Splitting.* ACS Applied Materials & Interfaces, 2014. **6**: p. 1843-1854. DOI: 10.1021/am4048317.

111. Mulyati, S., R. Takagi, A. Fujii, Y. Ohmukai, and H. Matsuyama, *Simultaneous improvement of the monovalent anion selectivity and antifouling properties of an anion exchange membrane in an electrodialysis process, using polyelectrolyte multilayer deposition.* J. Membr. Sci., 2013. **431**: p. 113-120. DOI: 10.1016/j.memsci.2012.12.022.

112. Femmer, R., A. Mani, and M. Wessling, *Ion transport through electrolyte/polyelectrolyte multi-layers.* Sci Rep, 2015. **5**: p. 11583. DOI: 10.1038/srep11583.

113. Rijnaarts, T., D.M. Reurink, F. Radmanesh, W.M. de Vos, and K. Nijmeijer, *Layer-by-layer coatings on ion exchange membranes: Effect of multilayer charge and hydration on monovalent ion selectivities.* J. Membr. Sci., 2019. **570-571**: p. 513-521. DOI: 10.1016/j.memsci.2018.10.074.

114. Sata, T., K. Teshima, and T. Yamaguchi, *Permselectivity between Two Anions in Anion Exchange Membranes Crosslinked with Various Diamines in Electrodialysis.* J. of Polymer Science: Part A-Polymer Chemistry, 1996. **34**: p. 1475-1482.

115. Golubenko, D.V., Y.A. Karavanova, S.S. Melnikov, A.R. Achoh, G. Pourcelly, and A.B. Yaroslavtsev, *An approach to increase the permselectivity and mono-valent ion selectivity of cation-exchange membranes by introduction of amorphous zirconium phosphate nanoparticles.* J. Membr. Sci., 2018. **563**: p. 777-784. DOI: 10.1016/j.memsci.2018.06.024.

116. Křivčík, J., D. Neděla, J. Hadrava, and L. Brožová, *Increasing selectivity of a heterogeneous ion-exchange membrane.* Desalin. Water Treat., 2015. **56**: p. 3160-3166. DOI: 10.1080/19443994.2014.980970.

117. Kariduraganavar, M.Y., R.K. Nagarale, A.A. Kittur, and S.S. Kulkarni, *Ion-exchange membranes: preparative methods for electrodialysis and fuel cell applications.* Desalination, 2006. **197**: p. 225-246. DOI: 10.1016/j.desal.2006.01.019.

118. Khodabakhshi, A.R., S.S. Madaeni, and S.M. Hosseini, *Comparative studies on morphological, electrochemical, and mechanical properties of S-polyvinyl chloride based heterogeneous cation-exchange membranes with different resin ratio loading.* Ind. Eng. Chem. Res., 2010. **49**: p. 8477-8487.

119. Kim, T., J.E. Dykstra, S. Porada, A. van der Wal, J. Yoon, and P.M. Biesheuvel, *Enhanced charge efficiency and reduced energy use in capacitive deionization by increasing the discharge voltage.* Journal of Colloid and Interface Science, 2014. DOI: 10.1016/j.jcis.2014.08.041.

120. Biesheuvel, P.M. and M.Z. Bazant *Nonlinear dynamics of capacitive charging and desalination by porous electrodes*. Phys. Rev. E, 2010. **81**: p. 031502. DOI: 10.1103/PhysRevE.81.031502.

121. Porada, S., R. Zhao, A. van der Wal, V. Presser, and P.M. Biesheuvel, *Review on the science and technology of water desalination by capacitive deionization.* Prog. Mater. Sci., 2013. **58**: p. 1388-1442. DOI: 10.1016/j.pmatsci.2013.03.005.

122. Dykstra, J.E., K.J. Keesman, P.M. Biesheuvel, and A. van der Wal, *Theory of pH changes in water desalination by capacitive deionization.* Water Res, 2017. **119**: p. 178-186. DOI: 10.1016/j.watres.2017.04.039.

123. Singh, K., H.J.M. Bouwmeester, L.C.P.M. de Smet, M.Z. Bazant, and P.M. Biesheuvel, *Theory of Water Desalination with Intercalation Materials.* Physical Review Applied, 2018. **9**. DOI: 10.1103/PhysRevApplied.9.064036.

124. Nikonenko, V., V. Zabolotsky, C. Larchet, B. Auclair, and G. Pourcelly, *Mathematical description of ion transport in membrane systems.* Desalination, 2002. **147**: p. 369-374.

125. Kim, Y., W.S. Walker, and D.F. Lawler, *Electrodialysis with spacers: Effects of variation and correlation of boundary layer thickness.* Desalination, 2011. **274**: p. 54-63. DOI: 10.1016/j.desal.2011.01.076.

126. Johnson, A.M. and J. Newman, *Desalting by Means of Porous Carbon Electrodes.* J. Electrochem. Soc., 1971. **118**: p. 510-517.

127. Tang, W., J. Liang, D. He, J. Gong, L. Tang, Z. Liu, D. Wang, and G. Zeng, *Various cell architectures of capacitive deionization: Recent advances and future trends.* Water Res., 2019. **150**: p. 225-251. DOI: 10.1016/j.watres.2018.11.064.

128. Wang, L., P.M. Biesheuvel, and S. Lin, *Reversible thermodynamic cycle analysis for capacitive deionization with modified Donnan model.* J. Colloid Interface Sci., 2018. **512**: p. 522-528. DOI: 10.1016/j.jcis.2017.10.060.

129. Porada, S., L. Borchardt, M. Oschatz, M. Bryjak, J.S. Atchison, K.J. Keesman, S. Kaskel, P.M. Biesheuvel, and V. Presser, *Direct prediction of the desalination performance of porous carbon electrodes for capacitive deionization.* Energy Environ. Sci., 2013. **6**: p. 3700-3712. DOI: 10.1039/c3ee42209g.

130. Tang, W., P. Kovalsky, D. He, and T.D. Waite, *Fluoride and nitrate removal from brackish groundwaters by batch-mode capacitive deionization.* Water Res., 2015. **84**: p. 342-349. DOI: 10.1016/j.watres.2015.08.012.

131. Singh, K., H.J.M. Bouwmeester, L.C.P.M.d. Smet, M.Z. Bazant, and P.M. Biesheuvel, *Theory of Water Desalination with Intercalation Materials.* Phys. Rev. Applied, 2018. **9**: p. 064036.

132. Hawks, S.A., M.R. Cerón, D.I. Oyarzun, T.A. Pham, C. Zhan, C.K. Loeb, D. Mew, A. Deinhart, B.C. Wood, J.G. Santiago, M. Stadermann, and P.G. Campbell, *Using Ultramicroporous Carbon for the Selective Removal of Nitrate with Capacitive Deionization.* Environ. Sci. Technol., 2019. DOI: 10.1021/acs.est.9b01374.

133. Song, J., J. Ma, C. Zhang, C. He, and T.D. Waite, *Implication of Non-electrostatic Contribution to Deionization in Flow-Electrode CDI: Case Study of Nitrate Removal From Contaminated Source Waters.* Frontiers in Chemistry, 2019. **7**. DOI: 10.3389/fchem.2019.00146.

134. Gao, X., S. Porada, A. Omosebi, K.L. Liu, P.M. Biesheuvel, and J. Landon, *Complementary surface charge for enhanced capacitive deionization.* Water Res., 2016. **92**: p. 275-282. DOI: 10.1016/j.watres.2016.01.048.

135. Mubita, T.M., S. Porada, P.M. Biesheuvel, A. van der Wal, and J.E. Dykstra, *Capacitive deionization with wire-shaped electrodes.* Electrochim. Acta, 2018. **270**: p. 165-173. DOI: 10.1016/j.electacta.2018.03.082.

136. Arulrajan, A.C., D.L. Ramasamy, M. Sillanpää, A. van der Wal, P.M. Biesheuvel, S. Porada, and J.E. Dykstra, *Exceptional Water Desalination Performance with Anion-Selective Electrodes.* Adv. Mater., 2019: p. 1806937. DOI: 10.1002/adma.201806937.

137. Kim, M., M.d. Cerro, S. Hand, and R.D. Cusick, *Enhancing capacitive deionization performance with charged structural polysaccharide electrode binders.* Water Res., 2019. **148**: p. 388-397. DOI: 10.1016/j.watres.2018.10.044.

138. Hiemstra, T., W.H.v. Riemsdijk, and G.H. Bolt, *Multisite Proton Adsorption Modeling at the Solid/Solution Interface of (Hydr)oxides: A New Approach.* J. Colloid Interface Sci., 1989. **133**: p. 91-104.

139. Hiemstra, T., H. Yong, and W.H.v. Riemsdijk, *Interfacial Charging Phenomena of Aluminum (Hydr)oxides.* Langmuir, 1999. **15**: p. 5942-5955.

140. Hemmatifar, A., D.I. Oyarzun, J.W. Palko, S.A. Hawks, M. Stadermann, and J.G. Santiago, *Equilibria model for pH variations and ion adsorption in capacitive deionization electrodes.* Water Res., 2017. **122**: p. 387-397. DOI: 10.1016/j.watres.2017.05.036.

141. Biesheuvel, P.M., H.V.M. Hamelers, and M.E. Suss, *Theory of Water Desalination by Porous Electrodes with Immobile Chemical Charge.* Colloids Interface Sci. Commun., 2015. **9**: p. 1-5. DOI: 10.1016/j.colcom.2015.12.001.

142. Biesheuvel, P.M., S. Porada, M. Levi, and M.Z. Bazant, *Attractive forces in microporous carbon electrodes for capacitive deionization.* J. Solid State Electr., 2014. **18**: p. 1365-1376. DOI: 10.1007/s10008-014-2383-5.

143. Zhao, R., P.M. Biesheuvel, and A. van der Wal, *Energy consumption and constant current operation in membrane capacitive deionization.* Energy Environ. Sci., 2012. **5**: p. 9520-9527. DOI: 10.1039/c2ee21737f.

144. Porada, S., L. Weinstein, R. Dash, A. van der Wal, M. Bryjak, Y. Gogotsi, and P.M. Biesheuvel, *Water Desalination Using Capacitive Deionization with Microporous Carbon Electrodes.* ACS Applied Materials & Interfaces, 2012. **4**: p. 1194-1199. DOI: 10.1021/am201683j.

145. Hatzell, M.C., M. Raju, V.J. Watson, A.G. Stack, A.C.T. van Duin, and B.E. Logan, *Effect of Strong Acid Functional Groups on Electrode Rise Potential in Capacitive Mixing by Double Layer Expansion.* Environ. Sci. Technol., 2014. **48**: p. 14041-14048. DOI: 10.1021/es5043782.

146. Dykstra, J.E., R. Zhao, P.M. Biesheuvel, and A. van der Wal, *Resistance identification and rational process design in Capacitive Deionization.* Water Res., 2016. **88**: p. 358–370.

147. Reale, E.R. and K.C. Smith, *Capacitive Performance and Tortuosity of Activated Carbon Electrodes with Macroscopic Pores.* J. Electrochem. Soc., 2018. **165**: p. A1685-A1693. DOI: 10.1149/2.0601809jes.

148. Li, L., P.A. Quinlivan, and D.R.U. Knappe, *Effects of activated carbon surface chemistry and pore structure on the adsorption of organic contaminants from aqueous solution.* Carbon, 2002. **40**: p. 2085–2100.

149. Chen, J.P. and Wu, *Acid/Base-Treated Activated Carbons: Characterization of Functional Groups and Metal Adsorptive Properties.* Langmuir, 2004. **20**: p. 2233-2242. DOI: 10.1021/la0348463.

150. Seredych, M., D. Hulicova-Jurcakova, G.Q. Lu, and T.J. Bandosz, *Surface functional groups of carbons and the effects of their chemical character, density and accessibility to ions on electrochemical performance.* Carbon, 2008. **46**: p. 1475-1488. DOI: 10.1016/j.carbon.2008.06.027.

151. Boehm, H.P., *Some aspects of the surface chemistry of carbon blacks and other carbons.* Carbon, 1994. **32**: p. 759-769.

152. Shafeeyan, M.S., W.M.A.W. Daud, A. Houshmand, and A. Shamiri, *A review on surface modification of activated carbon for carbon dioxide adsorption.* J. Anal. Appl. Pyrolysis, 2010. **89**: p. 143-151. DOI: 10.1016/j.jaap.2010.07.006.

153. Sun, Z., L. Chai, Y. Shu, Q. Li, M. Liu, and D. Qiu, *Chemical bond between chloride ions and surface carboxyl groups on activated carbon.* Colloids Surf. Physicochem. Eng. Aspects, 2017. **530**: p. 53-59. DOI: 10.1016/j.colsurfa.2017.06.077.

154. Ota, K., Y. Amano, M. Aikawa, and M. Machida, *Removal of nitrate ions from water by activated carbons (ACs)—Influence of surface chemistry of ACs and coexisting chloride and sulfate ions.* Appl. Surf. Sci., 2013. **276**: p. 838-842. DOI: 10.1016/j.apsusc.2013.03.053.

155. Zhao, R., P.M. Biesheuvel, H. Miedema, H. Bruning, and A.v.d. Wal, *Charge Efficiency: A Functional Tool to Probe the Double-Layer Structure Inside of Porous Electrodes and Application in the Modeling of Capacitive Deionization.* J. Phys. Chem. Lett., 2010. **1**: p. 205–210. DOI: 10.1021/jz900154h|J.

156. Biesheuvel, P.M., *Activated carbon is an electron-conducting amphoteric ion adsorbent.* ARXIV, 2015. **1509.06354**.

157. Marcus, Y., *Ion Properties*, in *Ionic Interactions in Natural and Synthetic Macromolecules*. 2012, John Wiley & Sons, Inc. p. 1-33.

158. Tansel, B., *Significance of thermodynamic and physical characteristics on permeation of ions during membrane separation: Hydrated radius, hydration free energy and viscous effects.* Sep. Purif. Technol., 2012. **86**: p. 119-126. DOI: 10.1016/j.seppur.2011.10.033.

159. Collins, K., *Sticky ions in biological systems.* Proc. Natl. Acad. Sci. USA, 1995. **92**: p. 5553-5557.

160. Epsztein, R., E. Shaulsky, N. Dizge, D.M. Warsinger, and M. Elimelech, *Role of Ionic Charge Density in Donnan Exclusion of Monovalent Anions by Nanofiltration.* Environ Sci Technol, 2018. **52**: p. 4108-4116. DOI: 10.1021/acs.est.7b06400.

161. Kalluri, R.K., M.M. Biener, M.E. Suss, M.D. Merrill, M. Stadermann, J.G. Santiago, T.F. Baumann, J. Biener, and A. Striolo, *Unraveling the potential and pore-size dependent capacitance of slit-shaped graphitic carbon pores in aqueous electrolytes.* PCCP, 2013. **15**: p. 2309. DOI: 10.1039/c2cp43361c.

162. Nightingale, E.R., *Phenomenological theory of ion solvation. Effective radii of hydrated ions.* J. Phys. Chem., 1959. **63**: p. 1381-1387. DOI: 10.1021/j150579a011.

163. Smith, D.W., *Ionic hydration enthalpies.* J. Chem. Educ., 1977. **54**: p. 540-542.

164. Haynes, W.M., *CRC Handbook of Chemistry and Physics, 93rd Edition*. 2012: Taylor & Francis.

165. Wang, Z., H. Gong, Y. Zhang, P. Liang, and K. Wang, *Nitrogen recovery from low-strength wastewater by combined membrane capacitive deionization (MCDI) and ion exchange (IE) process.* Chem. Eng. J., 2017. **316**: p. 1-6. DOI: 10.1016/j.cej.2017.01.082.

166. Sadrzadeh, M., A. Razmi, and T. Mohammadi, *Separation of different ions from wastewater at various operating conditions using electrodialysis.* Sep. Purif. Technol., 2007. **54**: p. 147-156. DOI: 10.1016/j.seppur.2006.08.023.

167. Lee, J.-B., K.-K. Park, H.-M. Eum, and C.-W. Lee, *Desalination of a thermal power plant wastewater by membrane capacitive deionization.* Desalination, 2006. **196**: p. 125-134. DOI: 10.1016/j.desal.2006.01.011.

168. Gao, H., B. Zhang, X. Tong, and Y. Chen, *Monovalent-anion selective and antifouling polyelectrolytes multilayer anion exchange membrane for reverse electrodialysis.* J. Membr. Sci., 2018. **567**: p. 68-75. DOI: 10.1016/j.memsci.2018.09.035.

169. Mohapatra, M., S. Anand, B.K. Mishra, D.E. Giles, and P. Singh, *Review of fluoride removal from drinking water.* J. Environ. Manage., 2009. **91**: p. 67-77. DOI: 10.1016/j.jenvman.2009.08.015.

170. Fu, F. and Q. Wang, *Removal of heavy metal ions from wastewaters: A review.* J. Environ. Manage., 2011. **92**: p. 407-418. DOI: 10.1016/j.jenvman.2010.11.011.

171. Binnemans, K., P.T. Jones, B. Blanpain, T. Van Gerven, and Y. Pontikes, *Towards zero-waste valorisation of rare-earth-containing industrial process residues: a critical review.* J. Clean. Prod., 2015. **99**: p. 17-38. DOI: 10.1016/j.jclepro.2015.02.089.

172. Yantasee, W., G.E. Fryxell, R.S. Addleman, R.J. Wiacek, V. Koonsiripaiboon, K. Pattamakomsan, V. Sukwarotwat, J. Xu, and K.N. Raymond, *Selective removal of lanthanides from natural waters, acidic streams and dialysate.* J. Hazard Mater., 2009. **168**: p. 1233-8. DOI: 10.1016/j.jhazmat.2009.03.004.

173. Jha, M.K., A. Kumari, R. Panda, J. Rajesh Kumar, K. Yoo, and J.Y. Lee, *Review on hydrometallurgical recovery of rare earth metals.* Hydrometallurgy, 2016. **161**: p. 77. DOI: 10.1016/j.hydromet.2016.01.003.

174. Elmidaoui, A., F. Elhannouni, M.A.M. Sahli, L. Chay, H. Elabbassi, M. Hafsi, and D. Largeteau, *Pollution of nitrate in Moroccan ground water: removal by electrodialysis.* Desalination, 2001. **136**: p. 325-332.

175. Shrimali, M. and K.P. Singh, *New methods of nitrate removal from water.* Environ. Pollut., 2001. **112**: p. 351-359.

176. Eyal, A. and O. Kedem, *Nitrate-selective anion-exchange membranes.* J. Membr. Sci., 1988. **38**: p. 101-111.

177. Wisniewski, C., F. Persin, T. Cherif, R. Sandeaux, A. Grasmick, and C. Gavach, *Denitrification of drinking water by the association of an electrodialysis process and a membrane bioreactor: feasibility and application.* Desalination, 2001. **139**: p. 199-205.

178. Midaoui, A.E., F. Elhannouni, M. Taky, L. Chay, M.A.M. Sahli, L. Echihabi, and M. Hafsi, *Optimization of nitrate removal operation from ground water by electrodialysis.* Sep. Purif. Technol., 2002. **29**: p. 235-244.

179. Menkouchi Sahli, M.A., S. Annouar, M. Mountadar, A. Soufiane, and A. Elmidaoui, *Nitrate removal of brackish underground water by chemical adsorption and by*

electrodialysis. Desalination, 2008. **227**: p. 327-333. DOI: 10.1016/j.desal.2007.07.021.

180. Banasiak, L.J. and A.I. Schäfer, *Removal of boron, fluoride and nitrate by electrodialysis in the presence of organic matter.* J. Membr. Sci., 2009. **334**: p. 101-109. DOI: 10.1016/j.memsci.2009.02.020.

181. Weinertova, K., R.S. Honorato, E. Stranska, and D. Nedela, *Comparison of heterogeneous anion-exchange membranes for nitrate ion removal from mixed salt solution.* Chem. Pap., 2017. **72**: p. 469-478. DOI: 10.1007/s11696-017-0299-0.

182. Xu, X., Q. He, G. Ma, H. Wang, N. Nirmalakhandan, and P. Xu, *Selective separation of mono- and di-valent cations in electrodialysis during brackish water desalination: Bench and pilot-scale studies.* Desalination, 2018. **428**: p. 146-160. DOI: 10.1016/j.desal.2017.11.015.

183. Zhang, Y., R. Liu, Q. Lang, M. Tan, and Y. Zhang, *Composite anion exchange membrane made by layer-by-layer method for selective ion separation and water migration control.* Sep. Purif. Technol., 2018. **192**: p. 278-286. DOI: 10.1016/j.seppur.2017.10.022.

184. Wang, X.-l., M. Wang, Y.-x. Jia, and B.-b. Wang, *Surface Modification of Anion Exchange Membrane by Covalent Grafting for Imparting Permselectivity between Specific Anions.* Electrochim. Acta, 2015. **174**: p. 1113-1121. DOI: 10.1016/j.electacta.2015.06.115.

185. Kingsbury, R.S., S. Zhu, S. Flotron, and O. Coronell, *Microstructure Determines Water and Salt Permeation in Commercial Ion-Exchange Membranes.* ACS Appl. Mater. Interfaces, 2018. **10**: p. 39745-39756. DOI: 10.1021/acsami.8b14494.

186. Hosseini, S.M., A. Gholami, S.S. Madaeni, A.R. Moghadassi, and A.R. Hamidi, *Fabrication of (polyvinyl chloride/cellulose acetate) electrodialysis heterogeneous cation exchange membrane: Characterization and performance in desalination process.* Desalination, 2012. **306**: p. 51-59. DOI: 10.1016/j.desal.2012.07.028.

187. Molau, G., *Heterogeneous ion-exchange membranes.* J. Membr. Sci., 1981. **8**: p. 309-330.

188. Han, S.-D., H.-J. Lee, and S.-H. Moon, *Influence of the ratio of resin to polymeric binder on the heterogeneity of cation-exchange membranes.* Desalin. Water Treat., 2015: p. 1-11. DOI: 10.1080/19443994.2014.1000386.

189. Shalimov, A.S., S.A. Novikova, I.A. Stenina, and A.B. Yaroslavtsev, *Ion transport in MF-4SK cation-exchange membranes modified with acid zirconium phosphate.* Russ. J. Inorg. Chem., 2006. **51**: p. 700-705. DOI: 10.1134/s0036023606050020.

190. Taylor-Pashow, K.M.L., T.C. Shehee, and D.T. Hobbs, *Advances in Inorganic and Hybrid Ion Exchangers.* Solvent Extr. Ion Exch., 2013. **31**: p. 122-170. DOI: 10.1080/07366299.2012.735510.

191. Hosseini, S.M., A.R. Hamidi, A.R. Moghadassi, P. Koranian, and S.S. Madaeni, *Fabrication of novel mixed matrix electrodialysis heterogeneous ion-exchange membranes modified by ilmenite (FeTiO3): electrochemical and ionic transport characteristics.* Ionics, 2014. **21**: p. 437-447. DOI: 10.1007/s11581-014-1186-0.

192. Bouzek, K., S. Moravcová, J. Schauer, L. Brožová, and Z. Pientka, *Heterogeneous ion-selective membranes: the influence of the inert matrix polymer on the membrane properties.* J. Appl. Electrochem., 2010. **40**: p. 1005-1018. DOI: 10.1007/s10800-009-9974-3.

193. Nagarale, R.K., V.K. Shahi, S.K. Thampy, and R. Rangarajan, *Studies on electrochemical characterization of polycarbonate and polysulfone based heterogeneous cation-exchange membranes.* React. Funct. Polym., 2004. **61**: p. 131-138. DOI: 10.1016/j.reactfunctpolym.2004.04.007.

194. Volodina, E., N. Pismenskaya, V. Nikonenko, C. Larchet, and G. Pourcelly, *Ion transfer across ion-exchange membranes with homogeneous and heterogeneous surfaces.* J. Colloid Interface Sci., 2005. **285**: p. 247-258. DOI: 10.1016/j.jcis.2004.11.017.

195. Choi, J.-H., S.-H. Kim, and S.-H. Moon, *Heterogeneity of Ion-Exchange Membranes: The Effects of Membrane Heterogeneity on Transport Properties.* J. Colloid Interface Sci., 2001. **241**: p. 120-126. DOI: 10.1006/jcis.2001.7710.

196. Gohil, G., *Comparative studies on electrochemical characterization of homogeneous and heterogeneous type of ion-exchange membranes.* J. Membr. Sci., 2004. **240**: p. 211-219. DOI: 10.1016/j.memsci.2004.04.022.

197. Křivčík, J., J. Vladařová, J. Hadrava, A. Černín, and L. Brožová, *The effect of an organic ion-exchange resin on properties of heterogeneous ion-exchange membrane.* Desalin. Water Treat., 2012. **14**: p. 179-184. DOI: 10.5004/dwt.2010.1025.

198. Oren, Y., V. Freger, and C. Linder, *Highly conductive ordered heterogeneous ion-exchange membranes.* J. Membr. Sci., 2004. **239**: p. 17-26. DOI: 10.1016/j.memsci.2003.12.031.

199. Miao, Y.-m., Y.-x. Jia, R.-q. Guo, and M. Wang, *Heterogeneous anion-exchange membrane: Influences of charged binders with crosslinking structure on electrodialytic performance.* J. Membr. Sci., 2018. **557**: p. 67-75. DOI: 10.1016/j.memsci.2018.04.030.

200. Farrokhzad, H., M.R. Moghbeli, T. van Gerven, and B. van der Bruggen, *Surface modification of composite ion exchange membranes by polyaniline.* React. Funct. Polym., 2015. **86**: p. 161-167. DOI: 10.1016/j.reactfunctpolym.2014.08.003.

201. Gohil, G.S., V.V. Binsu, and V.K. Shahi, *Preparation and characterization of monovalent ion selective polypyrrole composite ion-exchange membranes.* J. Membr. Sci., 2006. **280**: p. 210-218. DOI: 10.1016/j.memsci.2006.01.020.

202. Güler, E., W. van Baak, M. Saakes, and K. Nijmeijer, *Monovalent-ion-selective membranes for reverse electrodialysis.* J. Membr. Sci., 2014. **455**: p. 254-270. DOI: 10.1016/j.memsci.2013.12.054.

203. Sata, T., T. Yamaguchi, and K. Matsusaki, *Effect of Hydrophobicity of Ion Exchange Groups of Anion Exchange Membranes on Permselectivity between Two Anions.* J. Phys. Chem., 1995. **99**: p. 12875-12882. DOI: DOI: 10.1039/C39950001153

204. Epsztein, R., E. Shaulsky, M. Qin, and M. Elimelech, *Activation behavior for ion permeation in ion-exchange membranes: Role of ion dehydration in selective transport.* J. Membr. Sci., 2019. **580**: p. 316-326. DOI: 10.1016/j.memsci.2019.02.009.

205. Oh, C.-M., C.-W. Hwang, and T.-S. Hwang, *Synthesis of a quaternarized poly(vinylimidazole-co-trifluoroethylmethacrylate-co-divinylbenzene) anion-exchange membrane for nitrate removal.* J. Environ. Chem. Eng., 2014. **2**: p. 2162-2169. DOI: 10.1016/j.jece.2014.09.014.

206. Kikhavani, T., S.N. Ashrafizadeh, and B. Van der Bruggen, *Nitrate Selectivity and Transport Properties of a Novel Anion Exchange Membrane in Electrodialysis.* Electrochim. Acta, 2014. **144**: p. 341-351. DOI: 10.1016/j.electacta.2014.08.012.

207. Galama, A.H., D.A. Vermaas, J. Veerman, M. Saakes, H.H.M. Rijnaarts, J.W. Post, and K. Nijmeijer, *Membrane resistance: The effect of salinity gradients over a cation exchange membrane.* J. Membr. Sci., 2014. **467**: p. 279-291. DOI: 10.1016/j.memsci.2014.05.046.

208. Giorno, L., E. Drioli, and H. Strathmann, *Ion-Exchange Membrane Characterization*, in *Encyclopedia of Membranes*, E. Drioli and L. Giorno, Editors. 2016, Springer Berlin Heidelberg: Berlin, Heidelberg. p. 1052-1056.

209. Geise, G.M., M.A. Hickner, and B.E. Logan, *Ionic Resistance and Permselectivity Tradeoffs in Anion Exchange Membranes.* ACS Appl. Mater. Interfaces, 2013. **5**: p. 10294-10301. DOI: 10.1021/am403207w.

210. Shibuta, S. and H. Imamura, *Hydration Promoted by a Methylene Group: A Volumetric Study on Alkynes in Water.* J. Phys. Chem. B, 2018. **122**: p. 2985-2991. DOI: 10.1021/acs.jpcb.8b00843.

211. Gonzalez-Caballero, F. and F. de las nieves, *On the relation between the electrokinetic behavior of heterogeneous ion-exchange membranes and their structural characteristics.* J. Membr. Sci., 1983. **16**: p. 225-235.

212. Fritz, J.S. and D.T. Gjerde, *Ion Chromatography*. 2009: Wiley.

213. Richards, L.A., A.I. Schäfer, B.S. Richards, and B. Corry, *The Importance of Dehydration in Determining Ion Transport in Narrow Pores.* Small, 2012. **8**: p. 1701-1709. DOI: 10.1002/smll.201102056.

214. Corry, B., *Designing Carbon Nanotube Membranes for Efficient Water Desalination.* J. Phys. Chem. B, 2008. **112**: p. 1427-1434.

215. Clifford, D. and W.J. Weber, *The determinants of divalent/monovalent selectivity in anion exchangers.* Reactive Polym., 1983. **1**: p. 77-89.

216. Subramonian, S. and D. Clifford, *Monovalent/Divalent Selectivity and the Charge Separation Concept.* Reactive Polym., 1988. **9**: p. 195-209.

217. Baer, M.D., V.-T. Pham, J.L. Fulton, G.K. Schenter, M. Balasubramanian, and C.J. Mundy, *Is Iodate a Strongly Hydrated Cation?* J. Phys. Chem. Lett., 2011. **2**: p. 2650-2654. DOI: 10.1021/jz2011435.

218. Sharma, B. and A. Chandra, *Nature of hydration shells of a polyoxy-anion with a large cationic centre: The case of iodate ion in water.* J. Comput. Chem., 2018. **39**: p. 1226-1235. DOI: 10.1002/jcc.25185.

219. Campione, A., L. Gurreri, M. Ciofalo, G. Micale, A. Tamburini, and A. Cipollina, *Electrodialysis for water desalination: A critical assessment of recent developments on process fundamentals, models and applications.* Desalination, 2018. **434**: p. 121-160. DOI: 10.1016/j.desal.2017.12.044.

220. Zhao, R., O. Satpradit, H.H.M. Rijnaarts, P.M. Biesheuvel, and A. van der Wal, *Optimization of salt adsorption rate in membrane capacitive deionization.* Water Res., 2013. **47**: p. 1941-1952. DOI: 10.1016/j.watres.2013.01.025.

221. Porada, S., L. Zhang, and J.E. Dykstra, *Energy consumption in membrane capacitive deionization and comparison with reverse osmosis.* Desalination, 2020. **488**: p. 114383. DOI: 10.1016/j.desal.2020.114383.

222. Elattar, A., A. Elmidaoui, N. Pismenskaia, C. Gavach, and G. Pourcelly, *Comparison of transport properties of monovalent anions through anion-exchange membranes.* J. Membr. Sci., 1998. **143**: p. 249-261.

223. Münchinger, A. and K.-D. Kreuer, *Selective ion transport through hydrated cation and anion exchange membranes I. The effect of specific interactions.* J. Membr. Sci., 2019. **592**: p. 117372. DOI: 10.1016/j.memsci.2019.117372.

224. Mubita, T., S. Porada, P. Aerts, and A. van der Wal, *Heterogeneous anion exchange membranes with nitrate selectivity and low electrical resistance.* J. Membr. Sci., 2020. **607**: p. 118000. DOI: 10.1016/j.memsci.2020.118000.

225. Pintauro, P.N. and D.N. Bennion, *Mass Transport of Electrolytes in Membranes. 1. Development of Mathematical Transport Model.* Ind. Eng. Chem. Fundam., 1984. **23**: p. 230-234.

226. Pintauro, P.N. and D.N. Bennion, *Mass Transport of Electrolytes in Membranes. 2. Determination of NaCI Equilibrium and Transport Parameters for Nafion.* Ind. Eng. Chem. Fundam., 1984. **23**: p. 234-243. DOI: 10.1021/i100014a017,.

227. Tedesco, M., H.V.M. Hamelers, and P.M. Biesheuvel, *Nernst-Planck transport theory for (reverse) electrodialysis: I. Effect of co-ion transport through the*

membranes. J. Membr. Sci., 2016. **510**: p. 370-381. DOI: 10.1016/j.memsci.2016.03.012.

228. Ortiz, J.M., J.A. Sotoca, E. Expósito, F. Gallud, V. García-García, V. Montiel, and A. Aldaz, *Brackish water desalination by electrodialysis: batch recirculation operation modeling.* J. Membr. Sci., 2005. **252**: p. 65-75. DOI: 10.1016/j.memsci.2004.11.021.

229. Tado, K., F. Sakai, Y. Sano, and A. Nakayama, *An analysis on ion transport process in electrodialysis desalination.* Desalination, 2016. **378**: p. 60-66. DOI: 10.1016/j.desal.2015.10.001.

230. Zabolotsky, V.I., J.A. Manzanares, V.V. Nikonenko, K.A. Lebedev, and E.G. Lovtsov, *Space charge effect on competitive ion transport through ion-exchange membranes.* Desalination, 2002. **147**: p. 387-392.

231. Kim, Y., W.S. Walker, and D.F. Lawler, *Competitive separation of di- vs. mono-valent cations in electrodialysis: effects of the boundary layer properties.* Water Res, 2012. **46**: p. 2042-56. DOI: 10.1016/j.watres.2012.01.004.

232. Guzman-Garcia, A.G., P.N. Pintauro, M.W. Verbrugge, and R.F. Hill, *Development of a Space-Charge Transport Model for Ion-Exchange Membranes.* AICHE J., 1990. **36**: p. 1061-1074.

233. Yang, Y. and P.N. Pintauro, *Multicomponent Space-Charge Transport Model for Ion-Exchange Membranes.* AICHE J., 2000. **46**: p. 1177-1190.

234. Biesheuvel, P.M. and J.E. Dykstra, *Physics of electrochemical processes*. 2020.

235. Quenneville, E. and M. Buschmann, *A transport model of electrolyte convection through a charged membrane predicts generation of net charge at membrane/electrolyte interfaces.* J. Membr. Sci., 2005. **265**: p. 60-73. DOI: 10.1016/j.memsci.2005.04.032.

236. Galama, A.H., J.W. Post, M.A. Cohen Stuart, and P.M. Biesheuvel, *Validity of the Boltzmann equation to describe Donnan equilibrium at the membrane–solution interface.* J. Membr. Sci., 2013. **442**: p. 131-139. DOI: 10.1016/j.memsci.2013.04.022.

237. Kamcev, J., D.R. Paul, and B.D. Freeman, *Effect of fixed charge group concentration on equilibrium ion sorption in ion exchange membranes.* J. Mater. Chem. A, 2017. **5**: p. 4638-4650. DOI: 10.1039/c6ta07954g.

238. Uto, M., Hitoshi Yoshida, M. Sugawara, and Y. Umezawa, *Uphill Transport Membrane Electrodes.* Anal. Chem., 1986. **58**: p. 1798-1803.

239. Nonaka, T. and N. Matsumoto, *Uphill and selective transport of anions through 2,3-epithiopropyl methacrylate-butyl methacrylate-methacryloyloxyethyltrimethylammonium chloride terpolymer membranes.* J. Mem. Sci, 1994. **92**: p. 117-129.

240. Krishna, R., *Highlighting coupling effects in ionic diffusion.* Chem. Eng. Res. Des., 2016. **114**: p. 1-12. DOI: 10.1016/j.cherd.2016.08.009.

241. Higa, M. and A. Kira, *Theory and Simulation of Ion Transport in Nonstationary States against Concentration Gradients across Ion-Exchange Membranes.* J. Phys. Chem., 1992. **96**: p. 9518-9523. DOI: 10.1021/j100202a081,.

242. Tedesco, M., H.V.M. Hamelers, and P.M. Biesheuvel, *Nernst-Planck transport theory for (reverse) electrodialysis: III. Optimal membrane thickness for enhanced process performance.* J. Membr. Sci., 2018. **565**: p. 480-487. DOI: 10.1016/j.memsci.2018.07.090.

243. Rinzema, A., J. van Lier, and G. Lettinga, *Sodium inhibition of acetoclastic methanogens in granular sludge from a UASB reactor.* Enzyme Microb. Technol., 1988. **10**: p. 24-32. DOI: 10.1016/0141-0229(88)90094-4.

244. Vyrides, I., H. Santos, A. Mingote, M.J. Ray, and D.C. Stuckey, *Are Compatible Solutes Compatible with Biological Treatment of Saline Wastewater? Batch and Continuous Studies Using Submerged Anaerobic Membrane Bioreactors (SAMBRs).* Environ. Sci. Technol., 2010. **44**: p. 7437-7442. DOI: 10.1021/es903981k.

245. Fang, C., K. Boe, and I. Angelidaki, *Anaerobic co-digestion of desugared molasses with cow manure; focusing on sodium and potassium inhibition.* Bioresour. Technol., 2011. **102**: p. 1005-1011. DOI: 10.1016/j.biortech.2010.09.077.

246. De Vrieze, J., M. Coma, M. Debeuckelaere, P. Van der Meeren, and K. Rabaey, *High salinity in molasses wastewaters shifts anaerobic digestion to carboxylate production.* Water Res., 2016. **98**: p. 293-301. DOI: 10.1016/j.watres.2016.04.035.

247. Gagliano, M.C., S.B. Ismail, A.J.M. Stams, C.M. Plugge, H. Temmink, and J.B. Van Lier, *Biofilm formation and granule properties in anaerobic digestion at high salinity.* Water Res., 2017. **121**: p. 61-71. DOI: 10.1016/j.watres.2017.05.016.

248. Sudmalis, D., M.C. Gagliano, R. Pei, K. Grolle, C.M. Plugge, H.H.M. Rijnaarts, G. Zeeman, and H. Temmink, *Fast anaerobic sludge granulation at elevated salinity.* Water Res, 2018. **128**: p. 293-303. DOI: 10.1016/j.watres.2017.10.038.

249. Sudmalis, D., S.K. Millah, M.C. Gagliano, C.I. Butre, C.M. Plugge, H.H.M. Rijnaarts, G. Zeeman, and H. Temmink, *The potential of osmolytes and their precursors to alleviate osmotic stress of anaerobic granular sludge.* Water Res, 2018. **147**: p. 142-151. DOI: 10.1016/j.watres.2018.09.059.

250. Altaş, L., *Inhibitory effect of heavy metals on methane-producing anaerobic granular sludge.* J. Hazard. Mater., 2009. **162**: p. 1551-1556. DOI: 10.1016/j.jhazmat.2008.06.048.

251. Karri, S., R. Sierra-Alvarez, and J.A. Field, *Toxicity of copper to acetoclastic and hydrogenotrophic activities of methanogens and sulfate reducers in anaerobic sludge.* Chemosphere, 2006. **62**: p. 121-127. DOI: 10.1016/j.chemosphere.2005.04.016.

252. Kugelman, I.J. and P. Mccarty, *Cation Toxicity and Stimulation in Anaerobic Waste Treatment.* Journal (Water Pollution Control Federation), 1965. **37**: p. 97-116.

253. Lefebvre, O., S. Quentin, M. Torrijos, J.J. Godon, J.P. Delgenès, and R. Moletta, *Impact of increasing NaCl concentrations on the performance and community composition of two anaerobic reactors.* Appl. Microbiol. Biotechnol., 2007. **75**: p. 61-69. DOI: 10.1007/s00253-006-0799-2.

254. Lin, C.-Y. and C.-C. Chen, *Effect of heavy metals on the methanogenic UASB granule.* Water Res., 1999. **33**: p. 409-416. DOI: 10.1016/S0043-1354(98)00211-5.

255. McCarty, P.L. and R.E. McKinney, *Salt Toxicity in Anaerobic Digestion.* Journal (Water Pollution Control Federation), 1961. **33**: p. 399-415. DOI: 10.2307/25034396.

256. Chen, J.L., R. Ortiz, T.W.J. Steele, and D.C. Stuckey, *Toxicants inhibiting anaerobic digestion: A review.* Biotechnol. Adv., 2014. **32**: p. 1523-1534. DOI: 10.1016/j.biotechadv.2014.10.005.

257. Harrison, J., H. Ceri, and R.J. Turner, *Multimetal resistance and tolerance in microbial biofilms.* Nature Reviews Microbiology, 2007. **5**: p. 928.

258. Seviour, T., Z. Yuan, M.C.M. van Loosdrecht, and Y. Lin, *Aerobic sludge granulation: A tale of two polysaccharides?* Water Res., 2012. **46**: p. 4803-4813. DOI: 10.1016/j.watres.2012.06.018.

259. Zhou, W., T. Imai, M. Ukita, M. Sekine, and T. Higuchi, *Triggering forces for anaerobic granulation in UASB reactors.* Process Biochem., 2006. **41**: p. 36-43. DOI: 10.1016/j.procbio.2005.02.029.

260. Ajao, V., H. Bruning, H. Rijnaarts, and H. Temmink, *Natural flocculants from fresh and saline wastewater: Comparative properties and flocculation performances.* Chem. Eng. J., 2018. **349**: p. 622-632. DOI: 10.1016/j.cej.2018.05.123.

261. Liu, Y. and H.H.P. Fang, *Influences of Extracellular Polymeric Substances (EPS) on Flocculation, Settling, and Dewatering of Activated Sludge.* Crit. Rev. Environ. Sci. Technol., 2003. **33**: p. 237-273. DOI: 10.1080/10643380390814479.

262. Comte, S., G. Guibaud, and M. Baudu, *Biosorption properties of extracellular polymeric substances (EPS) resulting from activated sludge according to their type: Soluble or bound.* Process Biochem., 2006. **41**: p. 815-823. DOI: 10.1016/j.procbio.2005.10.014.

263. Comte, S., G. Guibaud, and M. Baudu, *Biosorption properties of extracellular polymeric substances (EPS) towards Cd, Cu and Pb for different pH values.* J. Hazard. Mater., 2008. **151**: p. 185-193. DOI: 10.1016/j.jhazmat.2007.05.070.

264. d'Abzac, P., F. Bordas, E. Joussein, E.D. van Hullebusch, P.N.L. Lens, and G. Guibaud, *Metal binding properties of extracellular polymeric substances*

extracted from anaerobic granular sludges. Environmental Science and Pollution Research, 2013. **20**: p. 4509-4519. DOI: 10.1007/s11356-012-1401-3.

265. Dobrowolski, R., A. Szcześ, M. Czemierska, and A. Jarosz-Wikołazka, *Studies of cadmium(II), lead(II), nickel(II), cobalt(II) and chromium(VI) sorption on extracellular polymeric substances produced by Rhodococcus opacus and Rhodococcus rhodochrous.* Bioresour. Technol., 2017. **225**: p. 113-120. DOI: 10.1016/j.biortech.2016.11.040.

266. Li, W.-W. and H.-Q. Yu, *Insight into the roles of microbial extracellular polymer substances in metal biosorption.* Bioresour. Technol., 2014. **160**: p. 15-23. DOI: 10.1016/j.biortech.2013.11.074.

267. Toner, B., A. Manceau, M.A. Marcus, D.B. Millet, and G. Sposito, *Zinc Sorption by a Bacterial Biofilm.* Environ. Sci. Technol., 2005. **39**: p. 8288-8294. DOI: 10.1021/es050528+.

268. Gutierrez, T., D.V. Biller, T. Shimmield, and D.H. Green, *Metal binding properties of the EPS produced by Halomonas sp. TG39 and its potential in enhancing trace element bioavailability to eukaryotic phytoplankton.* BioMetals, 2012. **25**: p. 1185-1194. DOI: 10.1007/s10534-012-9581-3.

269. Gutierrez, T., T. Shimmield, C. Haidon, K. Black, and D.H. Green, *Emulsifying and Metal Ion Binding Activity of a Glycoprotein Exopolymer Produced by Pseudoalteromonas sp. Strain TG12.* Appl. Environ. Microbiol., 2008. **74**: p. 4867-4876. DOI: 10.1128/aem.00316-08.

270. Flemming, H.C. and J. Wingender, *The biofilm matrix.* Nature Reviews Microbiology, 2010. **8**: p. 623-633.

271. Teitzel, G.M. and M.R. Parsek, *Heavy metal resistance of biofilm and planktonic Pseudomonas aeruginosa.* Appl. Environ. Microbiol., 2003. **69**: p. 2313-2320. DOI: 10.1128/aem.69.4.2313-2320.2003.

272. Wang, H., J.J. Wilksch, T. Lithgow, R.A. Strugnell, and M.L. Gee, *Nanomechanics measurements of live bacteria reveal a mechanism for bacterial cell protection: the polysaccharide capsule in Klebsiella is a responsive polymer hydrogel that adapts to osmotic stress.* Soft Matter, 2013. **9**: p. 7560-7567. DOI: 10.1039/C3SM51325D.

273. Horn, H. and E. Morgenroth, *Transport of oxygen, sodium chloride, and sodium nitrate in biofilms.* Chem. Eng. Sci., 2006. **61**: p. 1347-1356. DOI: 10.1016/j.ces.2005.08.027.

274. Hu, Z., J. Jin, H.D. Abruña, P.L. Houston, A.G. Hay, W.C. Ghiorse, M.L. Shuler, G. Hidalgo, and L.W. Lion, *Spatial Distributions of Copper in Microbial Biofilms by Scanning Electrochemical Microscopy.* Environ. Sci. Technol., 2007. **41**: p. 936-941. DOI: 10.1021/es061293k.

275. Gagliano, M.C., T.R. Neu, U. Kuhlicke, D. Sudmalis, H. Temmink, and C.M. Plugge, *EPS Glycoconjugate Profiles Shift as Adaptive Response in Anaerobic Microbial*

Granulation at High Salinity. Frontiers in Microbiology, 2018. **9**. DOI: 10.3389/fmicb.2018.01423.

276. Suzuki, I., D. Lee, B. Mackay, L. Harahuc, and J.K. Oh, *Effect of Various Ions, pH, and Osmotic Pressure on Oxidation of Elemental Sulfur by Thiobacillus thiooxidans.* Appl. Environ. Microbiol., 1999. **65**: p. 5163-5168. DOI: 10.1128/aem.65.11.5163-5168.1999.

277. Smith, W.R., F. Moučka, and I. Nezbeda, *Osmotic pressure of aqueous electrolyte solutions via molecular simulations of chemical potentials: Application to NaCl.* Fluid Phase Equilib., 2016. **407**: p. 76-83. DOI: 10.1016/j.fluid.2015.05.012.

278. Siegrist, H. and W. Gujer, *Mass transfer mechanisms in a heterotrophic biofilm.* Water Res., 1985. **19**: p. 1369-1378. DOI: 10.1016/0043-1354(85)90303-3.

279. Ismail, S.B., C.J. de La Parra, H. Temmink, and J.B. van Lier, *Extracellular polymeric substances (EPS) in upflow anaerobic sludge blanket (UASB) reactors operated under high salinity conditions.* Water Res., 2010. **44**: p. 1909-1917. DOI: 10.1016/j.watres.2009.11.039.

280. Au - Felz, S., S. Au - Al-Zuhairy, O.A. Au - Aarstad, M.C.M. Au - van Loosdrecht, and Y.M. Au - Lin, *Extraction of Structural Extracellular Polymeric Substances from Aerobic Granular Sludge.* JoVE, 2016: p. e54534. DOI: doi:10.3791/54534.

281. Körstgens, V., H.-C. Flemming, J. Wingender, and W. Borchard, *Influence of calcium ions on the mechanical properties of a model biofilm of mucoid Pseudomonas aeruginosa.* Water Sci. Technol., 2001. **43**: p. 49-57. DOI: 10.2166/wst.2001.0338.

282. Li, J., J. He, Y. Huang, D. Li, and X. Chen, *Improving surface and mechanical properties of alginate films by using ethanol as a co-solvent during external gelation.* Carbohydr. Polym., 2015. **123**: p. 208-216. DOI: 10.1016/j.carbpol.2015.01.040.

283. Steinbusch, K.J.J., H.V.M. Hamelers, and C.J.N. Buisman, *Alcohol production through volatile fatty acids reduction with hydrogen as electron donor by mixed cultures.* Water Res., 2008. **42**: p. 4059-4066. DOI: 10.1016/j.watres.2008.05.032.

284. Sowers, K.R. and R.P. Gunsalus, *Halotolerance in Methanosarcina spp.: Role of N(sup(epsilon))-Acetyl-(beta)-Lysine, (alpha)-Glutamate, Glycine Betaine, and K(sup+) as Compatible Solutes for Osmotic Adaptation.* Appl Environ Microbiol, 1995. **61**: p. 4382-8. DOI: 10.1128/aem.61.12.4382-4388.1995.

285. Chen, J.P., L. Hong, S. Wu, and L. Wang, *Elucidation of Interactions between Metal Ions and Ca Alginate-Based Ion-Exchange Resin by Spectroscopic Analysis and Modeling Simulation.* Langmuir, 2002. **18**: p. 9413-9421.

286. Ionita, G., A.M. Ariciu, D.K. Smith, and V. Chechik, *Ion exchange in alginate gels--dynamic behaviour revealed by electron paramagnetic resonance.* Soft Matter, 2015. **11**: p. 8968-74. DOI: 10.1039/c5sm02062j.

287. Liu, Y., M.C. Lam, and H.H.P. Fang, *Adsorption of heavy metals by EPS of activated sludge.* Water Sci. Technol., 2001. **43**: p. 59-66.

288. More, T.T., J.S. Yadav, S. Yan, R.D. Tyagi, and R.Y. Surampalli, *Extracellular polymeric substances of bacteria and their potential environmental applications.* J Environ Manage, 2014. **144**: p. 1-25. DOI: 10.1016/j.jenvman.2014.05.010.

289. Lee, K.Y. and D.J. Mooney, *Alginate: Properties and biomedical applications.* Prog. Polym. Sci., 2012. **37**: p. 106-126. DOI: 10.1016/j.progpolymsci.2011.06.003.

290. Nestle, N. and R. Kimmich, *Heavy metal uptake of alginate gels studied by NMR microscopy.* Colloids Surf. Physicochem. Eng. Aspects, 1996. **115**: p. 141-147. DOI: 10.1016/0927-7757(96)03608-4.

291. Ahmed, E.M., *Hydrogel: Preparation, characterization, and applications: A review.* Journal of Advanced Research, 2015. **6**: p. 105-121. DOI: 10.1016/j.jare.2013.07.006.

292. Svoboda, M., J. Beneš, L. Vobecká, and Z. Slouka, *Swelling induced structural changes of a heterogeneous cation-exchange membrane analyzed by micro-computed tomography.* J. Membr. Sci., 2017. **525**: p. 195-201. DOI: 10.1016/j.memsci.2016.10.046.

293. Fan, H. and N.Y. Yip, *Elucidating conductivity-permselectivity tradeoffs in electrodialysis and reverse electrodialysis by structure-property analysis of ion-exchange membranes.* J. Membr. Sci., 2019. **573**: p. 668-681. DOI: 10.1016/j.memsci.2018.11.045.

294. Welte, C. and U. Deppenmeier, *Bioenergetics and anaerobic respiratory chains of aceticlastic methanogens.* Biochimica et Biophysica Acta (BBA) - Bioenergetics, 2014. **1837**: p. 1130-1147. DOI: 10.1016/j.bbabio.2013.12.002.

295. Chen, Y. and J.J. Cheng, *Effect of Potassium Inhibition on the Thermophilic Anaerobic Digestion of Swine Waste.* Water Environ. Res, 2007. **79**: p. 667-674. DOI: 10.2175/106143007x156853.

296. Demirer, O.N., R.L. Clifton, C.A.R. Perez, R. Naylor, and C. Hidrovo *Characterization of Ion Transport and -Sorption in a Carbon Based Porous Electrode for Desalination Purposes*. J. Fluids Eng., 2013. **135**: p. 041201. DOI: 10.1115/1.4023294.

297. Lee, J.-H., W.-S. Bae, and J.-H. Choi *Electrode reactions and adsorption/desorption performance related to the applied potential in a capacitive deionization process*. Desalination, 2010. **258**: p. 159-163. DOI: 10.1016/j.desal.2010.03.020.

298. Rica, R.A., R. Ziano, D. Salerno, F. Mantegazza, and D. Brogioli, *Thermodynamic Relation between Voltage-Concentration Dependence and Salt Adsorption in Electrochemical Cells.* Phys. Rev. Lett., 2012. **109**: p. 156103. DOI: 10.1103/PhysRevLett.109.156103.

299. Kim, T., J.E. Dykstra, S. Porada, A. van der Wal, J. Yoon, and P.M. Biesheuvel *Enhanced charge efficiency and reduced energy use in capacitive deionization by increasing the discharge voltage*. J. Colloid Interf. Sci., 2015. **446**: p. 317-326. DOI: 10.1016/j.jcis.2014.08.041.

300. Wang, H. and L. Pilon, *Accurate Simulations of Electric Double Layer Capacitance of Ultramicroelectrodes.* J. Phys. Chem. C, 2011. **115**: p. 16711-16719. DOI: 10.1021/jp204498e.

301. Oldham, K.B., *A Gouy–Chapman–Stern model of the double layer at a (metal)/(ionic liquid) interface.* J. Electroanal. Chem., 2008. **613**: p. 131-138. DOI: 10.1016/j.jelechem.2007.10.017.

302. Rica, R.A., D. Brogioli, R. Ziano, D. Salerno, and F. Mantegazza, *Ions Transport and Adsorption Mechanisms in Porous Electrodes During Capacitive-Mixing Double Layer Expansion (CDLE).* J. Phys. Chem. C, 2012. **116**: p. 16934-16938. DOI: 10.1021/jp3059849.

303. Müller, M. and B. Kastening, *The double layer of activated carbon electrodes. Part 1. The contribution of ions in the pores.* J. Electroanal. Chem., 1994. **374**: p. 149-158.

304. Gao, X., A. Omosebi, J. Landon, and K. Liu, *Enhanced Salt Removal in an Inverted Capacitive Deionization Cell Using Amine Modified Microporous Carbon Cathodes.* Environ. Sci. Technol., 2015. **49**: p. 10920-10926. DOI: 10.1021/acs.est.5b02320.

305. Bouhadana, Y., E. Avraham, M. Noked, M. Ben-Tzion, A. Soffer, and D. Aurbach, *Capacitive Deionization of NaCl Solutions at Non-Steady-State Conditions: Inversion Functionality of the Carbon Electrodes.* Journal of Physical Chemistry C, 2011. **115**: p. 16567-16573. DOI: 10.1021/jp2047486.

306. Omosebi, A., X. Gao, J. Rentschler, J. Landon, and K. Liu, *Continuous operation of membrane capacitive deionization cells assembled with dissimilar potential of zero charge electrode pairs.* J. Colloid Interface Sci., 2015. **446**: p. 345-351. DOI: 10.1016/j.jcis.2014.11.013.

307. Mirzadeh, M., F. Gibou, and T.M. Squires *Enhanced Charging Kinetics of Porous Electrodes: Surface Conduction as a Short-Circuit Mechanism*. Phys. Rev. Lett., 2014. **113**: p. 097701. DOI: 10.1103/PhysRevLett.113.097701.

308. Suss, M.E., P.M. Biesheuvel, T.F. Baumann, M. Stadermann, and J.G. Santiago, *In Situ Spatially and Temporally Resolved Measurements of Salt Concentration between Charging Porous Electrodes for Desalination by Capacitive Deionization.* Environ. Sci. Technol., 2014. **48**: p. 2008-2015. DOI: 10.1021/es403682n.

309. Porada, S., B.B. Sales, H.V.M. Hamelers, and P.M. Biesheuvel, *Water Desalination with Wires.* J. Phys. Chem. Lett., 2012. **3**: p. 1613-1618. DOI: 10.1021/jz3005514.

310. ATSDR (Agency for Toxic Substances and Disease Registry), *Toxicological profile for acetone*. 1994, U.S. Department of Health and Human Services: Atlanta,GA.

311. Jouyban, A., M.A.A. Fakhree, and A. Shayanfar, *Review of Pharmaceutical Applications of N-Methyl-2-Pyrrolidone.* J. Pharm. Pharmaceut. Sci., 2010. **13**: p. 524-535.

312. Figueiredo, J.L., M.F.R. Pererira, M.M.A. Freitas, and J.J.M. Orfao, *Modification of the surface chemistry of activated carbons.* Carbon, 1999. **37**: p. 1379-1389.

313. Cohen, I., E. Avraham, Y. Bouhadana, A. Soffer, and D. Aurbach, *Long term stability of capacitive de-ionization processes for water desalination: The challenge of positive electrodes corrosion.* Electrochim. Acta, 2013. **106**: p. 91-100. DOI: 10.1016/j.electacta.2013.05.029.

314. Lopez-Ramon, M.V., F. Stoeckli, C. Moreno-Castilla, and F. Carrasco-Marin, *On the characterization of acidic and basic surface sites on carbons by various techniques.* Carbon, 1999. **37**: p. 1215-1221.

315. Dickinson, E.J.F. and R.G. Compton, *Influence of the diffuse double layer on steady-state voltammetry.* J. Electroanal. Chem., 2011. **661**: p. 198-212. DOI: 10.1016/j.jelechem.2011.08.002.

316. Dykstra, J.E., P.M. Biesheuvel, H. Bruning, and A. Ter Heijne, *Theory of ion transport with fast acid-base equilibrations in bioelectrochemical systems.* Phys. Rev. E Stat. Nonlin. Soft Matter Phys., 2014. **90**: p. 013302. DOI: 10.1103/PhysRevE.90.013302.

317. Paz-Garcia, J.M., J.E. Dykstra, P.M. Biesheuvel, and H.V.M. Hamelers, *Energy from CO2 using capacitive electrodes – A model for energy extraction cycles.* J. Colloid Interface Sci., 2015. **442**: p. 103-109. DOI: 10.1016/j.jcis.2014.11.045.

318. Bansal, R.C. and M. Goyal, *Activated Carbon Adsorption*. 2005: CRC Press.

319. Li, H. and L. Zou, *Ion-exchange membrane capacitive deionization: A new strategy for brackish water desalination.* Desalination, 2011. **275**: p. 62-66. DOI: 10.1016/j.desal.2011.02.027.

320. Salame, I. and T. Bandosz, *Surface Chemistry of Activated Carbons: Combining the Results of Temperature-Programmed Desorption, Boehm, and Potentiometric Titrations.* J Colloid Interface Sci, 2001. **240**: p. 252-258. DOI: 10.1006/jcis.2001.7596.

321. Collins, K.D., *Ion hydration: Implications for cellular function, polyelectrolytes, and protein crystallization.* Biophys Chem, 2006. **119**: p. 271-81. DOI: 10.1016/j.bpc.2005.08.010.

322. Collins, K.D., *Why continuum electrostatics theories cannot explain biological structure, polyelectrolytes or ionic strength effects in ion-protein interactions.* Biophys Chem, 2012. **167**: p. 43-59. DOI: 10.1016/j.bpc.2012.04.002.

323. Zachariah, Z., R.M. Espinosa-Marzal, and M.P. Heuberger, *Ion specific hydration in nano-confined electrical double layers.* J Colloid Interface Sci, 2017. **506**: p. 263-270. DOI: 10.1016/j.jcis.2017.07.039.

324. Feng, G., J. Huang, B.G. Sumpter, V. Meunier, and R. Qiao, *Structure and dynamics of electrical double layers in organic electrolytes.* Phys Chem Chem Phys, 2010. **12**: p. 5468-79. DOI: 10.1039/c000451k.

325. Dunwell, M., Y. Yan, and B. Xu, *Understanding the influence of the electrochemical double-layer on heterogeneous electrochemical reactions.* Current Opinion in Chemical Engineering, 2018. **20**: p. 151-158. DOI: 10.1016/j.coche.2018.05.003.

326. Ito, M., *Structures of water at electrified interfaces: Microscopic understanding of electrode potential in electric double layers on electrode surfaces.* Surf. Sci. Rep., 2008. **63**: p. 329-389. DOI: 10.1016/j.surfrep.2008.04.002.

327. Lee, S.S., P. Fenter, K.L. Nagy, and N.C. Sturchio, *Changes in adsorption free energy and speciation during competitive adsorption between monovalent cations at the muscovite (001)-water interface.* Geochim. Cosmochim. Acta, 2013. **123**: p. 416-426. DOI: 10.1016/j.gca.2013.07.033.

328. Brown, M.A., Z. Abbas, A. Kleibert, R.G. Green, A. Goel, S. May, and T.M. Squires, *Determination of Surface Potential and Electrical Double-Layer Structure at the Aqueous Electrolyte-Nanoparticle Interface.* Physical Review X, 2016. **6**. DOI: 10.1103/PhysRevX.6.011007.

329. Pashley, R.M., *DLVO and hydration forces between mica surfaces in Li+, Na+, K+, and Cs+ electrolyte solutions: A correlation of double-layer and hydration forces with surface cation exchange properties.* J. Colloid Interface Sci., 1981. **83**: p. 531-546. DOI: doi.org/10.1016/0021-9797(81)90348-9.

330. Sakuma, H. and K. Kawamura, *Structure and dynamics of water on Li+-, Na+-, K+-, Cs+-, H3O+-exchanged muscovite surfaces: A molecular dynamics study.* Geochim. Cosmochim. Acta, 2011. **75**: p. 63-81. DOI: 10.1016/j.gca.2010.10.007.

331. Jiang, G., C. Cheng, D. Li, and J.Z. Liu, *Molecular dynamics simulations of the electric double layer capacitance of graphene electrodes in mono-valent aqueous electrolytes.* Nano Research, 2016. **9**: p. 174-186. DOI: 10.1007/s12274-015-0978-5.

332. Bastos-González, D., L. Pérez-Fuentes, C. Drummond, and J. Faraudo, *Ions at interfaces: the central role of hydration and hydrophobicity.* Current Opinion in Colloid & Interface Science, 2016. **23**: p. 19-28. DOI: 10.1016/j.cocis.2016.05.010.

333. Ohkubo, T., T. Konishi, Y. Hattori, H. Kanoh, T. Fujikawa, and K. Kaneko, *Restricted Hydration Structures of Rb and Br Ions Confined in Slit-Shaped Carbon Nanospace.* J. Am. Chem. Soc., 2002. **124**: p. 11860-11861.

334. Marañón Di Leo, J. and J. Marañón, *Hydration and diffusion of cations in nanopores.* Journal of Molecular Structure: THEOCHEM, 2005. **729**: p. 53-57. DOI: 10.1016/j.theochem.2005.02.070.

335. Gouaux, E. and R. MacKinnon, *Principles of Selective Ion Transport in Channels and Pumps.* Science, 2005. **310**: p. 1461-1465. DOI: 10.1126/science.1113666.

336. Sahu, S., M.D. Ventra, and M. Zwolak, *Dehydration as a Universal Mechanism for Ion Selectivity in Graphene and Other Atomically Thin Pores.* Nano Lett., 2017. **17**: p. 4719–4724. DOI: 10.1021/acs.nanolett.7b01399.

337. Epsztein, R., W. Cheng, E. Shaulsky, N. Dizge, and M. Elimelech, *Elucidating the mechanisms underlying the difference between chloride and nitrate rejection in nanofiltration.* J. Membr. Sci., 2018. **548**: p. 694-701. DOI: 10.1016/j.memsci.2017.10.049.

338. Richards, L.A., B.S. Richards, B. Corry, and A.I. Schafer, *Experimental energy barriers to anions transporting through nanofiltration membranes.* Environ Sci Technol, 2013. **47**: p. 1968-76. DOI: 10.1021/es303925r.

339. Kwasny, M.T., L. Zhu, M.A. Hickner, and G.N. Tew, *Thermodynamics of Counterion Release Is Critical for Anion Exchange Membrane Conductivity.* J Am Chem Soc, 2018. **140**: p. 7961-7969. DOI: 10.1021/jacs.8b03979.

340. Tedesco, M., H.V.M. Hamelers, and P.M. Biesheuvel, *Nernst-Planck transport theory for (reverse) electrodialysis: II. Effect of water transport through ion-exchange membranes.* J. Membr. Sci., 2017. **531**: p. 172-182. DOI: 10.1016/j.memsci.2017.02.031.

341. Han, L., S. Galier, and H. Roux-de Balmann, *Ion hydration number and electro-osmosis during electrodialysis of mixed salt solution.* Desalination, 2015. **373**: p. 38-46. DOI: 10.1016/j.desal.2015.06.023.

342. Gur, Y., I. Ravina, and A. Babchin, *On the Electrical Double Layer Theory II. The Poisson-Boltzmann Equation Including Hydration Forces.* J. Colloid Interface Sci., 1978. **64**: p. 333-341.

343. Hawks, S.A., A. Ramachandran, S. Porada, P.G. Campbell, M.E. Suss, P.M. Biesheuvel, J.G. Santiago, and M. Stadermann, *Performance metrics for the objective assessment of capacitive deionization systems.* Water Res, 2019. **152**: p. 126-137. DOI: 10.1016/j.watres.2018.10.074.

344. Kim, Y.-J., J.-H. Kim, and J.-H. Choi, *Selective removal of nitrate ions by controlling the applied current in membrane capacitive deionization (MCDI).* J. Membr. Sci., 2013. **429**: p. 52-57. DOI: 10.1016/j.memsci.2012.11.064.

345. Mubita, T.M., J.E. Dykstra, P.M. Biesheuvel, A. van der Wal, and S. Porada, *Selective adsorption of nitrate over chloride in microporous carbons.* Water Res, 2019. **164**: p. 114885. DOI: 10.1016/j.watres.2019.114885.

346. Pasta, M., C.D. Wessells, Y. Cui, and F. La Mantia, *A desalination battery.* Nano Lett, 2012. **12**: p. 839-43. DOI: 10.1021/nl203889e.

347. Zhang, J., X. Cui, F. Yang, L. Qu, F. Du, H. Zhang, and J. Wang, *Hybrid Cation Exchange Membranes with Lithium Ion-Sieves for Highly Enhanced Li+ Permeation and Permselectivity.* Macromolecular Materials and Engineering, 2019. **304**: p. 1800567. DOI: 10.1002/mame.201800567.

348. Bazrgar Bajestani, M., A. Moheb, and M. Dinari, *Preparation of lithium ion-selective cation exchange membrane for lithium recovery from sodium contaminated lithium bromide solution by electrodialysis process.* Desalination, 2020. **486**: p. 114476. DOI: 10.1016/j.desal.2020.114476.

349. Razmjou, A., G. Eshaghi, Y. Orooji, E. Hosseini, A.H. Korayem, F. Mohagheghian, Y. Boroumand, A. Noorbakhsh, M. Asadnia, and V. Chen, *Lithium ion-selective membrane with 2D subnanometer channels.* Water Res, 2019. **159**: p. 313-323. DOI: 10.1016/j.watres.2019.05.018.

350. Reig, M., H. Farrokhzad, B. Van der Bruggen, O. Gibert, and J.L. Cortina, *Synthesis of a monovalent selective cation exchange membrane to concentrate reverse osmosis brines by electrodialysis.* Desalination, 2015. **375**: p. 1-9. DOI: 10.1016/j.desal.2015.07.023.

351. An, S.-S., J. Liu, J.-H. Wang, M.-C. Wang, Z.-Y. Ji, S.-S. Qi, and J.-S. Yuan, *Synthesis and characterization of a plat sheet potassium ion sieve membrane and its performances for separation potassium.* Sep. Purif. Technol., 2019. **212**: p. 834-842. DOI: 10.1016/j.seppur.2018.11.079.

352. Louati, I., F. Guesmi, A. Chaabouni, C. Hannachi, and B. Hamrouni, *Effect of ionic strength on the ion exchange equilibrium between AMX membrane and electrolyte solutions.* Water Qual. Res. J. Can., 2015: p. wqrjc2015006. DOI: 10.2166/wqrjc.2015.006.

353. Bruggen, B.V.d., *Chapter 7 - Ion-exchange membrane systems—Electrodialysis and other electromembrane processes*, in *Fundamental Modelling of Membrane Systems*, P. Luis, Editor. 2018, Elsevier. p. 251-300.

354. Luo, T., F. Roghmans, and M. Wessling, *Ion mobility and partition determine the counter-ion selectivity of ion exchange membranes.* J. Membr. Sci., 2020. **597**: p. 117645. DOI: 10.1016/j.memsci.2019.117645.

355. Luo, H., W.-A.S. Agata, and G.M. Geise, *Connecting the Ion Separation Factor to the Sorption and Diffusion Selectivity of Ion Exchange Membranes.* Industrial & Engineering Chemistry Research, 2020. **59**: p. 14189-14206. DOI: 10.1021/acs.iecr.0c02457.

356. Diallo, M.S., M.R. Kotte, and M. Cho, *Mining Critical Metals and Elements from Seawater: Opportunities and Challenges.* Environ Sci Technol, 2015. **49**: p. 9390-9. DOI: 10.1021/acs.est.5b00463.

357. Vikström, H., S. Davidsson, and M. Höök, *Lithium availability and future production outlooks.* Applied Energy, 2013. **110**: p. 252-266. DOI: 10.1016/j.apenergy.2013.04.005.

358. Choubey, P.K., M.-s. Kim, R.R. Srivastava, J.-c. Lee, and J.-Y. Lee, *Advance review on the exploitation of the prominent energy-storage element: Lithium. Part I: From mineral and brine resources.* Miner. Eng., 2016. **89**: p. 119-137. DOI: 10.1016/j.mineng.2016.01.010.

359. Baspineiro, C.F., J. Franco, and V. Flexer, *Potential water recovery during lithium mining from high salinity brines.* Sci Total Environ, 2020. **720**: p. 137523. DOI: 10.1016/j.scitotenv.2020.137523.

360. Stamp, A., D.J. Lang, and P.A. Wäger, *Environmental impacts of a transition toward e-mobility: the present and future role of lithium carbonate production.* Journal of Cleaner Production, 2012. **23**: p. 104-112. DOI: 10.1016/j.jclepro.2011.10.026.

361. Kushnir, D. and B.A. Sandén, *The time dimension and lithium resource constraints for electric vehicles.* Resources Policy, 2012. **37**: p. 93-103. DOI: 10.1016/j.resourpol.2011.11.003.

362. Iclodean, C., B. Varga, N. Burnete, D. Cimerdean, and B. Jurchiș, *Comparison of Different Battery Types for Electric Vehicles.* IOP Conference Series: Materials Science and Engineering, 2017. **252**: p. 012058. DOI: 10.1088/1757-899x/252/1/012058.

363. Liu, X., X. Chen, L. He, and Z. Zhao, *Study on extraction of lithium from salt lake brine by membrane electrolysis.* Desalination, 2015. **376**: p. 35-40. DOI: 10.1016/j.desal.2015.08.013.

364. Flexer, V., C.F. Baspineiro, and C.I. Galli, *Lithium recovery from brines: A vital raw material for green energies with a potential environmental impact in its mining and processing.* Sci Total Environ, 2018. **639**: p. 1188-1204. DOI: 10.1016/j.scitotenv.2018.05.223.

365. Agusdinata, D.B., W. Liu, H. Eakin, and H. Romero, *Socio-environmental impacts of lithium mineral extraction: towards a research agenda.* Environmental Research Letters, 2018. **13**: p. 123001. DOI: 10.1088/1748-9326/aae9b1.

366. An, J.W., D.J. Kang, K.T. Tran, M.J. Kim, T. Lim, and T. Tran, *Recovery of lithium from Uyuni salar brine.* Hydrometallurgy, 2012. **117-118**: p. 64-70. DOI: 10.1016/j.hydromet.2012.02.008.

Acknowledgments

Acknowledgments

Writing this part of the thesis is very exciting because it means that I am close to ending an important chapter in my life. I am very grateful for having had the opportunity to pursue a PhD. And I want to thank all the people who were with me throughout this period and made this journey pleasant and rewarding.

I would like to thank my promotor**, Albert van der Wal**, for giving me the opportunity to work on this project. I appreciate the freedom you gave me to perform the research and the encouragement to improve my writing skills and sharpen my thinking. **Slawomir Porada**, thank you for your guidance and your patience. I learned a lot from you, not only about science but also how to deal with challenging situations. I am also grateful to **Jouke Dykstra** for your timely suggestions and efforts to improve the quality of the project. **Maarten Biesheuvel**, you are one of the main reasons I did a PhD. Thank you for your constant help and support. In many ways, the interaction with you, Slawomir, and Jouke have positively influenced how I approach and do research.

Cees Buisman, **Johannes Boonstra**, and **Bert Hamelers** for constructive interactions and collaborative work during my time as PhD representative.

Michel Saakes, I appreciate the feedback you gave me to improve one of the most challenging paper I had to write.

My sincere thanks to all the people who work to keep Wetsus running: **Linda**, **Willy**, **Janny**, **Trienke**, **Anke, Tineke, Roely, Nynke, Lucy, Hester, Gerrit**, **Jan de Groot, Rienk, Wiebe.** Thank you to the analytical team, **Janneke**, **Marianne, Lisette**, **Jan-Willem**, and **Jelmer**. Special thanks to **Mieke** for developing the method used to measure iodate and iodide. To solve any technical issue with my set-up I always counted on **Harm**. And when he was not around, I received the support of **Jan Tuinstra**, **John**, **Ernst**, **Jan Jurjen,** and **Wim Borgonje.** Thank you, **Gerben, Catharina, and Riet** for taking care of my special diet during the theme meetings.

I would like to thank my officemates, **Ilse**, **Enas**, **Casper**, **Louis**, **Suyash**, **Zexin**, **Antoine**, **Rita, Nandini**, and **Yin**, for the lively discussions, unschedule intervision sessions, and

tasty food we occasionally shared. Enas, I enjoyed our talks about family and life in general.

I would like to thank Qian Jia and Rienk van Staalduinen for choosing me as their supervisor and helping me with the lab work and the collection of data.

Thank you to my fellow PhDs **Emad** and **Diego** for the feedback and informative discussions about how to characterize ion-exchange membranes and interpret data. **Ettore**, thank you for showing me how to measure the contact angle. **Gosia**, I enjoyed our long talks and dinners with tasty food and strong drinks. **Kaustub**, 'my fraand', it was a pleasure to share part of the PhD route with you.

Paulina, vivir contigo puso a prueba mis nervios, no sé cuántas veces lograste asustarme. Gracias por no llevar un gato a la casa, por hacer nuestra convivencia llevadera, y por deshacerte de las babosas.

Liesbeth, **Wies**, and **Marjolein** for all the support and assistance to deal with administrative requirements at Wageningen University.

Thank you to **Thomas, Laura, Dainis, Joeri, Rosanne, Farzaneh, Adrian, Carlos,** and **Paulina** for the excellent trip to Chile that we organized together**.**

Ingrid Weurman, thank you for your help and advice when the water was a bit rough and it was difficult for me to swim.

Thank you to my paranymphs, **Tanya Georgieva** and **Gerbrich de Jong**, you were the door outside my PhD life and everything related to it. Tanya, it is always relaxing to share with you a cake and tea on Sunday afternoon. It is priceless to see our girls interacting and having fun together. Благодаря ви приятели. Gerbrich, de Nederlandse lessen bij jou waren veel meer dan dat. Met jou praten was een uitstekende manier om wat druk te verminderen en te ontspannen toen ik een beetje overweldigd was. Bedankt dat je me hebt geleerd hoe ik mijn favoriete Hollandse eten kan bereiden: erwtensoep.

Mami, eres mi ejemplo a seguir. Siempre andas estimulándome y retándome para que sea una mejor persona y para que dé lo mejor en todo lo que hago. Gracias por tu apoyo

incondicional. **Vito**, ser tu hermana es lo mejor. Gracias por hacerme reir, por ser mi confidente, por siempre apoyarme. A doña **Luisa** su influencia está en cada parte de mi ser. Sin ella este logro no hubiese sido posible. A tío **Alfonso**, gracias por el apoyo que me brindaste cuando se dió la oportunidad de venirme a estudiar a los Países Bajos. A la **familia Zambrano**, a mis tíos y primos por estar siempre pendiente de mí.

Daini, es esmu svētīta, ka esi man līdzās, ejot mūsu kopīgo dzīves ceļu. Paldies, ka esi mans terapeits, redaktors un pašapziņa, bet pāri visam, mans gādīgais vīrs un mūsu ziņkārīgās, enerģiskās un skaistās **Amandas Luīzes** tēvs. Viņa ir mūsu ideālākais kopdarbs.

To all the people I inadvertently omitted, thank you very much.

Al principio y fin de todas las cosas, Gracias!

About the author

Tania M. Mubita Zambrano was born on February 21, 1983, in Mérida, Venezuela. Tania obtained a bachelor's degree in chemistry (graduated *cum laude*) and a master's degree in chemical engineering from Universidad de los Andes and Universidad Simón Bolívar, respectively. Both universities are located in her home country.

In 2013, Tania moved to the Netherlands to start a second master's, this time in water technology (joint degree) at Wetsus Academy in Leeuwarden. In 2016, after completing her master's studies, she started a PhD in the Environmental Technology Department (ETE) at Wageningen University. The research was carried out at Wetsus, European Centre of Excellence for Sustainable Water Technology. The results of the PhD project are presented in this thesis. In October 2020, Tania started working as a researcher in the separation and purification expertise at Wageningen Food and Biobased Research (Wageningen University & Research).

Netherlands Research School for the
Socio-Economic and Natural Sciences of the Environment

D I P L O M A

for specialised PhD training

The Netherlands research school for the
Socio-Economic and Natural Sciences of the Environment
(SENSE) declares that

Tania Maria Mubita Zambrano

born on 21 February 1983 in Mérida, Venezuela

has successfully fulfilled all requirements of the
educational PhD programme of SENSE.

Wageningen, 19 February 2021

Chair of the SENSE board

Prof. dr. Martin Wassen

The SENSE Director

Prof. Philipp Pattberg

The SENSE Research School has been accredited by the Royal Netherlands Academy of Arts and Sciences (KNAW)

KONINKLIJKE NEDERLANDSE
AKADEMIE VAN WETENSCHAPPEN

The SENSE Research School declares that **Tania Maria Mubita Zambrano** has successfully fulfilled all requirements of the educational PhD programme of SENSE with a work load of 43.7 EC, including the following activities:

SENSE PhD Courses

- Environmental research in context (2016)
- Research in context activity: 'Initiating, organizing and coordinating successful study trip to Chile for PhD candidates from the Dept. of Environmental Technology' (2019)

Other PhD and Advanced MSc Courses

- Presentation Skills, Wetsus / Van-Zelf (2016)
- Communication Styles, Wetsus / How Company (2016)
- Design of Experiments, Wetsus / Justinek Engineering (2017)
- Project and Time Management, Wageningen Graduate School (2017)
- How to Supervise BSc/MSc students, Wetsus (2017)
- Scientific Writing, Wageningen Graduate School (2017)
- Illustrations for Scientific Publications, Wetsus / somersault (2017)
- Talents, Wetsus (2017)
- 8th European Summer School on Electrochemical Engineering, Université Toulouse III. France (2018)
- Linear Models, PE&RC and WIMEK (2018)
- Critical Thinking and Argumentation, Wageningen Graduate School (2019)
- Career Assessment, Wageningen Graduate School (2019)

Management and Didactic Skills Training

- PhD representative at Wetsus (2017-2019)
- Supervising MSc student with thesis entitled 'Comparative studies of heterogeneous cation exchange membranes with different polymeric binders' (2018)
- Supervising BSc student internship (2019)

Oral Presentations

- Nitrate selectivity of heterogeneous membranes in membrane capacitive deionization. 11th International Congress on Membranes and Membrane Processes, 29 July – 4 August 2017, San Francisco, United States of America
- Water desalination with wires: transport modelling for ideal and leaky membranes. Membranes in the Production of Drinking and Industrial Water Conference, 6-8 February 2017, Leeuwarden, The Netherlands

SENSE coordinator PhD education

Dr. ir. Peter Vermeulen

This work was performed in the cooperation framework of Wetsus, European Centre of Excellence for Sustainable Water Technology (www.wetsus.nl). Wetsus is co-funded by the Dutch Ministry of Economic Affairs and Ministry of Infrastructure and Environment, the European Union Regional Development Fund, the Province of Fryslân, and the Northern Netherlands Provinces. The author would like to thank the participants of the research theme “Capacitive Deionization" for the fruitful discussions and financial support.

Cover design by Tania Mubita and Harrison Mubita
Printed by ProefschriftMaken